



THE UNIVERSITY
of ADELAIDE

Plastic Tuners for
Power Steering Pump Noise Reduction

James Wilkie

School of Mechanical Engineering

The University of Adelaide
South Australia 5005
Australia

A thesis submitted in fulfilment of the requirements
for the degree of Ph.D. in Mechanical Engineering
28th October 2011

Abstract

Tuning cables of various designs are commonly included in automotive power steering systems to reduce the undesirable effects of pressure pulsations generated in the power steering pump. A recent development which has the potential to reduce noise is the plastic tuner (PT). The main benefit of this device when compared with the existing spiral wound steel tuner (SWST) is the vastly reduced cost associated with the methods of manufacturing.

Despite the apparent attractiveness of such a device, the PT has not been widely implemented by automotive fluid system suppliers. The main reason is relatively little is known about the performance of these devices and indeed their comparative performance with respect to a SWST. This research seeks to address this issue by developing a better understanding of the PT using experimental and analytical techniques to examine the acoustic noise reduction mechanisms of a variety of PT designs.

This thesis examines the relevant literature associated with the subject and covers several noise reduction techniques that can be applied to this research. The literature review section highlights a general gap in the knowledge base, where little specific detail exists that has not been derived experimentally from SWSTs. As such the general aim of this research is to further the knowledge into PTs, investigate the significant parameters of PT designs, and generate a suitable system model. The methodology proposed to achieve these aims is explained in detail and experimental and theoretical approaches are outlined. Finally, conclusions derived from the experimental investigations are discussed and a comparison is drawn between experimental and predicted results. For all PT parameters evaluated, good agreement is illustrated between predicted and experimental results.

Statement of Originality

This work contains no material which has been accepted for the award of any other degree or diploma in any university or other tertiary institution to Jamie Wilkie and, to the best of my knowledge and belief, contains no material previously published or written by another person, except where due reference has been made in the text.

I give my consent to the copy of my thesis when deposited in the University Library, being made available for loan and photocopying, subject to the provisions of the Copyright Act 1968.

I also give my permission for the digital version of my thesis to be made available on the web, via the University's digital research repository, the Library catalogue, the Australian Digital Theses Program (ADTP) and also through web search engines, unless permission has been granted by the University to restrict access for a period of time.

Jamie Wilkie

Acknowledgements

I would like to acknowledge some people who have contributed to this thesis or supported me during my time as an industry based postgraduate student.

Firstly I would like to thank my two supervisors Anthony Zander and Con Doolan. Their flexibility with respect to my industry based working life has assisted enormously and without their ready knowledge and guidance, I simply would not have completed this thesis.

I would like to thank Cooper Standard Automotive and in particular Troy Kelly for assistance with my experiments. The un-foreseen plant closure drastically impacted my research plans and without his help in setting up, dismantling, re-assembling, cups of tea etc., the full experimental schedule may not have been possible in the time available.

I am also thankful to the University Electronics Laboratory, for the use of their equipment, and in particular to Silvio De Ieso for his assistance in the early stages.

Finally, I would like to thank my family and close friends for their support over the last few years. I didn't anticipate the demands that this project would thrust upon me or the twists and turns my life would take along the way. Thanks for the understanding and for giving me the strength to keep going.

This thesis is dedicated to my son Innes. I hope it inspires you to be everything you can be.

Research Background

It should be noted that a significant portion of this research, specifically the experimental phase, was conducted whilst the author was an employee of Cooper Standard Automotive (CSA), Woodville North, Adelaide. CSA very kindly granted access to their power steering noise tuning rig as well as data acquisition software. In addition, a number of the test samples as well as baseline comparison samples were derived from CSA products. As a consequence, this research contains some context which has been deemed to be commercially sensitive, and hence, CSA have requested that no journal or conference papers associated with this research be published at this time. It is hoped that the outcomes from this research will be able to be published in the future, once sufficient intellectual property protection is in place.

In mid 2008 CSA closed their manufacturing facility in Adelaide and as a consequence, the scope of the experimental phase was constrained. Furthermore, considering the phase of the project at that time (approximately half-way through), it was difficult to predict future outcomes that may require further experimental investigation. To reduce this impact, the author completed a series of final experiments in the lead-up to the closure, in an effort to capture as much data as possible before the experimental facility was dismantled. This approach proved very useful upon reflection, and has contributed to some of the main outcomes derived in this thesis.

Contents

Abstract	iii
Statement of Originality.....	iv
Acknowledgements.....	v
Research Background	vi
Contents	vii
List of Figures	xii
List of Tables	xxiii
1 Introduction	1
1.1 Objectives	6
1.2 Key Objectives.....	7
1.2.1 Baseline Evaluation	7
1.2.2 Tuner Length.....	7
1.2.3 Tuner Hole Location	7
1.2.4 Tuner Hole Diameter	8
1.2.5 Multi-hole Tuners	8
1.2.6 Plastic Tuner Model.....	8
1.3 Outline.....	8
2 Literature Review	9
2.1 General Features of Hydraulic Power Steering Systems	9
2.2 Noise Characteristics Overview.....	10
2.2.1 Noise Generation	10
2.2.2 Noise Reduction.....	12
2.2.3 Acoustic Behaviour.....	13
2.3 Existing Attenuation Devices	15
2.3.1 Quincke Tube.....	15

2.3.2	Standpipe.....	17
2.3.3	The Spiral Wound Steel Tuner	18
2.3.4	The Plastic Tuner	21
2.4	Other Noise Reduction Methods.....	22
2.4.1	Turbofan Engine Noise Control.....	22
2.4.2	Sound Absorption of Honeycomb Panels	25
2.4.3	Transfer Matrix Methodology.....	28
2.4.4	Perforated Muffler Tube Components	33
2.5	Existing Acoustic Test Methods	36
2.5.1	The Two Microphone Method	36
2.5.2	Test Bench for Power Steering Noise Assessment	38
2.5.3	Standardised Test Procedures	39
2.6	Summary	44
3	Theory.....	45
3.1	Plastic Tuner Model Development	45
3.2	Tuner System Definition.....	46
3.3	Performance of Tuner and Tuner Elements	47
3.4	Plane Wave Assumption	48
3.5	Tuner Element Modelling.....	49
3.5.1	Tuner Duct Element.....	49
3.5.2	Tuner Extension Element.....	50
3.5.3	Tuner Expansion Element.....	52
3.5.4	Tuner Contraction Element.....	52
3.5.5	Tuner Hole Element.....	53
3.5.6	Parallel Branch Element	55
3.6	Validation of Modelling Approach.....	57
3.6.1	Transmission Matrix Validation – Single Expansion Chamber	57
3.6.2	Transmission Matrix Validation – Extended Inlet.....	59
3.6.3	Transmission Matrix Validation – Noise Reduction	61
3.7	Model of Tuner with No Holes.....	64
3.8	Model of Tuner with single hole (fixed diameter varied location)	65
3.9	Model of Tuner with single hole (fixed location varied diameter)	66
3.10	Model of Tuner with multiple holes	66

3.11	Summary	69
4	Experiments	70
4.1	Experimental Approach	70
4.1.1	Experimental Layout – Benchmarking	71
4.1.2	Experimental Layout – Tuner Design Investigations	72
4.1.3	Plastic Tuner Design	73
4.1.4	Control Sample	74
4.1.5	Plastic Tuner / Hose Coupling	74
4.1.6	Plastic Tuner Material Properties	75
4.1.7	Experimental Procedure	75
4.1.8	Experimental Noise Reduction	76
4.1.9	Empirical Approach to Termination Impedance	77
4.2	Termination Impedance Measurement	77
4.3	Baseline Evaluation Testing	78
4.3.1	Baseline Evaluation Results	78
4.3.2	Discussion arising from baseline evaluation	80
4.4	Tuner Length Experiments	81
4.4.1	Tuner Length Test Procedure	82
4.4.2	Tuner Length Test Results	83
4.5	Tuner Hole Location Experiments	86
4.5.1	Tuner Hole Location Test Procedure	87
4.5.2	Tuner Hole Location Test Results	87
4.6	Tuner Hole Diameter Experiments	90
4.6.1	Hole Diameter Test Procedure	91
4.6.2	Hole Diameter Test Results	91
4.7	Multi-hole Tuner Experiments	93
4.7.1	Multi-hole Tuner Test Procedure	94
4.7.2	Multi-hole Tuner Test Results	95
4.8	Conclusions	100
4.9	Summary	101
5	Results and Analysis	102
5.1	Tuner Length Validation	102

5.1.1	Analysis and discussion	102
5.2	Hole Location Validation.....	112
5.2.1	Analysis and discussion	112
5.3	Hole Diameter Validation	121
5.3.1	Analysis and discussion	121
5.4	Multi-hole Validation.....	128
5.4.1	Analysis and discussion	128
5.5	Termination Impedance	142
5.5.1	Analysis and Discussion	142
5.5.2	Proposed Theory	143
5.5.3	Validation and Discussion	144
5.5.4	Tuner Length Termination Impedance Prediction	150
5.5.5	Developed Tuner Length Noise Reduction Prediction	152
5.5.6	Hole Location Termination Impedance Prediction.....	154
5.5.7	Developed Hole Location Noise Reduction Prediction	155
5.5.8	Hole Diameter Termination Impedance Prediction	157
5.5.9	Developed Hole Diameter Noise Reduction Prediction	158
5.5.10	Multi Hole Termination Impedance Prediction	164
5.5.11	Developed Multi Hole Noise Reduction Prediction	167
5.6	Summary	171
6	Conclusions and Future Work	172
6.1	Summary.....	172
6.2	Key Objectives Achieved	173
6.2.1	Baseline Evaluation Summary.....	173
6.2.2	Tuner Length Summary	173
6.2.3	Tuner Hole Location Summary	174
6.2.4	Tuner Hole Diameter Summary.....	174
6.2.5	Multi-hole Summary	175
6.2.6	Plastic Tuner Model Summary	176
6.3	Future Work	178
7	References.....	179

Appendix A.....	187
A.1 Matlab Code – Tuner Duct Element.....	187
A.2 Matlab Code – Tuner Expansion Element.....	188
A.3 Matlab Code – Tuner Contraction Element.....	189
A.4 Matlab Code – Parallel Branch Element.....	190
A.5 Matlab Code – Transmission Loss.....	191
A.4 Matlab Code – Noise Reduction.....	192

List of Figures

Figure 1-1 Hydraulic Power Assisted Steering System: Component layout (Hydraulic Equipment Manufacturers, 2011).....	1
Figure 1-2 Typical Power Steering Vane Pump (Howstuffworks, 2001)	2
Figure 1-3 Typical Power Steering Pump Response (Howstuffworks, 2001)	2
Figure 1-4 Photograph of a) spiral wound steel tuner and baffle b) spiral wound steel tuner located inside hose bore	2
Figure 1-5 SWST Manufacturing Process.....	3
Figure 1-6 Photographs of filter paper from internal cleanliness testing	4
Figure 1-7 a) Fixture and clamp device b) Plastic tuner inserted over mandrel c) Hose insert / tuner end d) Completed plastic tuner assembly cross-section.....	5
Figure 2-1 Hydraulic Power Steering System (ZF, 2011).....	9
Figure 2-2 a) ‘In-phase’: phase difference is zero, b) ‘Out-of-phase: phase difference is 180°	11
Figure 2-3 a) Illustration of standing wave generation b) Attenuation of a standing wave.....	12
Figure 2-4 Quincke Tube illustration	15
Figure 2-5 Standpipe mounting (M Long, 1999)	17
Figure 2-6 Spiral Wound Steel Tuner Operation	18
Figure 2-7 Illustration of wave propagation inside the hose	20
Figure 2-8 Leak path profile illustration	20
Figure 2-9 Existing plastic tuner designs a) PSA (Peugeot 307) Plastic Tuner, b) GM Opel Vectra Plastic Tuner	21
Figure 2-10 Quincke Tube concept applied to inlet of turbofan engine. (Burdisso and Smith, 2000)	23

Figure 2-11 Quincke tube representations a) physical representation. b) simplified model.	23
Figure 2-12 Perforated Panel illustration.....	27
Figure 2-13 The three basic elements in an equivalent electrical representation a) a distributed element b) an in-line element c) a branch element.	29
Figure 2-14 Basic silencer system – representation of elements.....	31
Figure 2-15 Beranek and Vér, ‘Silencer system’.....	32
Figure 2-16 Acoustic impedance of a small circular orifice (Stinson and Shaw, 1985)	34
Figure 2-17 Two Microphone Method illustration.....	36
Figure 2-18 Test bench description and measurement points (Sciortino and Bamdad-Soufi, 1998)	39
Figure 2-19 Example of Ford Australia Noise Tuning Test Record (Ford Motor Company of Australia, 1979).....	40
Figure 2-20 Illustrations of impedance representations a) simple circuit b) using impedance notation.....	42
Figure 2-21 Secondary Source technique.....	42
Figure 3-1 Power steering hose assembly incorporating a plastic tuner and component models a) Power steering hose containing plastic tuner b) Model of tuner body c) Model of hole profile d) Model of tuner body downstream of the hole profile e) Model outside tuner f) Model at tuner outlet	45
Figure 3-2 Tuner System a) Acoustic b) Electrical Analogy.....	46
Figure 3-3 Noise Reduction of Tuner.....	47
Figure 3-4 Tuner Duct Element.....	49
Figure 3-5 Tuner Extension Element a) 3D view b) 2D view.....	51
Figure 3-6 Tuner Expansion Element.....	52
Figure 3-7 Tuner Contraction Element.....	53

Figure 3-8 Tuner Hole Element a) 3D view b) 2D view	54
Figure 3-9 Parallel Branch Element a) physical arrangement b) transmission matrix representation	55
Figure 3-10 Single expansion chamber dimensions used for validation	58
Figure 3-11 Comparison of Theoretical and Transfer Matrix predictions of Transmission Loss	59
Figure 3-12 Extended Inlet Expansion Chamber dimensions	60
Figure 3-13 Comparison of Transfer Matrix and 1-D Experimental Model of an extended inlet by Selamet and Ji (1998)	61
Figure 3-14 Geometry of a Simple Duct System	62
Figure 3-15 Simple Duct System Noise Reduction.....	63
Figure 3-16 Tuner with no holes a) physical arrangement b) transmission matrix representation	64
Figure 3-17 Tuner with single hole a) physical arrangement b) transmission matrix representation	65
Figure 3-18 Tuner with two holes a) physical arrangement b) transmission matrix representation	66
Figure 3-19 Tuner with three holes a) physical arrangement b) transmission matrix representation	68
Figure 4-1 Experimental layout.....	71
Figure 4-2 a) Test rig for plastic tuner investigation b) plastic tuner mounting detail	72
Figure 4-3 a) Length dimension in mm b) internal bore dimension in mm	73
Figure 4-4 Plastic Tuner design.....	73
Figure 4-5 CSA Ford India (B265) Spiral Wound Steel Tuner (Cooper Standard Automotive, 2007).....	74

Figure 4-6 a) Tuner pull-off specification b) Graph of temperature effects (Merkel, 2004)	74
Figure 4-7 Sample auto-power spectra from SignalCalc.....	76
Figure 4-8 Auto Power Spectrum a) SWST b) PT	79
Figure 4-9 Tuner length test construction a) longitudinal cross-section b) end view	81
Figure 4-10 Photograph of experimental layout	82
Figure 4-11 Auto Power Spectrum for Test Rig containing No Tuner	83
Figure 4-12 Termination impedance constant for Tuner Length experiments	84
Figure 4-13 Power spectrum - Tuner inlet vs Tuner outlet for various tuner lengths	84
Figure 4-14 Tuner Length Experiments – Measured Noise Reduction	85
Figure 4-15 Hole location test sample a) longitudinal cross section b) end view	87
Figure 4-16 Termination Impedance Constant for Hole Position Experiments	88
Figure 4-17 Power spectrum - tuner inlet vs tuner outlet for various positions of a single hole.....	88
Figure 4-18 Hole Location Experiment – Measured Noise Reduction	90
Figure 4-19 Hole diameter test sample a) longitudinal cross section b) end view	91
Figure 4-20 Impact of changing hole diameter on noise reduction	92
Figure 4-21 Termination Impedance Constant for Hole Diameter Experiment	92
Figure 4-22 Tuner inlet signal vs tuner outlet signal for hole diameter experiment	93
Figure 4-23 BMW 5 Series Plastic Tuner.....	94
Figure 4-24 Multi-hole test sample a) longitudinal cross section b) end view	94
Figure 4-25 Comparison of one, two or three equally spaced holes of common diameter.	95
Figure 4-26 Tuner inlet vs tuner outlet for two-hole tuner experiments	96
Figure 4-27 Termination Impedance Constant for two-hole experiments.....	97
Figure 4-28 Tuner inlet vs tuner outlet for three-hole tuner experiments	97

Figure 4-29 Termination Impedance Constant for three-hole experiments	98
Figure 4-30 Selected broadband attenuation results for multi-hole test samples	99
Figure 5-1 Predicted Transmission Loss for a 50mm long tuner	103
Figure 5-2 Predicted versus Measured Noise Reduction for a 50mm long tuner	103
Figure 5-3 Predicted Transmission Loss for a 100mm long tuner	104
Figure 5-4 Predicted versus Measured Noise Reduction for a 100mm long tuner ...	104
Figure 5-5 Predicted Transmission Loss for a 150mm long tuner	105
Figure 5-6 Predicted versus Measured Noise Reduction for a 150mm long tuner ...	105
Figure 5-7 Predicted Transmission Loss for a 200mm long tuner	106
Figure 5-8 Predicted versus Measured Noise Reduction for a 200mm long tuner ...	106
Figure 5-9 Predicted Transmission Loss for a 250mm long tuner	107
Figure 5-10 Predicted versus Measured Noise Reduction for a 250mm long tuner .	107
Figure 5-11 Predicted Transmission Loss for a 300mm long tuner	108
Figure 5-12 Predicted versus Measured Noise Reduction for a 300mm long tuner .	108
Figure 5-13 Predicted Transmission Loss for a 350mm long tuner	109
Figure 5-14 Predicted versus Measured Noise Reduction for a 350mm long tuner .	109
Figure 5-15 Predicted Transmission Loss for a 400mm long tuner	110
Figure 5-16 Predicted versus Measured Noise Reduction for a 400mm tuner	110
Figure 5-17 Tuner Length - Predicted versus Measured, 1 st Pump Order.	111
Figure 5-18 Tuner Length - Predicted versus Measured, 2nd Pump Order	111
Figure 5-19 Predicted Transmission Loss for a 400mm long tuner with a 1mm hole located 50mm from the tuner inlet	113
Figure 5-20 Predicted versus Measured Noise Reduction for a 400mm long tuner with a 1mm hole located 50mm from the tuner inlet	113
Figure 5-21 Predicted Transmission Loss for a 400mm long tuner with a 1mm hole located 100mm from the tuner inlet	114

Figure 5-22 Predicted versus Measured Noise Reduction for a 400mm long tuner with a uniform hole located 100mm from the tuner inlet.....	114
Figure 5-23 Predicted Transmission Loss for a 400mm long tuner with a 1mm hole located 150mm from the tuner inlet.....	115
Figure 5-24 Predicted versus Measured Noise reduction for a 400mm long tuner with a 1mm hole located 150mm from the tuner inlet.....	115
Figure 5-25 Predicted Transmission Loss for a 400mm long tuner with a 1mm hole located 200mm from the tuner inlet.....	116
Figure 5-26 Predicted versus Measured Noise Reduction for a 400mm long tuner with a 1mm hole located 200mm from the tuner inlet.....	116
Figure 5-27 Predicted Transmission Loss for a 400mm long tuner with a 1mm hole located 250mm from the tuner inlet.....	117
Figure 5-28 Predicted versus Measured Noise Reduction for a 400mm long tuner with a 1mm hole located 250mm from the tuner inlet.....	117
Figure 5-29 Predicted Transmission Loss for a 400mm long tuner with a 1mm hole 300mm from the tuner inlet	118
Figure 5-30 Predicted versus Measured Noise Reduction for a 400mm long tuner with a 1mm hole located 300mm from the tuner inlet.....	118
Figure 5-31 Predicted Transmission Loss for a 400mm long tuner with a 1mm hole located 350mm from the tuner inlet.....	119
Figure 5-32 Predicted versus Measured Noise Reduction for a 400mm long tuner with a 1mm hole located 350mm from the tuner inlet.....	119
Figure 5-33 Hole Location – Predicted versus Measured Noise Reduction, 1st Pump Order	120
Figure 5-34 Hole Location - Predicted versus Measured Noise Reduction, 2nd Pump Order	120

Figure 5-35 Predicted Transmission Loss for a 400mm long tuner with a 1.0mm hole located 100mm from the tuner inlet	122
Figure 5-36 Predicted versus Measured Noise Reduction for a 400mm long tuner with a 1.0mm hole located 100mm from the tuner inlet	122
Figure 5-37 Predicted Transmission Loss for a 400mm long tuner with a 1.5mm hole located 100mm from the end of the tuner	123
Figure 5-38 Predicted versus Measured Noise Reduction for a 400mm long tuner with a 1.5mm hole located 100mm from the tuner inlet	123
Figure 5-39 Predicted Transmission Loss for a 400mm long tuner with a 2.0mm hole located 100mm from the tuner inlet	124
Figure 5-40 Predicted versus Measured Noise Reduction for a 400mm long tuner with a 2.0mm hole located 100mm from the tuner inlet	124
Figure 5-41 Predicted Transmission Loss for a 400mm long tuner with a 2.5mm hole located 100mm from the tuner inlet	125
Figure 5-42 Predicted versus Measured Noise Reduction for a 400mm long tuner with a 2.5mm hole located 100mm from the tuner inlet	125
Figure 5-43 Predicted Transmission Loss for a 400mm long tuner with a 3.0mm hole located 100mm from the tuner inlet	126
Figure 5-44 Predicted versus Measured Noise Reduction for a 400mm long tuner with a 3.0mm hole located 100mm from the tuner inlet	126
Figure 5-45 Hole Diameter – Predicted versus Measured Noise Reduction, 1 st Order	127
Figure 5-46 Hole Diameter – Predicted versus Measured Noise Reduction, 2nd Order	127
Figure 5-47 Predicted Transmission Loss for a 400mm long tuner with two 1.0mm holes located 100mm and 200mm from the tuner inlet.....	129

Figure 5-48 Predicted versus Measured Noise Reduction for a 400mm long tuner with two 1.0mm holes located 100mm and 200mm from the tuner inlet	129
Figure 5-49 Predicted Transmission Loss for a 400mm long tuner with two 1.5mm holes located 100mm and 200mm from the tuner inlet	130
Figure 5-50 Predicted versus Measured Noise Reduction for a 400mm long tuner with two 1.5mm holes located 100mm and 200mm from the tuner inlet	130
Figure 5-51 Predicted Transmission Loss for a 400mm long tuner with two 2.0mm holes located 100mm and 200mm from the tuner inlet	131
Figure 5-52 Predicted versus Measured Noise Reduction for a 400mm long tuner with two 2.0mm holes located 100mm and 200mm from the tuner inlet	131
Figure 5-53 Predicted Transmission Loss for a 400mm long tuner with two 2.5mm holes located 100mm and 200mm from the tuner inlet	132
Figure 5-54 Predicted versus Measured Noise Reduction for a 400mm long tuner with two 2.5mm holes located 100mm and 200mm from the tuner inlet	132
Figure 5-55 Predicted Transmission Loss for a 400mm long tuner with two 3.0mm holes located 100mm and 200mm from the tuner inlet	133
Figure 5-56–Predicted versus Measured Noise Reduction for a 400mm long tuner with two 3.0mm holes located 100mm and 200mm from the tuner inlet	133
Figure 5-57 Predicted versus Measured Noise Reduction for tuners with two holes, 1st Pump Order.....	134
Figure 5-58 Predicted versus Measured Noise Reduction for tuners with two holes, 2nd Pump Order.....	134
Figure 5-59 Predicted Transmission Loss for a 400mm long tuner with three 1.0mm holes located at 100mm, 200mm and 300mm from the tuner inlet	135
Figure 5-60 Predicted versus Measured Noise reduction for a 400mm long tuner with three 1.0mm holes located 100mm, 200mm and 300mm from the tuner inlet.....	136

Figure 5-61 Predicted Transmission Loss for a 400mm long tuner with three 1.5mm holes located 100mm, 200mm, and 300mm from the tuner inlet.....	136
Figure 5-62 Predicted versus Measured Noise Reduction for a 400mm long tuner with three 1.5mm holes located 100mm, 200mm and 300mm from the tuner inlet	137
Figure 5-63 Predicted Transmission Loss for a 400mm long tuner with three 1.5mm holes located 100mm, 200mm and 300mm from the tuner inlet.....	137
Figure 5-64 Predicted versus Measured Noise Reduction for a 400mm long tuner with three 2.0mm holes located 100mm, 200mm and 300mm from the tuner inlet	138
Figure 5-65 Predicted Transmission Loss for a 400mm long tuner with three 3.0mm holes located 100mm, 200mm and 300mm from the tune inlet.....	138
Figure 5-66 Predicted versus Measured Noise Reduction for a 400mm long tuner with three 2.5mm holes loated 100mm, 200mm and 300mm from the tuner inlet	139
Figure 5-67 Predicted Transmission Loss for a 400mm long tuner with three 3.0mm holes located 100mm, 200mm and 300mm from the tuner inlet.....	139
Figure 5-68 Predicted versus Experimental Noise Reduction for a 400mm long tuner with three 3.0mm holes located 100mm, 200mm and 300mm from the tuner inlet .	140
Figure 5-69 Predicted versus Experimental Noise Reduction for three holes tuners, 1st Pump Order.	140
Figure 5-70 Predicted versus Experimental Noise Reduction for three holes tuners, 2nd Pump Order.	141
Figure 5-71 Comparison of Termination Impedance Constant and New Theory	144
Figure 5-72 Predicted versus Empirical Termination Impedance for a 50mm long tuner	145
Figure 5-73 Predicted versus Empirical Termination Impedance for a 100mm long tuner.....	146
Figure 5-74 Predicted versus Empirical Termination Impedance for a 150mm long tuner.....	146

Figure 5-75 Predicted versus Empirical Termination Impedance for a 200mm long tuner	147
Figure 5-76 Predicted versus Empirical Termination Impedance for a 250mm long tuner	147
Figure 5-77 Predicted versus Empirical Termination Impedance for a 300mm long tuner	148
Figure 5-78 Predicted versus Empirical Termination Impedance for a 350mm long tuner	148
Figure 5-79 Predicted versus Empirical Termination Impedance for a 400mm long tuner	149
Figure 5-80 1st Pump Order Termination Impedance (Real) for a range of tuner lengths	151
Figure 5-81 1st Pump Order Termination Impedance (Imag) for a range of tuner lengths	151
Figure 5-82 Tuner Length - Predicted versus Measured Noise Reduction at 1 st Pump Order	152
Figure 5-83 1 st Pump Order Termination Impedance (Real) for a range of tuner hole locations	154
Figure 5-84 1st Pump Order Termination Impedance (Imag) for a range of tuner hole locations	155
Figure 5-85 Hole Location – Predicted vs Measured Noise Reduction at 1 st Pump Order	156
Figure 5-86 1 st Pump Order Termination Impedance (Real) for a range of tuner hole diameters	157
Figure 5-87 1st Pump Order Termination Impedance (Imag) for a range of tuner hole diameters	158

Figure 5-88 Hole Diameter – Predicted vs Measured Noise Reduction at 1 st Pump Order.....	159
Figure 5-89 Sketch of micro-perforated panel absorber (Maa, 1988), where d = diameter of orifice, b = spacing between orifices, t = thickness of panel and D = air cavity depth between panel and rigid backing wall.	160
Figure 5-90 Absorption coefficient for a single hole in the tuner wall with varying diameter	163
Figure 5-91 1st Pump Order Termination Impedance (Real) for two hole tuners with a range of hole diameters	165
Figure 5-92 1st Pump Order Termination Impedance (Imag) for two hole tuners with a range of holes diameters.....	165
Figure 5-93 1st Pump Order Termination Impedance (Real) for three hole tuners with a range of hole diameters	166
Figure 5-94 3-Hole 1st Pump Order Termination Impedance (Imag) for three hole tuners with a range of hole diameters.....	166
Figure 5-95 Two Hole Tuner – Predicted vs Measured Noise Reduction 1 st Pump Order	167
Figure 5-96 Three Hole Tuner – Predicted vs Measured Noise Reduction 1 st Pump Order.....	168
Figure 5-97 Absorption coefficient for a 2 hole tuners with varying diameter.....	170
Figure 5-98 Absorption coefficient for a 3 hole tuners with varying diameter.....	170

List of Tables

Table 4-1 Tuner properties table.....	75
Table 4-2 Preliminary Test Results	80
Table 4-3 Tuner Length Test Sample	81
Table 4-4 Hole location test sample construction.....	87
Table 4-5 Hole Diameter test sample construction.....	91
Table 4-6 Longitudinal cross section of multi-hole test sample.....	94
Table 5-1 Experimental Correlation Coefficients.....	142

1 Introduction

Power steering pumps used in automotive power assisted steering application can, as a result of their mechanical and hydrodynamic operation, combine with other system components to generate undesirable noise that originates from a pressure pulse wave in the hydraulic fluid. This wave has the ability to propagate through the fluid and system boundary, causing structural vibration which can produce noise which is audible to a vehicle occupant at particular operating conditions.

NOTE:

This figure/table/image has been removed to comply with copyright regulations. It is included in the print copy of the thesis held by the University of Adelaide Library.

Figure 1-1 Hydraulic Power Assisted Steering System: Component layout (Hydraulic Equipment Manufacturers, 2011)

A typical automotive power steering system is illustrated in Figure 1.1. Noise originating in the pump, is transmitted through the fluid via the hydraulic transmission lines eventually causing structural vibration in the steering column, which is sensed (acoustically and tactilely) by the vehicle driver, under particular driving conditions. In the worst case this noise will create severe noise, sometimes referred to as ‘moaning’ or ‘whining’ which, through its manifestation, has the potential to shorten component life through mechanical fatigue.

Figure 1.2 shows an illustration of a typical vane pump used in power steering applications. This type of pump generates system noise as the flow it produces is not continuous. The discontinuity arises as each vane passes over the high pressure (exit) port of the pump and a partial vacuum is created as the fluid behind the vane rushes to fill the void between the next and previous vane. This eventuates as a large negative pressure pulse which is illustrated in Figure 1.3.

NOTE:
This figure/table/image has been removed
to comply with copyright regulations.
It is included in the print copy of the thesis
held by the University of Adelaide Library.

Figure 1-2 Typical Power Steering Vane Pump (Howstuffworks, 2001)

NOTE:
This figure/table/image has been removed
to comply with copyright regulations.
It is included in the print copy of the thesis
held by the University of Adelaide Library.

Figure 1-3 Typical Power Steering Pump Response (Howstuffworks, 2001)

In the past, various techniques have been used to control the propagation of the pressure pulsations through the hydraulic power steering system. Typically, these techniques employ the use of attenuation devices such as in-line restrictors, tuner cables, or baffles, located inside the bore of the high pressure power steering hose (see Figure 1.4a and 1.4b).

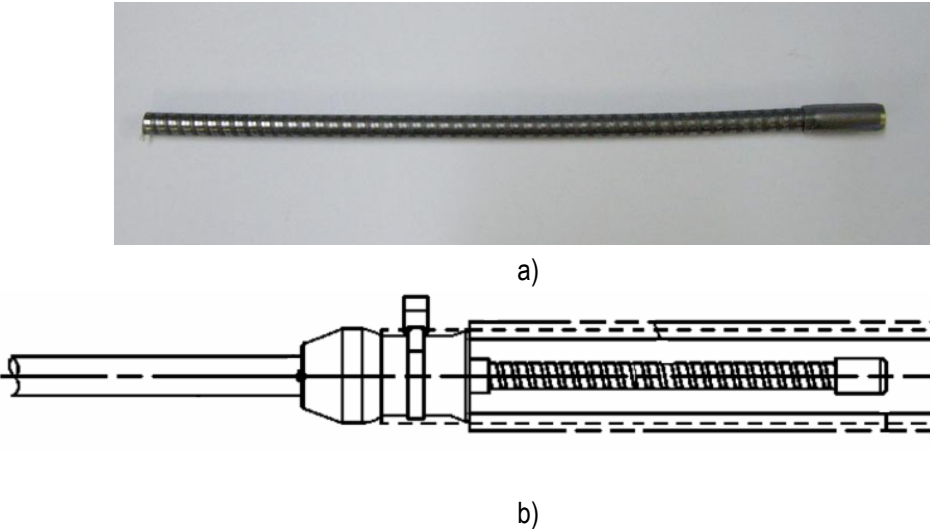


Figure 1-4 Photograph of a) spiral wound steel tuner and baffle b) spiral wound steel tuner located inside hose bore

These devices, while not completely eradicating the pressure pulse, can significantly reduce the transmitted wave magnitude so that it is below an acceptable threshold. The most common of all attenuation devices amongst automotive component suppliers is the tuner cable. Within this type of device, and from car to car, the tuner cable design can be as diverse as the range of pumps, hoses and power steering racks which drive this requirement. However, the basic operating principle is generally the same; the location of the tuner in the hose bore creates additional acoustic impedance, such that undesirable acoustic pressure waves in the fluid are dampened. One such tuner design, the spiral wound steel tuner, provides significant attenuation of pressure pulsations due to leakage through the tuner wall. Whilst the spiral wound steel tuner is probably the most commonly employed design, it requires a costly manufacturing process. Figure 1.5 illustrates the main assembly stages involved in the steel tuner construction.

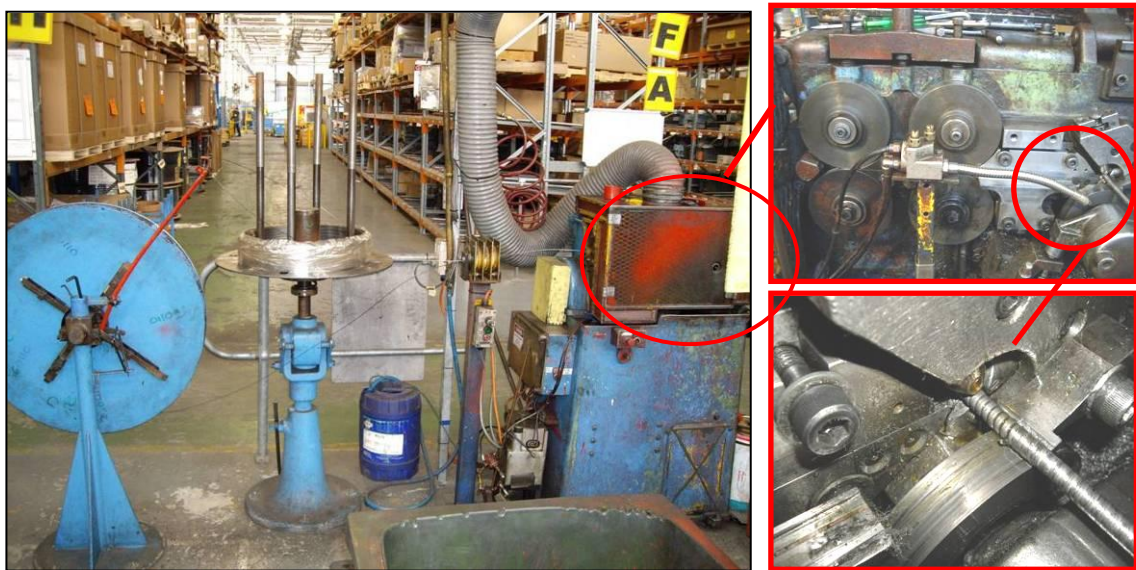
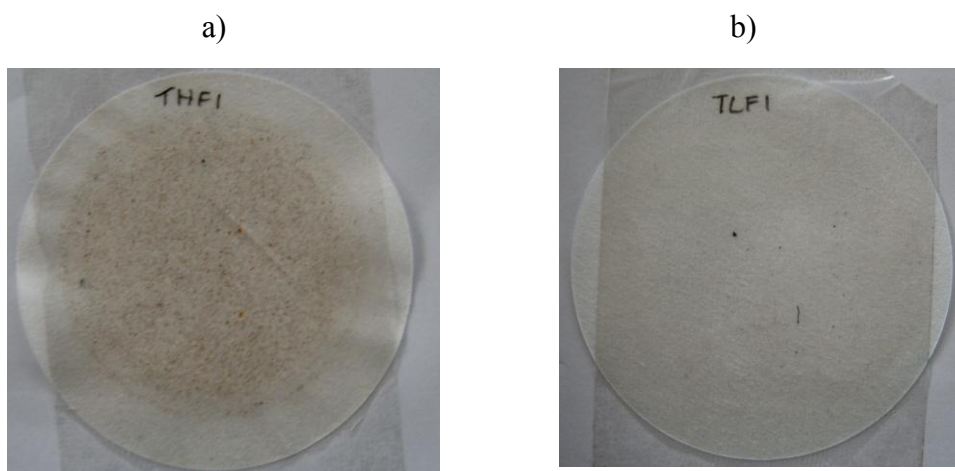


Figure 1-5 SWST Manufacturing Process

First, two separate coils of wire, each with different diameters, are fed through a demagnetising device which assists with the rolling process. Second, the wires are jointly passed through a series of rollers which flatten and coil the wire to a fixed diameter. The process is staggered where one of the flattened wires initiates the coil and the second is then wrapped to complete the cylindrical profile. The resultant ‘tube’ is not completely sealed but instead provides a leak path for the fluid and primarily allows the tuner to flex when mounted inside the hose bore.

Not only is the material, equipment and labour required for such a process significant, unfortunately the process itself is inherently dirty, which is undesirable in power steering component manufacture. Figure 1.6 shows two photographs of filter papers used in power steering assembly internal cleanliness testing. As can be observed from the spiral wound steel tuner image, significant particles are present which predominately include steel and rust deposits generated through the steel tuner assembly process. Metal chips formed during the steel tuner rolling process become entrained in the process lubrication fluid, and remain even after post assembly washing and are notoriously difficult to remove.

Without proper flushing of completed assemblies using kerosene or similar solvents, such contamination may cause significant damage to pump internals during operation. Protecting against such an eventuality translates as further costs in the form of stringent process controls to regulate contamination. It is not surprising therefore that some component suppliers are now turning their attention to the use of alternative materials such as plastics, for improved, cost efficient tuner cable design.



**Figure 1-6 Photographs of filter paper from internal cleanliness testing
a) spiral wound steel tuner filter paper b) plastic tuner filter paper**

The impact of utilising a plastic tuner design over a spiral wound steel tuner design on a typical fluid systems provider is therefore measurable in terms of raw material costs, manufacturing process costs, and cost of quality. The largest saving can be gained from the difference in related manufacturing and assembly costs. The manufacturing and assembly process associated with the plastic tuner is greatly simplified compared to its spiral wound steel counterpart. The main difference between the plastic tuner and the spiral wound steel tuner is the presence of pressure relief holes in lieu of the leak path

promoted by the spiral wound steel construction. Holes are positioned and cut using a variety of processes e.g. flow drilling, laser cutting and hot piercing. The tuner is then assembled into the power steering hose via an insert which is positioned at the mounting end of the tuner and then crimped to the insert tube on the hose coupling. The process for this stage of the tuner assembly is illustrated in Figure 1.7.

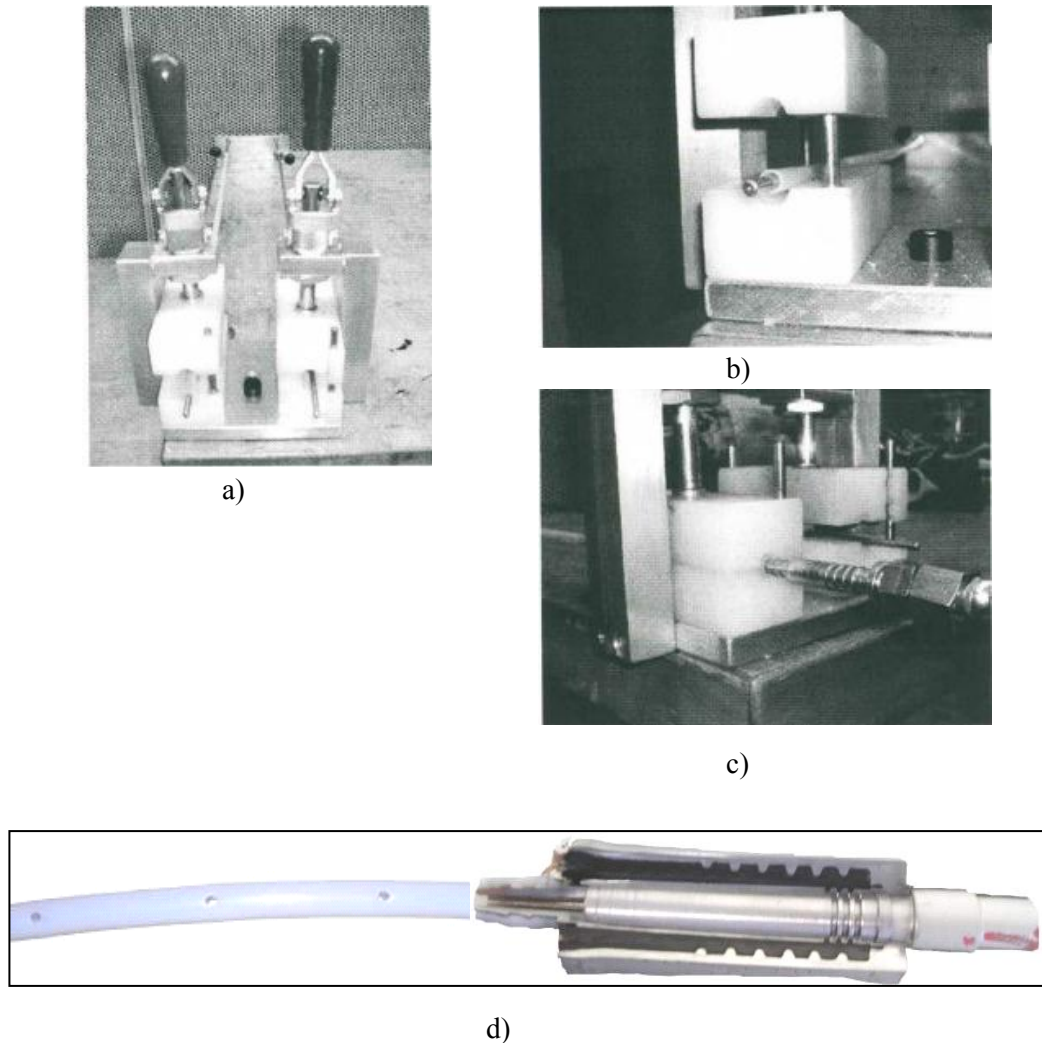


Figure 1-7 a) Fixture and clamp device b) Plastic tuner inserted over mandrel c) Hose insert / tuner end d) Completed plastic tuner assembly cross-section.

As can be seen from Figure 1.7, not only is the tuner manufacturing process greatly simplified, it is also significantly cleaner and easier to maintain. As a result the cost of setting up such an operation, compared with the spiral wound steel tuner, is greatly reduced. The main area of concern is controlling the tuner length and hole profile, which are normally considered ‘critical characteristics’ of each tuner design. Despite the obvious benefits of the plastic tuner manufacturing process, not enough is known about how these devices operate to permit routine design. Any design work performed

has been based on ad-hoc experimental tests, which are time consuming and tend to be based on a trial and error approach. Additionally, the overall cost of development, whilst not as high as the proposed savings, is still a significant outlay, taking the form of expensive test equipment and skilled resource to optimise the design. As a result, little work has been done by automotive companies in developing an understanding of plastic tuner devices to the point where they can be readily implemented. Typically manufacturers would use the ‘cut and try’ method in developing a solution to their particular application, as the time required for design optimisation is often unavailable. Considering this finite development time interval, the ‘cut and try’ method is extremely inefficient. Essentially it involves initially guessing at possible tuner solutions (normally two or three), and then following an iterative process to develop a best fit solution for the system. Breaking this process down into its separate elements, this includes the time associated with building new test samples i.e. manufacture of components and assembly, stripping down the test rig, mounting new test samples, and running the test. By far the longest time duration is the time associated with the manufacture of the test samples. Normally this would take around 1 to 2 days for a batch of assemblies. However, due to existing customer production schedules, it is often difficult to access critical manufacturing equipment freely. This can often postpone test sample construction by a number of days (for example until the weekend when the equipment is not in use). Due to the nature of an iterative process this delay can often be repeated from test sample to test sample. It soon becomes apparent that the total time for development begins to increase rapidly. A typical development phase can take as long as 2 to 3 months, and this is only at the component level. Subsequent system (vehicle) level testing may require further refinement. As a consequence, the nature of the ‘cut and try’ method can often contribute to a less than optimal solution being achieved. The development engineer can quickly become weary and stop at a point that is effective, but not necessarily optimal.

1.1 Objectives

It is clear that the ‘cut and try’ development methodology is in need of some attention. As a minimum, it would certainly be beneficial if the testing time could be reduced by some means, thereby making the iterative process more efficient. Ultimately there is a requirement for a system model which can be tailored to assist in the design and development of a tuner for particular vehicle application. Whilst this does exist to some degree for spiral wound steel tuners, the existing knowledge does not encompass plastic tuners containing pressure relief holes.

Hence, the overall aim of this research is to investigate the noise reduction characteristics of plastic tuners and use this knowledge to develop a new theoretical model.

1.2 Key Objectives

The overall aim of the research is quite broad and it is therefore prudent to define some key objectives which this research will cover. Following a benchmarking exercise, a number of parameters of the plastic tuner design are investigated, as described in the following sections. The knowledge generated during these tasks is then used to develop a suitable system model.

1.2.1 Baseline Evaluation

Initially, as little is understood about plastic tuners and their performance, it is logical to start with a comparative evaluation of a plastic tuner with the performance of an established design i.e. the spiral wound steel tuner. Additionally, with respect to the overall power steering system, there are other factors such as system back-pressure that can increase as a result of the introduction of a tuner device, which have to be considered in addition to the desired noise reduction benefits. Considering the impact of these factors it is important to firstly establish whether the plastic tuner is at least similar or better to the spiral wound steel tuner design. These effects need to be quantified and investigated by developing a suitable experimental test, which has the ability to evaluate the back-to-back performance of the plastic and spiral wound steel tuners.

1.2.2 Tuner Length

The geometry of the tuner, in particular the overall length of tuner, varies subtly in each application. It would appear that this is a key design requirement for the tuner, but it is not fully understood why or to what extent this feature will impact tuner performance. In order to quantify this element of the plastic tuner, a suitable experimental investigation is required.

1.2.3 Tuner Hole Location

Almost all commercially available plastic tuners contain pressure relief holes. The effect of including a hole to a plastic tuner is not fully understood. Additionally, the location of this uniform hole may also have some further effect on noise reduction when compared to a tuner containing no holes. This design parameter needs to be investigated through a series of suitable experiments to quantify the impact of the hole

inclusion, and to investigate the impact of the translation of the hole location along the tuner length.

1.2.4 Tuner Hole Diameter

From the literature review to be presented in Chapter 2, in particular with reference to perforated muffler tubes and sound absorption in honeycomb panels, the size or diameter of the perforation is of distinct significance when trying to optimise the attenuation of incident acoustic waves. It is believed that due to the conceptual similarities between these devices and the plastic tuner, that a similar behaviour may be observed when varying the size of the hole on the plastic tuner. To confirm this theory, a suitable set of experiments is required which will illustrate and quantify the impact of varying the hole diameter for a given tuner design.

1.2.5 Multi-hole Tuners

The concept of potentially improved performance from multi-hole plastic tuners has arisen mainly from the review of existing commercially available plastic tuners. It is assumed that an increase in performance may be gained by adding holes to the plastic tuner. In order to investigate this theory, a series of experiments is required to investigate the impact of adding holes to a tuner of fixed length. The results should confirm whether additional holes impact overall tuner noise reduction or not.

1.2.6 Plastic Tuner Model

In order to improve the design and development process related to plastic tuners, there is a need to develop a model which clearly illustrates the behaviour of acoustic wave propagation through the tuner system. The main purpose of the model is to predict the noise reduction of a pump generated acoustic wave, between clearly defined start and end points. The model should therefore cover all acoustic interactions between each discrete element over the tuner length. Ideally, this model will accurately predict the noise reduction magnitude at the pump fundamental frequency, which is the frequency of greatest interest in automotive power steering.

1.3 Outline

The thesis begins in Chapter 2 with a review of the relevant literature associated with the subject and explains several noise reduction techniques that can be applied to hydraulic power steering systems. This leads into the development of a theoretical model in Chapter 3 followed by a description of the methodology used to capture experimental data in Chapter 4. Experimental and theoretical results are presented in Chapter 5 and a summary of the conclusions is discussed in Chapter 6.

2 Literature Review

The general aim of this research is to investigate the noise reduction characteristics of plastic tuners. [Initially, the review will provide an overview of power steering systems and the generation of noise within the pump and its propagation through the system.] This chapter will then review the previously published knowledge concerning spiral wound steel tuners, plastic tuners and their associated noise reduction techniques. This section concludes with a summary of the relevant literature and identification of the gaps in the knowledge base.

2.1 General Features of Hydraulic Power Steering Systems

Typically, an automotive power steering system (Figure 2.1) is a hydraulically controlled system which comprises a rack and pinion type steering gear (4) and integral control valve (3), a hydraulic pump (5), a fluid reservoir (6), connecting fluid hoses (7) and a mechanical linkage connecting the steering column (8). New developments have seen the electronic control (2) of hydraulic assistance based on vehicle speed (1) for reasons of increased safety.

NOTE:
This figure/table/image has been removed
to comply with copyright regulations.
It is included in the print copy of the thesis
held by the University of Adelaide Library.

Figure 2-1 Hydraulic Power Steering System (ZF, 2011)

The hydraulic pump, driven via a belt coupled to the engine crankshaft pulley, draws fluid from the reservoir and provides fluid pressure for the system. Within the pump is a pressure relief valve, which governs the maximum pressure within the system. The

steering gear combines the manual (mechanical) aspects of a traditional steering system with the assistance of pressure from the hydraulic system. It performs this function by displacing fluid via the control valve to provide assistance when turning the steering wheel. The fluid also acts as a cushion to absorb minor road shocks although this is not its primary function. The route of the fluid after it has passed from the pump is via the high pressure line, through the control valve and rack feed lines, out of the rack into the low pressure return line, finally returning to the fluid reservoir. The high pressure line would normally contain some form of attenuation device. Examples of these devices are discussed in greater detail in Section 2.3.

2.2 Noise Characteristics Overview

In attempting to control the sound output from a hydraulic system, one must consider the transmission of energy through the fluid path from the pump, control valve, cylinders and other components of the system. The objectionable noise generated in a power steering system has been categorised in three distinct forms by Foster and Hannan (1977). Significant Fluid Borne Noise (FBN) or pressure fluctuations in the hydraulic fluid can excite resonant frequencies in system components, leading to vibration or Structure Borne Noise (SBN). This is in turn transmitted through various paths to generate Airborne Noise (ABN) which can be a source of discomfort to the vehicle occupant. The origin of FBN is essentially the power steering pump, although it has been shown by Kobayashi and Ohshima (2001) that significant effects can originate during power steering rack control valve operation. This phenomenon can compound pump noise (pressure fluctuations) and accelerate mechanical wear within the system. As the power steering rack control valve is essentially downstream of the high pressure power steering line, these effects can be ignored for the purposes of this research. The noise characteristic of greatest interest to this project is therefore FBN generated in the pump, as it can be argued that the most effective way to reduce noise is to treat the source.

2.2.1 Noise Generation

As described previously in Chapter 1, power steering pumps are typically multiple vane, positive displacement type which only vary subtly from car to car. These pumps generate noise as the flow they produce is not continuous. This flow discontinuity produces a fluid pressure fluctuation which has been summarised by Drew *et al* (1998) as follows:

- An acoustic waveform which is a function of the pumping mechanism geometry and fluid properties.
- The compression flow ripple, which is caused by the sudden compression of the fluid being pumped as it comes into contact with the high pressure port.
- Leakage flow ripple which is a result of pressure differentials across leak paths.

This pressure fluctuation is the subject of discussion hence. How this noise propagates through the system is a topic which is not entirely understood and this will be addressed as part of the main aims and objectives in Section 3. Further complicating any analysis is the fact that minor changes in pump speed can alter the pump generated waveform and overall system noise.

Dickenson (1994) has shown that vane pumps generate most of their noise at the fundamental or pumping frequency. Significant noise energy is also generated at multiples or harmonics of the fundamental frequency. The sound pressure levels of the harmonics generally reduce at higher frequencies, however, it has been found that fourth and fifth harmonics can have enough energy to produce audible noise. Variations in flow from the pump are converted to pressure pulsations when they meet resistance or impedance in the system. Pressure wave propagation follows the classical theory for sound transmission in pipes (Kinsler and Frey, 1962). As the pressure wave propagates through a hydraulic line it will eventually reach the system boundary. At this point, some of this wave will be reflected back towards the source. The pressure at any point along the line is therefore the vector sum of the forward travelling wave originating at the source (pump) and the total of all waves reflected from the system boundaries. The sum of the waves is a maximum when the phase difference between all waves is zero and a minimum when this difference is 180° . This principle is illustrated in Figure 2.2.

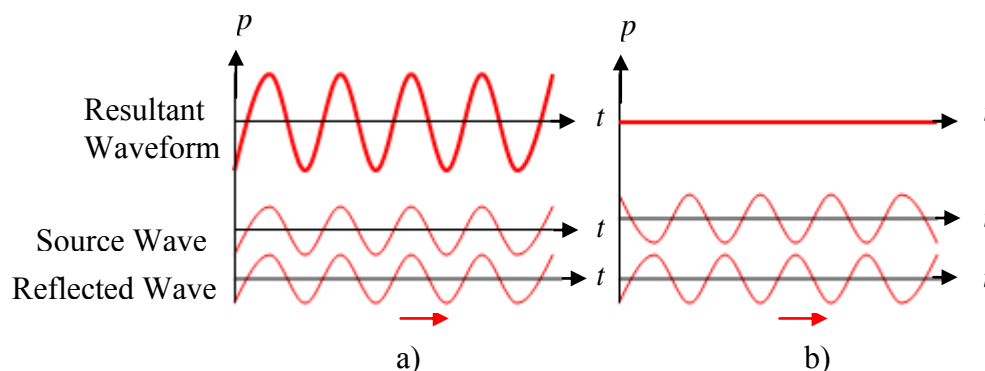


Figure 2-2 a) ‘In-phase’: phase difference is zero, b) ‘Out-of-phase: phase difference is 180°

2.2.2 Noise Reduction

Standing waves develop as a result of interference between two waves travelling in opposite directions. The result is a wave that appears stationary with a series of nodes (zero displacement) and anti-nodes (maximum displacement). This principle is illustrated in Figure 2.3. Considering once again the propagation of a pressure wave in the hydraulic fluid, and plotting the amplitudes along a line for a single frequency component against the distance along the line, the resultant curve is similar to a sine wave. This envelope of pressure amplitudes is the standing wave and one standing wave develops for each component frequency.

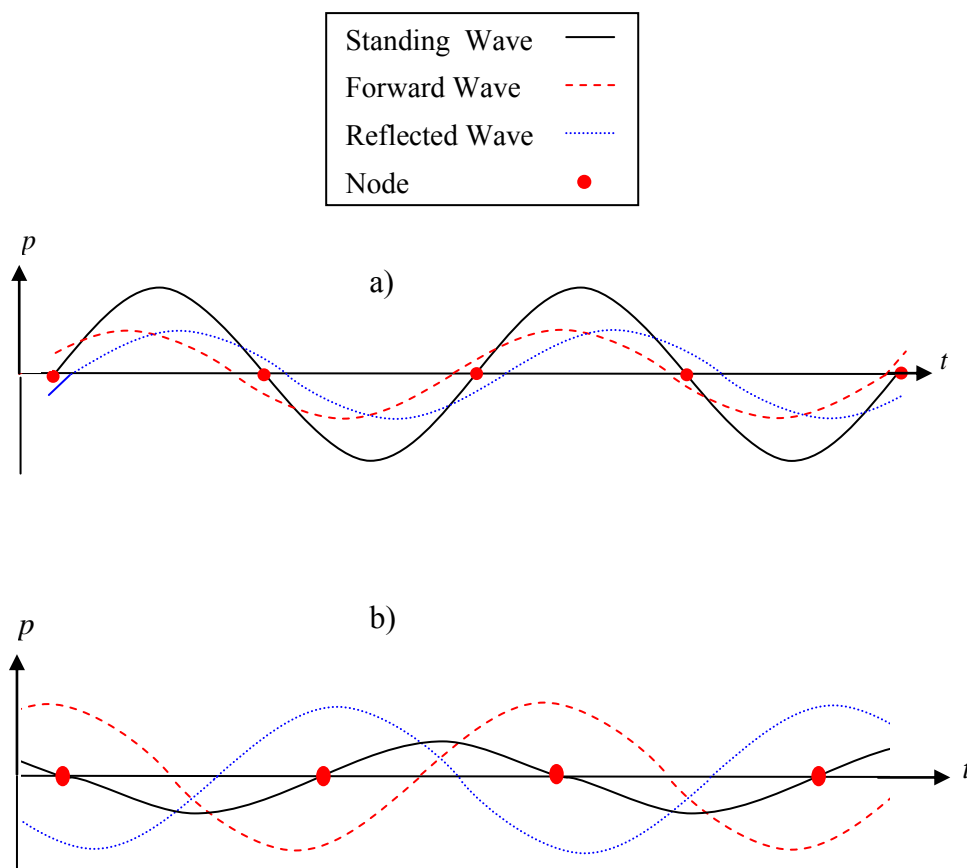


Figure 2-3 a) Illustration of standing wave generation b) Attenuation of a standing wave

In this research the component frequency of main interest is the fundamental vane pass frequency. In reality, this frequency is constantly changing through vehicle engine operation. However, in practice there are particular engine/pump speeds which generate higher audible noise levels than others. These speeds and associated frequencies are of particular interest in power steering noise tuning, which is the reduction of the pump standing wave ratio (ratio of adjacent node to anti-node amplitude) at a particular

frequency and corresponding pump speed. The reduction of this standing wave ratio is fundamentally influenced by attempting to control the dominant waveforms in the system, which can be considered to be the forward travelling wave, generated by the pump and the reflected wave travelling in the opposite direction. By influencing either of these waves, the standing waveform peak magnitude can be reduced or attenuated. This principle is illustrated in Figure 2.3b), where the forward travelling waveform has experienced a phase shift from Figure 2.3a) and as a result, has changed the standing wave peak magnitude. This is the fundamental principle upon which most reactive power steering noise attenuation devices work. Further attenuation can be achieved using resistive methods, where a constriction is inserted, or appropriately selected materials (elastomeric hose) are used, to dissipate the energy of the travelling wave.

It should be noted that pump generated noise reduction is not only a function of the pump and all interacting system components, but also of the point in the system where the pressure pulse is measured. In order to quantify the performance of an attenuation device, pressure is often measured at two points (typically pump outlet and steering gear inlet), and an attenuation metric defined as the ratio of outlet pressure to inlet pressure is calculated.

2.2.3 Acoustic Behaviour

Whilst the general acoustic behaviour of a power steering system, covering noise generation and subsequent noise reduction has been covered in Sections 2.2.1 & 2.2.2, it is important at this point to provide a summary of relevant acoustic theory, such that a foundation can be set for the development of a theoretical model of the plastic tuner.

Considering the geometry of a plastic tuner, it is clear that the most basic element for consideration is similar to a hollow tube or duct. A theoretical study of sound wave propagation in ducts is therefore important for the analysis of a plastic tuner for its acoustical properties. The purpose of this section is to outline the relevant existing acoustic theory concerning the simple case of a rigid tube filled with a flowing, non viscous fluid. This explanation will provide a basis for understanding the concepts discussed later in this thesis. Appropriate theory applicable to the plastic tuner will be discussed and developed later in this thesis and verified during the experimental campaign to confirm the significant interactions during wave propagation along the tuner length.

Munjal (1987) in his text on exhaust and ventilation system design has provided a complete derivation of acoustic theory related to sound wave propagation in ducts from the fundamental equations governing mass continuity, dynamic equilibrium and energy. In this case, the wave front is defined as a surface for which all points of acoustic pressure p and particle velocity u is in a plane normal to the direction of propagation. The author has shown that by manipulation of these equations in terms of time t and longitudinal coordinate x , one can obtain

$$\left[\frac{\partial^2}{\partial t^2} - c^2 \frac{\partial^2}{\partial x^2} \right] p = 0 \quad (2.1)$$

where c is the wave velocity.

Equation 2.1 is known as the classical one-dimensional (involving one spatial coordinate) wave equation. Assuming time dependence in the exponential form $e^{j\omega t}$, the general solution of this equation is

$$p(x, t) = Ae^{j\omega(t-x/c)} + Be^{j\omega(t+x/c)} \quad (2.2)$$

where $\omega = 2\pi f$.

The first part of this solution represents a progressive wave travelling forward with velocity c . Similarly, the second part of the solution represents a progressive wave travelling in the opposite direction with the same velocity. The wave velocity c is more commonly referred to as the speed of sound and Eqn 2.2 represents the superposition of two waves with amplitudes A and B moving in opposite directions.

Equation 2.2 can be re-arranged to the more common form

$$p(x, t) = \left(Ae^{-jkx} + Be^{+jkx} \right) e^{j\omega t} \quad (2.3)$$

where $k = \frac{\omega}{c} = \frac{2\pi}{\lambda}$ and k is the wave number and λ is the acoustic wavelength.

As particle velocity, u , also satisfies the same wave equation, it has also been shown that

$$u(x, t) = \frac{1}{Z} \left(A e^{-jkx} - B e^{+jkx} \right) e^{j\omega t} \quad (2.4)$$

where $Z = \rho c$ is the specific acoustic impedance of the medium, defined as the ratio of acoustic pressure and particle velocity of a plane progressive wave, and ρ is the density of the medium in which the wave is travelling.

Constants A and B are determined by the boundary conditions imposed by the acoustic elements that immediately precede and follow the particular element under investigation. This is explained in more detail in Section 4, where a system of connected elements is developed to represent the plastic tuner.

2.3 Existing Attenuation Devices

Since most objectionable power steering system noise conditions occur at more or less fixed power steering pump speed or frequency, a pressure wave interference type attenuating device is used to cancel pressure pulsations from the pump. There have been many variations on attenuation devices since the original patent submitted by Klees (1967). These devices are described in the following sections.

2.3.1 Quincke Tube

Klees (1967) proposed that passive in-line noise reduction devices acted like quarter wavelength or half wavelength side-branch resonators, and reduced the amplitude of the pressure wave by destructive interference. This theory comes from the original concept firstly proposed by Herschel (1883), then later verified experimentally by Quincke (1866) based on the acoustic interference of musical tones.

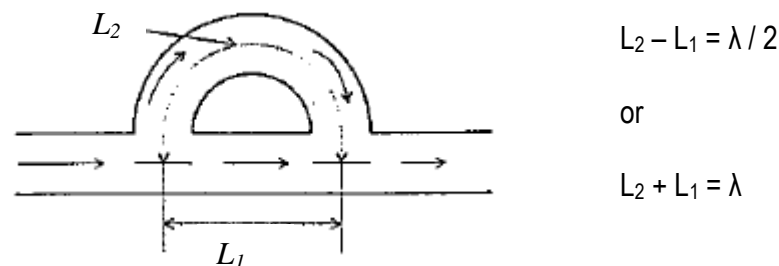


Figure 2-4 Quincke Tube illustration

The principle of this device is based on splitting the acoustic energy equally between two paths of lengths that differ by a half wavelength. As the two waves travel these different lengths, they are out of phase when they are recombined. This arrangement is called a Quincke Tube or Herschel-Quincke Tube (see Fig 2.4) and can be designed to cancel the pump fundamental frequency and its harmonics. Detailed analysis of Quincke tubes has been performed and can be found in the literature (Stewart, 1928; Selamet, 1994)

Of course this explanation, relating tube length to the acoustic wavelength of interest, is oversimplified as the actual system dynamics are more complicated. As previously explained, acoustic waves can propagate in both directions (source and reflected waves) and this normally occurs in both the main duct and Quincke tubes. Additionally, impedance characteristics associated with the tube/main duct boundary are not considered. The impedance at this point is determined by the size and geometry of the tube opening. It is proposed that this geometrical property is also potentially a major contributor to noise reduction in plastic tuners containing pressure relief holes. This concept will be investigated and covered in greater detail in Section 4.

Hastings and Chen (1993) modelled automotive power steering hoses on the basis of Quincke Tubes. Unfortunately, their approach was quite simplistic, ignoring important system effects such as hose wall interactions. The theory developed was based on calculations that are essentially relevant to coaxial steel pipes, not to flexible hoses. However, the authors did show that power steering attenuation devices can provide high attenuation, but only in extremely narrow frequency bands. If a Quincke Tube based design is effective in controlling FBN at one pump speed, it is ineffective if the pump speed changes even slightly. Attempts have been made to develop the Quincke tube with respect to this limitation (Griffen *et al.*, 1999). However, some limitation still exists in the selection of the materials used in this technique.

In automotive applications where pump speed constantly varies as a result of ever changing engine speed, this problem is tackled by utilising a combination of an attenuation device and high expansion elastomeric hose material to broaden the effective frequency range. Following an initial paper detailing an approach to modelling the transmission and attenuation of fluid borne noise in flexible hoses (Longmore, 1977) this subject has been researched extensively (Tuc, 1981; Longmore

and Schlesinger, 1991; Drew, 1997). Most recently, Johnston *et al* (2010) have developed this theory to include an understanding of a wide range of commonly used hoses, in particular nylon braided hoses and steel reinforced braids, and their varied effects on noise reduction. It should be noted that this arrangement would normally incur additional product expense and is not a complete solution.

2.3.2 Standpipe

Undesirable noise can be controlled by modification of the source or reflected waveforms, modification of the transmission path (Quincke Tube), or by modification at the receiver. The receiver in the power steering system is the power steering rack and integral control valve. One method of modification at the receiver is the Standpipe as proposed by Long (1999) of Delphi Automotive Systems.

NOTE:
This figure/table/image has been removed
to comply with copyright regulations.
It is included in the print copy of the thesis
held by the University of Adelaide Library.

Figure 2-5 Standpipe mounting (M Long, 1999)

The Standpipe as illustrated in Figure 2.5 contains a column of air, which dampens unwanted pressure pulsations to an acceptable level. The column of air in the Standpipe is more compressible than the hydraulic power steering fluid, and allows the pressure waves in the fluid line to be absorbed similar to the operation of a mechanical vibration absorber. The Standpipe is installed as close to the rack/control valve inlet as possible with the upper end of the hose positioned higher than the pump reservoir. This method has been shown to be highly effective over varying engine rpm and pump speeds. The Standpipe has also been shown to be capable of suppressing non-pump generated, non-coherent, sources of noise such as chatter from the gear rack, body vibration and tyre shudder. The main problem with this method is that the capability of the Standpipe is directly proportional to its length, and the column of air it contains. To cover all desired

frequency ranges, this is not always possible in an environment where space and component weight are at a premium.

2.3.3 The Spiral Wound Steel Tuner

The most common attenuation device in power steering systems is the spiral wound steel tuner cable. The tuner tube section is commonly constructed from spiral wound steel strip or wire, which has a cross-sectional form that interlocks with adjacent loops. This allows the cable to bend and flex within the hose and also allows fluid to leak through the tuner wall. End caps prevent abrasion with the inner hose bore surface.

The noise reduction mechanism of this device is illustrated in Fig. 2.6.

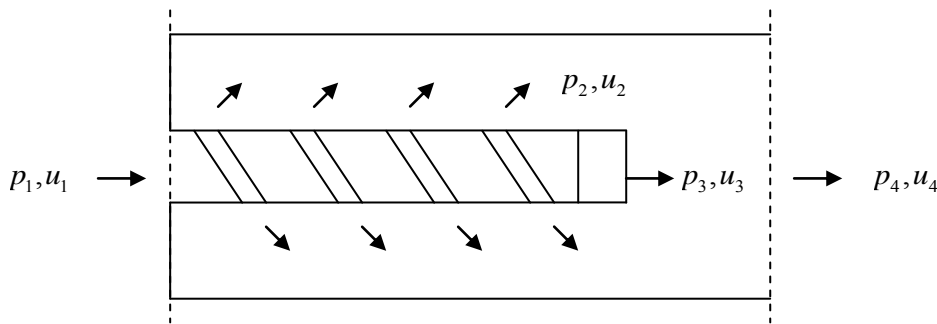


Figure 2-6 Spiral Wound Steel Tuner Operation

Fluid enters the spiral wound steel tuner with an acoustic pressure p_1 and acoustic velocity u_1 . Fluid progresses along the inside of the tuner with some fluid leaking through the gaps in the tuner wall. For the purpose of this description it is assumed that the fluid leaking through the tuner wall at each discrete point along the tuner length, has a resultant acoustic pressure and velocity in the annulus between the tuner and the internal hose wall, equal to p_2, u_2 . The remaining fluid that does not leak through the tuner wall continues along the tuner length and exits the tuner with an acoustic pressure and velocity of p_3, u_3 . As a result of the different fluid paths and associated energy loss, there is a magnitude and phase difference between the acoustic pressures p_2 and p_3 . The amalgamation of these two pressures at the tuner outlet results in a downstream pressure p_4 , which is typically a reduction of the tuner inlet pressure p_1 . Ideally the tuner is designed to target an acoustic pressure or ‘noise’ at a particular frequency of interest. In this case this is the power steering pump fundamental excitation frequency. This is normally achieved, but it should be noted that incorrectly specifying the tuner design can result in amplification of pump generated noise or higher order modes within the system.

Figure 2.6 is a much simplified explanation of the various interactions along the tuner length. In reality the tuner noise reduction mechanism is much more complex. Some attempts have been made to analyse the behaviour of the spiral wound steel tuner. In particular Washio and Konishi (1985) researched the behaviour of the fluid in the annulus between the tuner and the hose wall. They have shown that the radial motion of the hose wall is significant when a tuner is present. However, they have ignored important effects, in particular leakage through the tuner wall. Drew *et al* (1998) have tackled this problem by including leakage through the tuner wall in their theoretical model of pressure flow ripple in flexible hoses containing tuners. This work is probably the most relevant work to the current research. In their approach, the authors propose a method for modelling pressure pulsations in a power steering hose by analysing a frequency dependent impedance matrix. This matrix relates the Fourier transforms determined by pressure at each end of the hose, to the Fourier transforms of inward and outward flow.

$$\begin{Bmatrix} P_A \\ P_B \end{Bmatrix} = \begin{bmatrix} z_{11} & z_{12} \\ z_{21} & z_{22} \end{bmatrix} \begin{Bmatrix} Q_A \\ Q_B \end{Bmatrix} \quad (2.5)$$

where

P_A = Fourier transform of inlet pressure

P_B = Fourier transform of outlet pressure

Q_A = Fourier transform of inlet flow rate

Q_B = Fourier transform of outlet flow rate

$z_{11}..z_{22}$ = impedance matrix terms

The theoretical model is supported by experimental results. The methodology, which adopts the transmission matrix approach used in other automotive applications (Munjal, 1987), centres on the premise that sound wave propagation along the tuner is a result of three independent actions. The wave motion at any cross section of the hose can therefore be defined by deducing the resultant pressure and flow as a result of the three actions, which are defined as follows: the pressure wave motion inside the tuner, the pressure wave motion outside the tuner and the radial hose wall displacement. This concept is illustrated in Fig. 2.7.

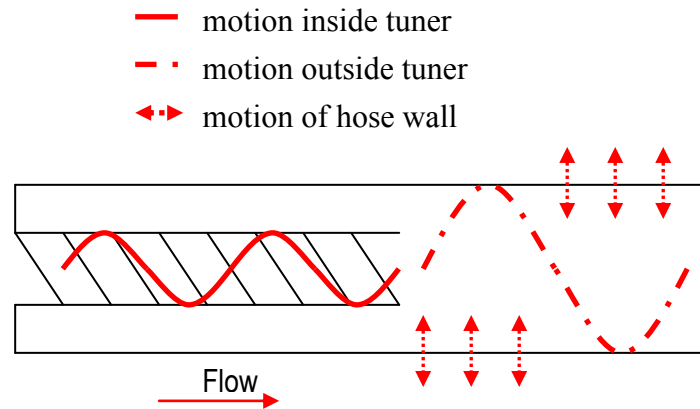


Figure 2-7 Illustration of wave propagation inside the hose

Drew (1998) categorises the system by independently analysing the damping effects at each progressive point in the system, and then combining them to provide a resultant impedance matrix covering the whole system between two measurement points of interest. It is noted however that these results follow an empirical best-fit methodology with respect to certain terms within the impedance matrix. The theory also assumes leakage through the tuner wall is continuously distributed, which may not be the case. This assumption lends itself to spiral wound steel tuners and not so much to plastic tuners containing discrete holes. Considering the plastic tuner, it is a fair assumption that there will be significant pressure drop over the tuner length which will also affect leakage through the tuner pressure relief holes at various points along the tuner. Furthermore, the fluid remaining in the tuner past the point of the pressure relief hole will also be affected. Additionally, the cross section of the leak path profile will play a significant part in the overall pressure drop for a given tuner construction. This is illustrated in Figure 2.8; for a given flow rate the pressure at points 1, 2 and 3 will vary according to the leak path profile.

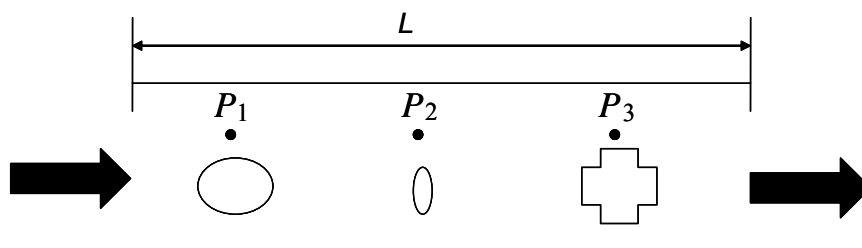


Figure 2-8 Leak path profile illustration

In summary, whilst the model proposed by Drew (1997) and Drew et al (1998) is probably the most relevant to the current work, it chiefly concerns itself with spiral wound steel tuners. As has been discussed there are some gaps, namely tuner wall leak rates and leak path profile, which need to be investigated before it can be applied to plastic tuners. The current work seeks to address these gaps by investigating the noise reduction characteristics of plastic tuners, and then use this knowledge to develop a new theoretical model.

2.3.4 The Plastic Tuner

A relatively new development on the spiral wound steel tuner is the plastic tuner, which normally contains pressure relief holes in lieu of the leak path promoted by the spiral wound steel construction. No work to date has been published specifically on plastic tuners and it is not surprising therefore that not much is understood about their operation. Despite this, a wide range of power steering hoses containing plastic tuners are currently available from various suppliers. Figure 2.9 illustrates two of the tuners and their vehicle applications.



a)



b)

Figure 2-9 Existing plastic tuner designs a) PSA (Peugeot 307) Plastic Tuner, b) GM Opel Vectra Plastic Tuner

2.4 Other Noise Reduction Methods

Apart from current and historically employed attenuation devices, there are a number of other noise reduction methods not specific to power steering that have some relevance to this research. The following section of the literature review examines some of these methods and their applications, outlining where relevant the potential for the existing knowledge to be developed and applied to this new research.

2.4.1 Turbofan Engine Noise Control

With the ever increasing demand for air travel and growing number of flights to rural locations, aircraft turbofan engines are becoming a significant source of noise pollution at airports and surrounding communities. The tones produced by the fan are a significant source of the problem, and together with other noise sources, have traditionally been targeted by a variety of noise control techniques (Casalino *et al.*, 2008). These techniques specifically include inlet duct wall or liner treatment (Mangiarotty, 1971) and more recently, active noise control systems to attenuate engine noise (Thomas *et al.*, 1993).

Of particular interest to the current research is the application of Quincke tube theory to the noise control problem, which has been most recently investigated by Burdisso (2000) and Hallez (2001). Burdisso (2000) has shown through experimental investigation of a Pratt and Whitney JT15D turbofan engine, that implementation of the Quincke tube concept provides very good reduction of tonal noise at discrete frequencies as well as broadband noise. Figure 2.10 illustrates the layout of the Quincke (HQ) tubes positioned on the inlet of the engine.

NOTE:
This figure/table/image has been removed
to comply with copyright regulations.
It is included in the print copy of the thesis
held by the University of Adelaide Library.

Figure 2-10 Quincke Tube concept applied to inlet of turbofan engine. (Burdisso and Smith, 2000)

The method of noise cancellation explained by Burdisso and Smith (2000) and validated experimentally by Hallez (2001) follows the simple explanation of the Quincke Tube given previously in Section 2.3.1.

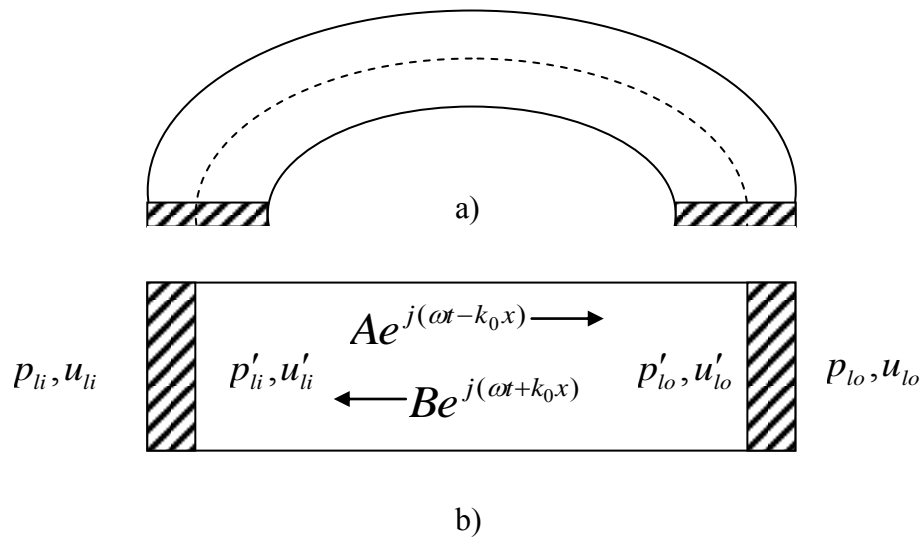


Figure 2-11 Quincke tube representations a) physical representation. b) simplified model.

Normally, Quincke tubes are constructed in a semi-circular or similar fashion. However for modelling purposes they are considered as straight tubes with uniform cross section as shown in Fig. 2.11. This assumption does not change the dynamics of the model as only plane waves are propagating in the tube. As per the explanation previously given in Section 2.2.3, the sound wave inside the tube is expressed in terms of positive and negative travelling plane waves of amplitude A and B , respectively. If x is the local tube coordinate, the pressure and particle velocity inside the tube are given as

$$p'(x, t) = (Ae^{-jkx} + Be^{+jkx})e^{j\omega t} \quad (2.6)$$

$$u'(x, t) = \left(\frac{Ae^{-jkx} - Be^{+jkx}}{\rho c} \right) e^{j\omega t} \quad (2.7)$$

The acoustic pressure and the particle velocity at the ends of the l^{th} tube are expressed in the following matrix form

$$\begin{Bmatrix} p'_{li} \\ \rho c u'_{li} \end{Bmatrix} = [T_t] \begin{Bmatrix} p'_{lo} \\ \rho c u'_{lo} \end{Bmatrix} = \begin{bmatrix} \cos(kL) & i \sin(kL) \\ i \sin(kL) & \cos(kL) \end{bmatrix} \begin{Bmatrix} p'_{lo} \\ \rho c u'_{lo} \end{Bmatrix} \quad (2.8)$$

where L is the centreline length of the tube and subscripts 'i' and 'o' refer to the tube input and output respectively and $[T_t]$ is the transfer matrix for the tube. In practice, the tube is connected to the main duct through a perforated screen. This minimises the potential for flow distortion (vortex shedding) due to the tube opening, which would create additional noise. The effect of the perforated screens is included as

$$\begin{Bmatrix} p_{li} \\ \rho c u_{li} \end{Bmatrix} = [T_{ps}] \begin{Bmatrix} p'_{li} \\ \rho c u'_{li} \end{Bmatrix} \quad \text{and} \quad \begin{Bmatrix} p_{lo} \\ \rho c u_{lo} \end{Bmatrix} = [T_{ps}] \begin{Bmatrix} p'_{lo} \\ \rho c u'_{lo} \end{Bmatrix} \quad (2.9)$$

where the transfer matrix of the perforated screen is

$$[T_{ps}] = \begin{bmatrix} 1 & \frac{Z_{ps}}{\rho c} \\ 0 & 1 \end{bmatrix} \quad (2.10)$$

Z_{ps} is the impedance of the perforated screen written as

$$Z_{ps} = i \frac{\omega \rho}{\sigma} \left(t_{ps} + 2a_{orif} \frac{8}{3\pi} \right) + \begin{cases} \frac{\sqrt{8\mu\rho\omega}}{\sigma} \left(1 + \frac{t_{ps}}{2a_{orif}} \right) & \text{linear model} \\ \rho v_{orif} & \text{non linear model} \end{cases} \quad (2.11)$$

where t_{ps} is the thickness of the screen, a_{orif} is the orifice radius, σ is the screen open area ratio, v_{orif} is the orifice fluid velocity (acoustic particle velocity divided by σ), and μ is the dynamic viscosity coefficient. Including the effects of the perforated screen, the matrix that relates pressure and particle velocity at the tube ends is therefore

$$\begin{Bmatrix} P_{li} \\ \rho c u_{li} \end{Bmatrix} = \begin{bmatrix} T_{ps} \\ T_t \\ T_{ps} \end{bmatrix} \begin{Bmatrix} P_{lo} \\ \rho c u_{lo} \end{Bmatrix} = \begin{bmatrix} T_{11} & T_{12} \\ T_{21} & T_{22} \end{bmatrix} \begin{Bmatrix} P_{lo} \\ \rho c u_{lo} \end{Bmatrix} \quad (2.12)$$

Whilst this theory is relevant to sound waves present in stationary air or low Mach number flows, it is believed that the same methodology may be used to develop the theoretical model for sound pressure waves propagating through moving power steering fluid, exiting the plastic tuner through the pressure relief hole and then recombining with the main body of fluid flow at the tuner exit. The limits of the existing theory will be associated with the differences in impedance characteristics at each end of the model i.e. perforated screen (inlet) versus pressure relief hole profile and perforated screen (outlet) versus main body of fluid impedance. New terms will have to be developed at these points in order for the theory to be representative, although the resultant transfer matrix governing the pressure and particle velocity at each end will be similar in form to Eqn. 2.12.

2.4.2 Sound Absorption of Honeycomb Panels

In many engineering applications, not specifically within the automotive industry, it is often a requirement of a particular application to have some degree of noise reduction. This can be achieved by various methods including sound absorption, which is essentially a reduction of the sound pressure level through energy dissipation in the absorbing structure. Honeycomb panels, which are traditionally used in many different applications including buildings, ship hulls and airplane turbofan engines, actually provide very little absorption to sound approaching them. Low to middle frequency

ranges can only be effectively controlled using this method by employing layers of significant thickness. Unfortunately due to subsequent weight and associated cost this is not always possible.

Leading from the work defining the Helmholtz panel absorber (Morse and Ingard, 1968), Maa (1988) investigated the effects of adding micro-perforations to the honeycomb profile and the resultant impact on the sound absorption performance. Micro-perforated panels are tuned absorbers that require an air-gap between the perforated panel and the backing plate in which they are installed. Whilst the impact of introducing the micro-perforations was significant when compared to standard honeycomb panels, the controllable frequency range was somewhat limited. This work was later developed by Zhang and Gu (1998) who increased the effective bandwidth by including a second layer of micro-perforations, where the second layer is slightly offset from the first. Others have investigated the flexibility of the panel (Dupont *et al.*, 2003) and the influence of various panel materials backed by a common air gap (Kang, J and Fuchs, 1999). Finite Element Analysis (F.E.A.) techniques have also been employed (Burgemeister and Hansen, 1996) to examine the impact of perforations on panel material properties i.e. material density.

Most studies in this area follow an approach where the system absorption performance is estimated by interrogating an equivalent electro-acoustic circuit, based upon the analogy between the electric circuit and the acoustic system. This approach becomes quite complex for multiple layers of micro-perforations and therefore the transfer matrix methodology, which is discussed in greater detail in section 2.4.3, is more convenient for systems containing multiple layers of perforations (Lee, D and Kwon, 2004).

The literature reviewed in this area is consistent with a finding that the absorption performance of a perforated panel can usually be attributed to the acoustic impedance of the perforations. Lee and Swenson (1992) have suitably summarised this where the acoustic impedance of the panel illustrated in Fig. 2.12 is given by

$$Z_{panel} = \frac{32\eta t}{p_r d^2} \left(\sqrt{1 + \frac{x^2}{32}} + \frac{\sqrt{2}}{8} x \frac{d}{t} \right) + j \frac{\omega \rho_{air} t}{p_r} \left(1 + \frac{1}{\sqrt{9 + \frac{x^2}{2}}} + 0.85 \frac{d}{t} \right) \quad (2.13)$$

where

η	=	dynamic viscosity of air
ρ_{air}	=	density of air
t	=	thickness of plate
p_r	=	perforation ratio of plate
d	=	diameter of holes
x	=	$\frac{d}{2} \sqrt{\frac{\omega \rho_{air}}{\eta}}$
ω	=	angular frequency of wave

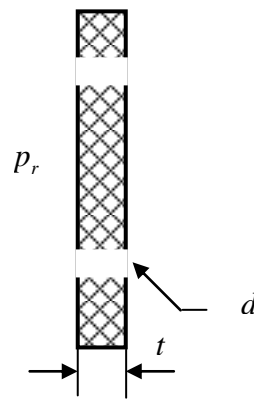


Figure 2-12 Perforated Panel illustration

With reference to the perforated panel illustration in Fig 2.12, a comparison can be drawn with the passage of fluid through the tuner wall in the plastic tuner for power steering pump noise reduction. It is thought that whilst this model has been constructed for sound waves moving in air, there may be a possibility that this theory could in fact be developed for fluid borne sound pressure waves moving in power steering fluid. This will be investigated in greater detail in Section 3 of this thesis.

Pan *et al.* (2005) has shown through detailed experimental results, that the perforation rate and core size are critical in maximising sound absorption over the widest frequency range. Relating this theory to the plastic tuner application, it becomes apparent that pressure relief hole size and the number of holes along the tuner may similarly have an effect on maximising pump generated noise reduction over the widest frequency range. This is of particular interest when considering the dynamic nature of the pump fundamental vane pass frequency which is controlled directly from a pulley mounted to the engine crankshaft. Hence the wider the frequency range covered by the tuner, the potentially more effective the tuner will be under changing engine conditions.

Honeycomb panels are constructed by adhesively bonding facing sheets to the honeycomb core. Pan *et al.* (2005) have also described the effect of glue, where this causes a partial blockage of the hole, to result in a reduction in expected sound absorption performance. There are two main reasons for this, firstly, total blockage of some holes which causes a reduction in the perforation ratio (i.e. number of holes). Secondly, glue partially covering some holes, which affects the acoustic resistance of the hole and increases the viscous friction between the moving air particles within the core profile. Once again, this knowledge is of particular interest to plastic tuner design. Where the pressure relief holes in the plastic tuner could become partially blocked as a result of swarf or the formation of burrs during the hole drilling process, it would be fair to assume that a similar reduction in performance may become apparent. It would be unlikely in a multi-hole tuner configuration that all or some of the holes would become completely blocked. However, it is still an important effect to consider and avoid.

At first glance, plastic tuners and honeycomb panels appear to be two completely unrelated applications of noise reduction. However, considering that the two applications follow basic acoustic principles derived from the same laws covering the conservation of energy and mass, it is likely that similarities will be able to be drawn between them. With this in mind, the theory reviewed in this section, is likely to have relevance when considering noise reduction in power steering hoses containing plastic tuners.

2.4.3 Transfer Matrix Methodology

The undesirable noise generated by gas handling equipment, such as fans used in air-conditioning systems, is typically controlled by passive silencers and lined ducts, whose performance is a function of their geometric and sound absorbing properties. In the automotive industry this knowledge is applied in the design of complex exhaust components used in the control of noise originating in the engine. Substantial research has been conducted in this field, particularly in modelling the interactions between different boundary conditions within the system (Munjal, 1987). Similar to the modelling of turbofan engines previously discussed in Section 2.4.1, researchers have chiefly employed the use of the transfer matrix methodology in the modelling of automotive exhaust silencer systems.

The transfer matrix (also called transmission matrix or four pole parameter representation) is used extensively (Igarashi, 1958) and is the most common approach to the acoustical analysis of automotive exhaust silencer systems. The original work by Sreenath and Munjal (1970) defines this approach by modelling noise characteristics of exhaust silencers on elements of a simple straight-through low pass filter. By adopting acoustic pressure p and particle velocity u as the two state variables, the following matrix relation can be written to relate the state variables on the two sides of the element subscripted r in the equivalent circuit.

$$\begin{bmatrix} p_r \\ u_r \end{bmatrix} = \begin{bmatrix} \text{a } 2 \times 2 \text{ transfer matrix} \\ \text{for the } r \text{ th element} \end{bmatrix} \begin{bmatrix} p_{r-1} \\ u_{r-1} \end{bmatrix} \quad (2.14)$$

$\begin{bmatrix} p_r & u_r \end{bmatrix}$ is called the state vector at the upstream point r , and $\begin{bmatrix} p_{r-1} & u_{r-1} \end{bmatrix}$ is called the state vector at the downstream point $r-1$. The transfer matrix for the r th element can be denoted by $[T_r]$, and each r th element of the exhaust silencer is modelled on one of the three elements of the straight-through low pass filter as shown in electrical representation in Fig 2.13.

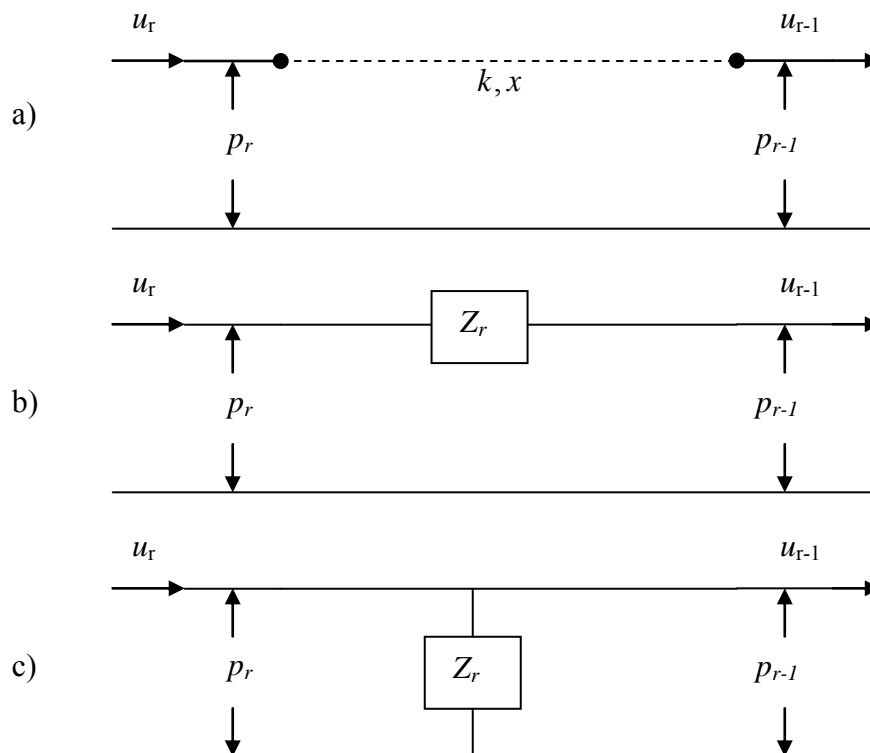


Figure 2-13 The three basic elements in an equivalent electrical representation a) a distributed element b) an in-line element c) a branch element.

For the distributed element shown in Fig 2.13a, making use of Eqn. 2.8, the following transfer matrix can be constructed

$$\begin{Bmatrix} p_r \\ u_r \end{Bmatrix} = \begin{bmatrix} \cos(kx) & -jZ_r \sin(kx) \\ -j\frac{1}{Z_r} \sin(kx) & \cos(kx) \end{bmatrix} \begin{Bmatrix} p_{r-1} \\ u_{r-1} \end{Bmatrix} \quad (2.15)$$

For the in line element illustrated in Fig 2.13b, one can observe

$$p_r = p_{r-1} + Z_r \cdot u_{r-1} \quad (2.16)$$

and

$$u_r = u_{r-1} \quad (2.17)$$

which yields the transfer matrix:

$$\begin{bmatrix} p_r \\ u_r \end{bmatrix} = \begin{bmatrix} 1 & Z_r \\ 0 & 1 \end{bmatrix} \begin{bmatrix} p_{r-1} \\ u_{r-1} \end{bmatrix} \quad (2.18)$$

For the lumped shunt or branch element illustrated in Fig 2.13c, one can observe

$$p_r = p_{r-1} \quad (2.19)$$

and

$$u_r = p_{r-1} / Z_r + u_{r-1} \quad (2.20)$$

which yields the transfer matrix

$$\begin{bmatrix} p_r \\ u_r \end{bmatrix} = \begin{bmatrix} 1 & 0 \\ 1/Z_r & 1 \end{bmatrix} \begin{bmatrix} p_{r-1} \\ u_{r-1} \end{bmatrix} \quad (2.21)$$

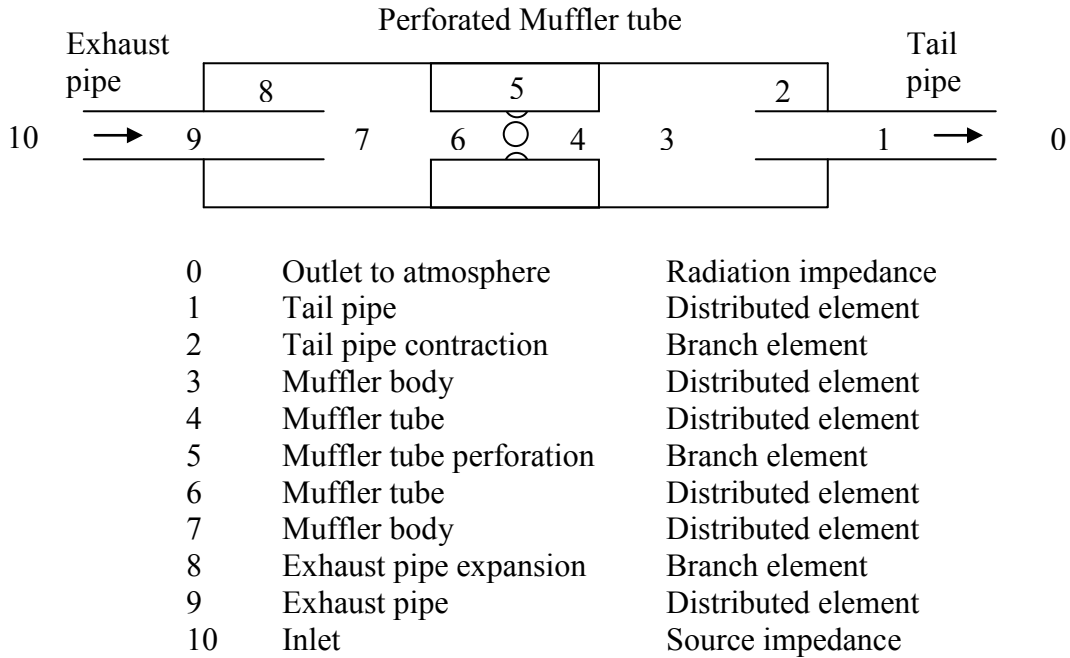


Figure 2-14 Basic silencer system – representation of elements

In this way, individual elements of the silencer system can be modelled between discrete points. Considering now the illustration of a basic silencer system as shown in Fig. 2.14, it is possible to generate the transfer matrix relation by successive application of Eqn. 2.14.

$$\{S_{n+1}\} = [T_{n+1}][T_n] \dots [T_r] \dots [T_1] \{S_0\} \quad (2.22)$$

where the state vector $\{S_0\} = [p_0 u_0]^T$

can be written as

$$\{S_0\} = \begin{bmatrix} p_0 \\ u_0 \end{bmatrix} = \begin{bmatrix} 1 & Z_0 \\ 0 & 1 \end{bmatrix} \begin{bmatrix} 0 \\ u_0 \end{bmatrix} \quad (2.23)$$

where Z_0 is the radiation impedance of the system. The radiation impedance represents the impedance imposed by the atmosphere on the acoustic radiation from the end of the exhaust tube, that is

$$Z_0 = \frac{\text{average acoustic pressure } p \text{ at outlet}}{\text{average mass velocity } v \text{ at outlet}} \quad (2.24)$$

where

$$\begin{aligned} v &= \rho S u \\ \rho &= \text{gas density} \\ S &= \text{cross sectional area} \end{aligned}$$

By performing multiplication of all the matrices outlined in Eqn. 2.22 one would obtain the resultant transfer matrix relation

$$\begin{bmatrix} p_9 \\ u_9 \end{bmatrix} = \begin{bmatrix} T_{11} & T_{12} \\ T_{21} & T_{22} \end{bmatrix} \begin{bmatrix} p_0 \\ u_0 \end{bmatrix} \quad (2.25)$$

where $[T_{ij}]$ is the resultant transfer matrix.

The methodology can be summarised as follows:

- Make an equivalent circuit for the system, drawing on the basic elements illustrated in Figure 2.14.
- Construct transfer matrices for all the elements starting with the source impedance and ending with the radiation impedance.
- Multiply these matrices sequentially.

Beranek and Vér (1992) have adequately summarised the transfer matrices for common exhaust elements, thus simplifying the theoretical approach developed by Sreenath and Munjal (1970). Their concept is illustrated in Fig 2.15.

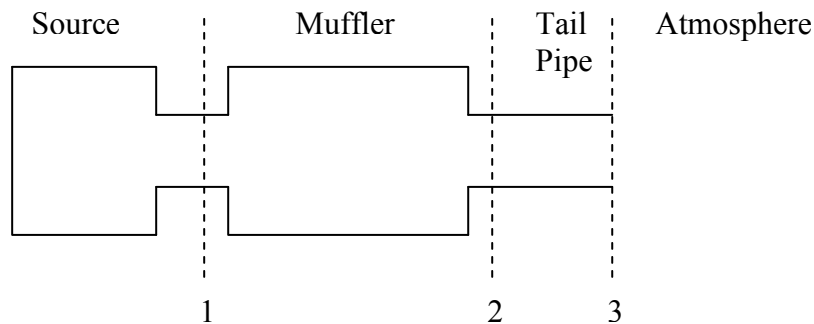


Figure 2-15 Beranek and Vér, ‘Silencer system’

$$\begin{bmatrix} p_3 \\ \rho S_3 u_3 \end{bmatrix} = \begin{bmatrix} T_{11} & T_{12} \\ T_{21} & T_{22} \end{bmatrix} \begin{bmatrix} p_2 \\ \rho S_2 u_2 \end{bmatrix} \quad (2.26)$$

where

p_i	=	acoustic pressure at i th location of element
ρ	=	mean density of gas
S_i	=	cross section of element at i th location of element
u_i	=	particle velocity at i th location of element
T_{ij}	=	element of transmission matrix

Following a similar approach to the modelling of sound transmission through lined ducts in parallel (Patrick, 1968), Beranek and Vér (1992) propose basic building blocks (transmission matrix terms) for each section of the exhaust model e.g. ‘pipe with uniform cross section’, ‘simple area expansion’, ‘simple area contraction’, and in this way build up terms for each boundary interaction between related points in the system. The overall transmission loss is then calculated via multiplication of the individual transmission matrices for each section.

This model has been based on sound pressure waves moving in air and it is expected that this type of model, or elements of the silencer system model, can be applied to sound pressure fluctuations in a power steering fluid. It is likely that the basic building blocks proposed by Beranek and Vér (1992) will form the basis for development of a model for a power steering hose containing a plastic tuner. In any case, the overall approach of both Beranek and Vér (1992) and Sreenath and Munjal (1970) i.e. dividing the system into simple element blocks separated by a boundary impedance, provides a useful guideline to modelling similar systems. Indeed most recently it has been proven effective in modelling plane waves in Respiratory Medical Devices (Jones and Kessissoglou, 2010).

2.4.4 Perforated Muffler Tube Components

Of particular interest is the perforated muffler tube. The main reason for this is the striking similarity in geometrical properties between that of this device and that of the plastic tuner; a feature which, as previously highlighted, has a major influence on noise reduction. Following an original paper by Sullivan (1979), research in this area has been plentiful (Jayaraman and Yam, 1981; Thawani and Jayaraman, 1983; Chen *et al.*, 1992) and has been comprehensively summarised in a book dedicated to muffler component

design by Munjal (1987). All authors agree that the acoustic impedance of perforates is a complex function of several physical variables, namely porosity, mean flow velocity through the holes, hole diameter, thickness of the tube, but is more or less independent of the diameter of the holes for the size of holes used in muffler components. Much of the theory in relation to the perforations has been developed with reference to the radiation of sound into circular tubes (Ingard, 1948) and the acoustic impedance of orifices (Ingard and Ising, 1967; Ronneberger, 1972). More recently Stinson and Shaw (1985) have summarised the acoustic impedance of small circular orifices as the sum of two separate components. The first of these Z_o represents the acoustic wave propagation within the orifice i.e. within the cylinder radius a and thickness t , as illustrated in Figure 2.16.

NOTE:
This figure/table/image has been removed
to comply with copyright regulations.
It is included in the print copy of the thesis
held by the University of Adelaide Library.

Figure 2-16 Acoustic impedance of a small circular orifice (Stinson and Shaw, 1985)

The second acoustic impedance denoted by Z_e represents the effects of the regions immediately adjacent to the orifice. Hence, the acoustic impedance of a small orifice is given by

$$Z = Z_o + Z_e \quad (2.27)$$

It should be noted that whilst this approach is convenient in terms of separating the two regions, the wave propagation between these two regions is not independent. In fact, the wave propagation is related i.e. what happens in one can influence the other. As it is very difficult to model the interaction of flow and waves located in close proximity, Rao (1984) has resorted to direct measurement. In his evaluation of the impedance of perforates with grazing flow, Rao (1984) summarised the acoustic impedance of the perforation as

$$\zeta = [7.337 \times 10^{-3}(1 + 72.23M) + j2.2245 \times 10^{-5}(1 + 51t)(1 + 204d)f] / \sigma \quad (2.28)$$

where

M	=	Mean flow Mach number in the tube
t	=	thickness of the perforated tube
d	=	hole diameter
f	=	frequency (Hz)
σ	=	porosity

Making use of a simple experimental set-up containing a uniform cross-section, rigid wall pipe, Rao evaluated the impedance of a perforated plate by measuring the impedance without the plate and subtracting this value from all the measured values with the plate in position.

In relation to the current research into plastic tuners, it would be suitable to use a similar method to evaluate the impact of the physical variables in this application, i.e. tuner length, pressure relief hole diameter and number of holes (perforation rate). Utilising Rao's proven experimental methodology each variable could be experimentally evaluated in isolation, obtaining the corresponding attenuation for a given variable, by subtracting a constant base sample from each set of test results.

Whilst this theory seems relevant in principle, the limits of its suitability will mainly be defined by the propagation of sound through a medium of vastly different density. It is likely that viscous effects in the power steering fluid will have to be considered, where the elasticity of air could previously be considered negligible in exhaust muffler component modelling. Despite this, the theory still provides a path for investigation and a firm basis for experimental analysis.

2.5 Existing Acoustic Test Methods

Experimental measurements are often required to provide certain basic data about a system that cannot be predicted precisely. Typically, measurement of noise reduction or transmission loss is not difficult to obtain, considering one only has to measure sound at two discrete points across the system under evaluation. It is much more difficult to evaluate the impedance or reflection coefficient of a boundary or termination. In order to assess these noise characteristics appropriate test apparatus and methods must be utilised. Historically, there have been different approaches to the problem, these are described in the following sections.

2.5.1 The Two Microphone Method

The two microphone method, as its name suggests, makes use of two microphones located at fixed positions. The measured signal may be random (containing all frequencies of interest) or a discrete frequency signal, pre-filtered via a low pass filter. A schematic diagram of the methodology originally proposed by Seybert and Ross (1977) is shown in Fig. 2.17.

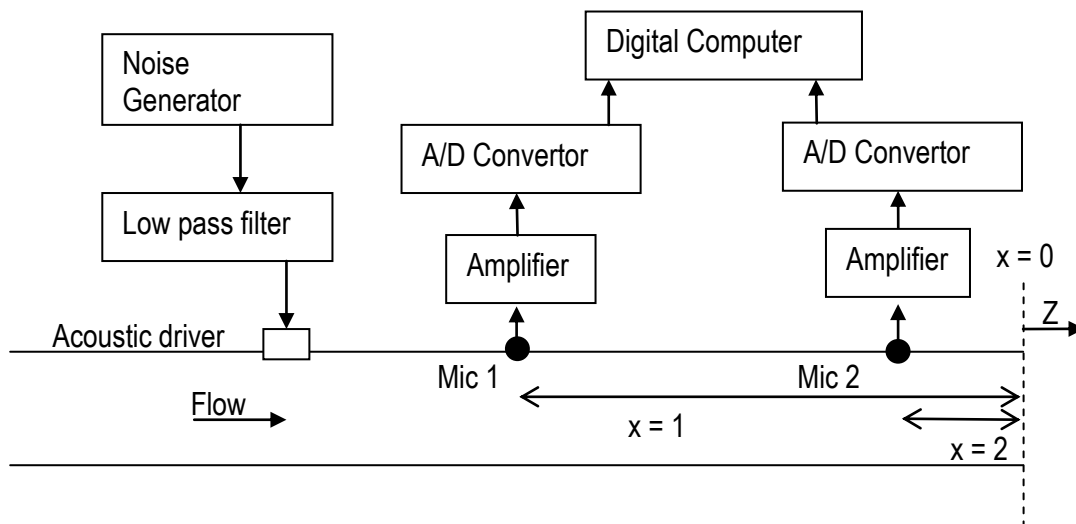


Figure 2-17 Two Microphone Method illustration

A random noise generator provides the required random noise signal, which is passed through a low-pass filter so as to obtain only the desired frequency range. This signal is then passed to an electro-pneumatic driver, which creates an acoustic pressure field on the moving medium inside the measurement tube. The signal picked up by each microphone is then amplified and converted before being fed to a digital computer capable of performing Fourier analysis. The measured data are autospectral densities of the signals at the two microphone locations and the cross-spectral density between

them. Making use of this measured data, the impedance and reflection coefficient of the system can be calculated.

A development of the two-microphone method is the Transfer Function method (Chung and Blaser, 1980). The experimental set-up is similar to that shown in Fig 2.17. However the reflection coefficient, defined as the ratio of the reflected wave pressure to that of the incident wave, is calculated from the acoustic transfer function H_{12} between the two microphone signals rather than the spectral densities as follows

From plane wave theory (see Section 2.2.3)

$$p(x, t) = (Ae^{-jkx} + Be^{+jkx})e^{j\omega t} \quad (2.29)$$

Working in the frequency domain and referring to Fig 2.17

$$p_1(\omega) = A(\omega)e^{+jkx_1} + B(\omega)e^{-jkx_1} \quad (2.30)$$

$$p_2(\omega) = A(\omega)e^{+jkx_2} + B(\omega)e^{-jkx_2} \quad (2.31)$$

and

$$R(\omega) = \frac{B(\omega)}{A(\omega)} \quad (2.32)$$

where $R(\omega)$ is the frequency dependant complex reflection coefficient and $A(\omega)$ and $B(\omega)$ are the complex amplitudes of the forward and rearward travelling waves, and $p_1(\omega)$ and $p_2(\omega)$ are the pressures measured at microphone 1 and 2 relative to a common reference.

$$H_{12}(\omega) = \frac{p_2(\omega)}{p_1(\omega)} = \frac{e^{jkx_2} + R(\omega)e^{-jkx_2}}{e^{jkx_1} + R(\omega)e^{-jkx_1}} \quad (2.33)$$

which is rearranged using Equations 2.29-2.31 to give

$$R(\omega) = \frac{H_{12}(\omega) - e^{-jk(x_1-x_2)}}{e^{+jk(x_1-x_2)} + H_{12}(\omega)} e^{-j(k^+ - k^-)x_1} \quad (2.34)$$

where

k^+ = wave number of forward travelling wave

k^- = wave number of rearward travelling wave

A limitation of this technique has been highlighted by the authors where at certain frequencies, $R(\omega)$ becomes indeterminate. To avoid this, microphone spacing has to be selected appropriately. Seybert and Soenarko (1981) have shown that random errors can also be reduced by maintaining a high coherence between the two microphones, and hence the distance between them should be minimized. However, the authors have also shown that this can prove problematic at low frequencies and at locations that correspond to a node point in the acoustic wave. Consequently, there is a concept of an optimal microphone location for the wave and frequency range being studied. Most recently, the technique has been demonstrated successfully using a single microphone, which is repositioned accordingly between measurements (Fahy, 1984; Chu, 1986).

Although this method was originally proposed for the stationary medium case, it has since been used successfully for the exhaust system of an internal combustion engine (Davies *et al.*, 1980). In this case, a comparison can be drawn to pressure waves moving in power steering fluid. This methodology is therefore also suitable for experimentally evaluating pressure waves propagating through the plastic tuner and a similar approach will be employed during the experimental phase. The experimental procedure is discussed in Section 3.4.1.

2.5.2 Test Bench for Power Steering Noise Assessment

The most commonly employed test apparatus for power steering noise assessment is similar to that described by Sciortino and Bamdad-Soufi (1998) for hydraulic pump assessment. The test bench as illustrated in Fig 2.18 consists of

1. A main supply pump driven by an asynchronous motor and internal gearbox.
2. A hydraulic fluid reservoir.
3. A test bench pump driven by an asynchronous motor and internal gearbox.

4. A complete valve assembly for the hydraulic circuit which allows separate testing of the power steering pump.
5. An automatic quick-clamping mechanism for making hydraulic circuit connections to the steering pumps.
6. A drive motor for speeds 900 to 4000 rpm.
7. A flexible coupling between the motor and the pump.
8. The steering pump.
9. A mechanical clamping system to aid back-support mounting of the pump.

NOTE:
This figure/table/image has been removed
to comply with copyright regulations.
It is included in the print copy of the thesis
held by the University of Adelaide Library.

Figure 2-18 Test bench description and measurement points (Sciortino and Bamdad-Soufi, 1998)

In addition to the listed apparatus a tachometer is often positioned on the shaft of the pump to measure speed when performing an order tracking process. Pressure transducers are positioned at the inlet and outlet of the pump to monitor static and dynamic pressures. Measurements are recorded directly from the instrumentation using an appropriate multi-channel data acquisition unit.

2.5.3 Standardised Test Procedures

There are many different procedural approaches currently available for pump generated fluid borne noise evaluation. Original Equipment Manufacturers (OEM's) typically split their development and testing between in-vehicle testing (cabin acoustic measurements) and laboratory based (experimental NVH tuning) tests. This split is an important consideration in power steering tuner design, as simply reducing the noise associated with the 1st order pump frequency at a given engine rpm, without any

reduction in broadband levels, may result in little or no reduction in perceived noise level, which is the metric used to quantify vehicle cabin noise.

Ford Motor Company of Australia in their test procedure DVT 11.07 (Ford Motor Company of Australia, 1979) has a basic approach to power steering hose attenuation performance assessment. Firstly, mounting the power steering hose to be tested on a similar rig to that described in Section 2.5.2, the pump is driven at a constant rpm (2000 rpm) and fluid temperature is raised to $170 \pm 10^{\circ}\text{F}$. Fluid pressure measurements are then recorded at the inlet and outlet of the power steering hose. Measurements (sound pressure levels) are recorded for the 10th, 20th and 30th engine order, where the pump pulley to engine drive pulley ratio is typically 1 to 10. An attenuation metric is then calculated from the ratio of the outlet pressure to the inlet pressure. As a performance characteristic this ratio is typically desired to be at least 1:5. A typical results table is shown in Fig 2.19.

NOTE:
This figure/table/image has been removed
to comply with copyright regulations.
It is included in the print copy of the thesis
held by the University of Adelaide Library.

Figure 2-19 Example of Ford Australia Noise Tuning Test Record (Ford Motor Company of Australia, 1979)

This process is then repeated on modified versions of the initial test sample, based on a ‘cut and try’ approach. All samples are then compared and the ‘best performer’, based on evaluation at different steering extremes, is selected as the ‘tuning solution’.

As discussed previously, this is a very simplistic approach to the problem, and little is understood about system component interactions, such that predictions could be made regarding component modification.

Whilst specific power steering system research is scarce, there has been some work to develop a predictive procedure for evaluating pressure waves originating in centrifugal and positive displacement vane pumps. Much of this work has led to the development of the original British Standard method (1990) which has now been superseded by ISO 10767-1 (1996). This approach utilises the root mean square pressure that would be generated with a pump discharging into a circuit of infinite acoustic impedance, termed the ‘blocked acoustic pressure’. The root mean square pressure is used in this calculation because it is a statistical measure of the magnitude of the varying (positive

and negative) pump pressure. Effectively the procedure consists of squaring the entire positive and negative points on a waveform, averaging those squared values and then taking the square root of the answer. The problem with this approach is that it is essentially a function of the pump alone and not of the whole system in which it interacts. The ‘blocked acoustic pressure’ tends to be unrepresentative of the pressure wave that would be generated in a real circuit and is dominated by the impedance characteristics of the pump. Edge and Johnston further developed the British Standard method in their Secondary Source method (Edge and Johnston, 1990). Using the impedance notation illustrated in Fig. 2.20, a harmonic of the pressure p and flow q at a position x in a uniform, rigid pipe at radian frequency ω can be described by

$$p = Fe^{-jkx} + Ge^{jkx} \quad (2.35)$$

$$q = \frac{Fe^{-jkx} - Ge^{jkx}}{Z} \quad (2.36)$$

where the Fe^{-jkx} term in these equations represents a wave travelling in the direction of increasing distance x along the pipe. Similarly, the Ge^{jkx} term represents a wave travelling in the opposite direction. The ‘characteristic impedance’ Z is therefore the complex ratio of the pressure wave to the flow wave and can be represented by

$$Z = \frac{p}{q} = \frac{\sqrt{\rho_f B_{eff}}}{A} \xi \quad (2.37)$$

where

- ρ_f = fluid density
- B_{eff} = ‘effective’ bulk modulus of fluid in pipe
- A = internal cross-sectional area of pipe
- ξ = complex coefficient representing viscosity effects.

This theory is better suited to acoustic wave propagation modelling when compared to the British Standard method as it takes into account damping effects as a result of fluid elasticity as well as considering two separate waveforms travelling in opposite directions.

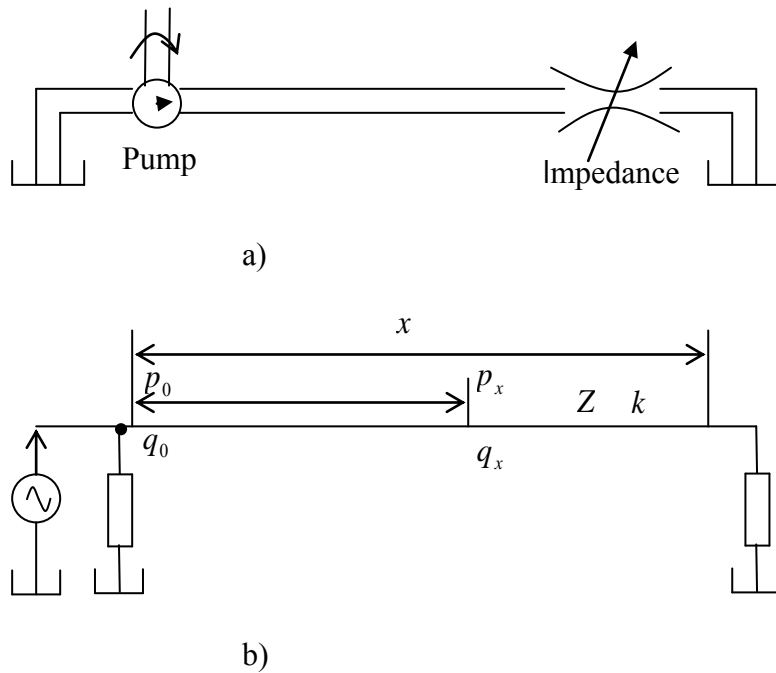


Figure 2-20 Illustrations of impedance representations a) simple circuit b) using impedance notation

The basis of this technique is to use a secondary source of fluid borne noise, as illustrated in Fig. 2.21. Various types of secondary source have been described including; electromagnetic vibrator and piston mechanism, positive displacement pump, and pulse generator. Each device must meet the minimum requirement of being capable of generating stable harmonic frequencies and covering a broad frequency band including the range of the pressure ripple generated by the test pump.

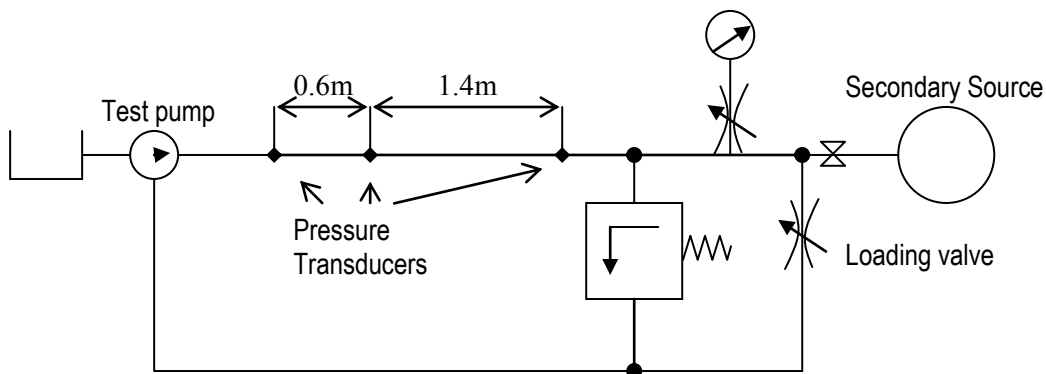


Figure 2-21 Secondary Source technique

Provided the frequencies of the pressure ripple from the two sources are different, the pressure ripple produced by either source can be examined in isolation. Considering the pressure wave from the secondary source, the termination becomes the impedance of the test pump. By manipulation of Eqns. 2.35 and 2.36, and analysis of the standing wave characteristics, it is then possible to derive terms for the source impedance and subsequently the source flow ripple. This method provides good measurement of the impedance characteristics of a range of pumps with good accuracy. Unfortunately it is unsuitable for a power steering hose application in the fact that it assumes rigid pipe walls. The impedance characteristics of a full hydraulic power steering system model are significantly more complex in that they must also give consideration to hose wall, hose/tuner and tuner damping effects.

2.6 Summary

This literature review has covered a wide range of existing knowledge and many practical methods associated with the noise reduction of pump generated power steering noise. In addition, other noise reduction methods and applications, such as inlet ducts on airplane turbofans or perforated exhaust muffler tubes, which have some relevance to this research, have been reviewed in detail.

It is clear that little applied research has been completed to date in relation to the noise reduction mechanisms of the plastic tuner. This review has demonstrated that the most relevant academic study, which is based on the attenuation mechanism of the spiral wound steel tuner (Drew *et al.*, 1998), raises some significant questions when applied to the plastic tuner. The main difference between the two designs, the pressure relief hole employed in lieu of the spiral wound leak path, is certainly not fully understood with respect to the acoustic impedance it generates in the system.

Furthermore, the effect of the geometry of the tuner body, the geometry of the pressure relief hole and the perforation rate of the tuner on the noise attenuation provided by the tuner have not been investigated.

These gaps in the literature confirm the need for addressing the key objectives for this research described in Section 1.2. This will be achieved by investigating the noise reduction characteristics of plastic tuners, and then use this knowledge to develop a new theoretical model.

3 Theory

In this chapter the theory used to develop a new model for the plastic tuner is presented. The chapter starts with an explanation of the modelling approach, followed by an illustration of the theory representing each section of the tuner. Expressions for the transmission matrix models of various tuner designs are also presented and discussed.

3.1 Plastic Tuner Model Development

The technique used in the modelling approach is illustrated in Figure 3.1 and follows the well known transfer matrix methodology discussed in Section 2.4.3. The model for the wave propagation inside the tuner (Figure 3.1b), passing through the pressure relief hole (Figure 3.1c), outside the tuner (Figure 3.1d), inside the tuner past the pressure relief hole (Figure 3.1e), and at the tuner outlet (Figure 3.1f) are developed individually and then fully coupled by matching the acoustic variables, i.e. pressure and particle velocity at the relevant boundary locations. Once the system transfer matrix is fully assembled the system performance can be analysed for various acoustic parameters of interest.

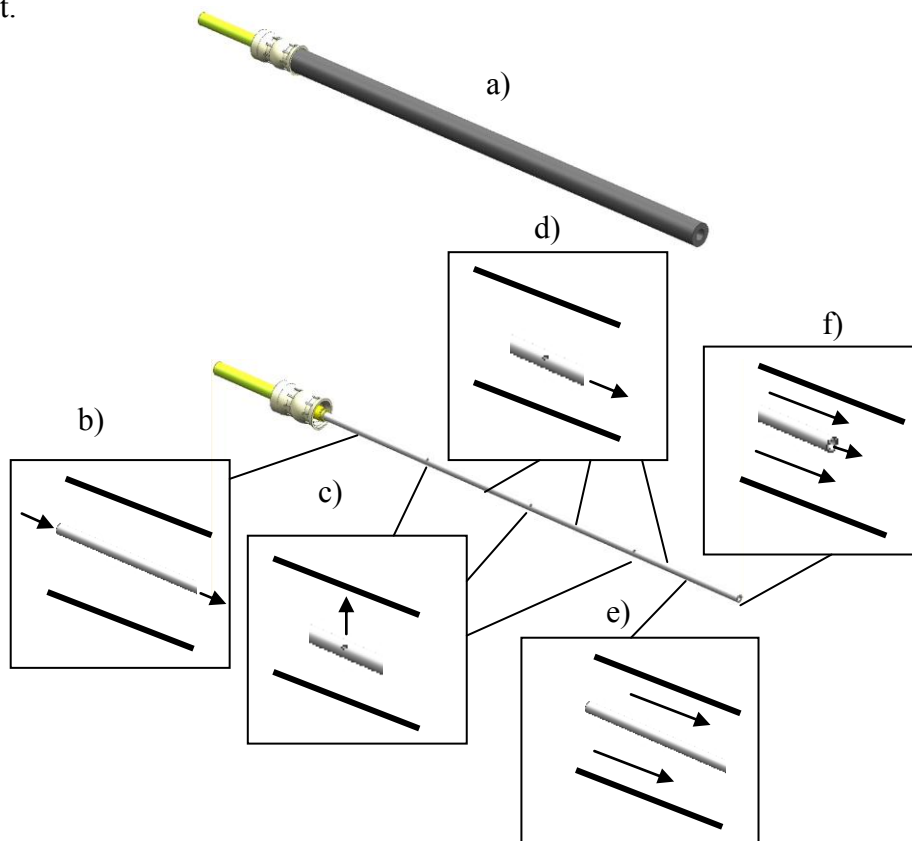


Figure 3-1 Power steering hose assembly incorporating a plastic tuner and component models a) Power steering hose containing plastic tuner b) Model of tuner body c) Model of hole profile d) Model of tuner body downstream of the hole profile e) Model outside tuner f) Model at tuner outlet

3.2 Tuner System Definition

The components of the hydraulic power steering system (herein referred to as the ‘system’) that are considered for the purposes of modelling the plastic tuner are illustrated in Fig. 3.2.a. These include the pump, the plastic tuner, the connecting pipes and the fluid reservoir.

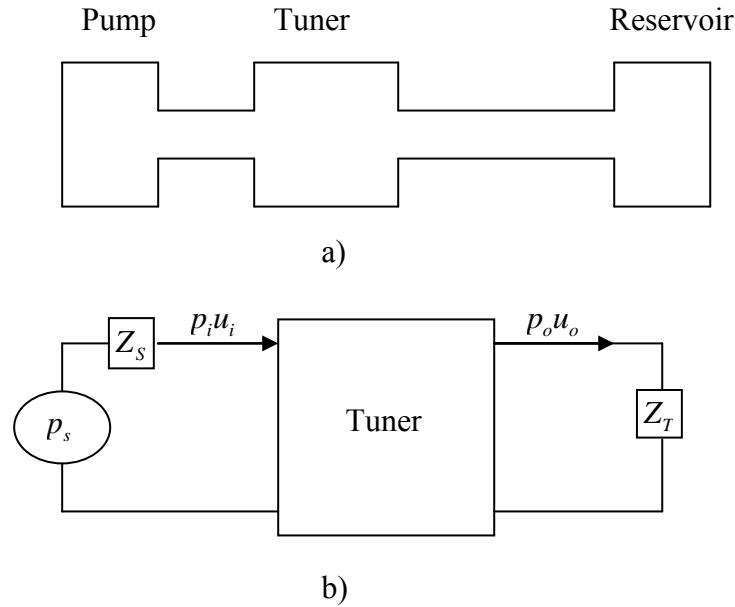


Figure 3-2 Tuner System a) Acoustic b) Electrical Analogy

The pipe connecting the pump to the tuner is considered to be part of the pump. This assumption leads to the corresponding electrical analogy illustrated in Fig. 3.2b, where acoustic pressure p and particle velocity u are used instead of voltage and current. The pump generates a source pressure p_s and contains an internal impedance Z_s . The tuner is represented by its four-pole transfer matrix elements T_{SYSij} , and the connecting pipe downstream of the tuner including the fluid reservoir, are treated as a single lumped impedance Z_T . Using the transfer matrix methodology, an expression relating the tuner input and output variables can be generated as

$$\begin{Bmatrix} P_i \\ \rho S u_i \end{Bmatrix} = [T_{SYS}] \begin{Bmatrix} P_o \\ \rho S u_o \end{Bmatrix} = \begin{bmatrix} T_{SYS11} & T_{SYS12} \\ T_{SYS21} & T_{SYS22} \end{bmatrix} \begin{Bmatrix} P_o \\ \rho S u_o \end{Bmatrix} \quad (3.1)$$

where ρ is the density of the fluid and S is the cross sectional area of the inlet/outlet duct. Subscripts i and o represent the inlet and outlet respectively.

3.3 Performance of Tuner and Tuner Elements

For the purpose of analysis, the performance of the system must be quantified. The three main acoustic performance parameters of any given system are Transmission Loss, Insertion Loss and Noise Reduction. These parameters are well understood and widely utilised in conjunction with the transfer matrix methodology. In this case, due to the in-situ location of the tuner between the pump and the reservoir, the most appropriate parameter for system analysis is Noise Reduction. The Noise Reduction of the tuner is defined as the difference in sound pressure levels at two arbitrarily selected points upstream and downstream of the tuner, as shown in Figure 3.3.

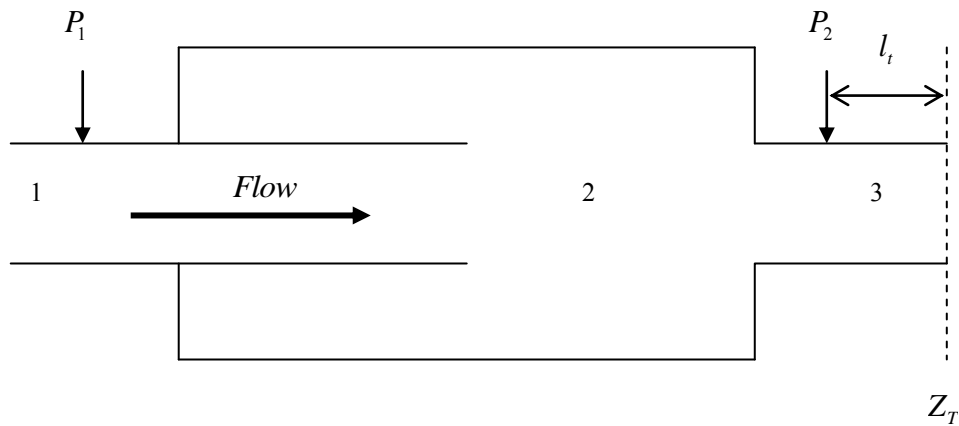


Figure 3-3 Noise Reduction of Tuner

The noise reduction (NR) is given by (Munjal, 1987)

$$NR = 20 \log_{10} \left| \frac{T_{SYS11} + T_{SYS12} / Z_T}{\cos(kl_t) + jY \sin(kl_t) / Z_T} \right| \quad (3.2)$$

where Z_T is the termination impedance of the system, Y is the characteristic impedance of the tuner outlet ($Y = \frac{c}{S}$), and T_{SYS**} are the fourpole parameters of combined system transfer matrix. As previously described in Section 3.2, the termination impedance represents the lumped impedance associated with the connecting pipes and fluid reservoir downstream of the tuner. Due to the complex interactions experienced by the pressure wave as it progresses through the power steering system, it is very difficult to predict the termination impedance of the system accurately. Additionally, any change to the system geometry can further affect the termination impedance and consequently the theoretical value of Noise Reduction.

Considering the Key Objectives of this thesis, it is considered that an empirical approach to modelling the termination impedance is appropriate here. This approach is discussed in greater detail in Chapter 4.

The system transfer matrix is obtained by successive multiplication of the transfer matrices representing the tuner inlet (1), the tuner contained within the hose body (2), and ending at the tuner outlet (3). Transfer matrices for these elements are presented in Section 3.5.

Individual elements, such as those outlined in Fig. 3.1, are typically assessed in terms of Transmission Loss. Transmission Loss is defined as the acoustic power level difference between the incident and transmitted waves of an anechoically terminated system (Munjaj, 1987). In terms of the resultant system transfer matrix, Transmission Loss (TL) is given as

$$TL = 20 \log_{10} \left| \frac{T_{SYS11} + \frac{1}{Y} T_{SYS12} + Y T_{SYS21} + T_{SYS22}}{2} \right| \quad (3.3)$$

This parameter is not suited to the plastic tuner application, because the termination is not anechoic. However, transmission loss is useful for validating the transfer matrix methodology as alternative modelling approaches are typically analysed using this parameter. This is covered in greater detail in Section 3.4.

3.4 Plane Wave Assumption

The transfer matrix methodology works on a principle which assumes that only plane waves are present in the system under analysis. The internal geometry of the tuner defines the wave path with respect to the frequency of interest; in this case the first order of the pump which is 333 Hz.

The frequency below which only plane waves propagate is called the ‘cut-off’ frequency and is given by (Beranek and Ver, 1992)

$$f_c = \frac{1.8412c}{2\pi r} \quad (3.4)$$

where c is the speed of sound in the fluid and r is the radius of the largest duct in the system. The speed of sound c in the fluid, in this case power steering fluid, is determined using the approach outlined by Drew (1997), where $c = 546 \text{ m/s}$.

For the system analyzed here, which has a maximum duct radius of 0.00537m, the cut-off frequency is 29,567 Hz. Therefore, it is clear that only plane waves are propagating in the system, since the cut-off frequency is well above the frequency range of interest from 0 to 1 kHz.

3.5 Tuner Element Modelling

Following the simplified definition of the tuner system in Section 3.2, the discrete elements of the tuner are now described for the purpose of generating a detailed model of the acoustic wave propagation within the tuner.

3.5.1 Tuner Duct Element

The tuner duct is modelled as a rigid walled uniform cross section duct (Kinsler and Frey, 1962). All fluid passes through the centre of the tuner. Frictional losses due to the tuner surface are considered negligible.

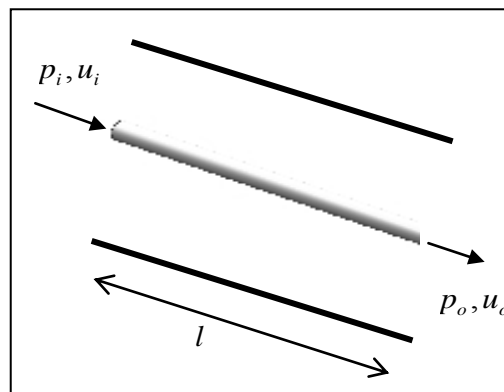


Figure 3-4 Tuner Duct Element

Figure 3.4 illustrates the geometry of this particular element. Using the transfer matrix methodology, an expression for this element can be constructed as

$$\begin{Bmatrix} p_i \\ \rho S u_i \end{Bmatrix} = [T_{DUCT}] \begin{Bmatrix} p_o \\ \rho S u_o \end{Bmatrix} = \begin{bmatrix} T_{11} & T_{12} \\ T_{21} & T_{22} \end{bmatrix} \begin{Bmatrix} p_o \\ \rho S u_o \end{Bmatrix} \quad (3.5)$$

where

p_i	=	acoustic pressure at inlet
p_o	=	acoustic pressure at outlet
u_i	=	particle velocity at inlet
u_o	=	particle velocity at outlet
T_{11}	=	$C \cos(k_c l)$
T_{12}	=	$C jY \sin(k_c l)$
T_{21}	=	$C \frac{j}{Y} \sin(k_c l)$
T_{22}	=	$C \cos(k_c l)$
k	=	$\frac{\omega}{c} = \frac{2\pi f}{c}$
k_c	=	$k / (1 - M^2)$
C	=	$e^{-jMk_c l}$
M	=	mean flow Mach number
Y	=	characteristic impedance of duct = $\frac{c}{S}$
ρ	=	fluid density
c	=	speed of sound in fluid
S	=	duct cross sectional area
l	=	duct element length
f	=	frequency of sound wave

3.5.2 Tuner Extension Element

The tuner extension is based on an extended inlet (Munjal, 1987), where the acoustic wave travelling along the tuner exits the tuner body and joins the wave travelling external to the tuner.

Figure 3.5 illustrates the geometry of this particular element.

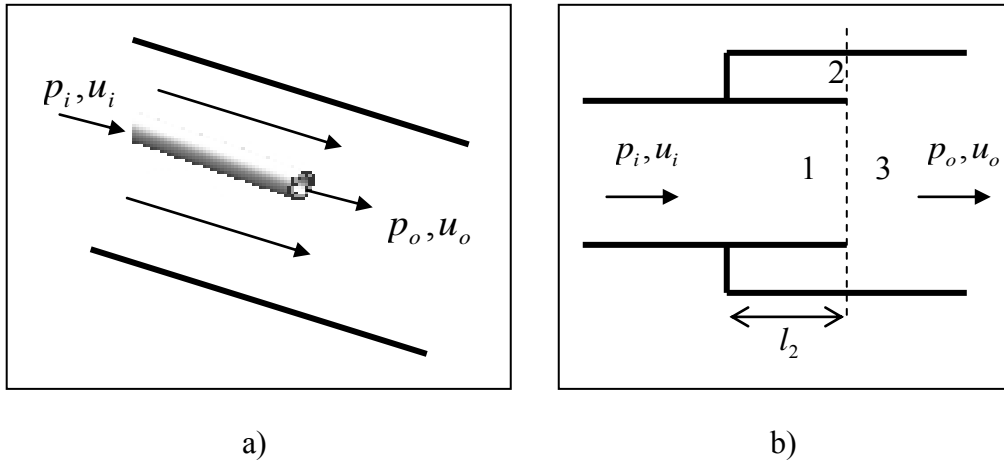


Figure 3-5 Tuner Extension Element a) 3D view b) 2D view

Using the transfer matrix methodology, an expression for this element can be constructed as

$$\begin{Bmatrix} P_i \\ \rho S u_i \end{Bmatrix} = [T_{EXT}] \begin{Bmatrix} P_o \\ \rho S u_o \end{Bmatrix} \quad (3.6)$$

where $[T_{EXT}]$ is modelled as an extended inlet.

In this case the mach number in the power steering fluid is less than 0.2. Therefore the transfer matrix can be simplified further into a simple branched impedance representing the annulus between duct 2 and duct 1 as illustrated in Figure 3.5 b and is given by

$$[T_{EXT}] = \begin{bmatrix} 1 & 0 \\ 1/Z_B & 1 \end{bmatrix} \quad (3.7)$$

where

$$Z_B = -jY \cot(kl_2) \quad (3.8)$$

3.5.3 Tuner Expansion Element

At the end of the tuner extension, there is an increase in cross sectional area where the acoustic wave travelling along the tuner exits the tuner and enters the hose cavity. This section of the system is modelled as a sudden area expansion (Munjal, 1987).

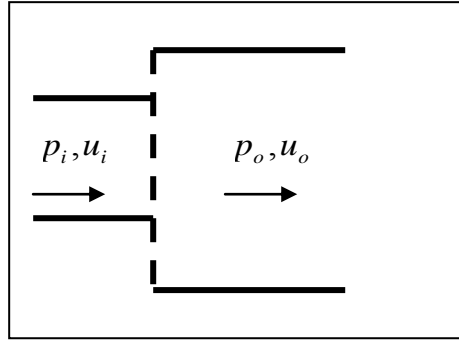


Figure 3-6 Tuner Expansion Element

Figure 3.6 illustrates the geometry of this particular element. for $M < 0.2$ in the smaller diameter tube, using the transfer matrix methodology, an expression for this element can be constructed as

$$\begin{Bmatrix} p_i \\ \rho S u_i \end{Bmatrix} = [T_{EXP}] \begin{Bmatrix} p_o \\ \rho S u_o \end{Bmatrix} \quad (3.9)$$

where

$$[T_{EXP}] = \begin{bmatrix} 1 & KMY \\ 0 & 1 \end{bmatrix} \quad (3.10)$$

and

$$K = \left(\frac{S_i}{S_o} - 1 \right)^2 \quad (3.11)$$

3.5.4 Tuner Contraction Element

At the end of the hose cavity there is a reduction in cross sectional area where the hose couples to the steel tube. This section of the system is modelled as a sudden area contraction (Munjal, 1987), where the acoustic wave travelling along the hose cavity enters the steel tube coupled to the hose. Figure 3.7 illustrates the geometry of this particular element.

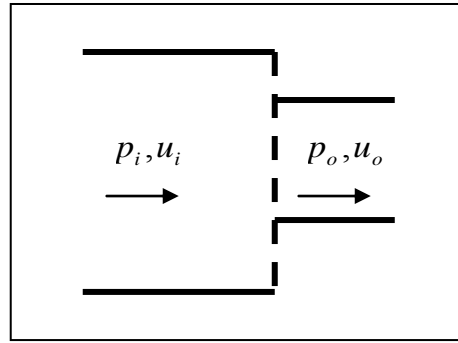


Figure 3-7 Tuner Contraction Element

The assumptions for this element are similar to the Tuner Expansion Element discussed previously, where the loss factor K is modified accordingly. The transfer matrix for this element can be constructed as

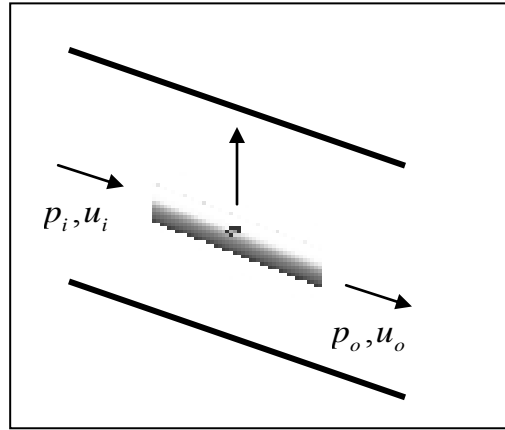
$$\begin{Bmatrix} p_i \\ \rho S u_i \end{Bmatrix} = [T_{CON}] \begin{Bmatrix} p_o \\ \rho S u_o \end{Bmatrix} = \begin{bmatrix} 1 & KMY \\ 0 & 1 \end{bmatrix} \begin{Bmatrix} p_o \\ \rho S u_o \end{Bmatrix} \quad (3.12)$$

where

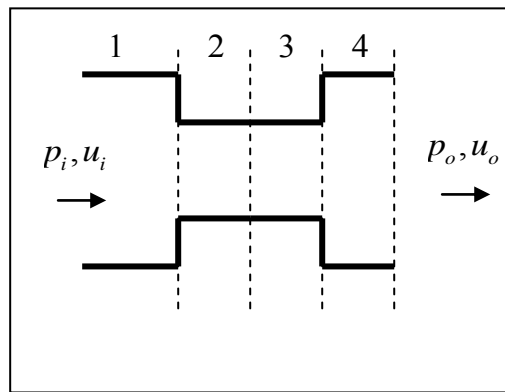
$$K = \left(1 - \frac{S_o}{S_i}\right) / 2 \quad (3.13)$$

3.5.5 Tuner Hole Element

The tuner hole element encompasses the acoustic intersections between the point in the system immediately prior to the hole opening, the hole itself, the point immediately after the hole, and the fluid region downstream of the hole where the fluid stream bends to run parallel with the hose axis. Following an approach similar to that outlined by Furnell and Bies (1989) in modelling curved duct systems, this element is modelled using a series of element types already discussed, with the addition of a new element representing the acoustic impedance at the hole opening.



a)



b)

Figure 3-8 Tuner Hole Element a) 3D view b) 2D view

Figure 3.8 illustrates the geometry of this particular element where the boundary between component 1 and 2 represents the area change the travelling wave experiences when transitioning from the relatively large cross section of the tuner body, into the smaller cross section of the hole. At the hole aperture (2), the travelling wave experiences an impedance associated with the hole geometry, before travelling through a constant cross section of length which is equal to the tube wall thickness (3). At this point, the travelling wave experiences another area change where the cross sectional area changes from relatively small (3) to relatively large (4).

Using the transfer matrix methodology, an expression for this element can be constructed as

$$\begin{Bmatrix} P_i \\ \rho S u_i \end{Bmatrix} = [T_{HOLE}] \begin{Bmatrix} P_o \\ \rho S u_o \end{Bmatrix} = [T_{CON}] [T_{ORI}] [T_{DUCT}] [T_{EXP}] \begin{Bmatrix} P_o \\ \rho S u_o \end{Bmatrix} \quad (3.14)$$

where $[T_{CON}]$, $[T_{DUCT}]$, and $[T_{EXP}]$ are as previously noted in Eqns 3.12, 3.5 and 3.10 respectively.

A term representing the tuner hole opening can be formulated as

$$[T_{ORI}] = \begin{bmatrix} 1 & Z_o \\ 0 & 1 \end{bmatrix} \quad (3.15)$$

where the impedance acoustic impedance of the hole opening Z_o is as defined in Equation 2.28.

3.5.6 Parallel Branch Element

Due to the inclusion of the holes in the tuner, the acoustic wave has the choice of discrete flow paths. This is illustrated in Fig 3.9, where the wave travelling along the inside of the tuner can flow out through the tuner hole into the hose wall cavity (Branch 1), or continue on its path and exit the tuner at the tuner end (Branch 2).

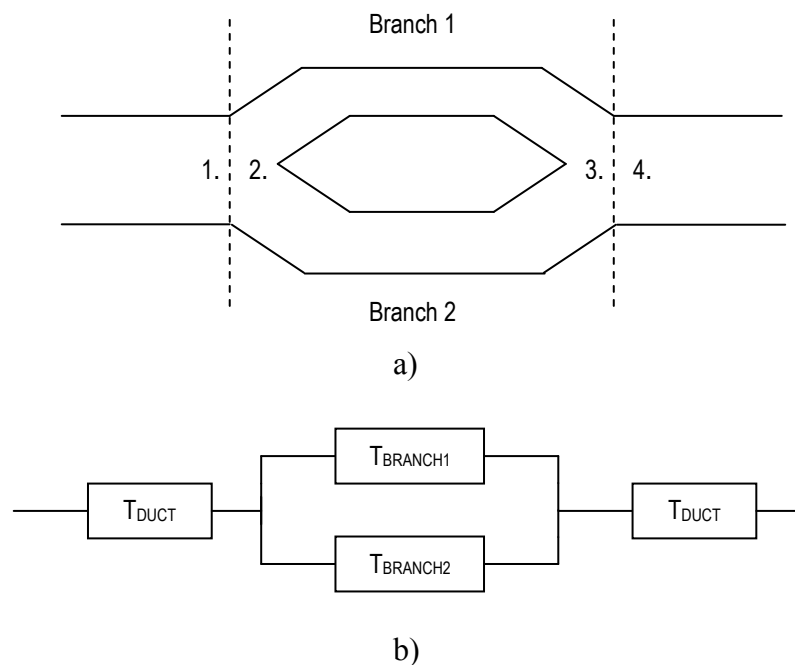


Figure 3-9 Parallel Branch Element a) physical arrangement b) transmission matrix representation

For a system of N branches

where

i	=	branch number
p	=	acoustic pressure
Q	=	mass flow

Assuming plane wave propagation

$$p_1 = p_{2i} \quad (3.16)$$

$$p_4 = p_{3i} \quad (3.17)$$

$$Q_1 = \sum_{i=1}^N Q_{2i} \quad (3.18)$$

$$Q_4 = \sum_{i=1}^N Q_{3i} \quad (3.19)$$

where Q_1 is the mass flow i.e. $\rho_1 S_1 u_1$.

Using the transmission matrix methodology, each branch can be described by

$$\begin{bmatrix} p_{2i} \\ Q_{2i} \end{bmatrix} = \begin{bmatrix} A_i & B_i \\ C_i & D_i \end{bmatrix} \begin{bmatrix} p_{3i} \\ Q_{3i} \end{bmatrix} \quad (3.20)$$

and the transmission matrix for the complete parallel branch system is

$$\begin{bmatrix} p_{1i} \\ Q_{1i} \end{bmatrix} = [T_{PBRN}] \begin{bmatrix} p_{4i} \\ Q_{4i} \end{bmatrix} = \begin{bmatrix} A & B \\ C & D \end{bmatrix} \begin{bmatrix} p_{4i} \\ Q_{4i} \end{bmatrix} \quad (3.21)$$

where

$$A = \frac{\sum_{i=1}^N \frac{A_i}{B_i}}{\sum_{i=1}^N \frac{1}{B_i}} \quad (3.22)$$

$$B = \frac{1}{\sum_{i=1}^N \frac{1}{B_i}} \quad (3.23)$$

$$C = \sum_{i=1}^N \left(C_i - \frac{D_i A_i}{B_i} \right) + \frac{\sum_{i=1}^N \frac{A_i}{B_i} \sum_{i=1}^N \frac{D_i}{B_i}}{\sum_{i=1}^N \frac{1}{B_i}} \quad (3.24)$$

$$D = \frac{\sum_{i=1}^N \frac{D_i}{B_i}}{\sum_{i=1}^N \frac{1}{B_i}} \quad (3.25)$$

3.6 Validation of Modelling Approach

Before constructing the transfer matrix model for the relatively complex interactions of the tuner system using the elements defined in section 3.5, it is important to firstly validate this approach by analysing some simple systems. Initially, this is conducted using Transmission Loss as the performance parameter, to remove any ambiguity associated with the termination impedance. Once the transmission matrix approach is confirmed, a simple system is then analysed in terms of Noise Reduction, to validate the model in this respect.

3.6.1 Transmission Matrix Validation – Single Expansion Chamber

The single expansion chamber is a widely used system where values of TL are well established and the geometry is relatively simple. The theoretical value of TL for the expansion chamber is given by (Bell, 1994)

$$TL = 10 \log_{10} \left[1 + \frac{1}{4} \left(m - \frac{1}{m} \right)^2 \sin^2 kL \right] \quad (3.26)$$

where m is the area ratio of inlet/outlet section to expansion chamber section, k is the wave number and L is the expansion chamber length.

The geometry of the modelled system is given in Figure 3.10.

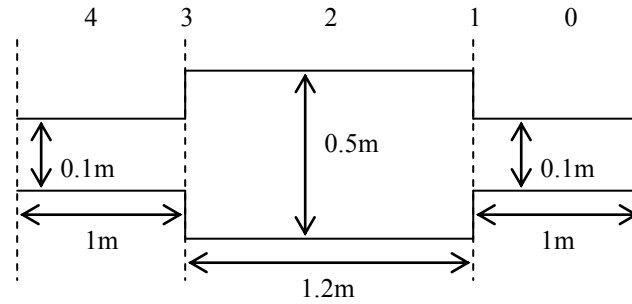


Figure 3-10 Single expansion chamber dimensions used for validation

Using the transfer matrix methodology, an expression for this system can be constructed as

$$\begin{Bmatrix} P_i \\ \rho S u_i \end{Bmatrix} = [T_{SYS}] \begin{Bmatrix} P_o \\ \rho S u_o \end{Bmatrix} \quad (3.27)$$

where

$$[T_{SYS}] = [T_{DUCT4}] [T_{EXP3}] [T_{DUCT2}] [T_{CON1}] [T_{DUCT0}] \quad (3.28)$$

The TL for this system can then be calculated using Equation 3.3.

Figure 3.13 illustrates the TL calculated using the analytical expression given by equation 3.27.

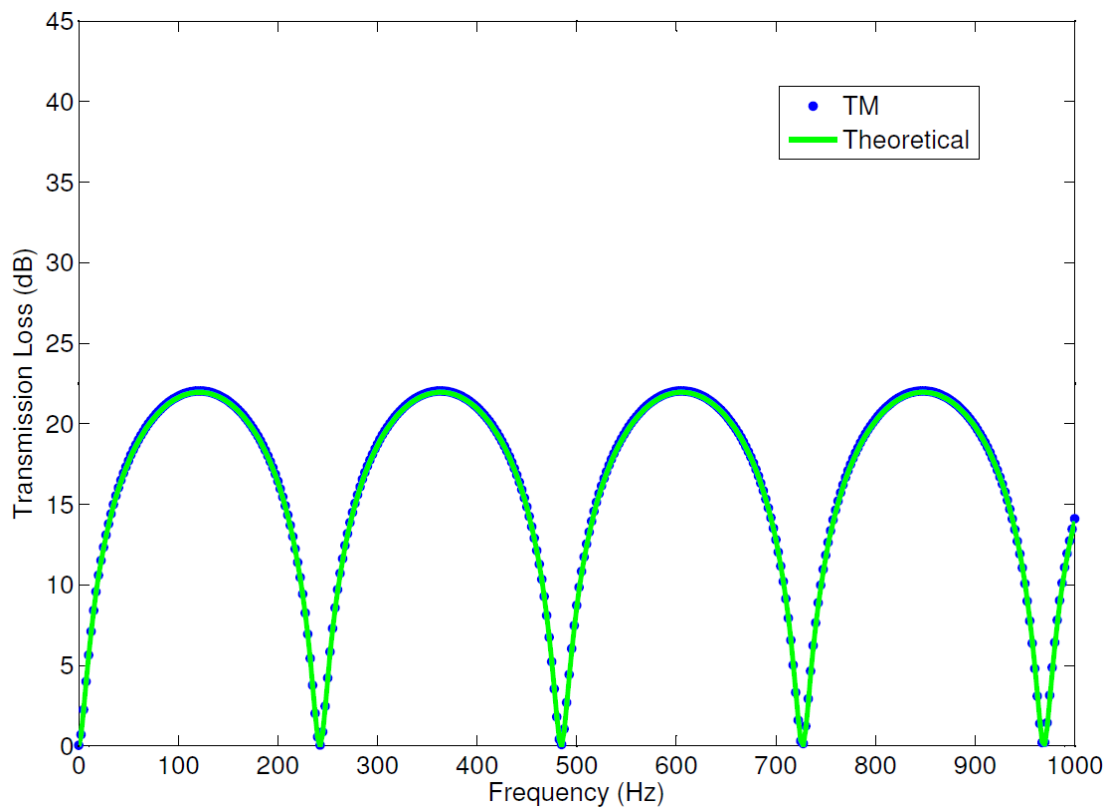


Figure 3-11 Comparison of Theoretical and Transfer Matrix predictions of Transmission Loss

It can be seen that the TL values for the transmission matrix model overlay the theoretical model exactly, with only a very small difference in magnitude at the peak values of transmission loss. This increase is attributed to the difference between the mean flow assumptions in the two models, and is considered negligible for tuner modelling purposes. From this analysis, the construction of the transmission matrix elements, and indeed their coupling to derive the transmission loss for the overall system, is considered valid.

3.6.2 Transmission Matrix Validation – Extended Inlet

Whilst the Single Expansion Chamber validation confirms the construction of the transfer matrix, it is a relatively simple model when compared to the plastic tuner. The example illustrated in Figure 3.12 is much more closely related to the plastic tuner located inside the hose body (see Fig 1.4 b).

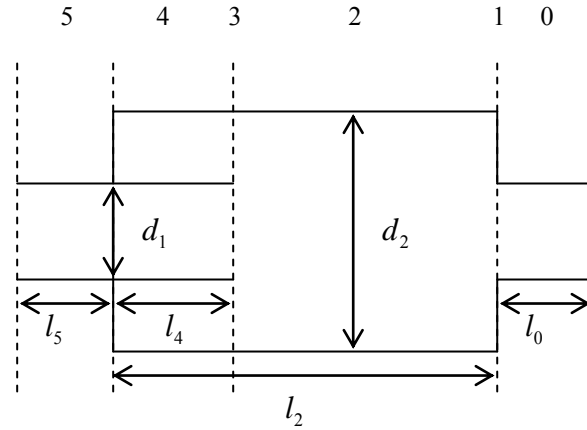


Figure 3-12 Extended Inlet Expansion Chamber dimensions

The extended inlet expansion chamber is again widely understood and utilized extensively as a ‘building-block’ in modern muffler design.

Using the transfer matrix methodology, an expression for this system can be constructed as

$$\begin{Bmatrix} P_i \\ \rho S u_i \end{Bmatrix} = [T_{SYS}] \begin{Bmatrix} P_o \\ \rho S u_o \end{Bmatrix} \quad (3.29)$$

where

$$[T_{SYS}] = [T_{DUCT5}] [T_{EXT4}] [T_{EXP3}] [T_{DUCT2}] [T_{CON1}] [T_{DUCT0}] \quad (3.30)$$

The TL for this system can then be calculated using Equation 3.3.

In order to verify the TL predicted using Equation 3.30, the results are compared to the 1-D experimental results presented by Selamet and Ji (1998) for an identical system geometry i.e. $d_1 = 4.86 \text{ cm}$, $d_2 = 15.32 \text{ cm}$, $l_4 = 8.00 \text{ cm}$ and $l_2 = 28.23 \text{ cm}$. Figure 3.13 illustrates the comparison of results.

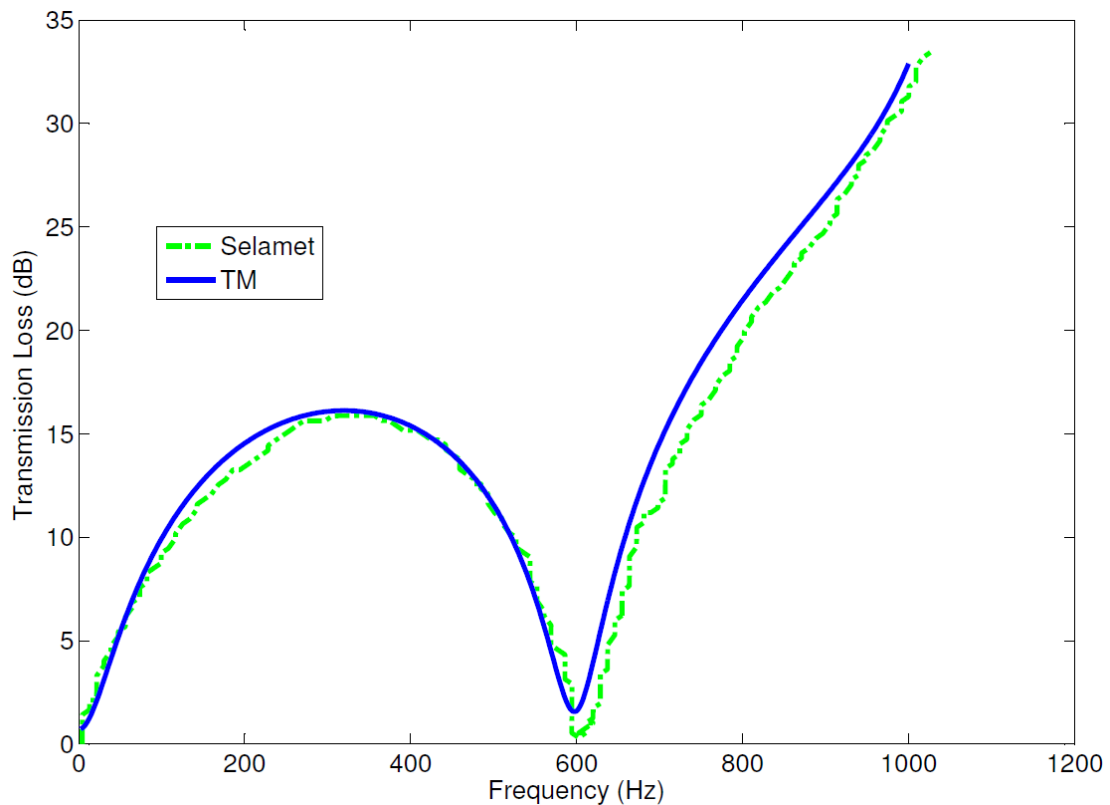


Figure 3-13 Comparison of Transfer Matrix and 1-D Experimental Model of an extended inlet by Selamet and Ji (1998)

As can be seen from Figure 3.13, there is excellent agreement between the two data sets. This validation further confirms the suitability of the modelling approach and additionally validates the assumptions outlined as part of the tuner element modelling in Section 3.7.

3.6.3 Transmission Matrix Validation – Noise Reduction

As the transmission matrix has been validated in the two previous sections, it is important to also consider the construction of the model, and its ability to predict noise reduction as a performance parameter. As previously outlined, the termination impedance that is present in the power steering system is difficult to model analytically. However, there is still a requirement to validate the theory as applied to this system. For this purpose a simple duct system 1m in length and 125mm in diameter was analyzed. The system is illustrated in Figure 3.14.

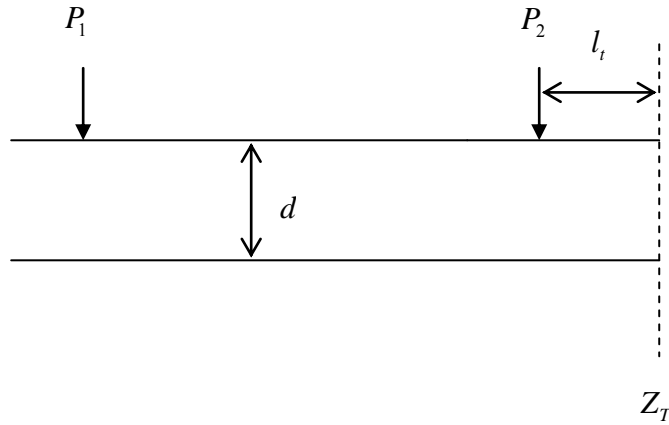


Figure 3-14 Geometry of a Simple Duct System

Using the transfer matrix methodology, an expression for this system can be constructed as

$$\begin{Bmatrix} P_i \\ \rho S u_i \end{Bmatrix} = [T_{SYS}] \begin{Bmatrix} P_o \\ \rho S u_o \end{Bmatrix} \quad (3.31)$$

where

$$[T_{SYS}] = [T_{DUCT}] \quad (3.32)$$

The Noise Reduction for this system is calculated using Equation 3.2, where the termination impedance Z_T is modelled as an open ended pipe radiating to an unbounded region.

At sufficiently low frequencies such that the propagating wave characteristic $(kr_0)^2 \ll 1$, Z_T can be expressed in terms of its zero mean flow counterpart (Munjaj, 1987)

$$Z_T = Y \left(\left(\frac{1}{2} k r_0 \right)^2 + j(k l_e) \right) \quad (3.33)$$

where

- l_e = end correction = $0.61 r_0$
- r_0 = termination duct radius

In order to validate the results calculated using Equation 3.2, the results are compared to the experimentally measured and Finite Element Analysis result presented by Lapka and Cempel (2007) as shown in Figure 3.15.

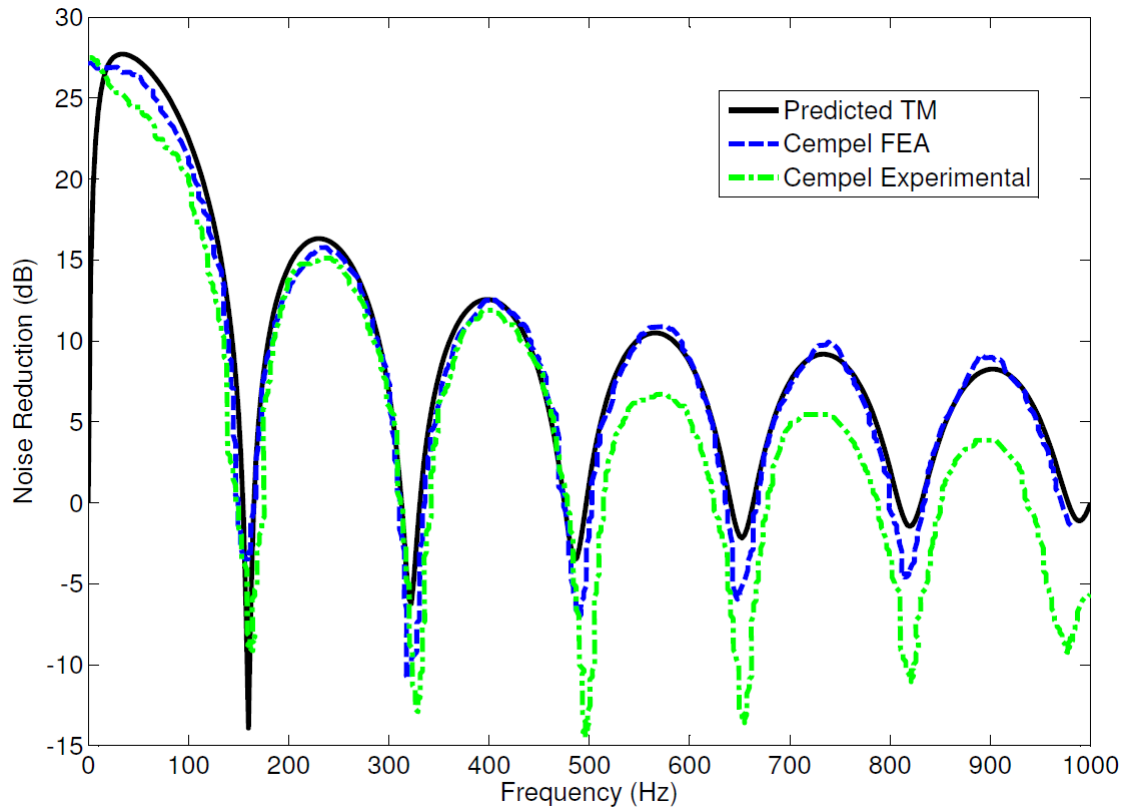


Figure 3-15 Simple Duct System Noise Reduction

There is excellent agreement between the modelled data sets. The minor deviations at frequencies higher than 500Hz are attributed to differences in mean flow and rigid wall assumptions. It is unclear from Lapka and Cempel's paper exactly how they have modelled these attributes.

With this final validation of the noise reduction theory, it is now possible to proceed with confidence in modelling the relatively complex constructions of the plastic tuner, using the transmission matrix approach. The following sections outline the theory defining the models for each of the systems to be investigated to address the key objectives of this research.

3.7 Model of Tuner with No Holes

The tuner with no holes illustrated in Figure 3.16. In order to model this type of tuner, Tuner Duct, Tuner Expansion and Tuner Contraction elements are utilised, representing the acoustic wave motion starting at Transducer 1 (location 5), then inside the tuner, at the tuner outlet and inside the hose body as far as Transducer 2 (location 0). This type of tuner is very similar to the extended inlet chamber muffler analysed in Section 3.6.

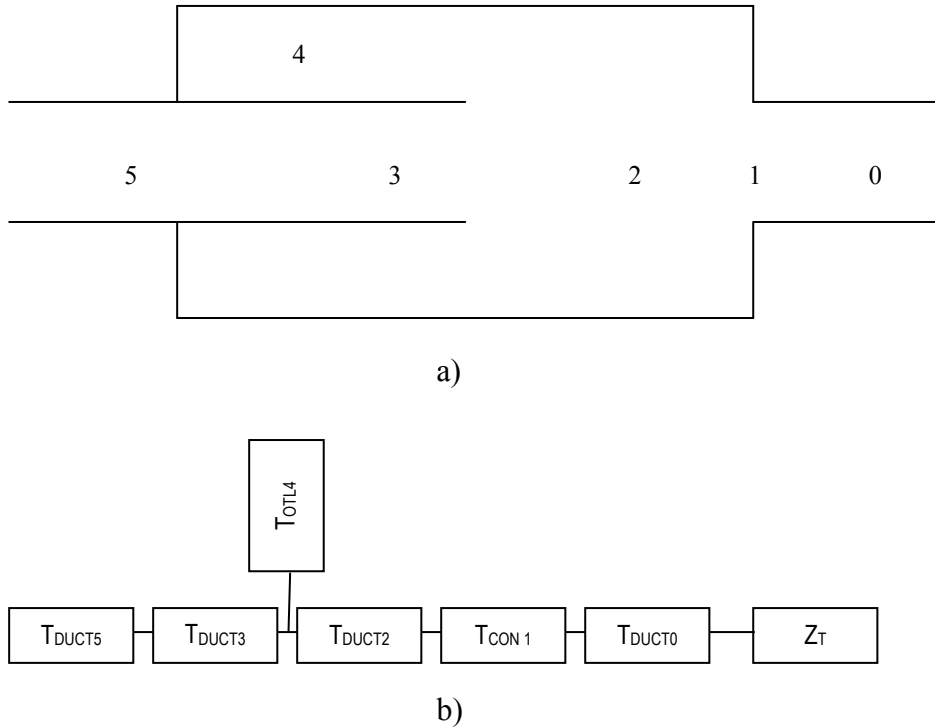


Figure 3-16 Tuner with no holes a) physical arrangement b) transmission matrix representation

Using the transmission matrix methodology, an expression for this element can be constructed as

$$\begin{Bmatrix} p_i \\ \rho S u_i \end{Bmatrix} = [T_{SYS}] \begin{Bmatrix} p_o \\ \rho S u_o \end{Bmatrix} \quad (3.34)$$

where

$$[T_{SYS}] = [T_{DUCT5}] [T_{DUCT3}] [T_{OTL4}] [T_{DUCT2}] [T_{CON1}] [T_{DUCT0}] \quad (3.35)$$

3.8 Model of Tuner with single hole (fixed diameter varied location)

The tuner with a single hole in the sidewall of the tuner is illustrated in Figure 3.17. In order to model this type of tuner, Tuner Duct, Tuner Expansion, Parallel Branch, Tuner Hole and Tuner Contraction elements are utilised representing the acoustic wave motion starting at Transducer 1 (location 8), then inside the tuner, at the tuner hole, in the duct parallel to the tuner, and inside the hose body as far as Transducer 2 (location 0).

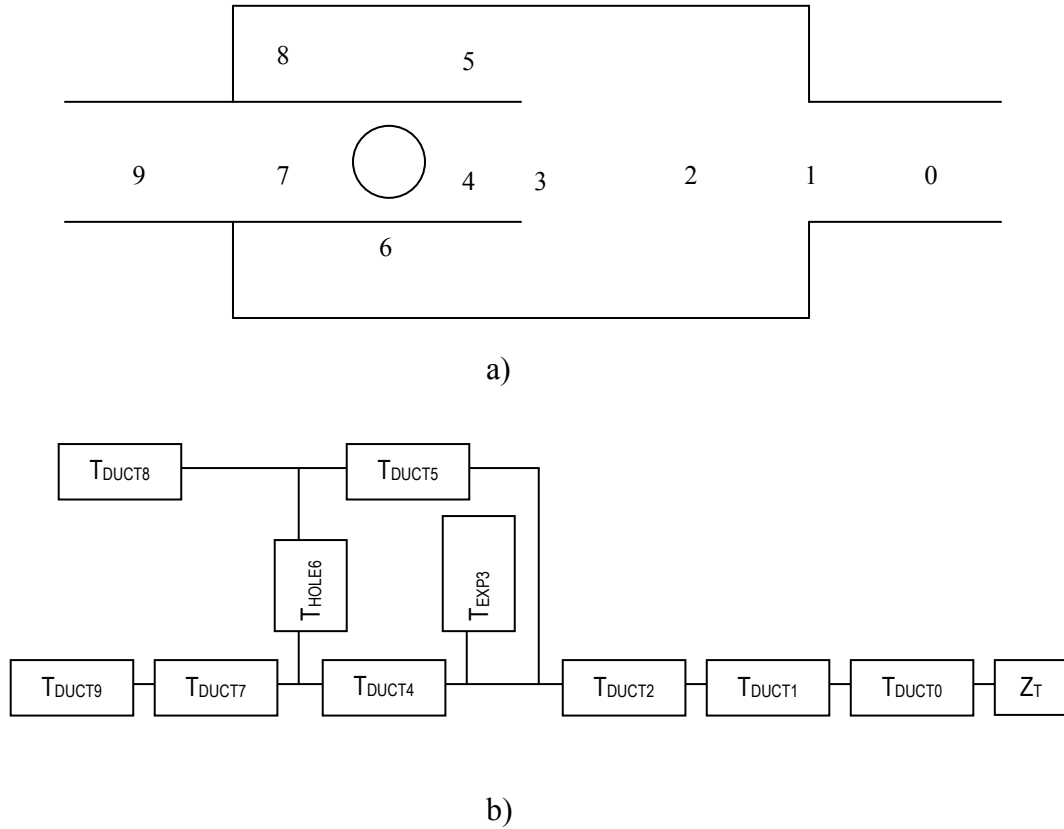


Figure 3-17 Tuner with single hole a) physical arrangement b) transmission matrix representation

Using the transmission matrix methodology, an expression for this element can be constructed as

$$\begin{Bmatrix} p_i \\ \rho S u_i \end{Bmatrix} = [T_{SYS}] \begin{Bmatrix} p_o \\ \rho S u_o \end{Bmatrix} \quad (3.36)$$

where

$$[T_{SYS}] = [T_{DUCT8}] [T_{DUCT6}] [T_{PB1}] [T_{DUCT2}] [T_{CON1}] [T_{DUCT0}] \quad (3.37)$$

and

$$[T_{PB1}]_{BRANCH1} = [T_{DUCT4}][T_{HOLE5}][T_{DUCT7}] \quad (3.38)$$

$$[T_{PB1}]_{BRANCH2} = [T_{DUCT3}] \quad (3.39)$$

3.9 Model of Tuner with single hole (fixed location varied diameter)

The model used for this investigation is identical to that described in Section 3.8, where the diameter d and open area ratio p are modified accordingly for each experiment.

3.10 Model of Tuner with multiple holes

The tuner with multiple holes is illustrated in Figure 3.18 for the case of two holes and Figure 3.19 for the case of three holes in the tuner sidewall. In order to model this type of tuner, Tuner Duct, Tuner Expansion, Parallel Branch, Tuner Hole and Tuner Contraction elements are utilised, representing the acoustic wave motion starting at Transducer 1 (location 11 for two holes and location 14 for three holes), then inside the tuner, at the tuner holes, at the tuner outlet and inside the hose body as far as Transducer 2 (location 0).

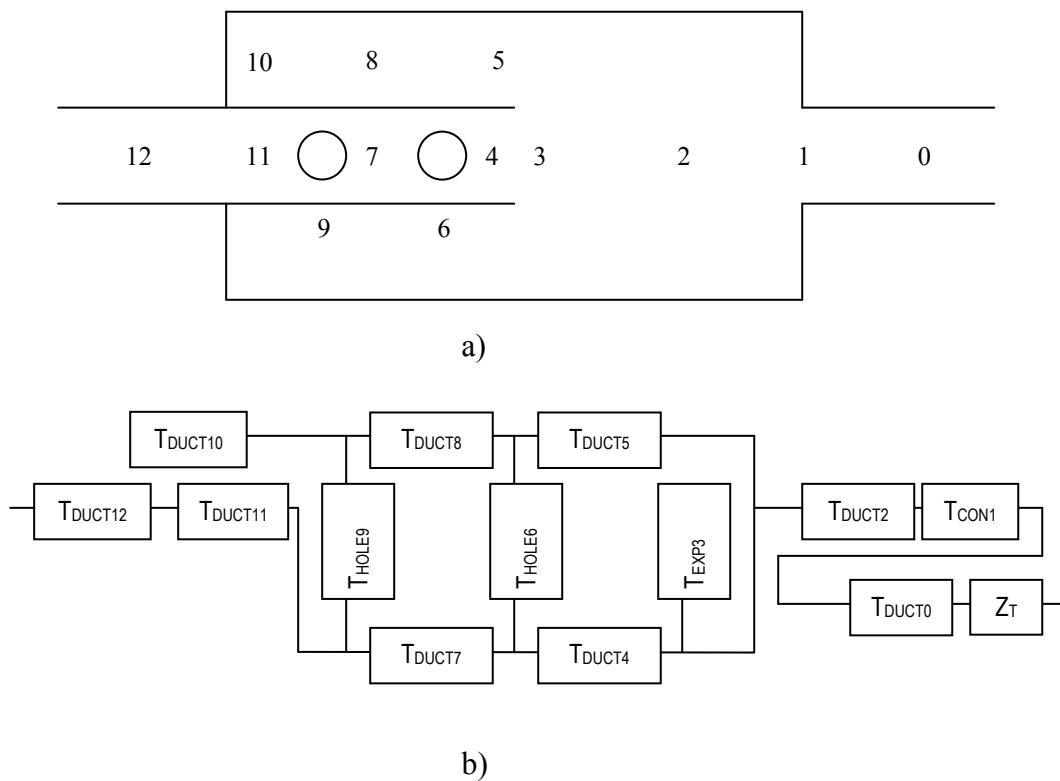


Figure 3-18 Tuner with two holes a) physical arrangement b) transmission matrix representation

Using the transmission matrix methodology, an expression for this element can be constructed as

$$\begin{Bmatrix} P_i \\ \rho S u_i \end{Bmatrix} = [T_{SYS}] \begin{Bmatrix} P_o \\ \rho S u_o \end{Bmatrix} \quad (3.40)$$

where, for a two-hole tuner

$$[T_{SYS}] = [T_{DUCT11}] [T_{DUCT9}] [T_{PB2}] [T_{DUCT2}] [T_{DUCT0}] \quad (3.41)$$

and

$$[T_{PB2}]_{BRANCH1} = [T_{DUCT3}] [T_{DUCT6}] \quad (3.42)$$

$$[T_{PB2}]_{BRANCH2} = [T_{DUCT4}] [T_{HOLE5}] [T_{DUCT6}] [T_{DUCT7}] [T_{DUCT10}] \quad (3.43)$$

$$[T_{PB2}]_{BRANCH3} = [T_{DUCT4}] [T_{DUCT7}] [T_{HOLE8}] [T_{DUCT10}] \quad (3.44)$$

$$[T_{PB2}]_{BRANCH4} = [T_{DUCT3}] [T_{HOLE5}] [T_{DUCT7}] [T_{HOLE8}] [T_{DUCT10}] \quad (3.45)$$

For a three hole tuner $[T_{SYS}]$ is modified to

$$[T_{SYS}] = [T_{DUCT14}] [T_{DUCT12}] [T_{PB3}] [T_{DUCT2}] [T_{DUCT0}] \quad (3.46)$$

and

$$[T_{PB3}]_{BRANCH1} = [T_{DUCT3}] [T_{DUCT6}] [T_{DUCT9}] \quad (3.47)$$

$$\begin{aligned} [T_{PB3}]_{BRANCH2} &= [T_{DUCT4}] [T_{HOLE5}] [T_{DUCT7}] [T_{DUCT10}] [T_{DUCT13}] \\ &\times [T_{DUCT6}] [T_{DUCT9}] \end{aligned} \quad (3.48)$$

$$\begin{aligned} [T_{PB3}]_{BRANCH3} &= [T_{DUCT4}] [T_{DUCT7}] [T_{HOLE8}] [T_{DUCT10}] \\ &\times [T_{DUCT13}] [T_{DUCT9}] \end{aligned} \quad (3.49)$$

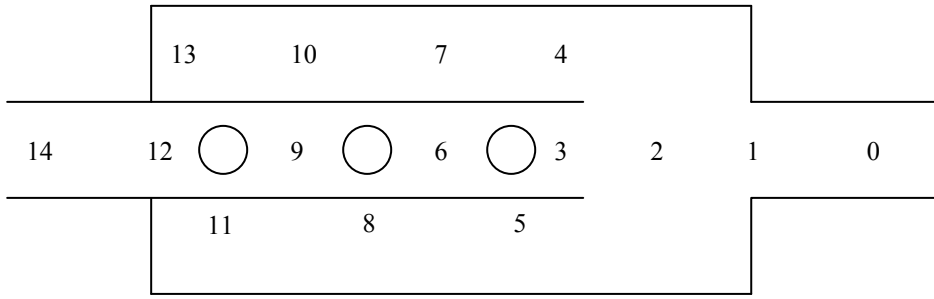
$$[T_{PB3}]_{BRANCH4} = [T_{DUCT4}][T_{DUCT7}][T_{DUCT10}][T_{HOLE11}][T_{DUCT13}] \quad (3.50)$$

$$[T_{PB3}]_{BRANCH5} = [T_{DUCT3}][T_{HOLE5}][T_{DUCT7}][T_{HOLE8}][T_{DUCT9}] \times [T_{DUCT10}][T_{DUCT13}] \quad (3.51)$$

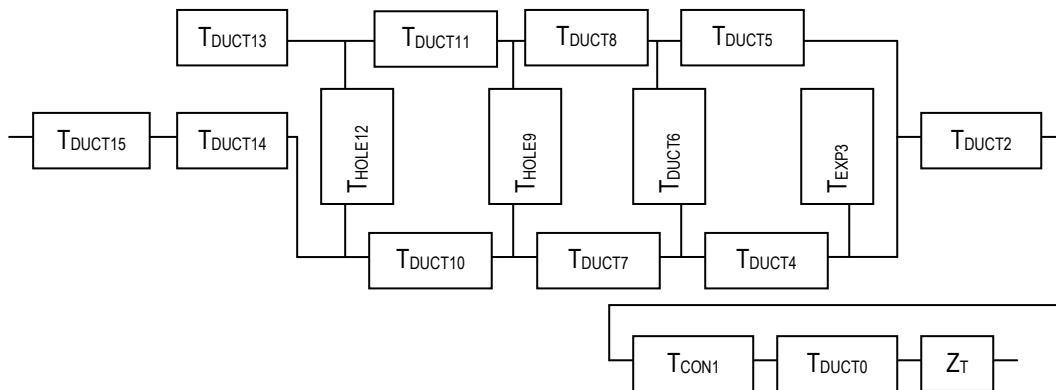
$$[T_{PB3}]_{BRANCH6} = [T_{DUCT3}][T_{HOLE5}][T_{DUCT7}][T_{DUCT10}][T_{HOLE11}] \times [T_{DUCT13}] \quad (3.52)$$

$$[T_{PB3}]_{BRANCH7} = [T_{DUCT3}][T_{HOLE5}][T_{DUCT7}][T_{DUCT10}][T_{HOLE11}] \times [T_{DUCT13}] \quad (3.53)$$

$$[T_{PB3}]_{BRANCH8} = [T_{DUCT3}][T_{DUCT6}][T_{HOLE8}][T_{DUCT10}][T_{HOLE11}] \times [T_{DUCT13}] \quad (3.54)$$



a)



b)

Figure 3-19 Tuner with three holes a) physical arrangement b) transmission matrix representation

3.11 Summary

An approach to modelling the plastic tuner has been presented. Discrete elements of the tuner have been outlined and are coupled using the transmission matrix methodology. Using this approach, results for various tuner designs can be analysed in terms of their noise reduction.

Chapter 4 describes the experimental approach used to measure the noise reduction for comparable tuner designs. These results are then analysed in Chapter 5.

4 Experiments

In this chapter the methodology used to experimentally investigate the various design parameters of the tuner, and additionally quantify their associated performance, are presented.

The chapter starts with an explanation of the experimental approach including a description of the test rig set-up and test apparatus used. The chapter explains the purpose of each experiment and the detail of each test sample. Additionally, the empirical approach to modelling the termination impedance is outlined and validated with experimental measurements. Finally, the chapter ends with initial thesis conclusions arising from the experiments and a discussion of their significance.

4.1 Experimental Approach

The experimental approach described in this section is concerned with achieving the key objectives defined in section 1.2. These discrete objectives can be summarised as an investigation of the noise reduction characteristics of plastic tuners and use this knowledge to develop a new theoretical model.

In all experiments, pump pressure noise reduction is derived from measurements using similar test apparatus to that which is described in Section 2.5.2.

In order to investigate the impedance characteristics of the tuner hole profile, it was necessary to set up a secondary test rig capable of isolating impedance effects associated with the hose / tuner boundary. This secondary rig is discussed in more detail in Section 4.1.2.

Whilst the system has resonances; the effects of these are only experienced by the vehicle driver under particular driving conditions. An example would be performing a sharp left turn (into driveway) at high engine revs, and low exterior sources of noise. For this reason, and regardless of the test rig configuration, all measurements were obtained at fixed pump rpm (2000 rpm), and stable fluid temperature (70°C).

Measurement data was analysed using SignalCalc signal processing software, which has the capability of generating auto power spectra based on inputs from rig mounted transducers.

Data captured using SignalCalc software can be converted to Matlab data files, which is then used to derive experimental and predicted noise reduction values used to validate the new system model. Comparison of experimental and predicted noise reduction values is covered in greater detail in Chapter 5.

4.1.1 Experimental Layout – Benchmarking

The experimental layout used for initial benchmarking against the spiral wound steel tuner is shown in Figure. 4.1. The flow path for the fluid in the system is as follows: fluid enters the pump inlet from the Reservoir Feed Line and passes to the pump outlet. The pump outlet is connected to the High Pressure Line which transmits the fluid to the Power Steering Rack inlet. The fluid then exits the Rack via the control valve and enters the Low Pressure Return Line. The Return Line feeds the Oil Cooler which maintains a stable system oil temperature. The outlet of the cooler is connected to the Reservoir via the Reservoir Return line, which returns the fluid back to the Reservoir.

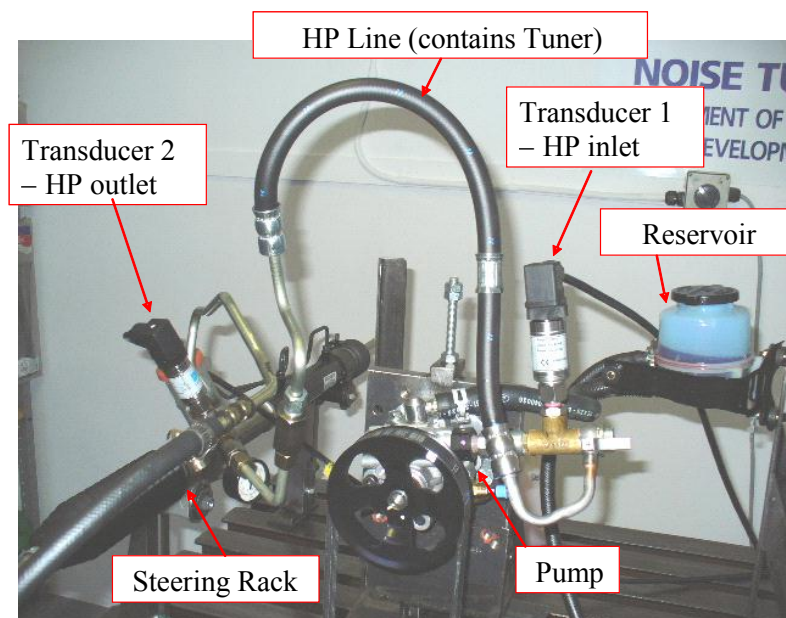


Figure 4-1 Experimental layout

The main area of interest in this experiment is the High Pressure Line which contains the plastic tuner. The pressure at the point in the system immediately after the pump outlet and immediately before the High Pressure Line inlet is captured by Transducer 1. At the other end, i.e. the point immediately after the High Pressure Line outlet and before the inlet to the Rack, the system pressure is captured by Transducer 2. Although the set-up is similar to the set-up for the ‘Two-Microphone Method’ discussed previously in Section 2.5.1, it should be noted the methodology used to analyse the transducer signals is not the same.

Ideally, when investigating the impact of the tuner on the system it is desirable to locate the transducers as close to the tuner inlet / outlet as possible. Unfortunately, this is not practical as it would require ‘tapping’ into the high pressure hose and sealing it effectively, without influencing the system pressure in that region. It is recognised therefore that the fluid pressure measured at Transducer 2 is not solely a representation of the fluid pressure exiting the tuner.

Both transducers are GE PTX1400 type 0-4bar_g (GE Sensing, 2005). The ten vane Kayaba pump is driven by a Baldor 0.56 kW DC motor (via a power steering drive belt) which is controlled by a Penta KBMD DC speed controller. In order to reduce the experimental error associated with the speed controller reading, RPM is measured directly from the pump pulley using an infra-red Onosokki Tachometer. All instrumentation was calibrated prior to experiments.

4.1.2 Experimental Layout – Tuner Design Investigations

In order to evaluate the effects of various tuner construction variables on the system, it is more practical to reduce the system to as ‘simple’ a level as possible. This is achieved by replacing the existing rubber hose assembly with a rigid steel tube, to remove the damping affects associated with the rubber, which are difficult to model and replicate theoretically.

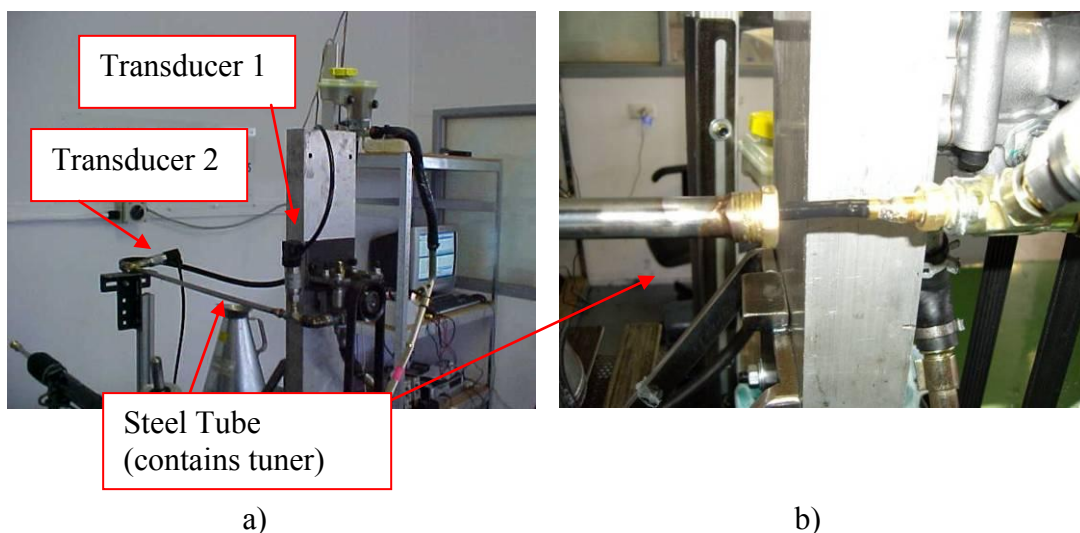


Figure 4-2 a) Test rig for plastic tuner investigation b) plastic tuner mounting detail

In the experimental set-up illustrated in Figure 4.2, the flow path for the fluid in the system is as follows: fluid enters the pump inlet from the Reservoir Feed Line and passes to the Pump outlet. The pump outlet is connected to the steel tube (12.7mm

outer diameter x 0.98mm wall thickness), which contains the plastic tuner. At either end of the steel tube, two T-ports support the mounting of transducers to allow for pressure measurement at the inlet and outlet. The fluid then exits the steel tube and enters the Low Pressure Return Line. The Low Pressure Return Line is connected to the reservoir which returns the fluid back to the start of the loop. Dimensional detail of the fluid path between the two transducers (T1 and T2) is illustrated in Figure 4.3.

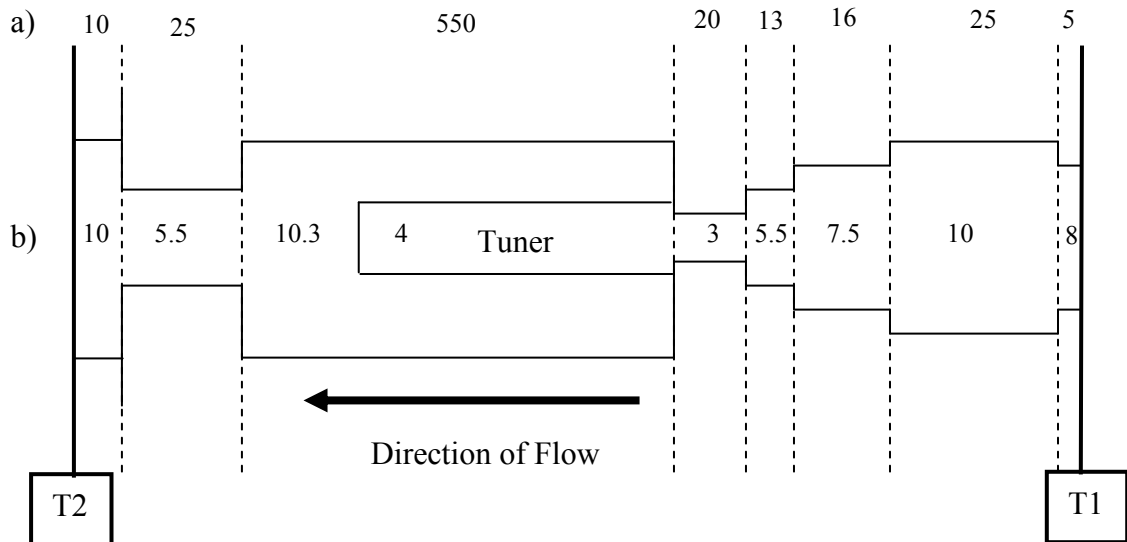


Figure 4-3 a) Length dimension in mm b) internal bore dimension in mm

4.1.3 Plastic Tuner Design

The plastic tuner used in the experiments forms a different configuration and hose mounting from the spiral wound steel tuner. The construction is illustrated in Figure 4.4, which also details the plastic tuner to tube coupling. A metal insert is mounted on the end of the extruded plastic tube. The insert/tube assembly is then attached to the pump-end tube by a crimping process.

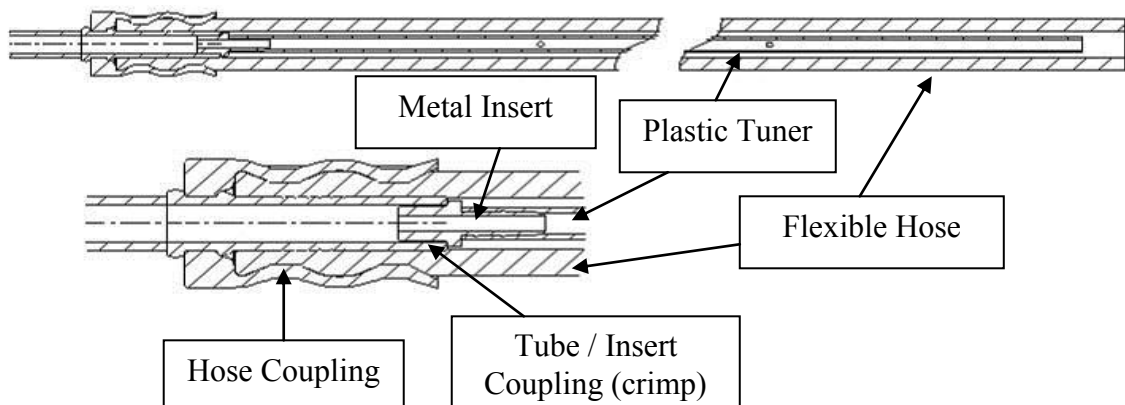


Figure 4-4 Plastic Tuner design

4.1.4 Control Sample

For the purpose of the benchmarking experiment, an appropriate control sample is required. The assembly selected was a spiral wound steel tuner used by Ford India (B265) and produced by Cooper Standard Automotive. A dimensional drawing detailing this tuner is given in Figure 4.5.

NOTE:
This figure/table/image has been removed
to comply with copyright regulations.
It is included in the print copy of the thesis
held by the University of Adelaide Library.

Figure 4-5 CSA Ford India (B265) Spiral Wound Steel Tuner (Cooper Standard Automotive, 2007)

4.1.5 Plastic Tuner / Hose Coupling

The connection between the plastic tuner, the tuner insert and the hose ferrule must be oil-sealed and tight. The tuner must remain in position throughout any operational state and must not slide out of position under any circumstance. Figure 4.6a) shows the minimum tensile forces which two standard tuner sizes must follow at room temperature (20°C approx).

The tuner selected for this design is $\text{Ø}6 \times 1$ mm. The specified values are based on calculations by Merkel (2004), which show that values of 225N occur as a result of fluid flow at a volumetric flow rate of 15 l/min in a cold start performance at -40°C. The correlation is displayed in Figure 4.6b)

NOTE:
This figure/table/image has been removed
to comply with copyright regulations.
It is included in the print copy of the thesis
held by the University of Adelaide Library.

Figure 4-6 a) Tuner pull-off specification b) Graph of temperature effects (Merkel, 2004)

4.1.6 Plastic Tuner Material Properties

In addition to the tensile strength requirement associated with the tuner / hose coupling, the plastic tubing itself must possess certain material properties which are derived from the mechanical and environmental requirements invoked by the power steering system. For this application there are several properties of interest which are summarised in Table 4.1.

Table 4-1 Tuner properties table

Mechanical Properties	Unit	Requirement
Hardness	Shore D	55 - 72
Burst Pressure at $T_{OIL}=100^{\circ}C$	bar	> 33
Thermal Properties	Unit	Requirement
Operating Temperature	$^{\circ}C$	-40 to +150
Chemical Properties	Unit	Requirement
Fluid Resistance	Inert to:	Dexron ATF Shell ATF Pentosin CHF11S Mobil 424

Typically these properties would be evaluated on the power steering hose assembly during the design and development phase as part of a Pressure Impulse Test. For the purposes of this research the test samples used throughout are constructed from DuPont ‘Zytel’ material grade 350PHS2.

4.1.7 Experimental Procedure

For a given point in the system, in order to maintain a stable fluid pressure and temperature, which can have a major impact on other system parameters used to calculate corresponding acoustic pressure and velocity for the common point of interest, it is important to control the system inputs which affect these two key parameters. For each experiment the pump is driven at the test RPM (2000 RPM). The system temperature which varies with pump RPM is controlled by ensuring the temperature stabilises over a period of 20 minutes to $70^{\circ}C$, prior to commencement of data acquisition. It is also important to maintain the system boundaries throughout the stabilisation and test period. This parameter can be altered by ‘steering’ the rack, which is therefore maintained at the zero degree position, which corresponds to straight ahead.

For each experiment, data was captured using the SignalCalc digital acquisition software. The software is set-up to capture pressure data based on a stable (linear) averaging function (50 averages). The frequency resolution was set at 2.5Hz.

The frequency range is set from 0-1000Hz as this is the range of greatest interest when considering the natural frequency of the pump at the test RPM. A typical plot is illustrated in Figure 4.7. Spectral amplitudes are displayed in units of Sound Pressure Level (dB) with respect to 20×10^{-6} Pascals.

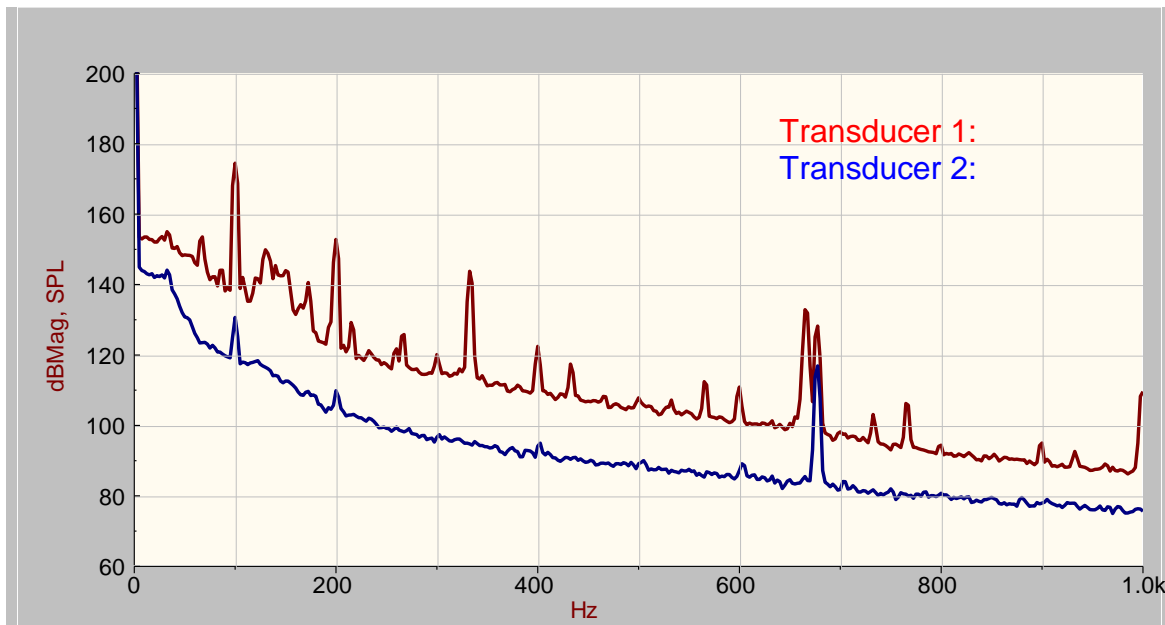


Figure 4-7 Sample auto-power spectra from SignalCalc

The tones at 100Hz, 200Hz and 300Hz are associated with electrical noise generated by the electric motor utilised in the test rig, and should not be considered with respect to the pump or tuner system. Despite several attempts to isolate the rig and system under test from this noise, it was not possible without the use of filters. As the tones do not coincide with the frequencies of greatest interest i.e. 333Hz, 666Hz and 999Hz, they are considered negligible for the purpose of this evaluation.

4.1.8 Experimental Noise Reduction

Following data capture through the experimental procedure described in Section 4.1.7, the data is converted to a readable format and imported into Matlab. The theoretical model presented in Chapter 3 is validated in Chapter 5 using Noise Reduction as a performance parameter. The formula used to calculate the experimental noise reduction is given by (Beranek and Ver, 1992)

$$NR = 20 \log_{10} \left| \frac{P_2}{P_1} \right| \quad (4.1)$$

where P_1 and P_2 are measured at transducer locations 1 and 2 respectively.

4.1.9 Empirical Approach to Termination Impedance

As discussed in Section 3.3, it is very difficult to model the termination impedance of the power steering system. The main reason for this is that the termination load, which is a function of the system geometry and fluid, is inadvertently changed from experiment to experiment, in-line with the changing plastic tuner samples. In this case, it was considered best to adopt an empirical approach, where the termination impedance is related to the particular system under analysis.

Initially, as a starting point, the empirical termination impedance Z_{T_e} , is defined as

$$Z_{T_e} = X_u \times Z_T \quad (4.2)$$

where Z_T is as previously defined in Section 3.6.3 (i.e. the termination impedance of an open ended pipe, radiating to an unbounded region, with zero mean flow), and X_u is a constant derived from 1st order pump magnitude experimental results. Following analysis of X_u for each experiment, a proposed value for this constant is suggested in Section 5.5.3. The detail of the termination impedance experimental procedure is discussed in Section 4.2, and the analysis of the results is discussed in Section 5.5.3.

4.2 Termination Impedance Measurement

Considering the key objectives of this research, the transmission matrix model proposed in Chapter 3 should accurately predict the 1st order pump noise reduction magnitude, for a range of different tuner constructions. In order to achieve this, the common system environmental parameters need to be matched. As these parameters are difficult to predict theoretically, the following procedure was used.

- Step 1: Capture experimental data and calculate associated experimental noise reduction using procedures defined in Section 4.1.
- Step 2: Calculate theoretical noise reduction (first pass), using Equations. 3.2 & 4.2, where X_u is selected to be an arbitrary value.

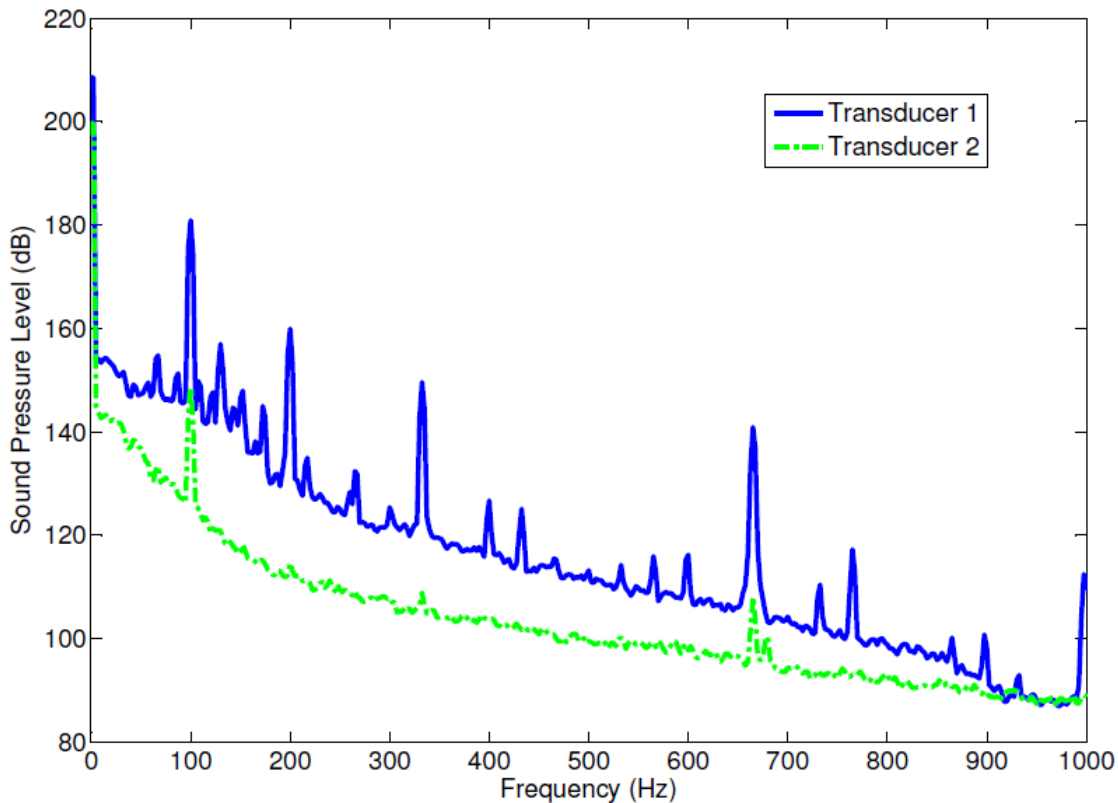
- Step 3: Repeat step 2, where X_u is now ‘tuned’ such that the predicted 1st order noise reduction magnitude coincides with the associated experimentally measured value.
- Step 4: Record final value of X_u .

4.3 Baseline Evaluation Testing

In order to evaluate the suitability of the proposed design described in Section 4.1.3, it is firstly important to compare the tuner performance with an ‘equivalent’ spiral wound steel construction. All tests are performed on the test rig illustrated in Figure 4.1. Test results were recorded at 2000 RPM based on the procedure outlined in Section 4.1.1. The construction of the two test samples was maintained where possible i.e. hose couplings, hose length, hose material and tuner location inside hose. The spiral wound steel construction was identical to that described in section 4.1.4. The plastic tuner consisted of a 400mm long plastic tuner with a 1mm diameter through hole located 350mm from the tuner inlet.

4.3.1 Baseline Evaluation Results

The results of the test on the spiral wound steel tuner and the plastic tuner are illustrated in Figure 4.8



a)

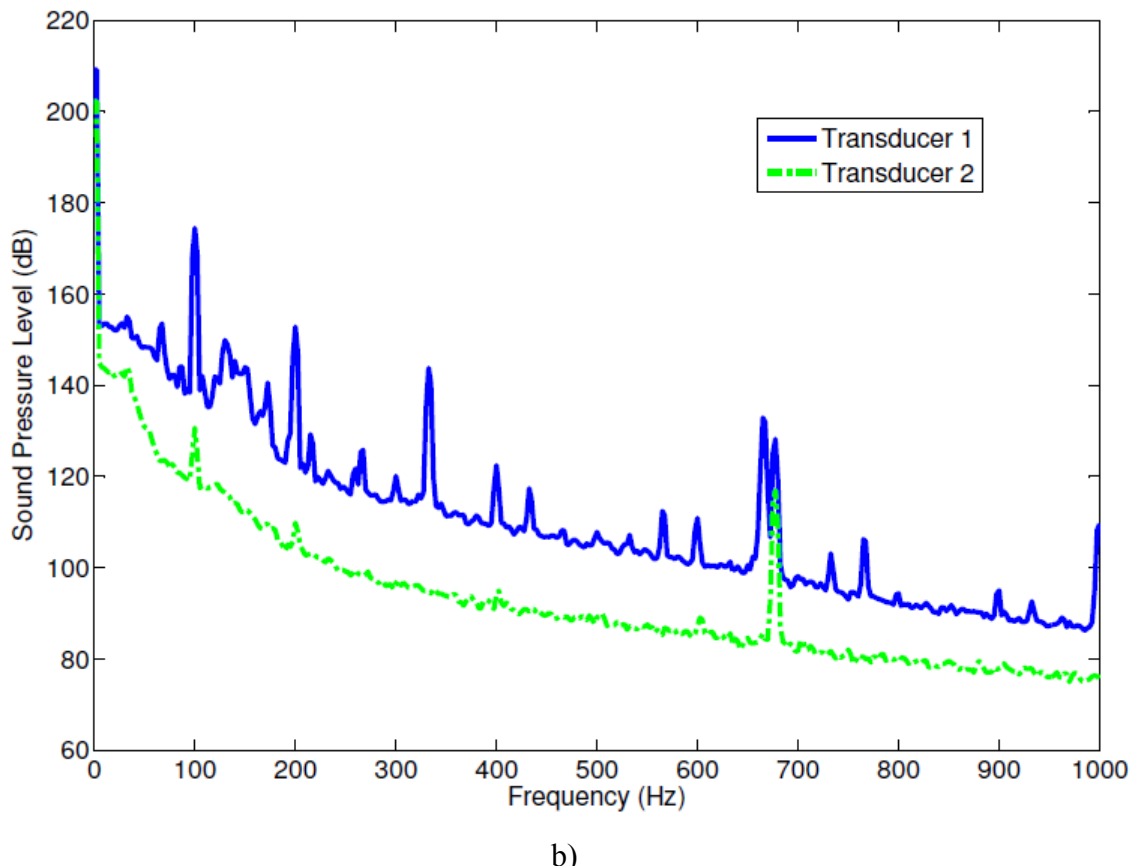


Figure 4-8 Auto Power Spectrum a) SWST b) PT

It can be observed from Figure 4.8 that for this particular plastic tuner construction, at the critical pump order frequencies of 333Hz, 666Hz and 999Hz, there appears to be an improved noise reduction performance, when compared to the spiral wound steel construction. It is noted however, that at approximately 680 Hz, the plastic tuner performs poorly. Overall it can be observed that there is a marginal reduction in system pressure with the plastic tuner configuration. This is best illustrated when comparing peaks for ‘Transducer 1’ at key pump frequencies in Figure 4.8a) and Figure 4.8b). High system pressure can be undesirable due to its impact on system component life. The tones at 100Hz, 200Hz and 300Hz are considered negligible as per description in Section 4.1.7.

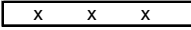
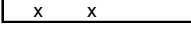
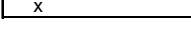
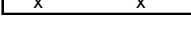
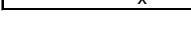


In summary, the results show that utilising a plastic tuner configuration in lieu of a spiral wound steel construction, it is possible to achieve an improved level of noise reduction performance and a reduced system pressure.

In addition to this single comparative test, an additional experiment was conducted to evaluate several plastic tuner constructions, chosen to evaluate the variation in noise reduction performance across systems design parameters.

This further test covered a range of high pressure power steering hose assemblies containing plastic tuners 400mm in length and constructed with hole positions according to the Table 4.2, where ‘X’ represents a hole location. The results were quickly quantified by comparing the noise reduction performance i.e. the noise reduction magnitude at the pump fundamental frequency 333 Hz of the test assembly, with that of a ‘control sample’, which was the spiral wound steel tuner configuration described in section 4.1.4. The results and PT configurations are summarised in Table 4.2.

Table 4-2 Preliminary Test Results

1	Significantly Better Than Control Sample	10dB or more difference
2	Marginally Better Than Control Sample	5 to 10 dB difference
3	Approximately the Same as Control Sample	within ± 5 dB difference
4	Marginally Worse Than Control Sample	-5 to -10dB difference
5	Significantly Worse Than Control Sample	-10 dB or more difference

Assembly	Configuration	Result
Control	Spiral Wound Steel	
Tube A		5
Tube B		1
Tube C		5
Tube D		4
Tube E		1
Tube F		5
Tube G		2

4.3.2 Discussion arising from baseline evaluation

Comparing the results for the different tube constructions, a number of observations can be made, which indicate the need for further investigation. In relation to the main aim of this experiment it is clear when comparing the results for Tube C and Tube E, that the leakage coefficient is not necessarily linear with pressure difference along the tuner length as has been suggested for the spiral wound steel tuner. This conclusion can be drawn because the 200mm difference in tuner hole position between Tube C and Tube E provides a significantly different noise reduction. As highlighted by Drew

(1998) in their previous experiments, it is difficult to measure tuner noise reduction accurately. The present observations would however indicate that there is scope for further investigation.

4.4 Tuner Length Experiments

The purpose of this experiment is to investigate the impact of a varied tuner length on overall tuner noise reduction. There are several reasons for this; firstly, of the commercially available tuners investigated, the tuner lengths vary quite considerably – what is the main reason for this? Additionally, it is not known if two tuners of different length will provide similar noise reduction in a given system. In this case, for commercial reasons, it would be desirable to utilise the shorter material length to obtain the same result.

The tuners used in this experiment contain no pressure relief holes and are constructed according to Figure 4.11 and Table 4.3.

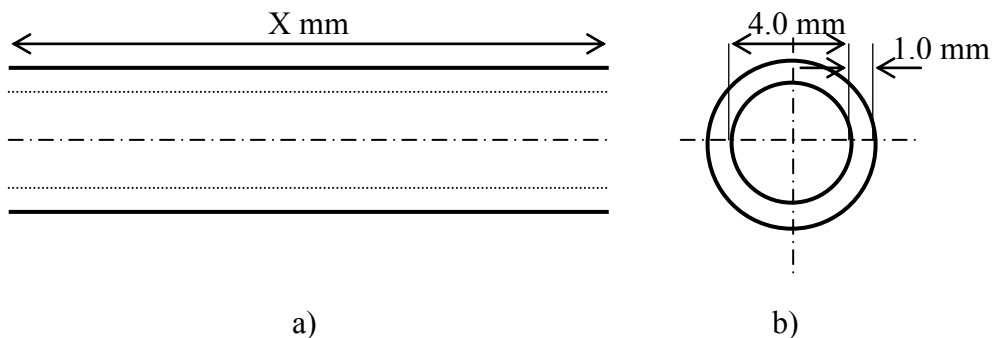


Figure 4-9 Tuner length test construction a) longitudinal cross-section b) end view

Table 4-3 Tuner Length Test Sample

Tuner length 'X' mm	Sample Designation
50	A
100	B
150	C
200	D
250	E
300	F
350	G
400	H

4.4.1 Tuner Length Test Procedure

The experimental equipment used for this test is the same as described in Section 4.1.2. For each experimental construction, the test samples were mounted on the test rig and the test pump was driven until the fluid in the system stabilised at a test temperature of 70°C. The pump RPM was then fixed at 2000 RPM and a series of data captures (50 averages) were taken using the Signal Calc software. A photograph of the test set-up can be seen in Figure 4.10.



Figure 4-10 Photograph of experimental layout

In order to quantify the noise reduction gained solely from the test sample, an initial test was first run to obtain data from the steel tube containing no tuner. The results for this test are illustrated in Figure 4.11.

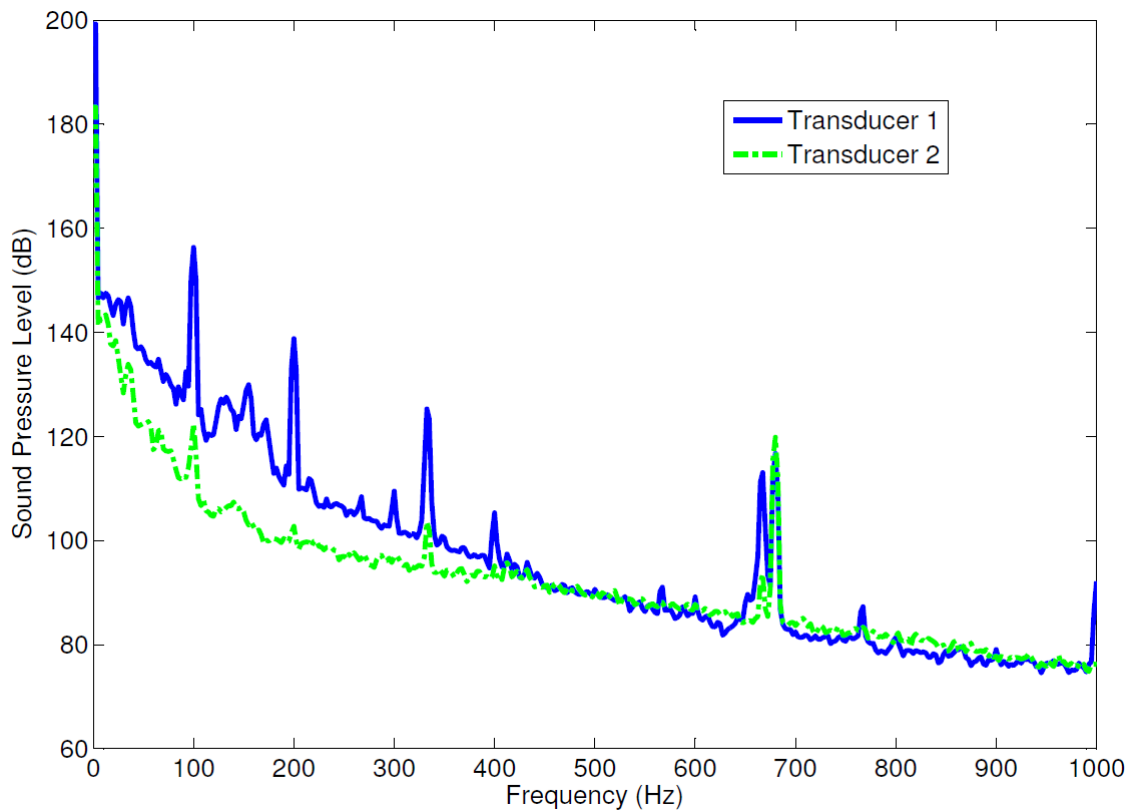


Figure 4-11 Auto Power Spectrum for Test Rig containing No Tuner

The result of the ‘no-tuner’ test was then subtracted from each of the test sample runs, to obtain the noise reduction magnitude relevant to each test sample. By plotting the resultant noise reduction magnitude of the 1st pump order (in this case at ~333Hz) against the corresponding value of ‘X’ in Table 4.3, an understanding of the impact of tuner length impact can be gained.

4.4.2 Tuner Length Test Results

The data captured during the experiment was analysed between the 0 – 1 kHz frequency range. This permitted analysis of the significant area of interest i.e. the noise reduction magnitude of pump generated noise (1st and 2nd Order) solely by each test sample.

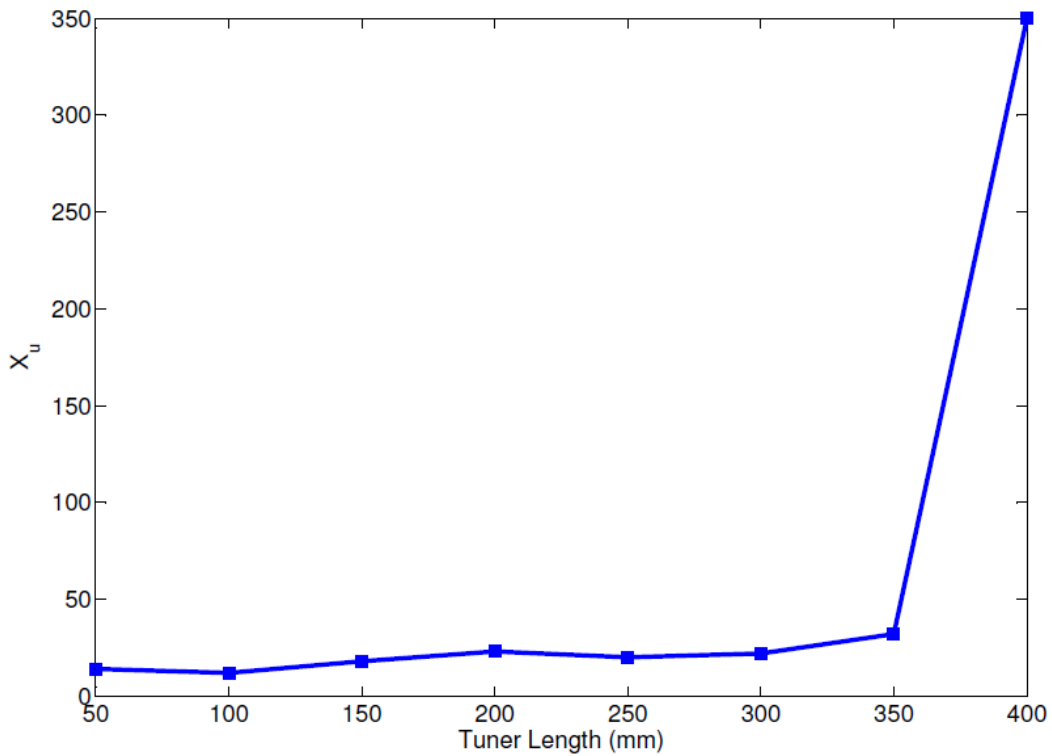


Figure 4-12 Termination impedance constant for Tuner Length experiments

Figure 4.13 illustrates the recorded values of X_u for the termination impedance. This is compared to the associated average power of the tuner inlet and tuner outlet pressure signals, at the 1st order pump frequency in Figure 4.14.

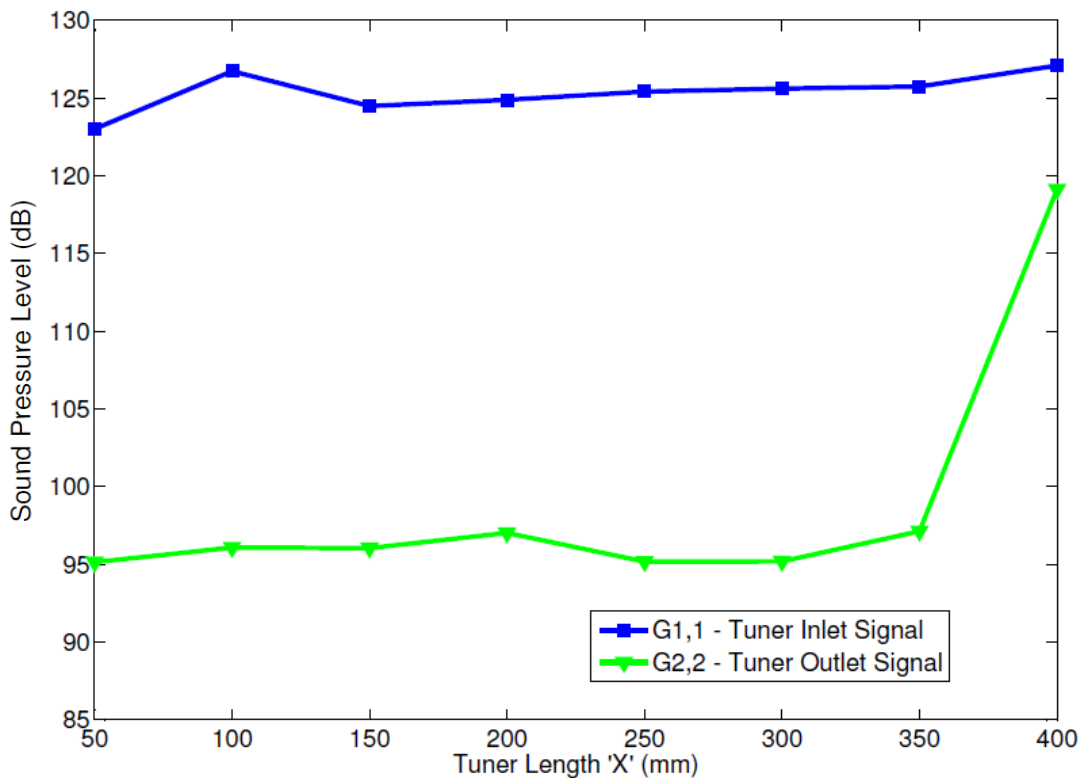


Figure 4-13 Power spectrum - Tuner inlet vs Tuner outlet for various tuner lengths

As can be seen from Figure 4.14, the magnitudes at the inlet and outlet remain reasonably constant with Tuner Length, fluctuating around 125 and 95 dB respectively for each tuner construction. However a sharp increase in outlet magnitude is noted for the 400mm tuner. Interestingly, whilst the magnitudes are different, the trend of the X_u plot has resemblance to the Tuner Outlet signal. It is possible that the two are related. This will be discussed in greater detail in Chapter 5.

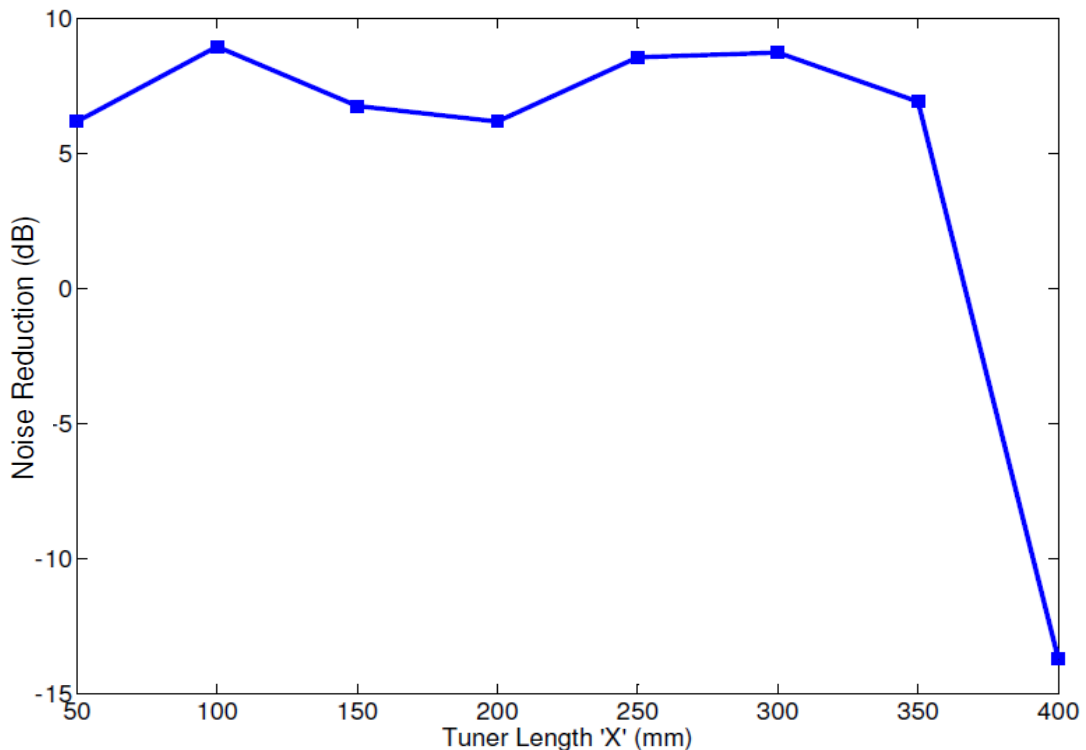


Figure 4-14 Tuner Length Experiments – Measured Noise Reduction

In any case, these results suggest that the introduction of the different tuner test samples have a significant impact on the downstream pressure in the system. This confirms the reasoning in adopting an empirical approach to model the system termination impedance as proposed in Chapter 3.

The first order noise reduction magnitude of each tuner construction versus tuner length is shown in Figure 4.14. The first observation that can be made from the results is that the noise reduction recorded is quite small in terms of total attenuation observed for a power steering hose assembly – in the range between 5-10dB. This is quite apparent when comparing the difference in magnitudes in Figure 4.14. This would suggest that the tuner length itself has a minor influence in overall system noise reduction.

The peak attenuation is provided by the 100mm tuner with a noise reduction value of 8.9 dB. However observing the apparent oscillatory pattern in the results, it may be the case that there is an optimal tuner with a length somewhere between 250mm and 300mm. Further testing would be required to confirm this.

The 400mm tuner is an outlier in this result set, and the reason for this large negative spike is not understood from this experiment alone. Excluding this result, the oscillatory pattern of the results with frequency may suggest that the introduction of the tuner is influencing wave propagation in the system, where the peaks for the 100mm and 300mm tuners are the result of destructive interference with the propagating wave. In contrast the 50mm and 200mm tuners would appear to be attenuating the propagating wave to a lesser extent. Further testing is required to confirm the existence of this trend.

Whilst the magnitudes of the noise reduction results presented in Figure 4.14 are quite small, they are nonetheless significantly different, which would go some way to explaining the reason for the spread of different length tuners in the current market. Additionally, the oscillatory pattern would suggest that it is possible to minimise and therefore optimise tuner construction from a commercial point of view.

4.5 Tuner Hole Location Experiments

As previously discussed, almost all commercially available power steering hoses containing plastic tuners incorporate pressure relief holes. The purpose of this experiment is to understand the impact of the location of a single hole (through bore) on overall tuner noise reduction for a fixed tuner length. Additionally this will investigate the claim (Merkel, 2004) that the holes can change the acoustic performance of the line. The tuners used in this experiment were constructed according to Figure 4.15 and Table 4.4.

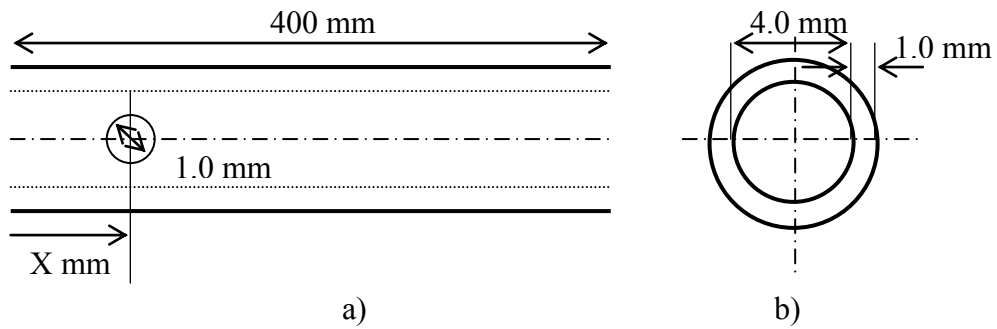


Figure 4-15 Hole location test sample a) longitudinal cross section b) end view

Table 4-4 Hole location test sample construction

Hole Position 'X' mm	Sample Designation
50	I
100	J
150	K
200	L
250	M
300	N
350	O

4.5.1 Tuner Hole Location Test Procedure

The procedure and equipment used in this test were identical to that used in the Tuner Length experiments described in Section 4.4.1. However, in this case the sample tuners were assessed against a tuner 400mm in length containing no holes (sample H from Tuner Length experiments). The result of sample H was subtracted from the result of each sample I-O, to provide an approximation of the resultant noise reduction attributed solely to the pressure relief hole introduction at each location in Table 4.4. By plotting the magnitude of the 1st pump order (in this case at ~333Hz) against 'X', an understanding of hole location impact on overall system noise reduction can be gained.

4.5.2 Tuner Hole Location Test Results

Figure 4.16 illustrates the recorded values of X_u for the termination impedance. Figure 4.17 illustrates the relationship between the power spectrum of the tuner inlet and tuner outlet pressure signals, at the 1st order pump frequency.

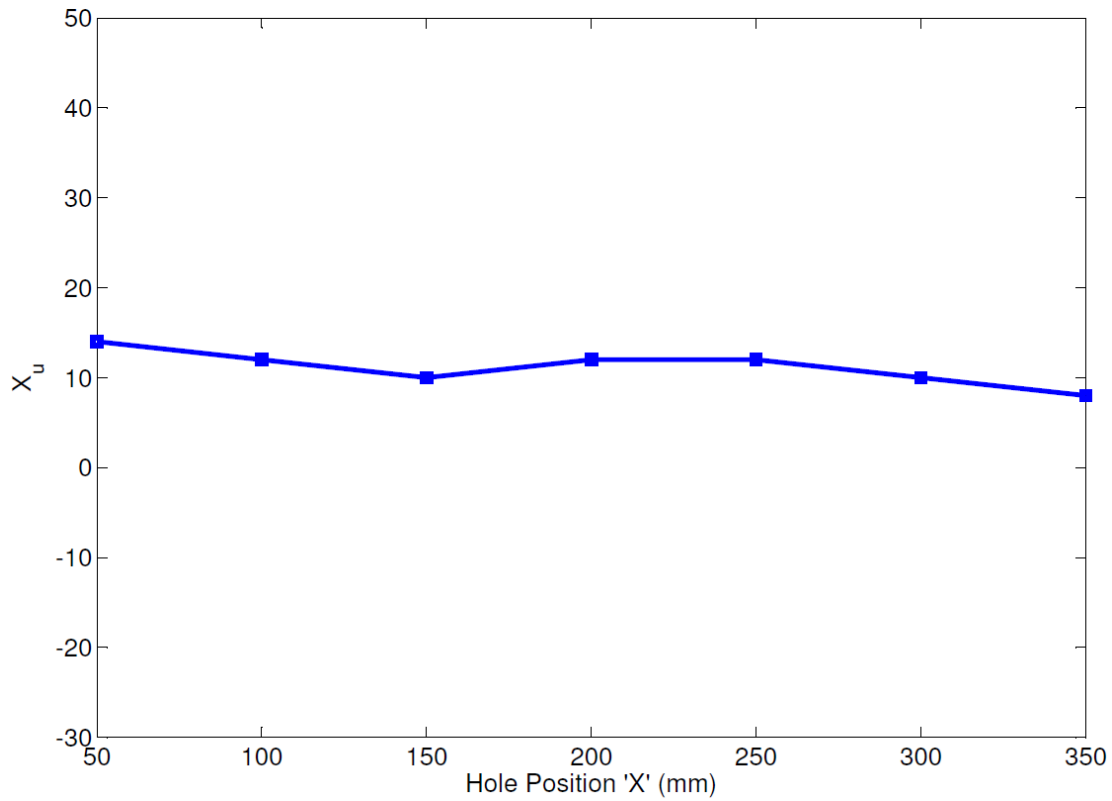


Figure 4-16 Termination Impedance Constant for Hole Position Experiments

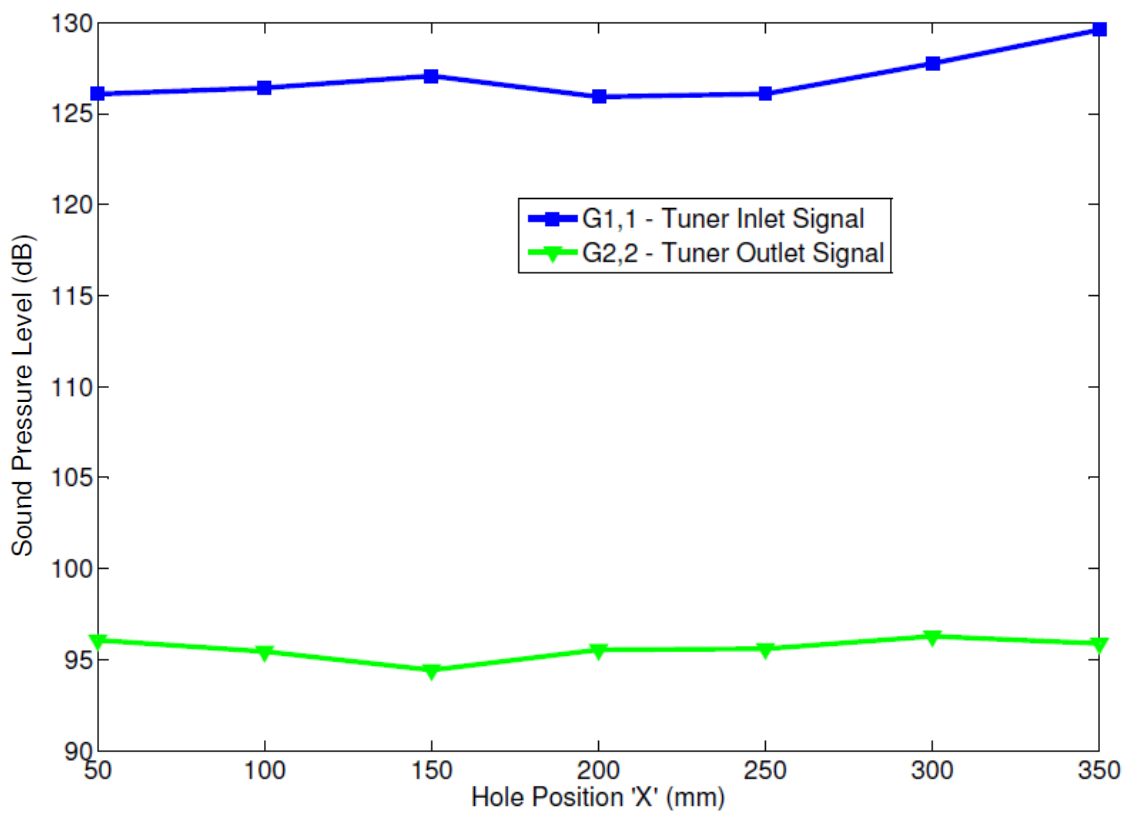


Figure 4-17 Power spectrum - tuner inlet vs tuner outlet for various positions of a single hole

Once again, there is a striking similarity when comparing the trend of the X_u plot to the tuner outlet signal. Additionally, when comparing the plot in Figure 4.17 to that illustrated in Figure 4.13, it can be observed that there is an increase in the sound pressure level at the tuner inlet over the range of test samples. It is proposed that this increase is a result of the increase in acoustic impedance between the two measuring points, when comparing a tuner without a pressure relief hole (Figure 4.13) to a tuner containing a pressure relief hole (Figure 4.17).

It should be noted that the position of the holes was measured with a steel rule and marked accordingly. Minor variances in actual versus desired hole position and diameter as a result of the measurement and drilling process may account for a variance in results. Further testing is required to quantify the impact of the hole, particularly holes of different size, and is explained in Section 4.6.

Focussing on hole position effects, Figure 4.18 illustrates the relationship between hole position and 1st order pump noise reduction for each of the test samples. Once again the change in noise reduction from sample to sample is quite small – approximately 4dB maximum. Despite this, it appears from the results that the location of the hole has a significant influence on the noise reduction. Whilst the magnitudes are relatively small when compared to total noise reduction, the results show that a translation of the hole position by as little as 50mm can have more than a 10% change in noise reduction magnitude between two locations such as between the 150mm and 200mm tuner. This is important, as whilst it would appear that there is additional benefit to be gained from adding pressure relief holes to the tuner, it may also be desirable to optimise overall tuner performance by appropriately selecting a pressure relief hole location, i.e. potentially gaining an extra 3dB in noise reduction.

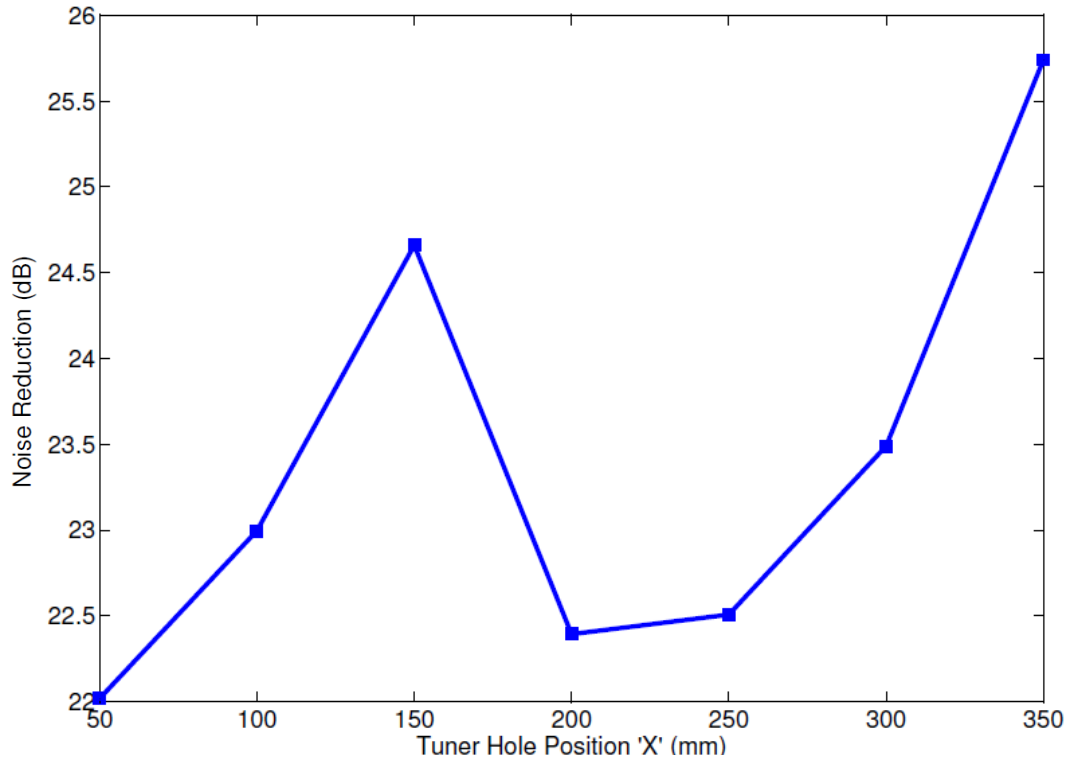


Figure 4-18 Hole Location Experiment – Measured Noise Reduction

4.6 Tuner Hole Diameter Experiments

The purpose of these experiments is to investigate the noise reduction performance of a tuner with a varied pressure relief hole diameter, at a fixed location, for a fixed length of tuner.

The test samples used in this experiment were constructed according to Figure 4.19 and Table 4.5. As the purpose of the relief hole is not fully understood at this stage, it is noted that in all existing examples reviewed, the pressure relief holes are normally located in the 1st quarter of the overall tuner length. For the purpose of this experiment the hole location is not considered critical, but for consistency the hole is positioned at 100mm from the inlet of the 400mm tuner.

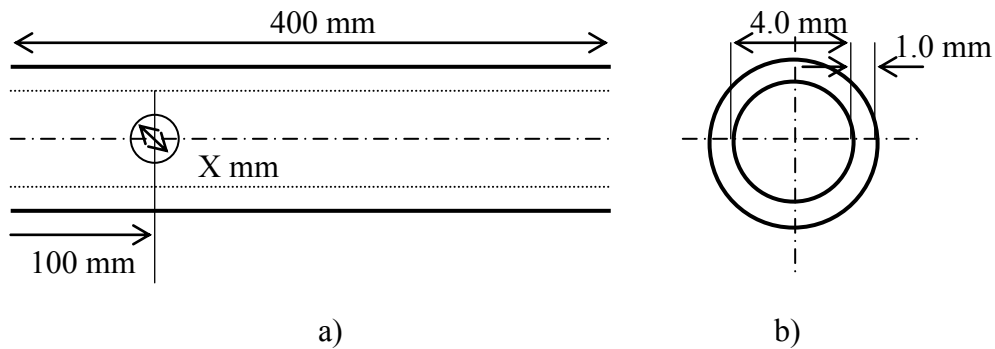


Figure 4-19 Hole diameter test sample a) longitudinal cross section b) end view

Table 4-5 Hole Diameter test sample construction

Hole Diameter 'X' mm	Sample Designation
1.0	A1
1.5	B1
2.0	C1
2.5	D1
3.0	E1

4.6.1 Hole Diameter Test Procedure

The procedure and equipment used in this test were identical to that used in the Tuner Length experiments described in Section 4.4.1. The noise reduction attributed to the hole profile was approximated by deriving a noise reduction for each test sample from experimental measurements and then subtracting the noise reduction of a tuner of identical length (400mm) containing no holes. Plotting the resultant noise reduction at the coinciding 1st order pump frequency against hole diameter, an understanding of varying hole diameter on attenuation performance can be gained.

4.6.2 Hole Diameter Test Results

The results illustrated in Figure 4.20 show that the diameter of a hole for a given location along the tuner length is a significant factor with respect to overall system noise reduction. It is noted that for some samples the prefix of the resultant magnitudes is negative. This indicates an amplification of the pump generated noise as a result of introducing each varied hole diameter profile to the tuner. Comparing the results for the 1.0mm and 1.5mm hole test samples, there is more than a 25dB drop with respect to noise reduction, which based on previous experimental results, is almost enough to completely negate the overall noise reduction developed by the entire tuner/hose solution.

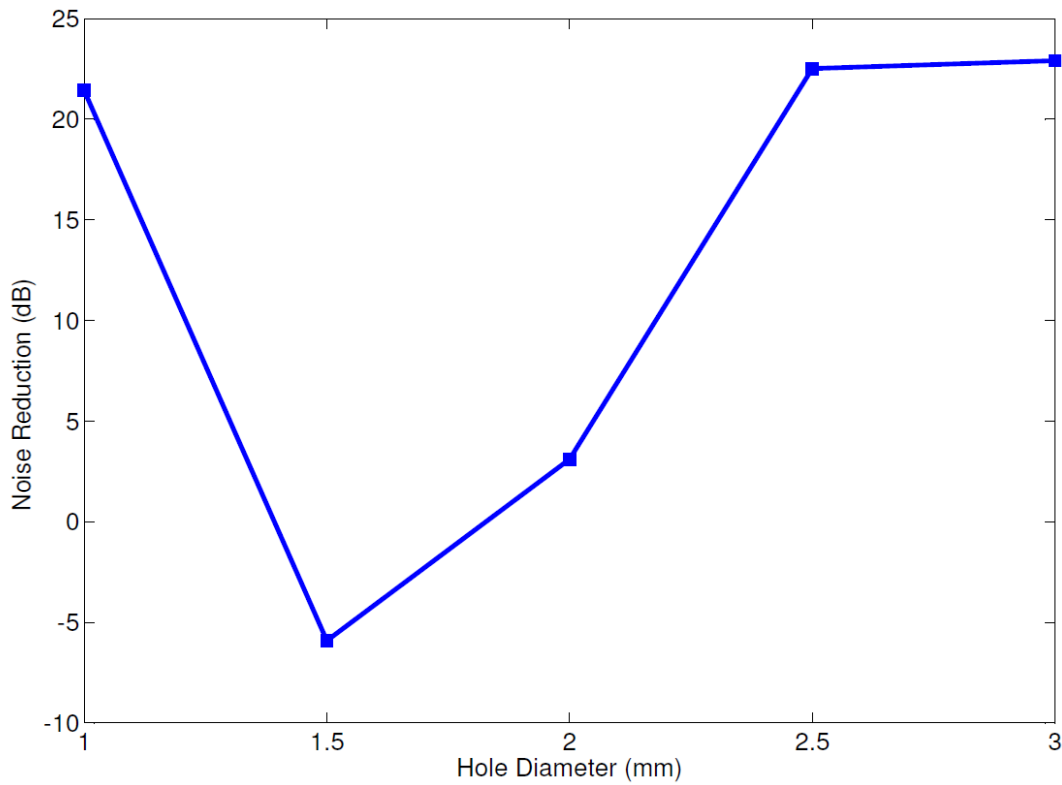


Figure 4-20 Impact of changing hole diameter on noise reduction

Considering the termination impedance for this experiment, Fig. 4.21 illustrates the recorded values of X_u . Figure 4.22 illustrates the relationship between the power of the tuner inlet and tuner outlet pressure signals, at the 1st order pump frequency.

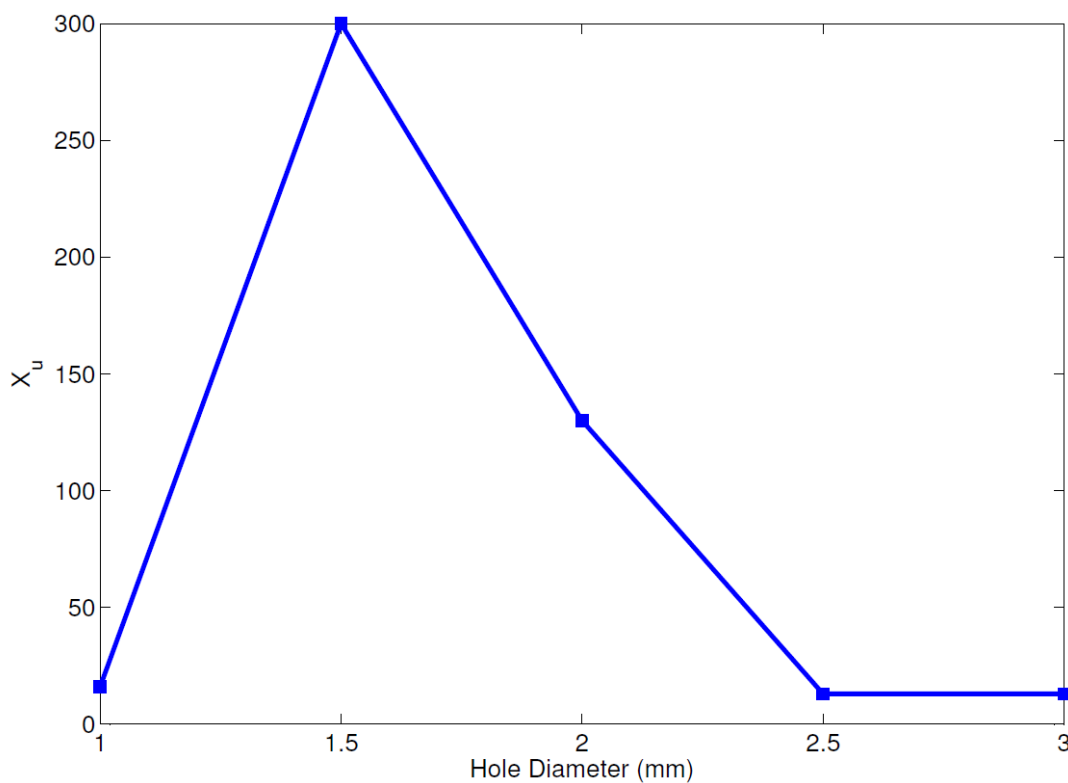


Figure 4-21 Termination Impedance Constant for Hole Diameter Experiment

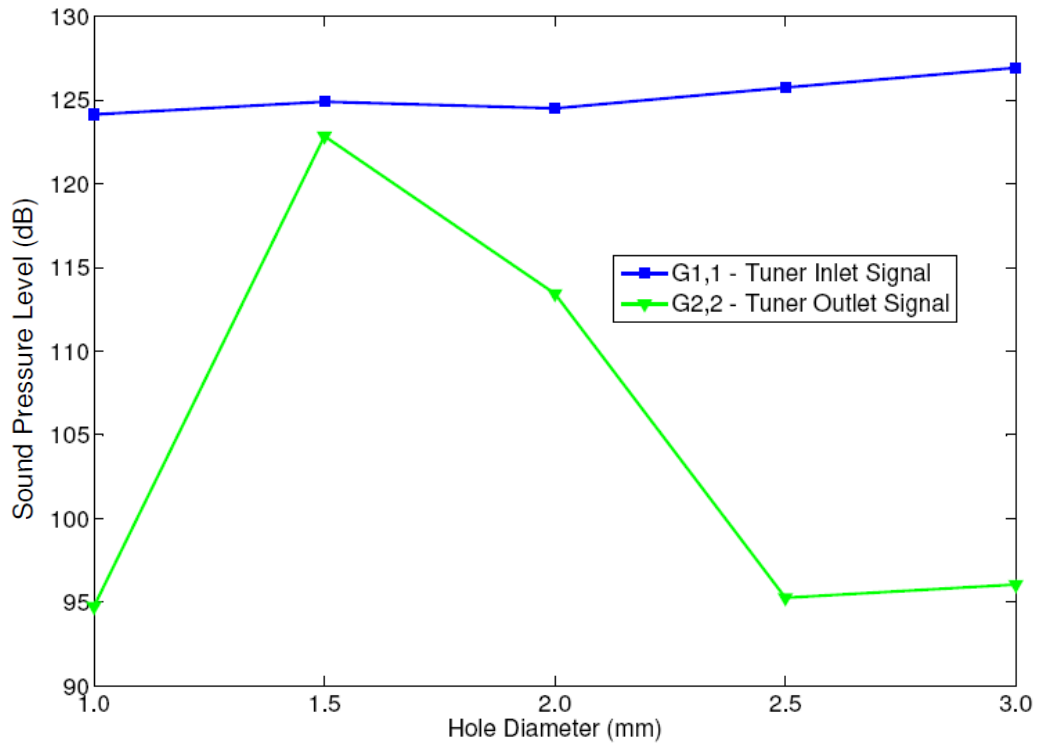


Figure 4-22 Tuner inlet signal vs tuner outlet signal for hole diameter experiment

It should be noted that the holes were created in the test samples by a drilling process and subsequent de-burring operation. Minor differences in hole profile from the desired test sample size may be contributing to varied results. If this manufacturing process proves to be critical, i.e. the hole diameter is a significant factor in tuner attenuation properties, it will be a process that will need to be refined and developed for a production environment. Suggested alternatives to the drilling operation include ‘Hot Piercing’ and ‘Laser Cutting’.

4.7 Multi-hole Tuner Experiments

Several of the commercially available tuners that have been reviewed earlier in this document contain multiple pressure relief holes, of the same diameter, at fixed intervals along the tuner length. An example of such a tuner is illustrated in Fig. 4.23, which is a photograph of a tuner used on BMW Series 5 vehicles. The purpose of this experiment is to understand the use or benefit of such tuner constructions when compared to tuners of singular hole design. There may be some commercial benefit to minimising the number of holes on a tuner for a given system and therefore it is important to understand why some designs employ multiple holes and others contain only one.

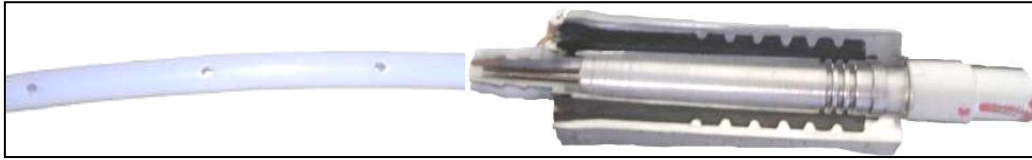


Figure 4-23 BMW 5 Series Plastic Tuner

The test samples used in this experiment were constructed according to Figure 4.24 and Table 4.6.

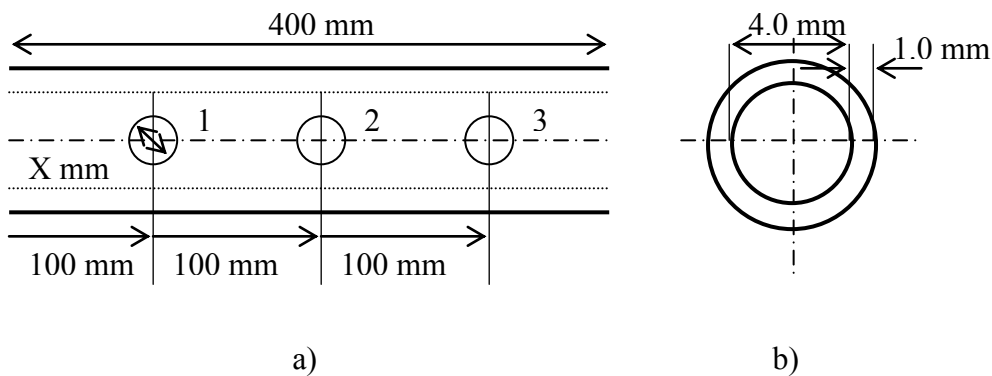


Figure 4-24 Multi-hole test sample a) longitudinal cross section b) end view

Table 4-6 Longitudinal cross section of multi-hole test sample

Hole Diameter 'X' mm	Sample Designation		
1.0	A1	A2	A3
1.5	B1	B2	B3
2.0	C1	C2	C3
2.5	D1	D2	D3
3.0	E1	E2	E3

4.7.1 Multi-hole Tuner Test Procedure

The procedure and equipment used in this test were identical to that which was used in the Tuner Length experiments described in Section 4.2.1. The noise reduction attributed to the hole profile was approximated by obtaining results for each test sample and then subtracting the result of a tuner of identical length (400mm) containing no holes. The results for tuner constructions A1-E1 have already been obtained from a previous experiment detailed in Section 4.6. These results together with the new results will be plotted to compare noise reduction for each diameter hole and each tuner construction i.e. one, two or three holes per tuner.

4.7.2 Multi-hole Tuner Test Results

Figure 4.25 illustrates the results of the multi-hole tuner test specimens. The first conclusion that can be drawn from the results is that multi-hole tuner configurations have a significantly different impact on the system attenuation when compared to singular hole tuner constructions.

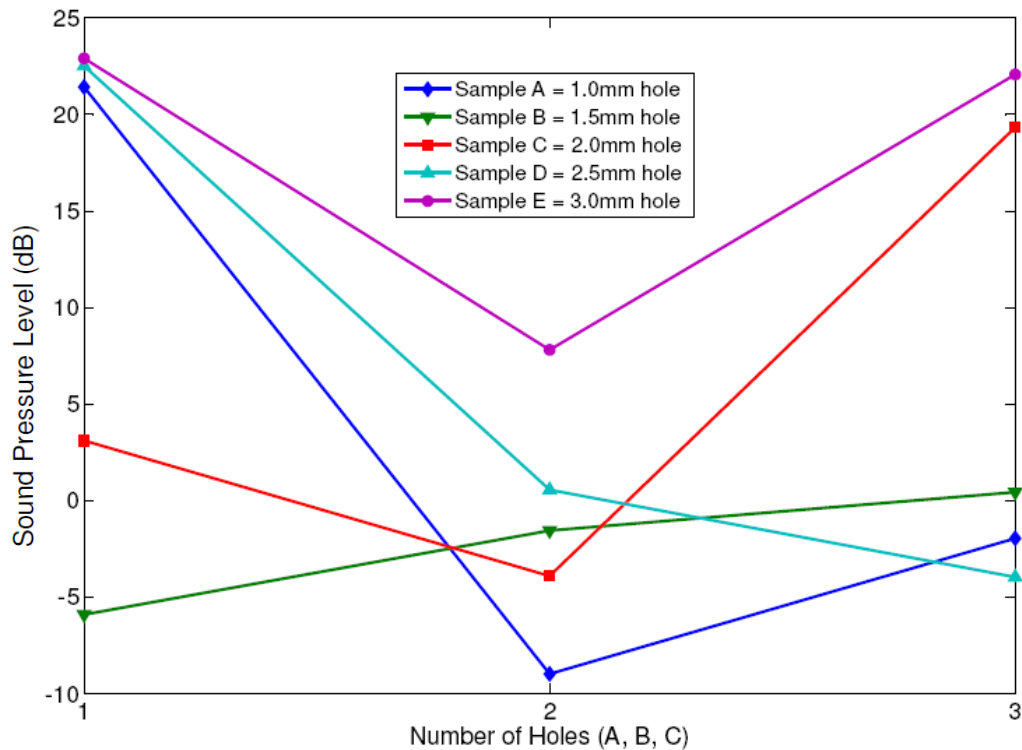


Figure 4-25 Comparison of one, two or three equally spaced holes of common diameter.

Within the bounds of this experiment it can be observed that there is a potential of 30dB to be gained from multi-hole tuner constructions when considering the difference between minimum (sample A2) and maximum (sample E3) results. However, a similar potential could be lost by moving from a single hole tuner (sample A1) to the multi-hole tuner construction (sample A2). This experiment has emphasised the significance of the tuner hole diameter.

For example, in nearly all cases two holes are less effective than one (except Sample B) and similarly three holes are more effective than two (except Sample D). In most cases multi-hole tuners are only better than single hole tuners if hole diameter is varied in addition to the perforation rate. One result that is significant is that there are two instances of three holes out-performing one (Sample B and Sample C). In both of these cases the tuner hole diameters are very close to each other in size. This may suggest

that the hole diameter is perhaps a primary function whilst the perforation rate is secondary when calculating optimal noise reduction. This would explain why some commercially available products have multiple hole constructions whilst others have only single holes. Interestingly, the BMW tuner discussed in Figure 4.23 has holes with a diameter of 2.0mm. Based on the results in this test, it would be logical to assume that an engineer following the ‘cut and try’ development method for a similar application, would arrive at a three hole tuner. It should be noted, however, that there are a number of factors that may have an influence on the results obtained here and those obtained elsewhere e.g. tuner length, tuner diameter, tuner material, pump geometry etc.

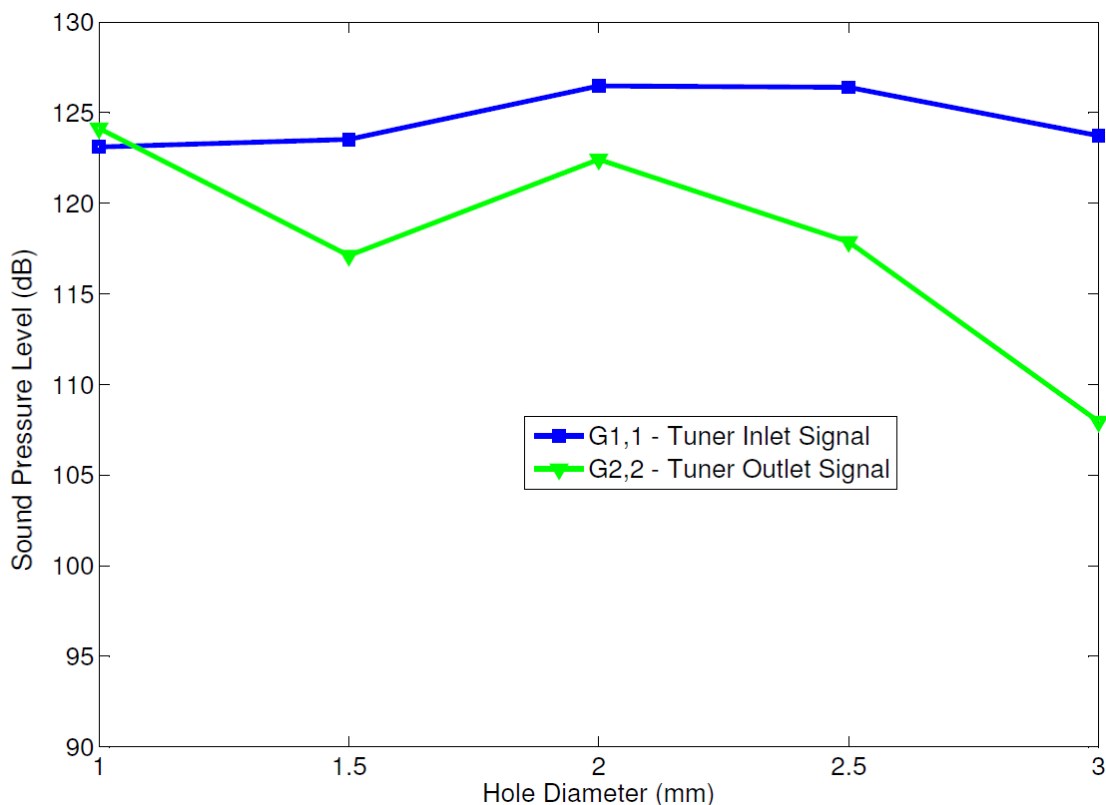


Figure 4-26 Tuner inlet vs tuner outlet for two-hole tuner experiments

Figure 4.26 illustrates the input and output sound pressure level for the two-hole configuration. Figure 4.27 illustrates the associated values of X_u for the termination impedance. Three hole auto power spectra and termination impedance constant plots are shown in Figures 4.28 and 4.29 respectively.

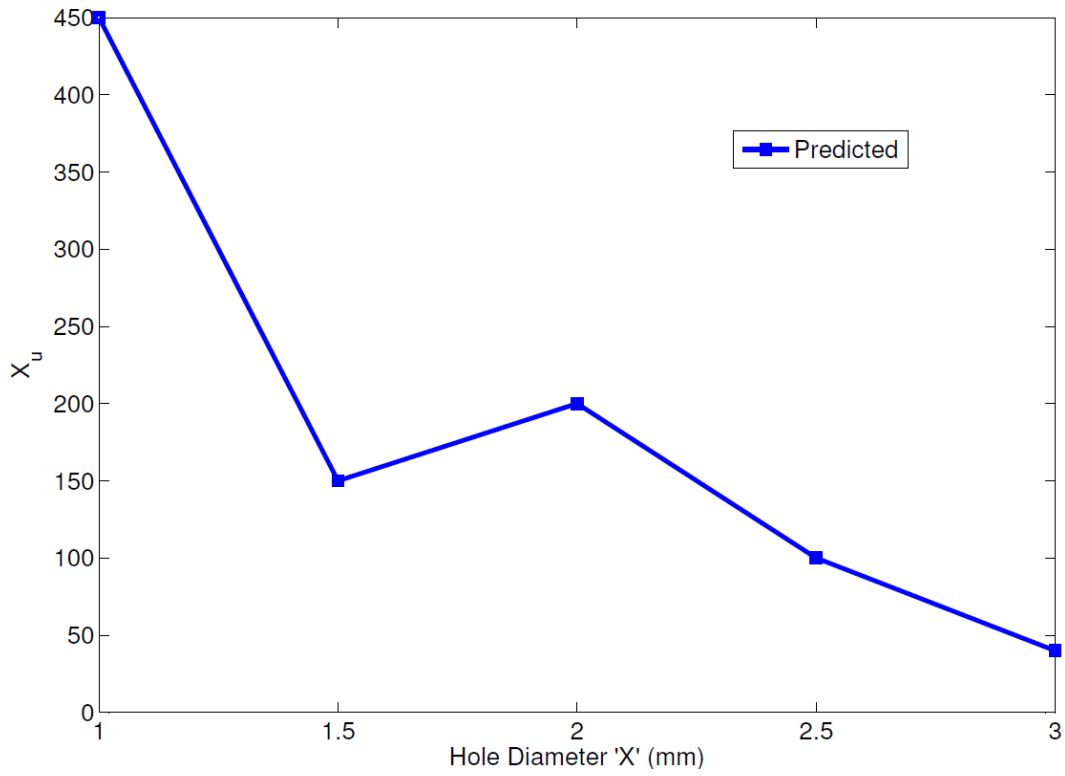


Figure 4-27 Termination Impedance Constant for two-hole experiments

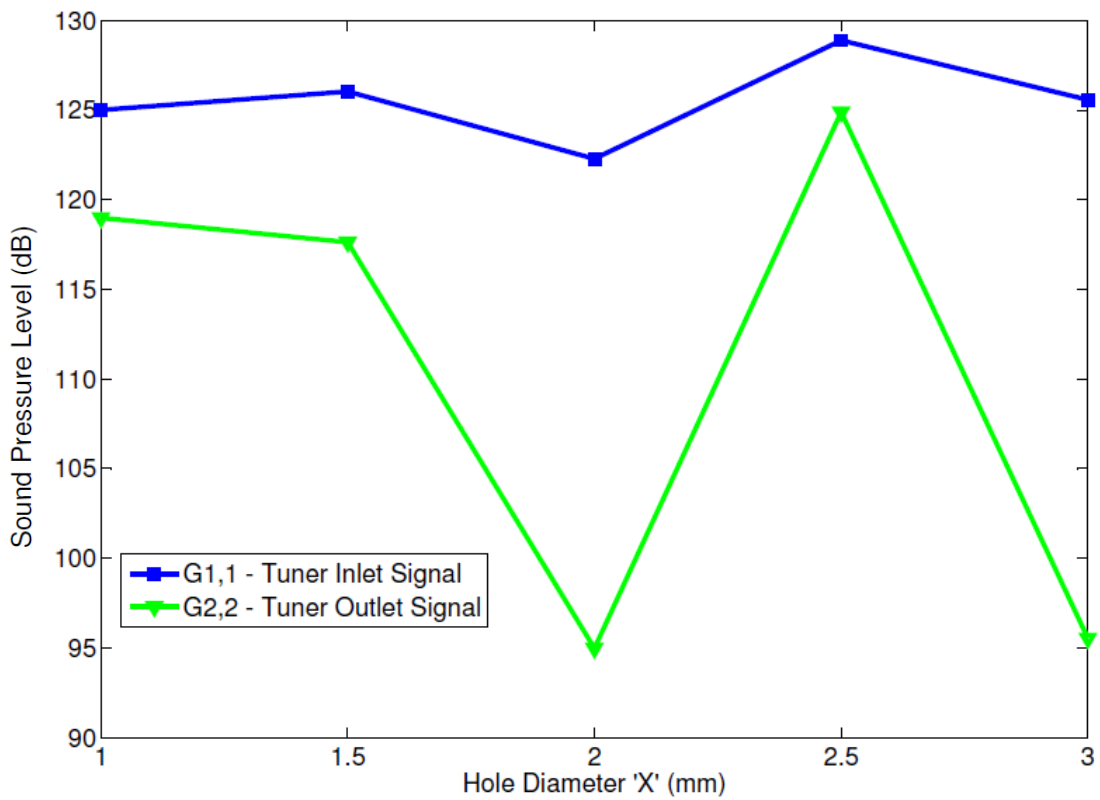


Figure 4-28 Tuner inlet vs tuner outlet for three-hole tuner experiments

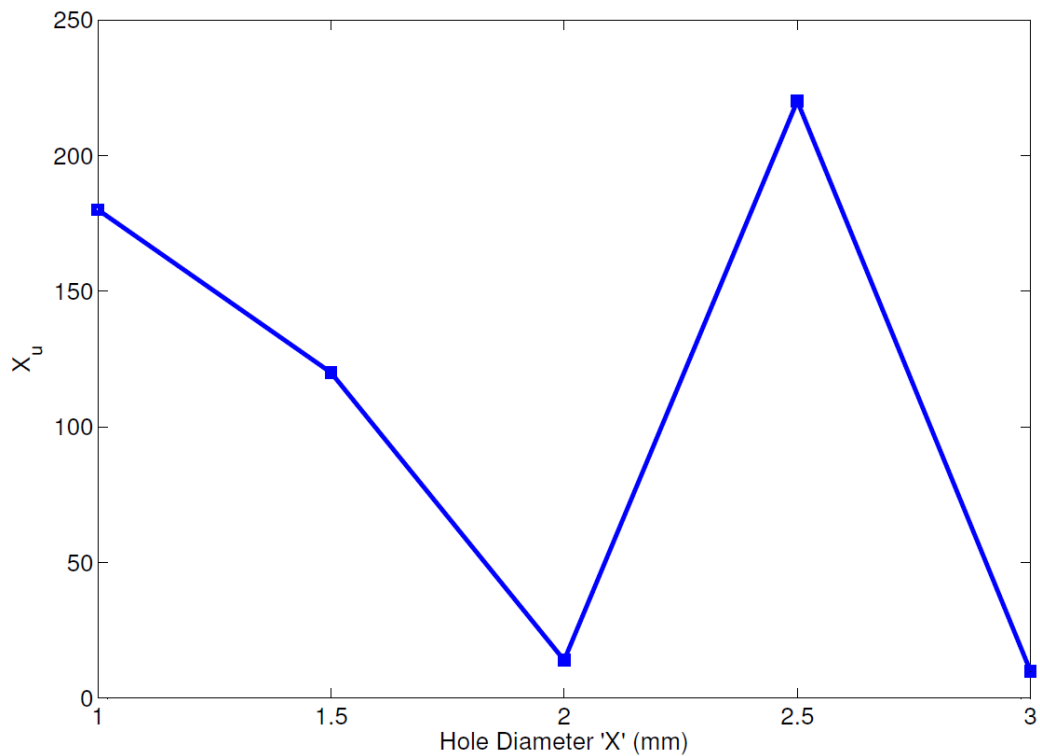


Figure 4-29 Termination Impedance Constant for three-hole experiments

As with all the other experiments described previously, Figures 4.28 and 4.29 suggest a relationship between the pressure measured at the tuner outlet and the constant used to calculate the termination impedance. At this stage it is unclear exactly what this relationship may be, however it is possible that it may be similar to the relationship proposed by Ichiyanagi (2008) when investigating the insertion loss characteristics of a side branch resonator. This theory is discussed further in Chapter 5.

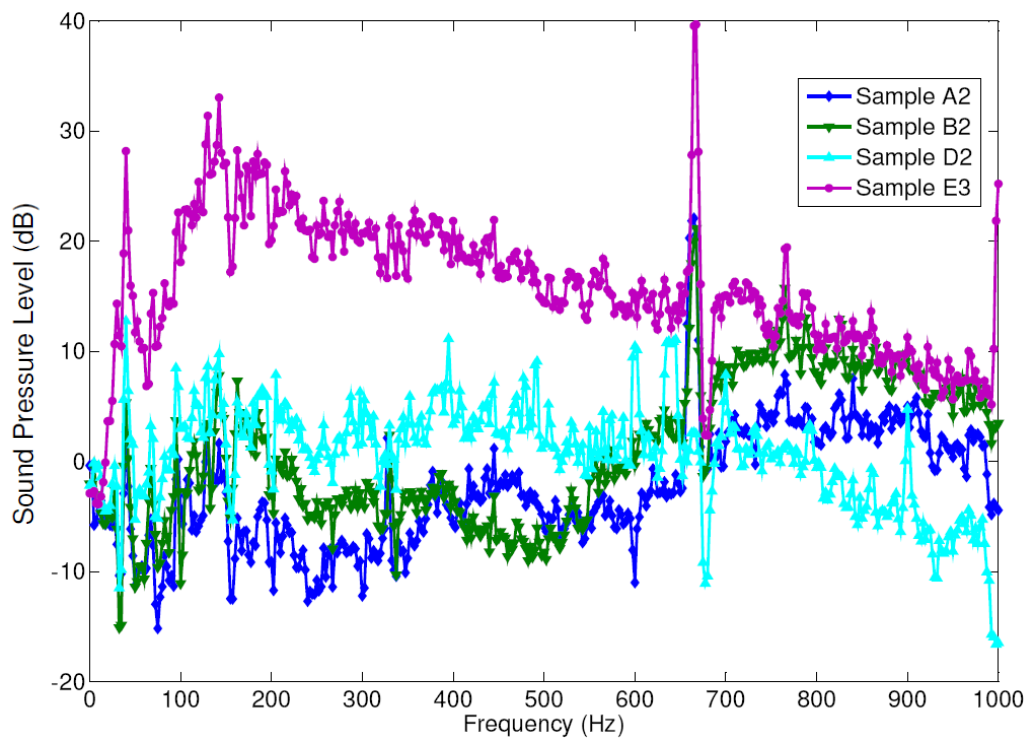


Figure 4-30 Selected broadband attenuation results for multi-hole test samples

Another important performance characteristic that needs to be considered with plastic tuner design is broadband noise level attenuation, as described in Section 2.5.3. Figure 4.30 illustrates the associated broadband noise levels for some of the multi-hole test sample results described previously.

As can be observed from the test results, the best multi-hole tuner construction E3 also provides significant attenuation at 2nd and 3rd pump orders and is generally >10dB over the 0-1000Hz range. In comparison, sample D2 which provides little noise reduction over the whole range, deteriorates rapidly in performance for higher pump orders. Sample B2 amplifies pump noise at lower frequencies and attenuates pump noise as frequency is increased.

From this set of results it is clear that 1st pump order noise reduction cannot be the only consideration when selecting an appropriate tuner construction. At the very least, broadband results should be checked to ensure the tuner construction is not creating a noise issue at other frequencies. This conclusion is aligned with the explanation previously given in Section 2.5.3 and relates to similar broadband noise concerns associated with Turbofan engines, as highlighted by Burdisso (2000).

4.8 Conclusions

A series of experiments have been completed to examine the various design parameters of plastic tuners, and to evaluate the gaps in the knowledge base as identified by the literature review in Chapter 2. The key findings addressing the key objectives may be summarised as follows;

- In comparing the plastic tuner with the spiral wound steel tuner, the plastic tuner has a similar level of performance when compared to the spiral wound steel tuner, dependant on its construction. A key finding is that the plastic tuner invokes a lower system back pressure than the spiral wound steel tuner, which is good for system component life.
- The evaluation of tuner length, has illustrated that the overall length of tuner is considered a minor factor in optimising tuner performance and overall system noise reduction. The maximum reduction to be gained from this feature falls in the range 5-10dB. However, as tuner length performance appears to oscillate between fixed maximum and minimum values as tuner length is increased, it is possible to minimise tuner length and so optimise tuner length from a commercial (materials use) viewpoint.
- Introducing pressure relief holes to the tuner design has the potential to provide a significant increase in noise reduction when compared to a tuner of identical length containing no holes. Additionally, depending on the location of the hole, there can be a further gain in noise reduction of up to approximately 3dB. This result also promotes the concept of an optimal hole location.
- The diameter of a pressure relief hole at a fixed location is critical in determining the resultant noise reduction of the tuner. Varying the hole diameter by as little as 0.5mm can significantly alter (>25dB) the noise reduction of the tuner.
- Depending on hole diameter and perforation rate, multi-hole tuner constructions can perform significantly better (>30dB) than single hole tuner constructions. Additionally as part of experimental results gained during the completion of the

multi-hole tuner experiments, it has been noted that broadband noise levels can be significantly affected depending on plastic tuner construction. It is important to check these levels as fundamental pump frequency noise reduction levels cannot be viewed in isolation when selecting an appropriate tuner design.

4.9 Summary

An experimental method for obtaining noise reduction for a number of different plastic tuner designs has been presented. Design parameters have been quantified within the bounds of the experiments and observations discussed. Further analysis of these results will be presented in Chapter 5.

In addition, it appears that a relationship exists between the termination impedance and the pressure measured at the point immediately downstream of the tuner. Further analysis is required to define this relationship and a theoretical model is outlined in Chapter 5.

5 Results and Analysis

In this chapter the theoretical model presented in Chapter 3 is validated using the experimental data captured using the methodology presented in Chapter 4.

The chapter starts with a brief summary of the approach which is applied to the experimental and theoretical results for each tuner configuration. Results for each configuration are then analysed and presented in relation to the pump fundamental frequency, which is the frequency of greatest interest in power steering noise reduction. The chapter ends with an analysis of the suggested relationship between the tuner outlet pressure and the system termination impedance.

5.1 Tuner Length Validation

The first configuration of the model to be validated, relates to the key objective concerned with the tuner length. The purpose of this section is to validate the elements of the model concerned with a tuner containing no holes, where the overall length of the tuner is varied. The model should represent the change observed during the associated experiments, where an oscillatory pattern of results was observed for the results pertaining to the pump fundamental frequency.

5.1.1 Analysis and discussion

As described previously in Section 3.3, noise reduction is the parameter best suited to evaluating plastic tuner noise performance. Having said this, it is also important to analyse the model construct, and for this reason, transmission loss is utilised to evaluate the predicted performance of the model in isolation of any termination effects. Equation 3.3 was used to calculate the theoretical transmission loss of the samples in this experiment.

To validate the accuracy of the model, noise reduction is used to compare predicted and experimental performance of the tuner samples. Firstly, Equation 3.2 was used to calculate the theoretical noise reduction of the samples in this experiment. Following this, Equation 4.1 was used to calculate the experimental noise reduction using the measured data captured during the experimental phase. Each discrete sample is illustrated in Figures 5.1 – 5.16.

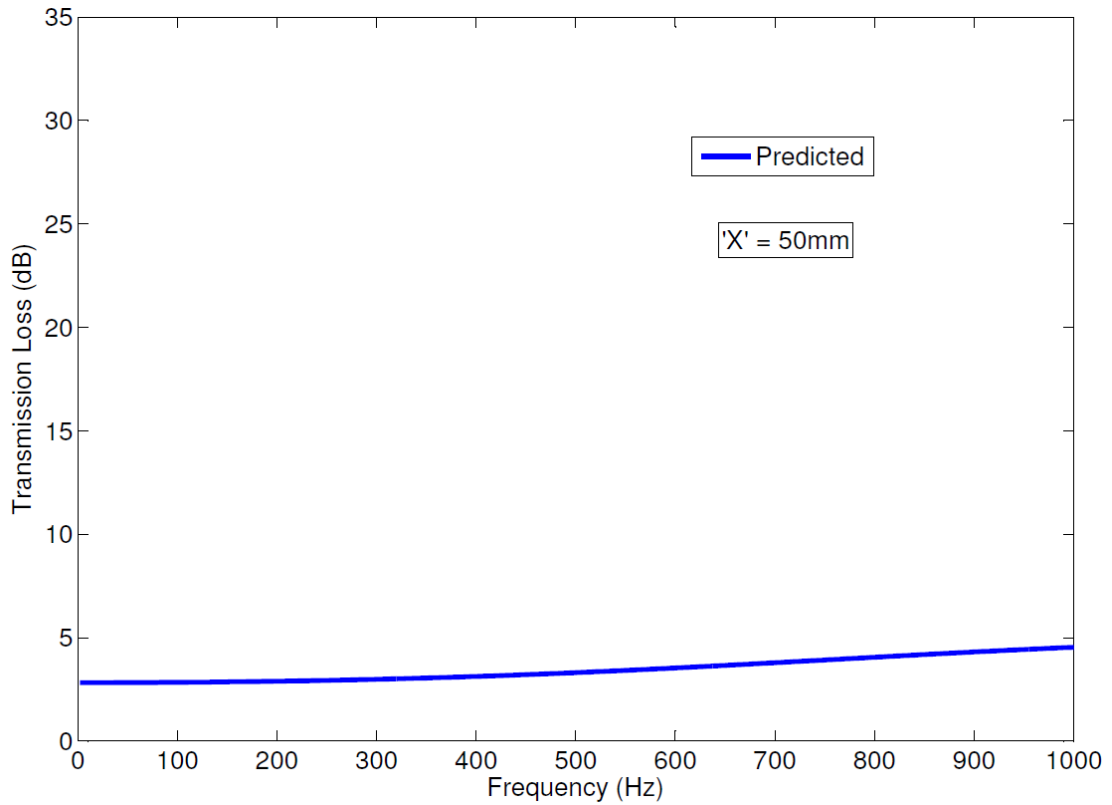


Figure 5-1 Predicted Transmission Loss for a 50mm long tuner

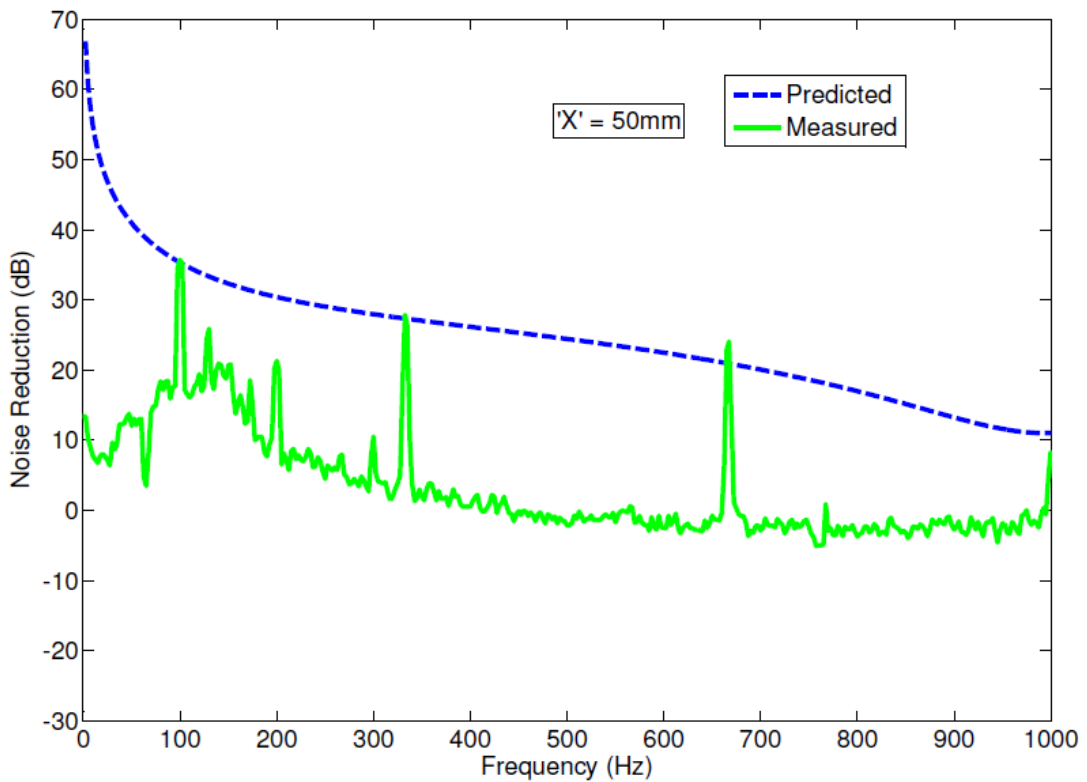


Figure 5-2 Predicted versus Measured Noise Reduction for a 50mm long tuner

It should be noted that for the measured results, the system is excited by the pump, therefore only the pump orders at approximately 333Hz, 666Hz and 999Hz are significantly excited.

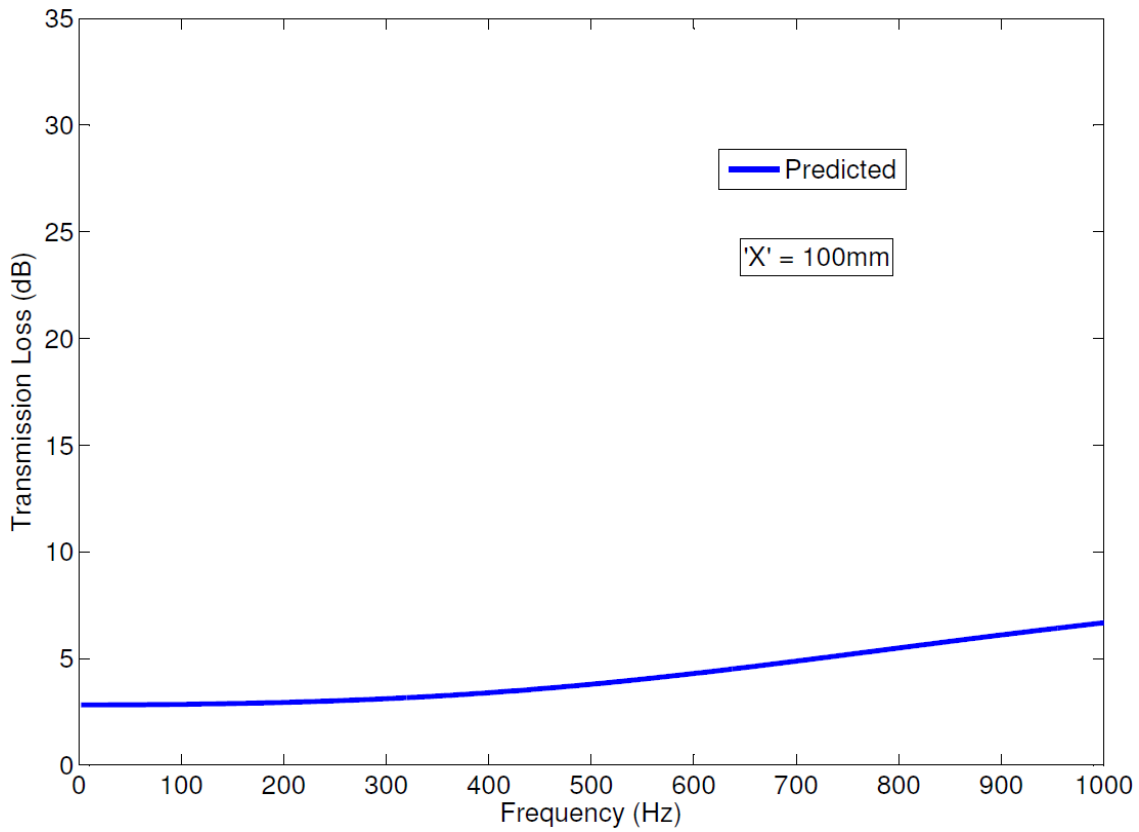


Figure 5-3 Predicted Transmission Loss for a 100mm long tuner

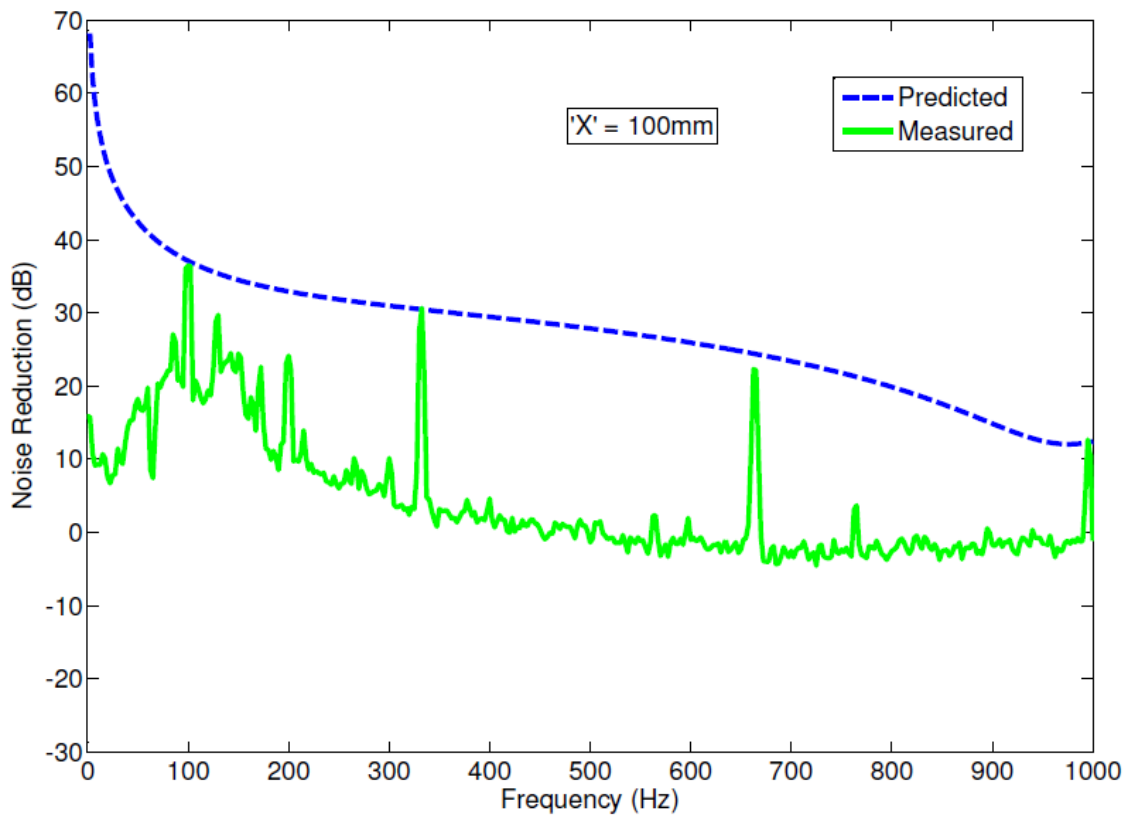


Figure 5-4 Predicted versus Measured Noise Reduction for a 100mm long tuner

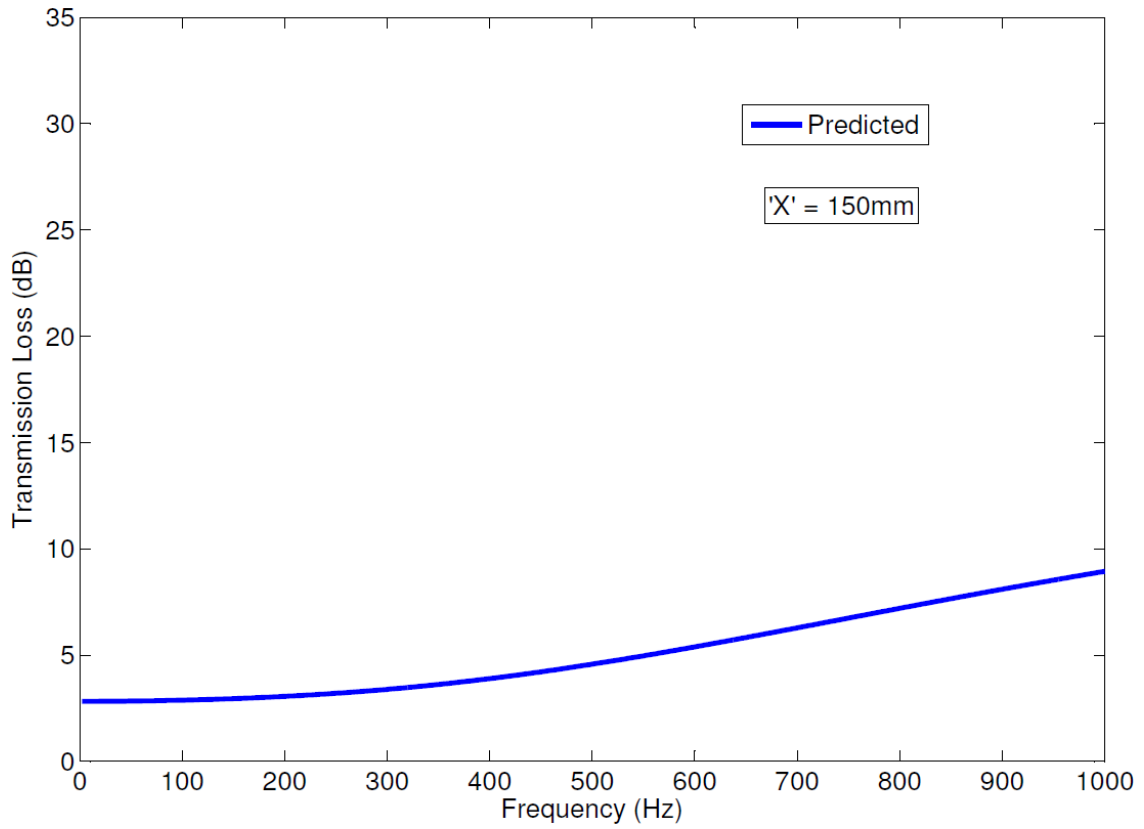


Figure 5-5 Predicted Transmission Loss for a 150mm long tuner

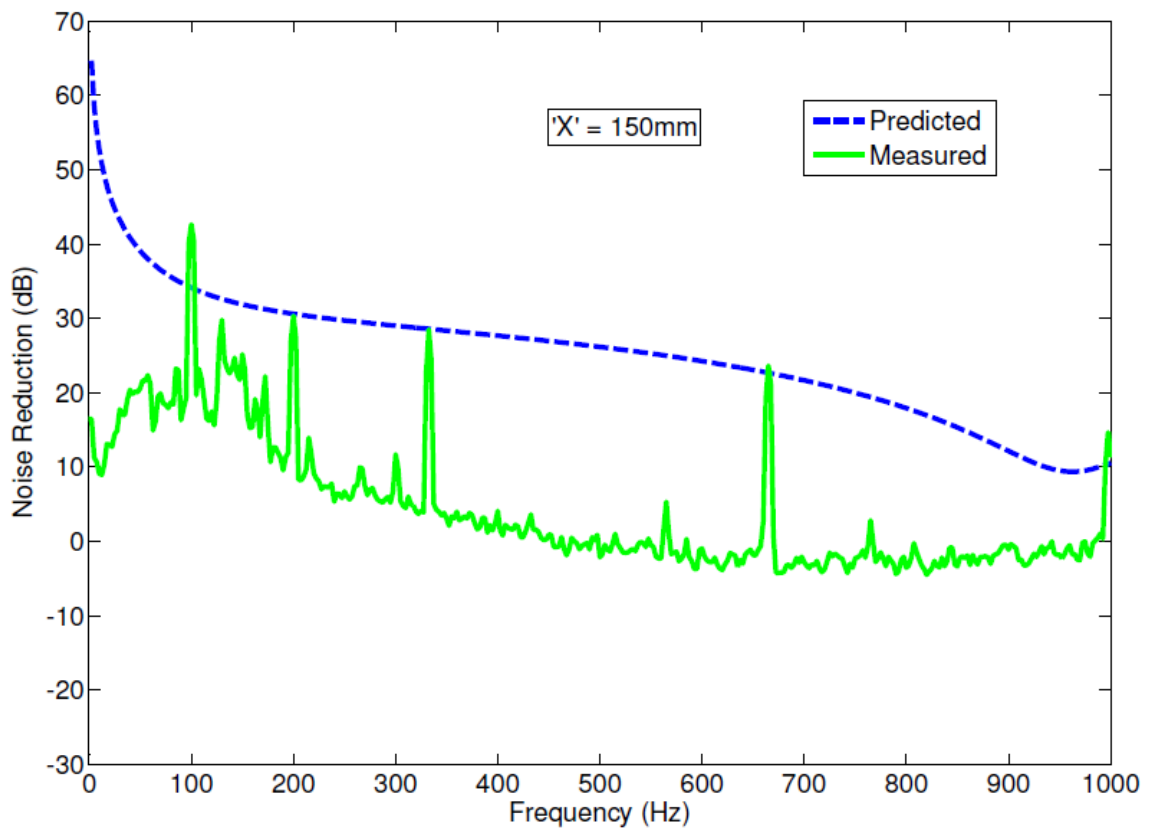


Figure 5-6 Predicted versus Measured Noise Reduction for a 150mm long tuner

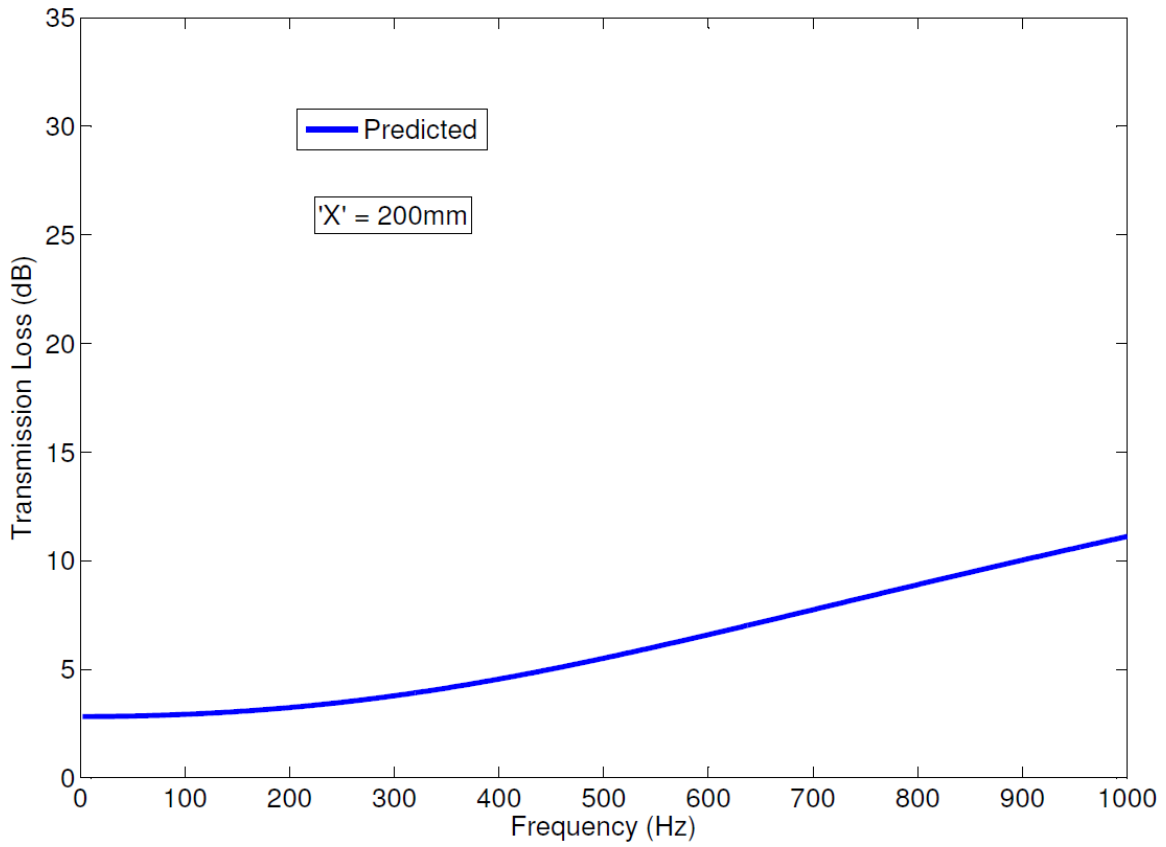


Figure 5-7 Predicted Transmission Loss for a 200mm long tuner

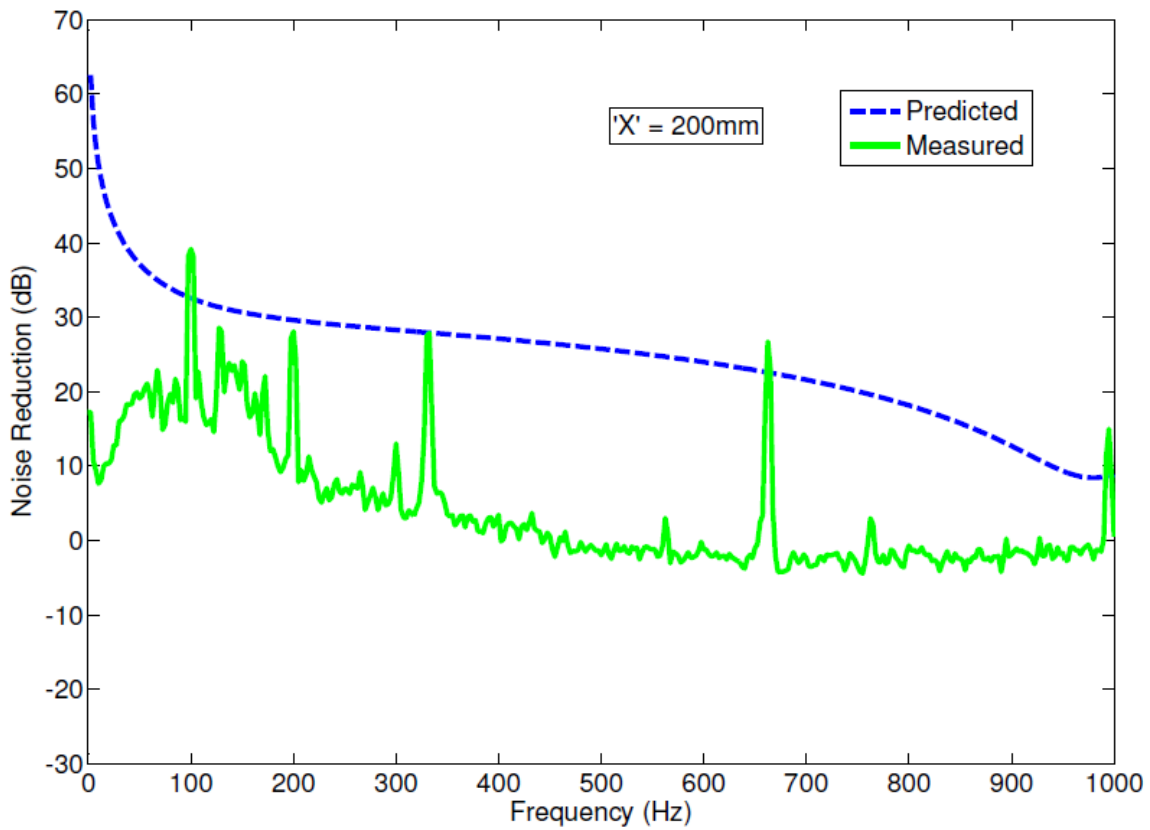


Figure 5-8 Predicted versus Measured Noise Reduction for a 200mm long tuner

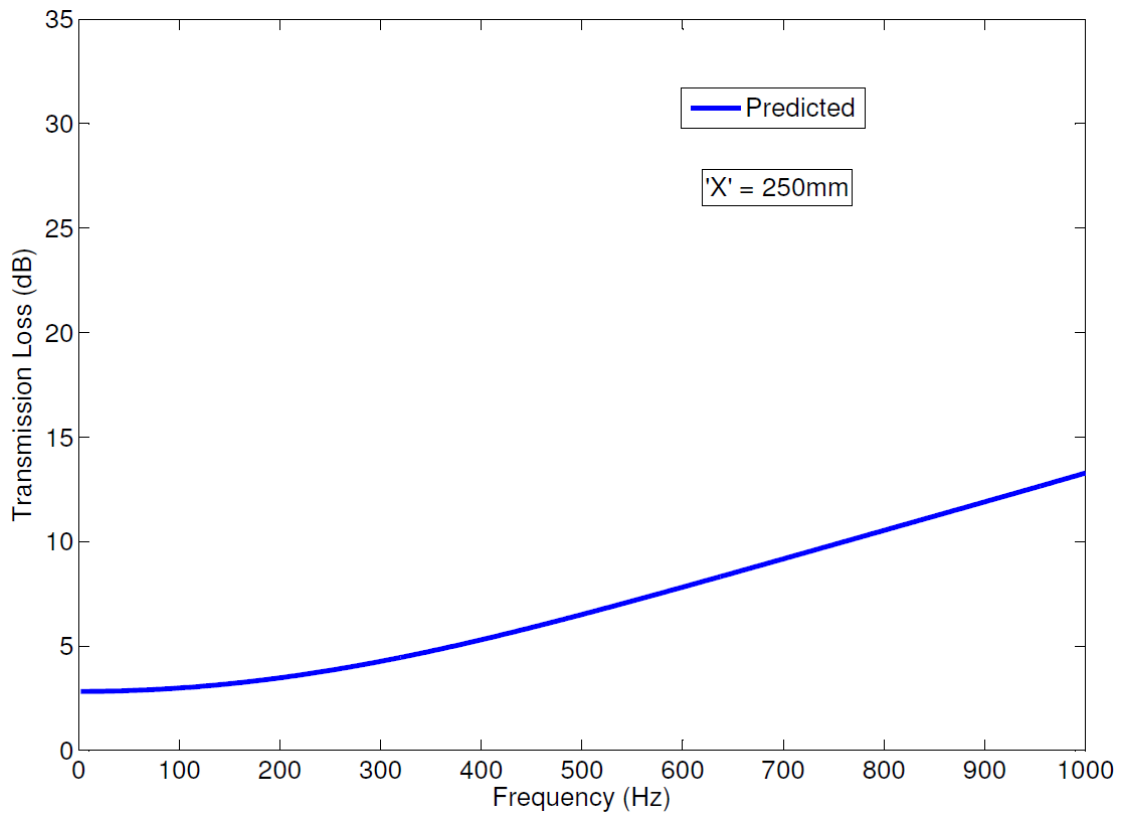


Figure 5-9 Predicted Transmission Loss for a 250mm long tuner

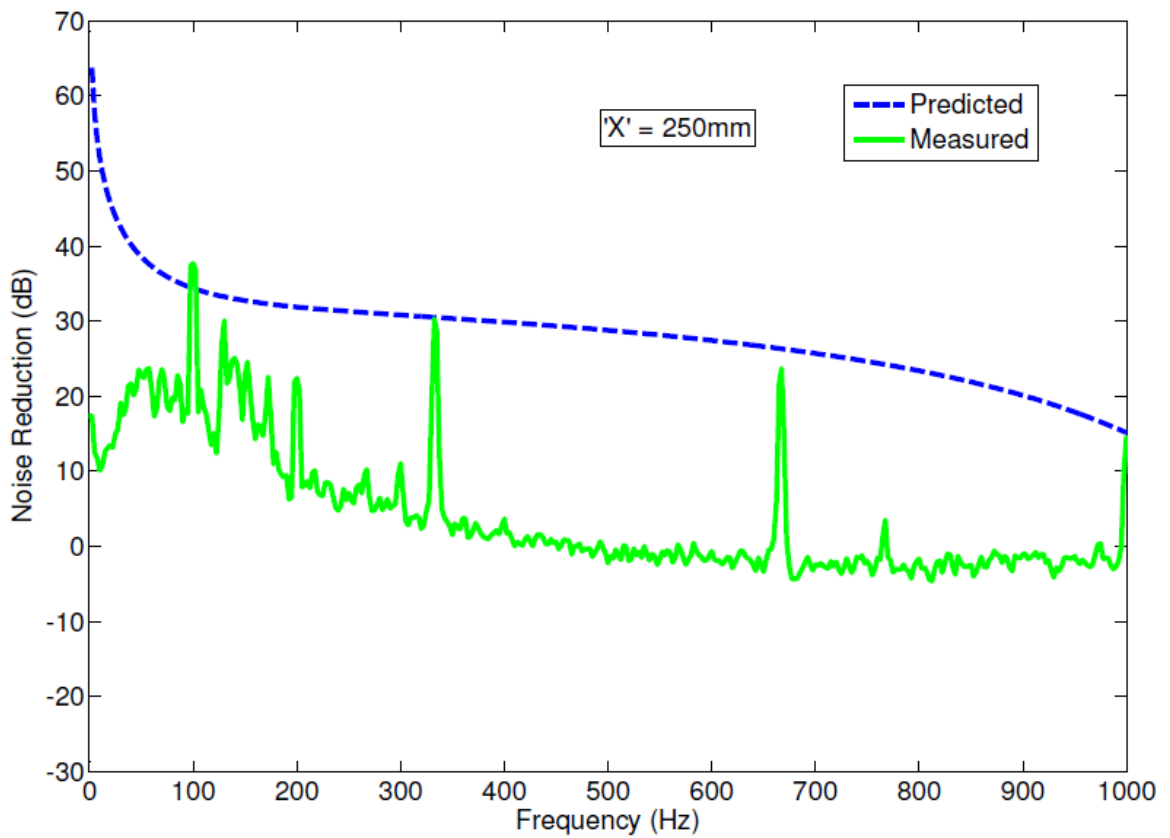


Figure 5-10 Predicted versus Measured Noise Reduction for a 250mm long tuner

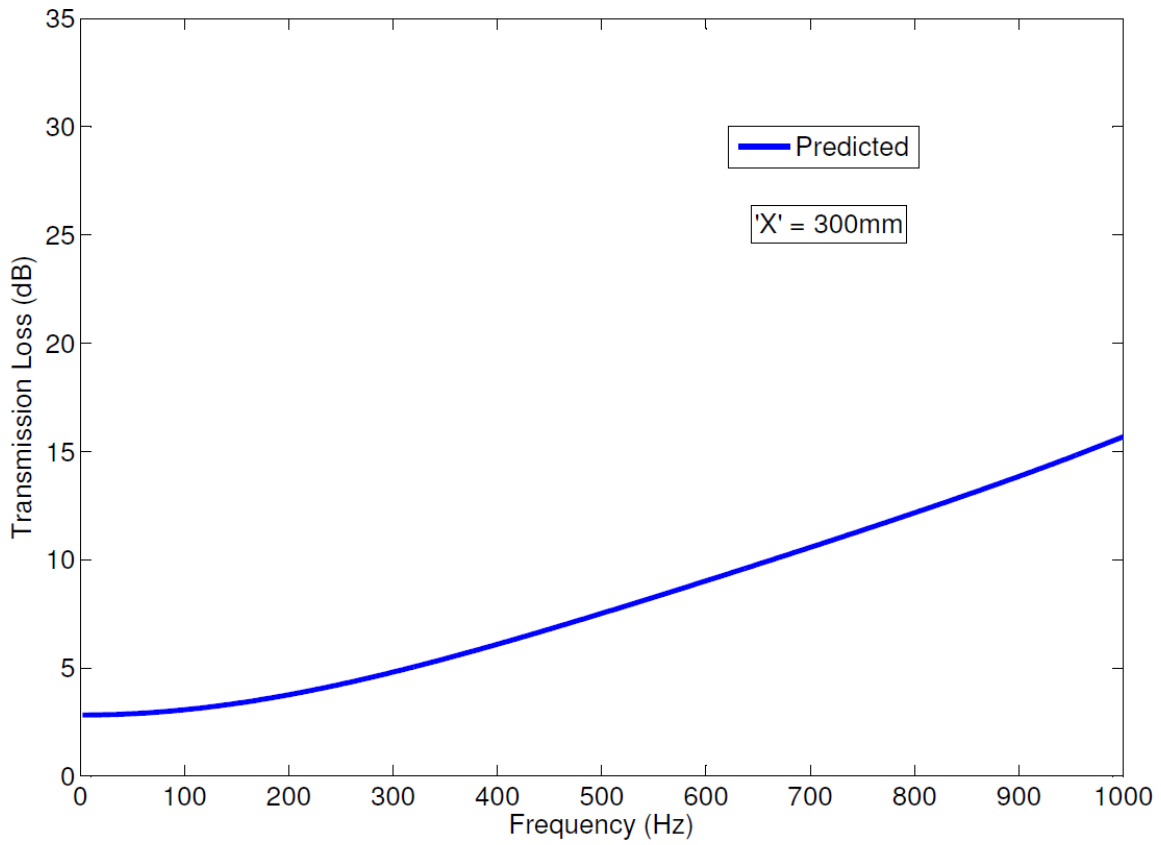


Figure 5-11 Predicted Transmission Loss for a 300mm long tuner

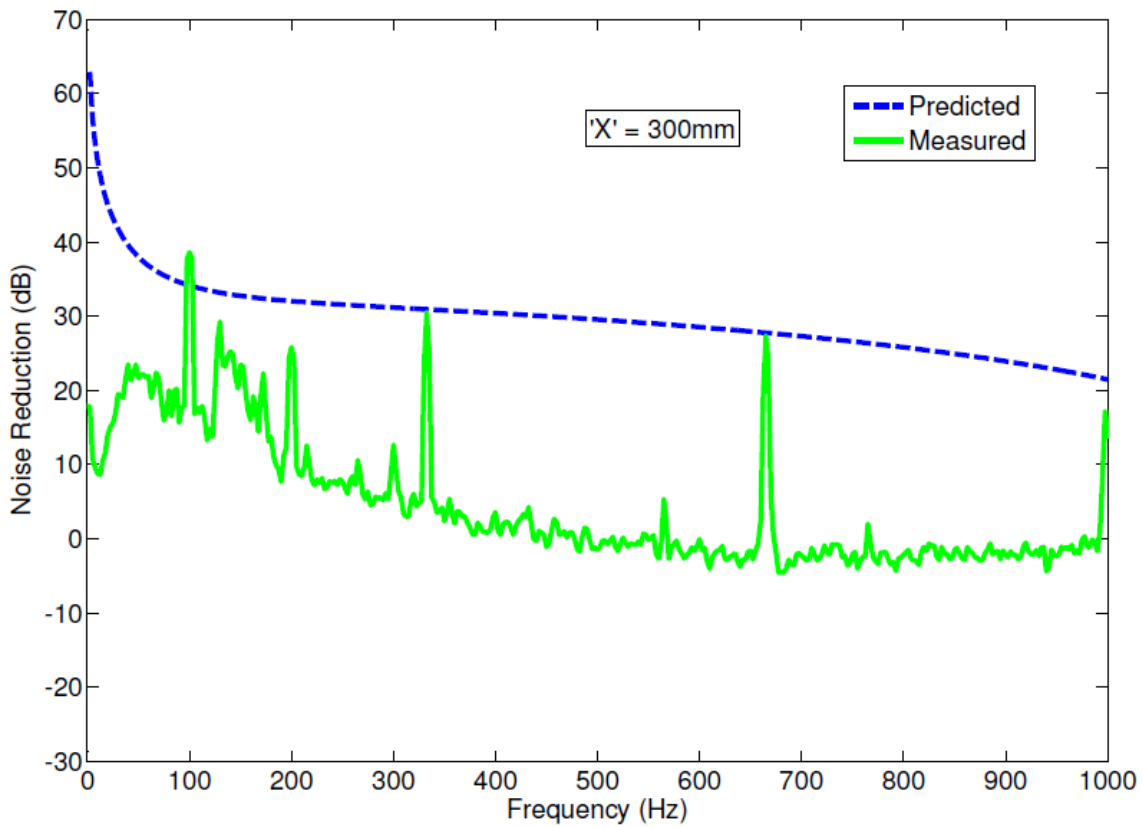


Figure 5-12 Predicted versus Measured Noise Reduction for a 300mm long tuner

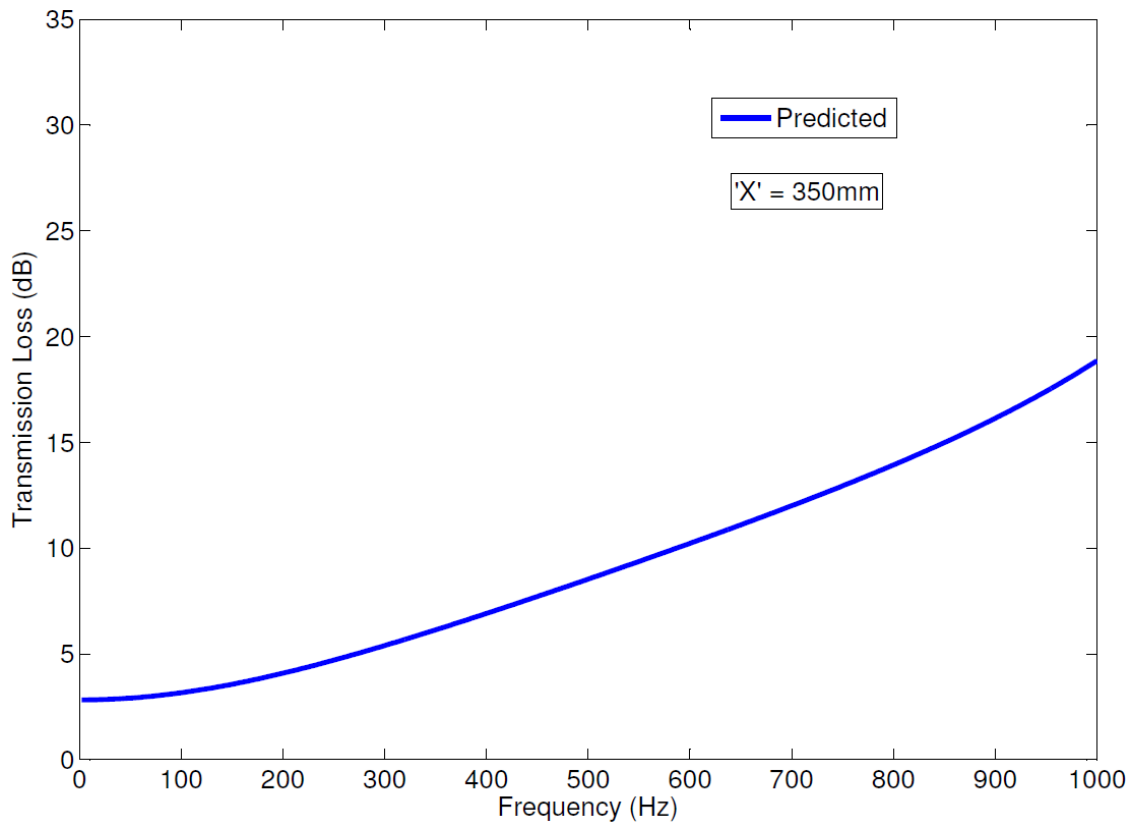


Figure 5-13 Predicted Transmission Loss for a 350mm long tuner

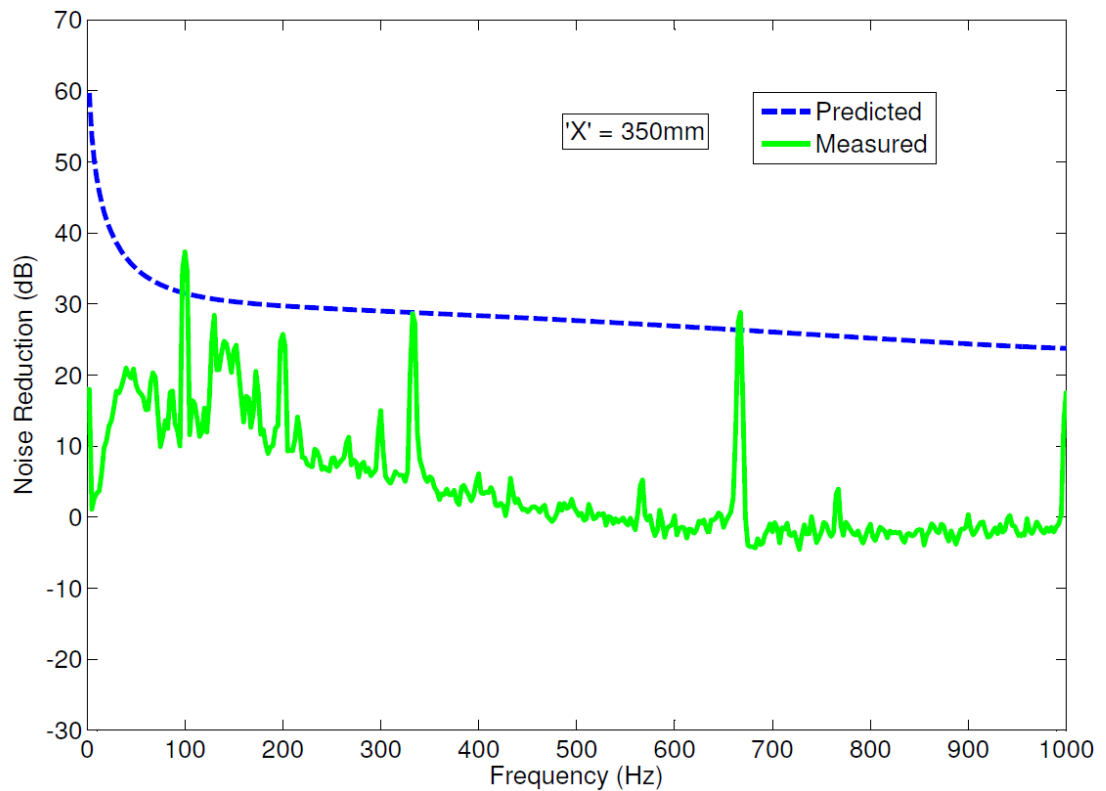


Figure 5-14 Predicted versus Measured Noise Reduction for a 350mm long tuner

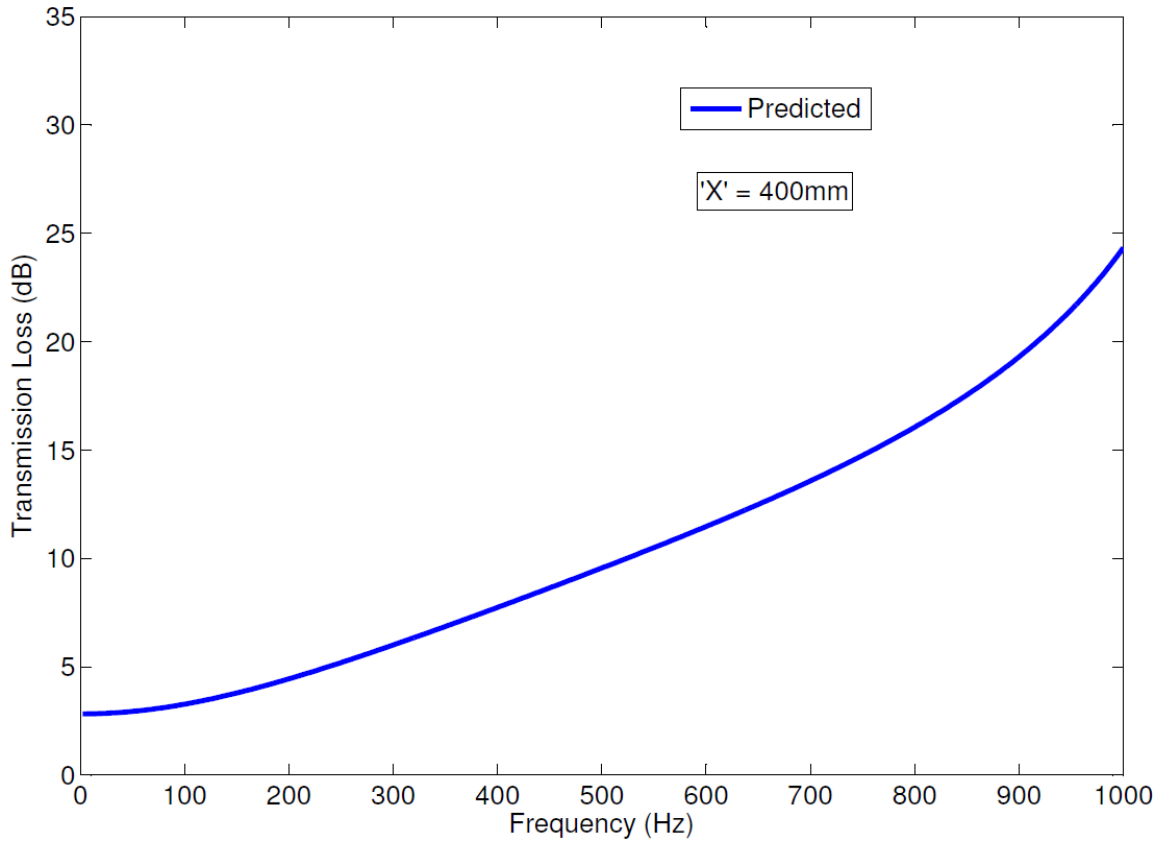


Figure 5-15 Predicted Transmission Loss for a 400mm long tuner

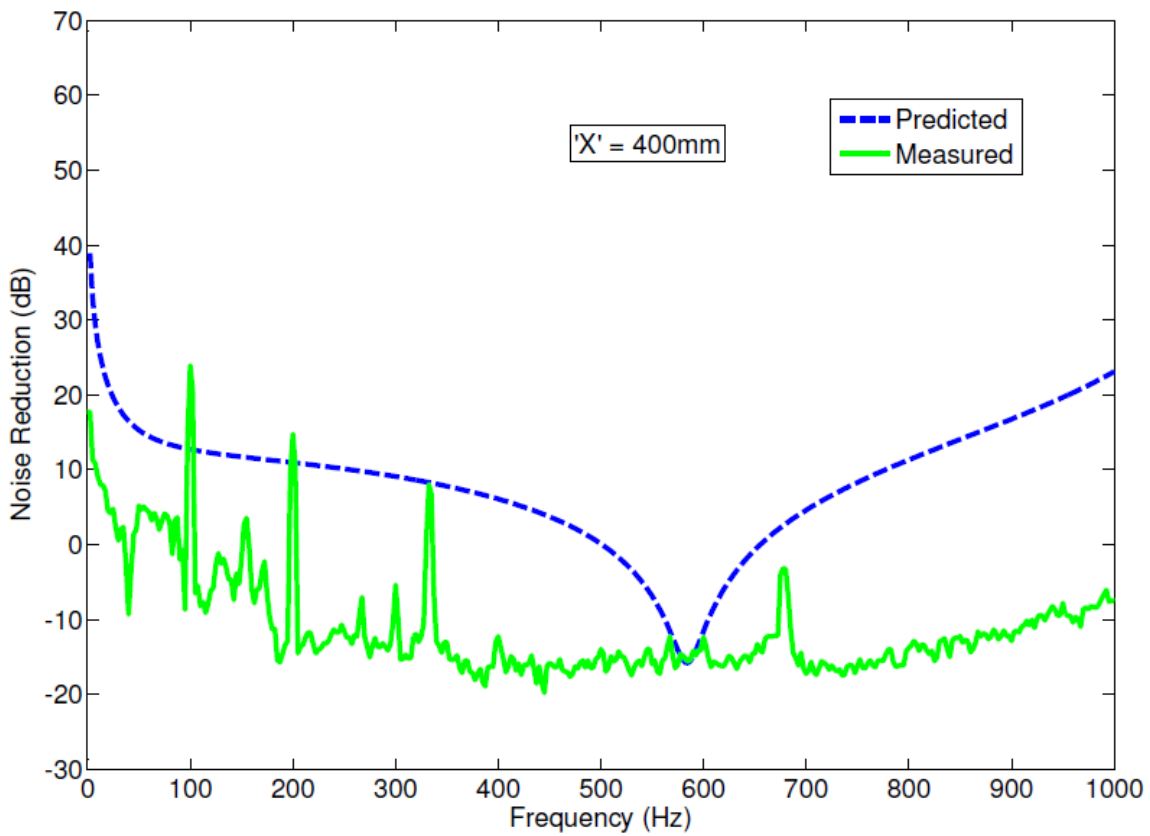


Figure 5-16 Predicted versus Measured Noise Reduction for a 400mm tuner

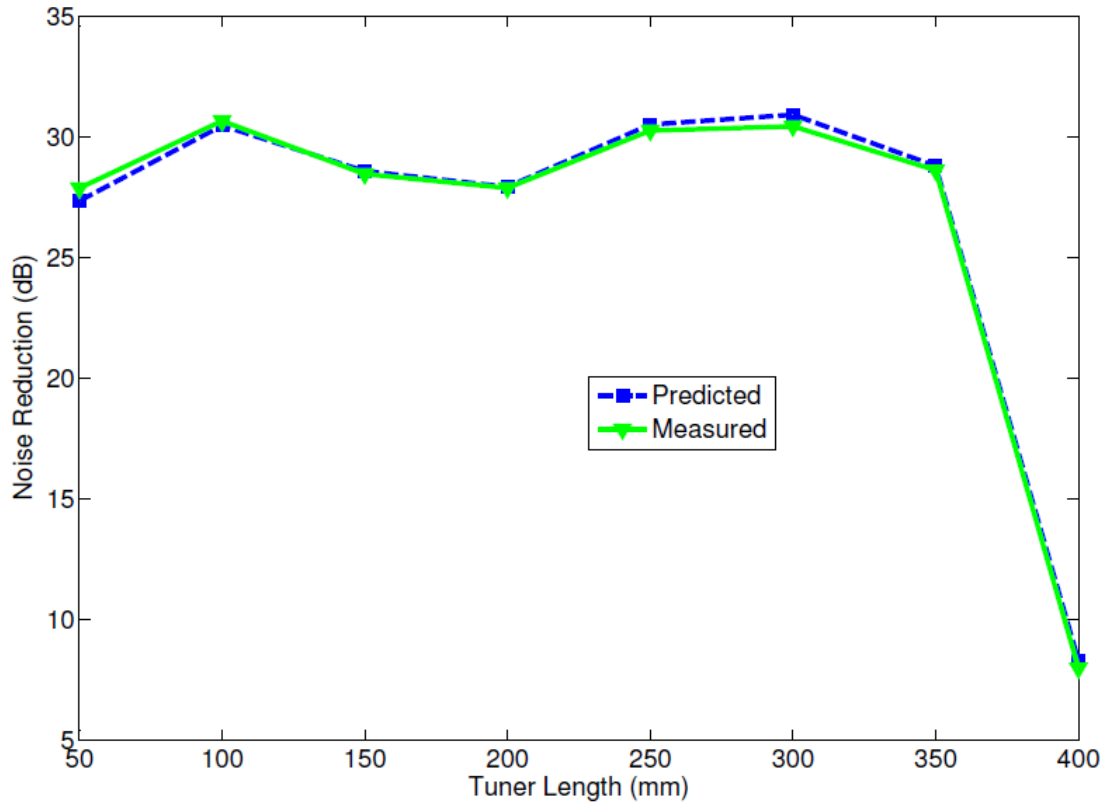


Figure 5-17 Tuner Length - Predicted versus Measured, 1st Pump Order.

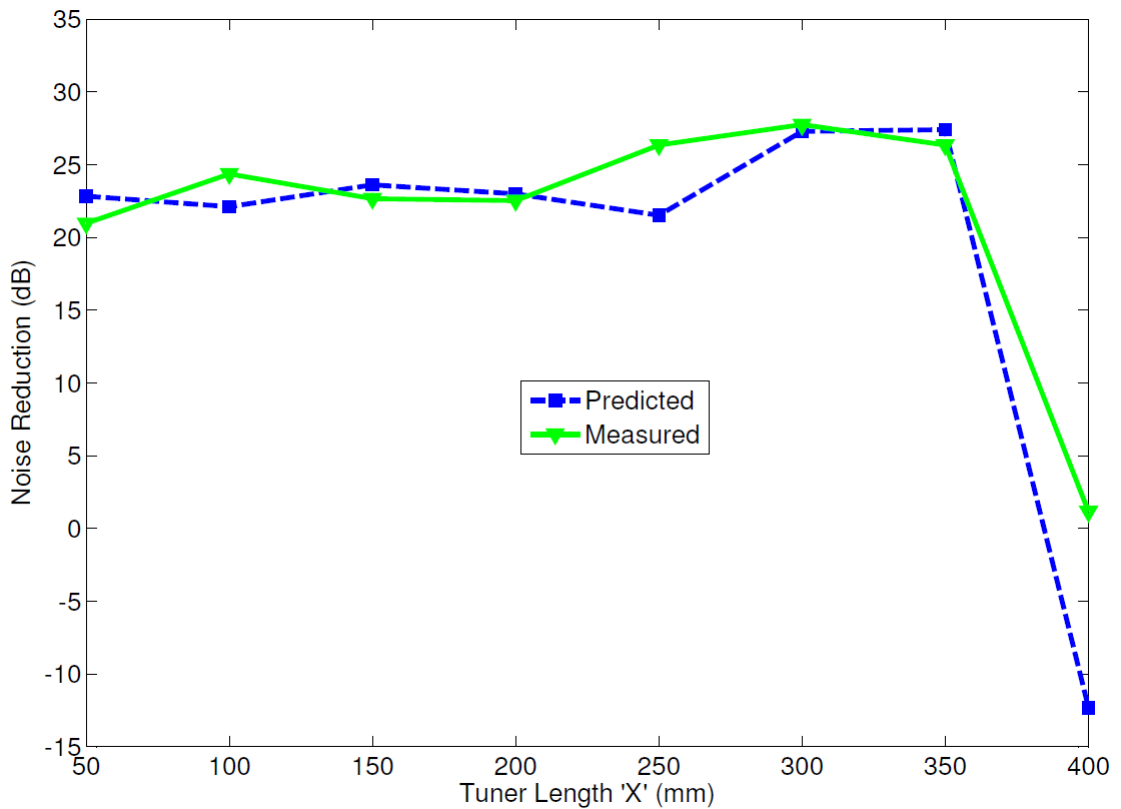


Figure 5-18 Tuner Length - Predicted versus Measured, 2nd Pump Order

As can be seen from Figure 5.17, there is excellent agreement between 1st pump order predicted and experimental noise reduction results for all tuner configurations. Considering the key objectives of this research, the model can be considered to be successful in this regard.

When comparing the transmission loss and noise reduction predictions, it is clear that the noise reduction mechanism is not only a function of the tuner itself, but rather the effect the tuner is having on the overall system. This is best demonstrated with the 100mm tuner, where the transmission loss for this configuration is around 4dB, however the predicted and experimental noise reductions are around 30dB. Transmission loss is clearly increasing with tuner length, however noise reduction does not appear to follow a linear relationship. Further analysis is provided in section 5.5.5.

5.2 Hole Location Validation

The purpose of this section is to validate the elements of the model concerned with the location of a fixed diameter hole along the tuner length. The model should represent the relatively constant noise reduction values observed during the experiments, where little change was observed for each sample at the pump fundamental frequency.

5.2.1 Analysis and discussion

Following the approach to Tuner Length analysis described in Section 5.1.1, Equation 3.3 was used to calculate the theoretical transmission loss of the samples in this experiment. Equation 3.2 was used to predict the theoretical noise reduction of the system in this experiment and Equation 4.1 was used to calculate the experimental noise reduction based on the measured data captured during the experimental phase. Each discrete sample is illustrated in Figures 5.18 – 5.31.

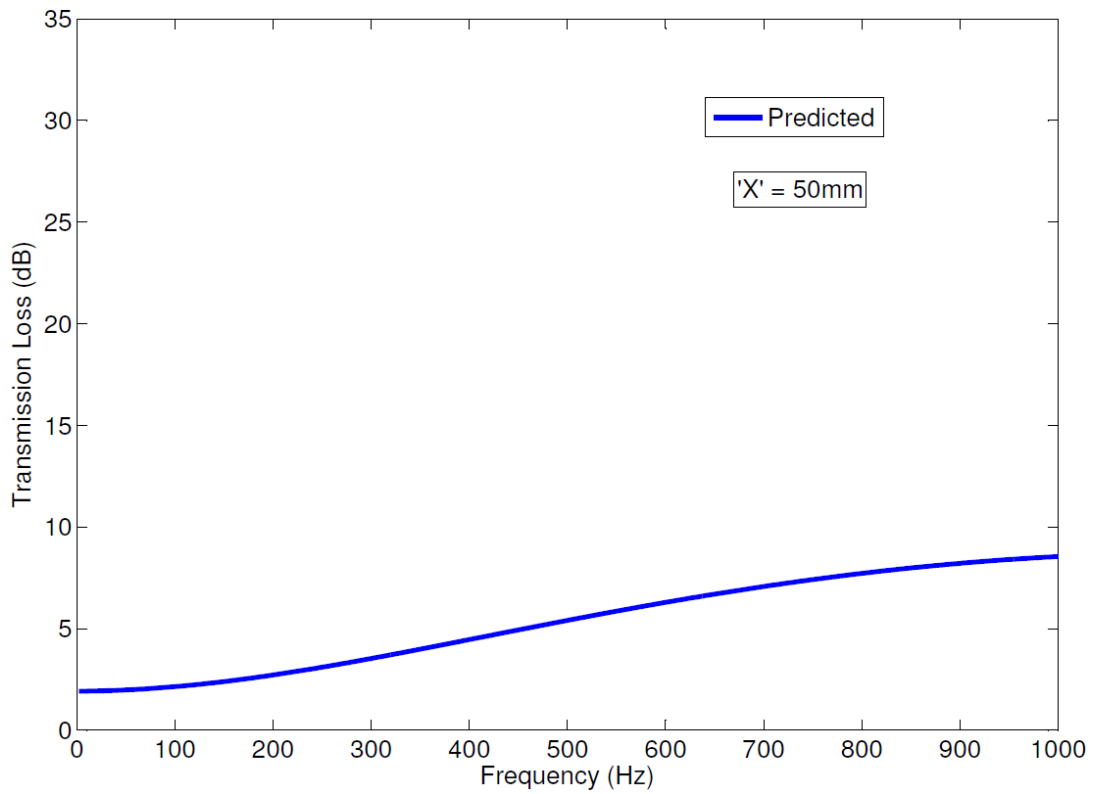


Figure 5-19 Predicted Transmission Loss for a 400mm long tuner with a 1mm hole located 50mm from the tuner inlet

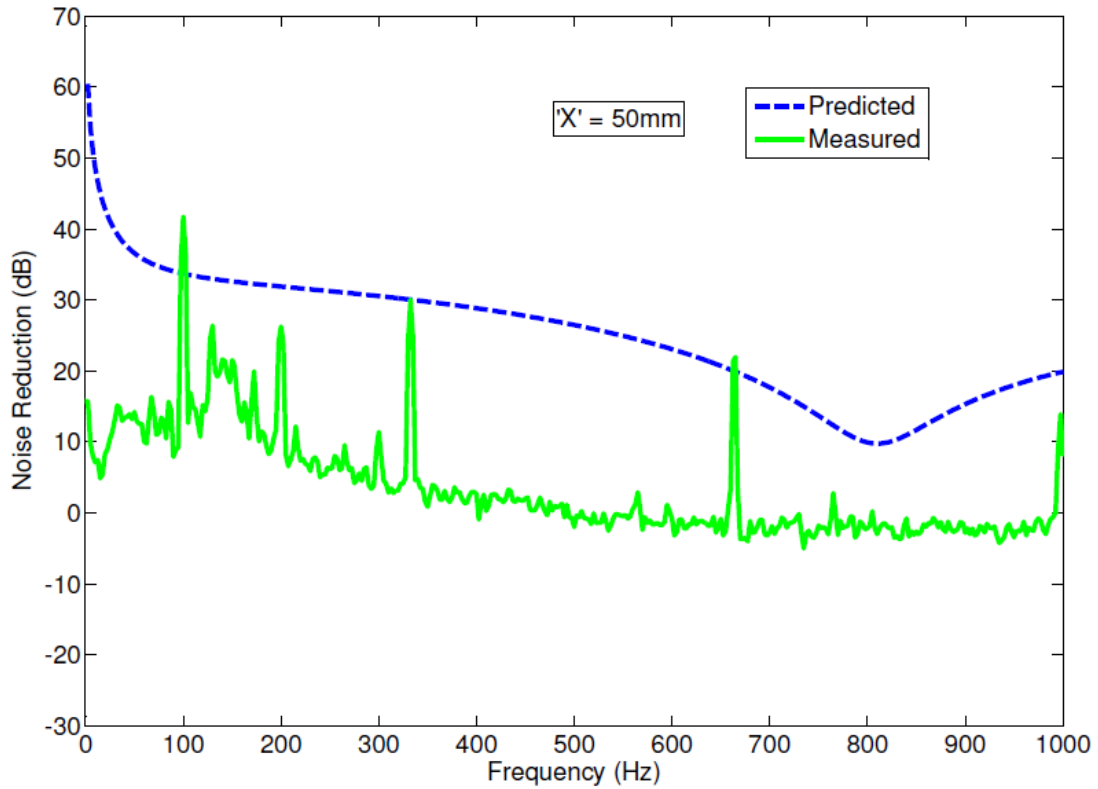


Figure 5-20 Predicted versus Measured Noise Reduction for a 400mm long tuner with a 1mm hole located 50mm from the tuner inlet

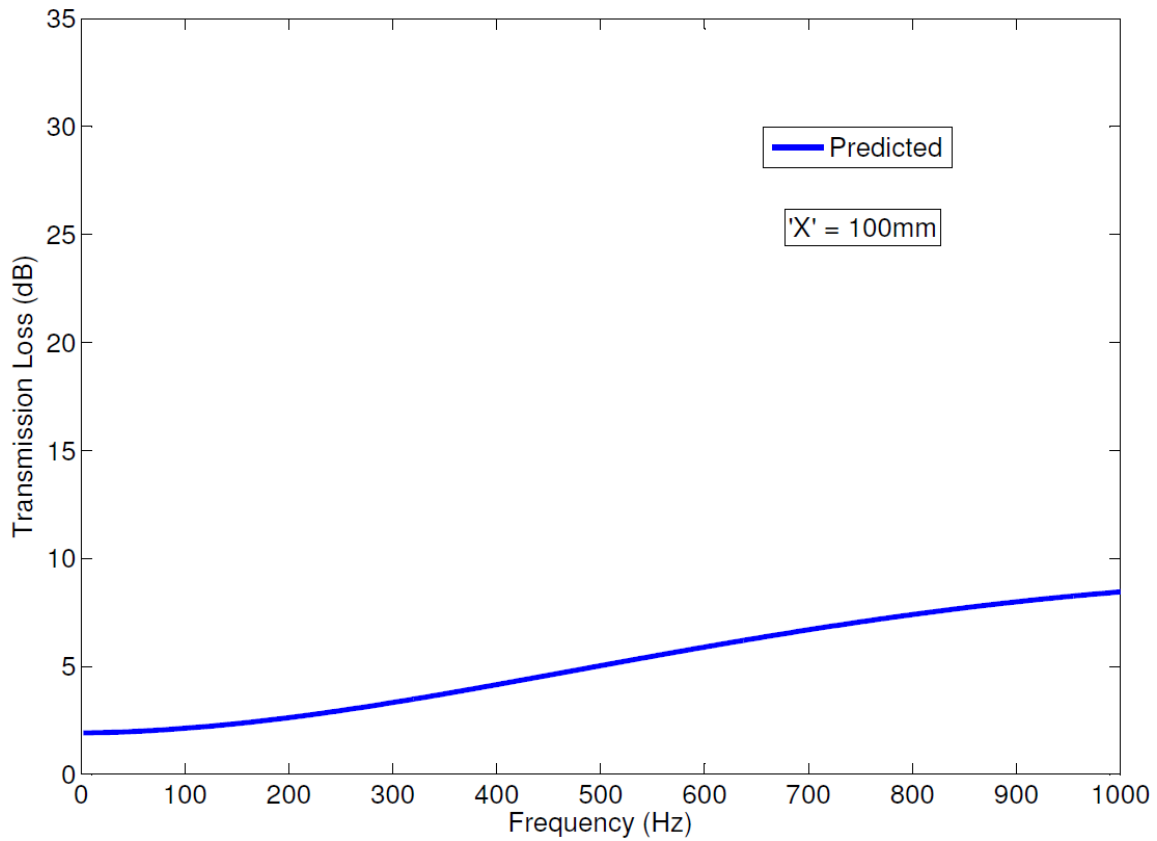


Figure 5-21 Predicted Transmission Loss for a 400mm long tuner with a 1mm hole located 100mm from the tuner inlet

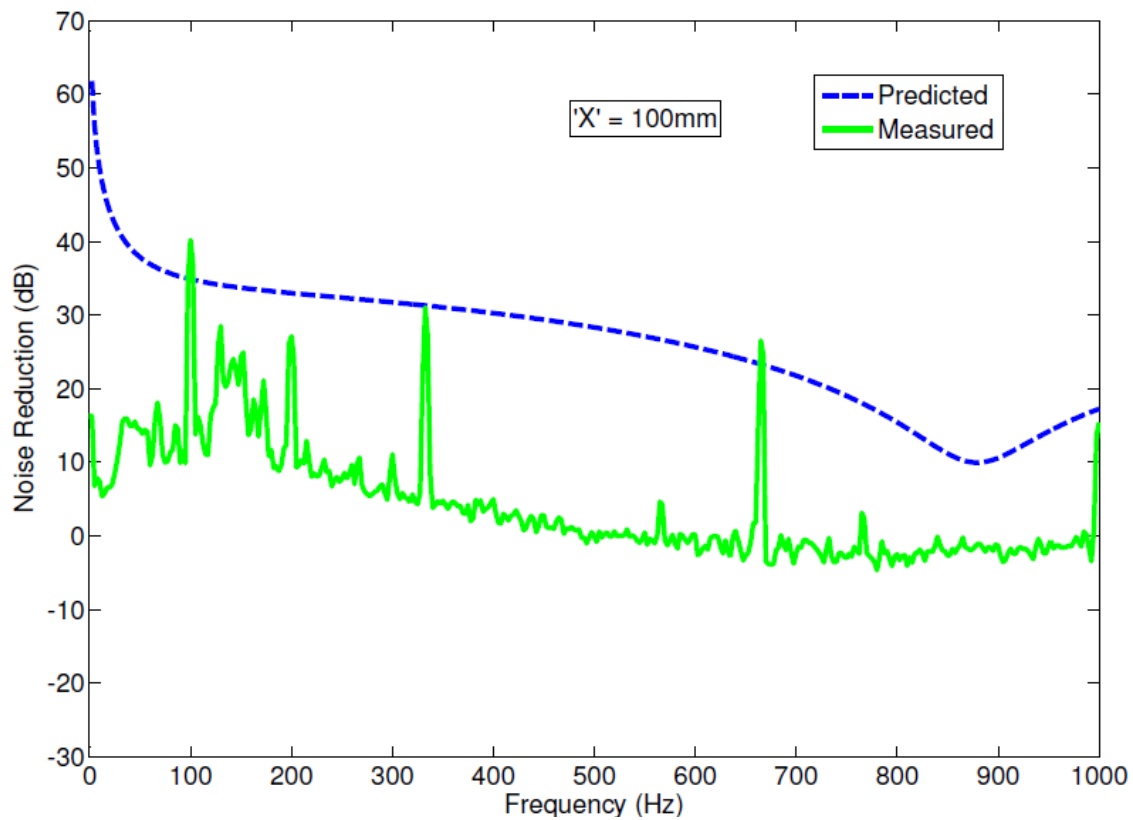


Figure 5-22 Predicted versus Measured Noise Reduction for a 400mm long tuner with a uniform hole located 100mm from the tuner inlet

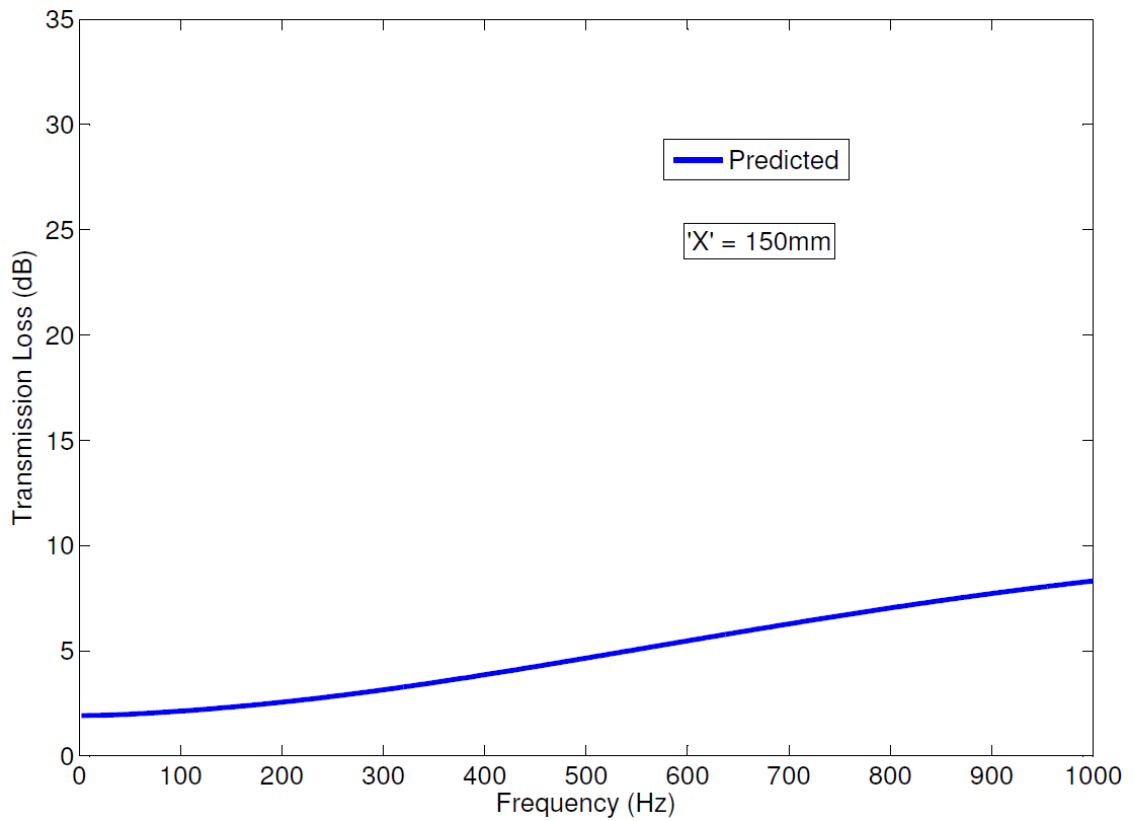


Figure 5-23 Predicted Transmission Loss for a 400mm long tuner with a 1mm hole located 150mm from the tuner inlet

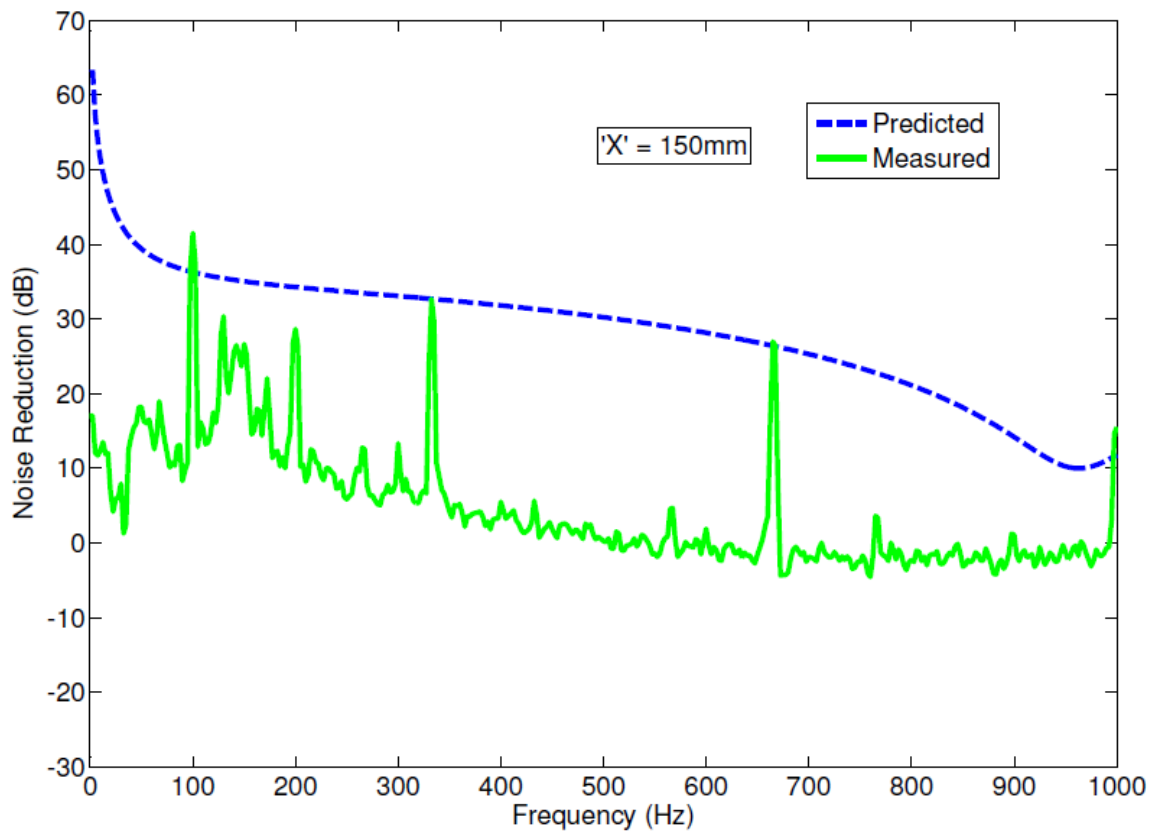


Figure 5-24 Predicted versus Measured Noise reduction for a 400mm long tuner with a 1mm hole located 150mm from the tuner inlet

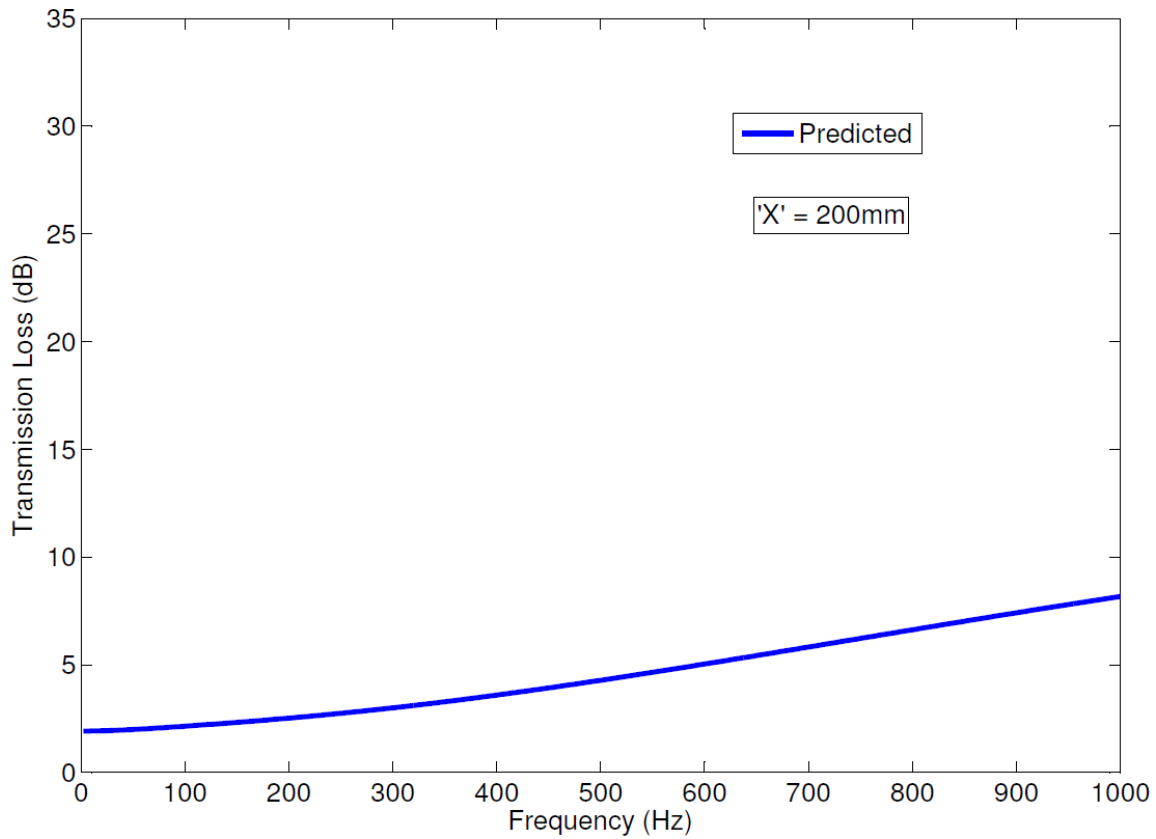


Figure 5-25 Predicted Transmission Loss for a 400mm long tuner with a 1mm hole located 200mm from the tuner inlet

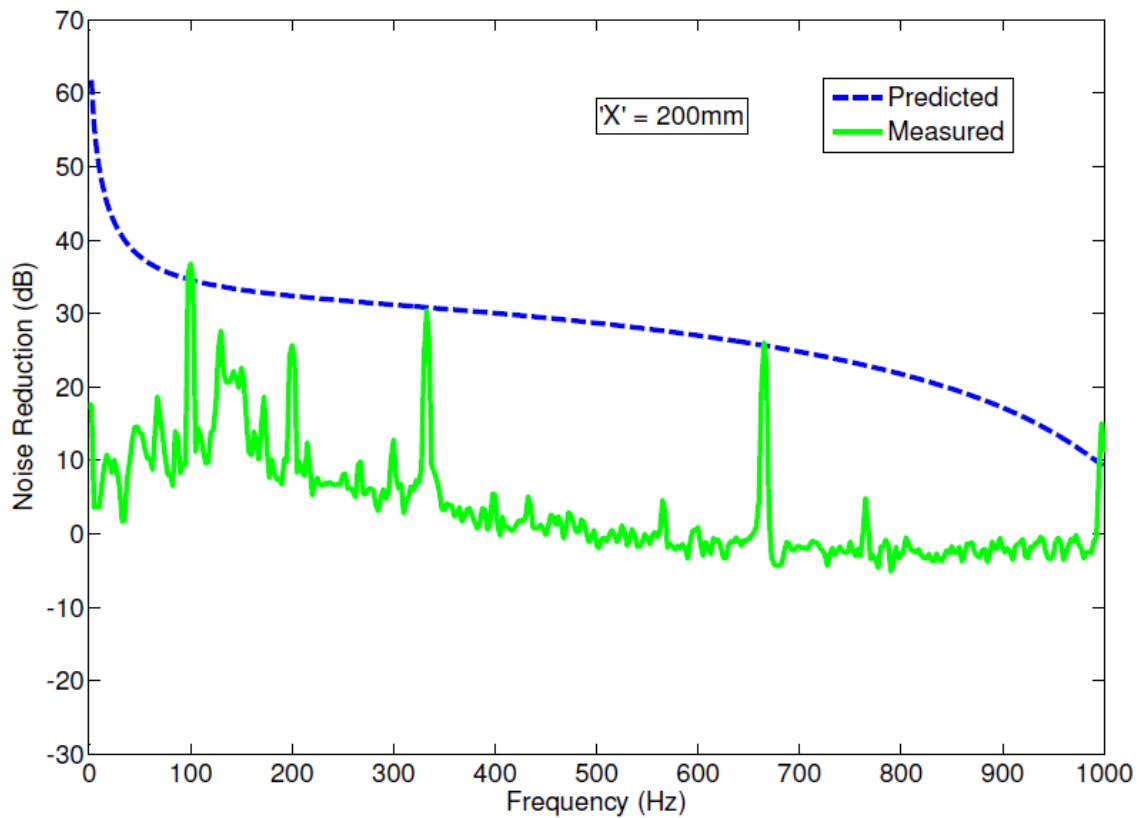


Figure 5-26 Predicted versus Measured Noise Reduction for a 400mm long tuner with a 1mm hole located 200mm from the tuner inlet

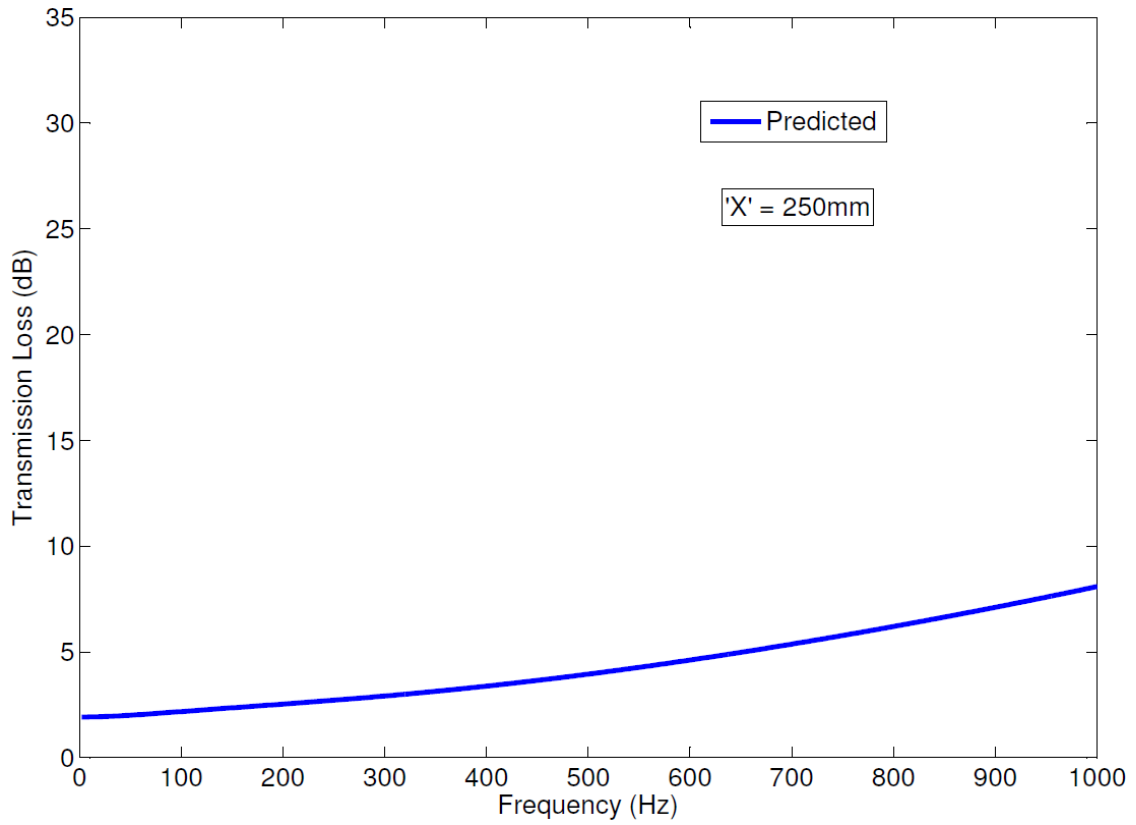


Figure 5-27 Predicted Transmission Loss for a 400mm long tuner with a 1mm hole located 250mm from the tuner inlet

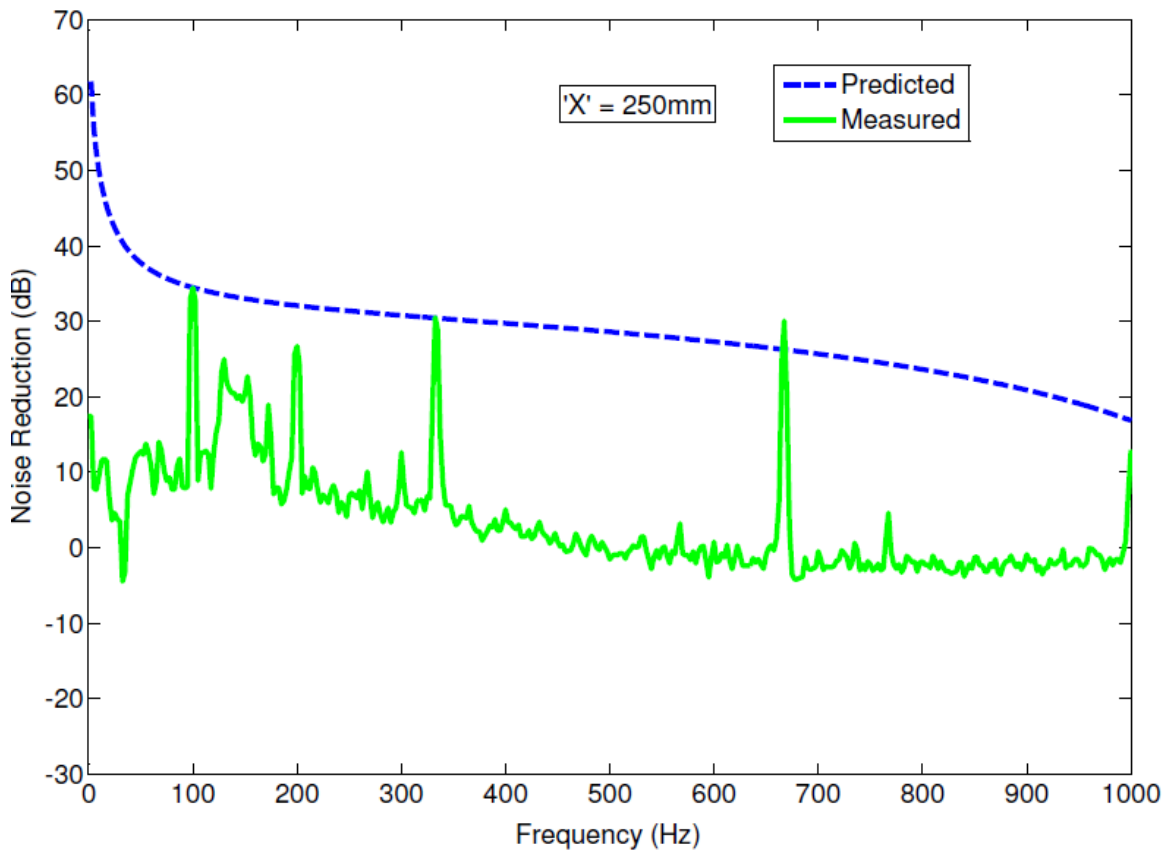


Figure 5-28 Predicted versus Measured Noise Reduction for a 400mm long tuner with a 1mm hole located 250mm from the tuner inlet

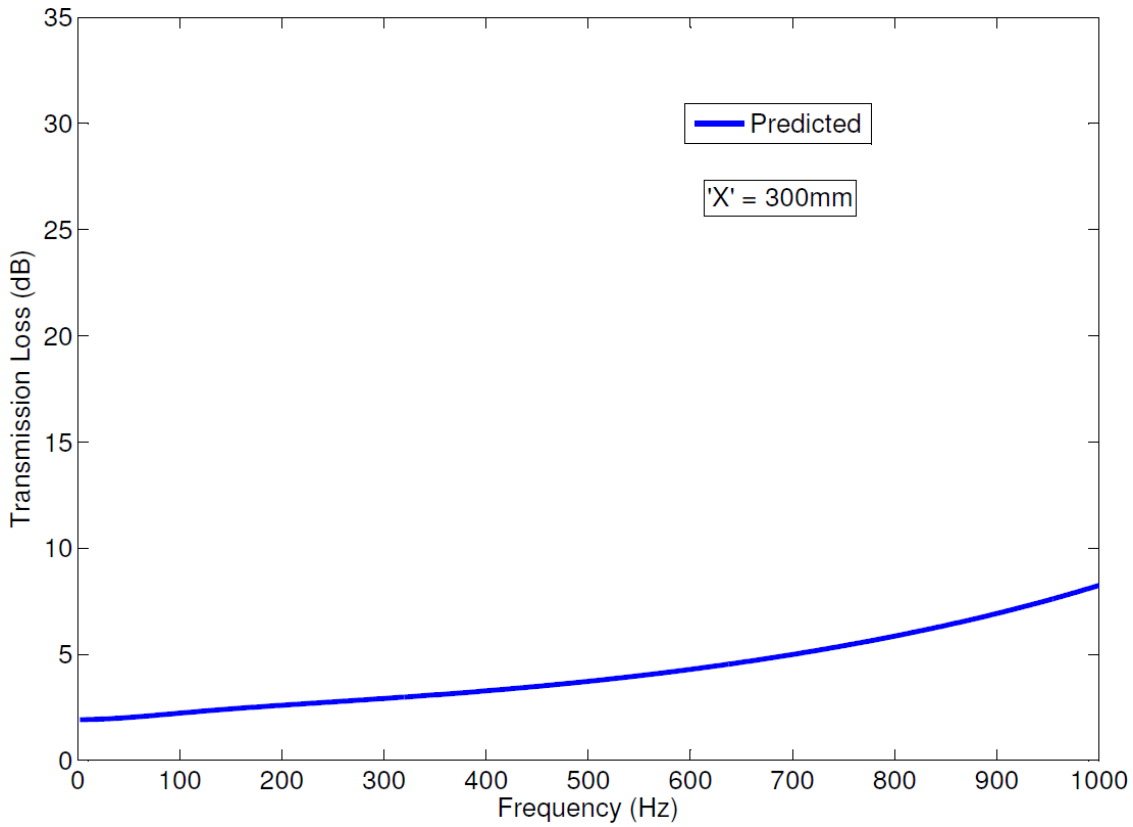


Figure 5-29 Predicted Transmission Loss for a 400mm long tuner with a 1mm hole 300mm from the tuner inlet

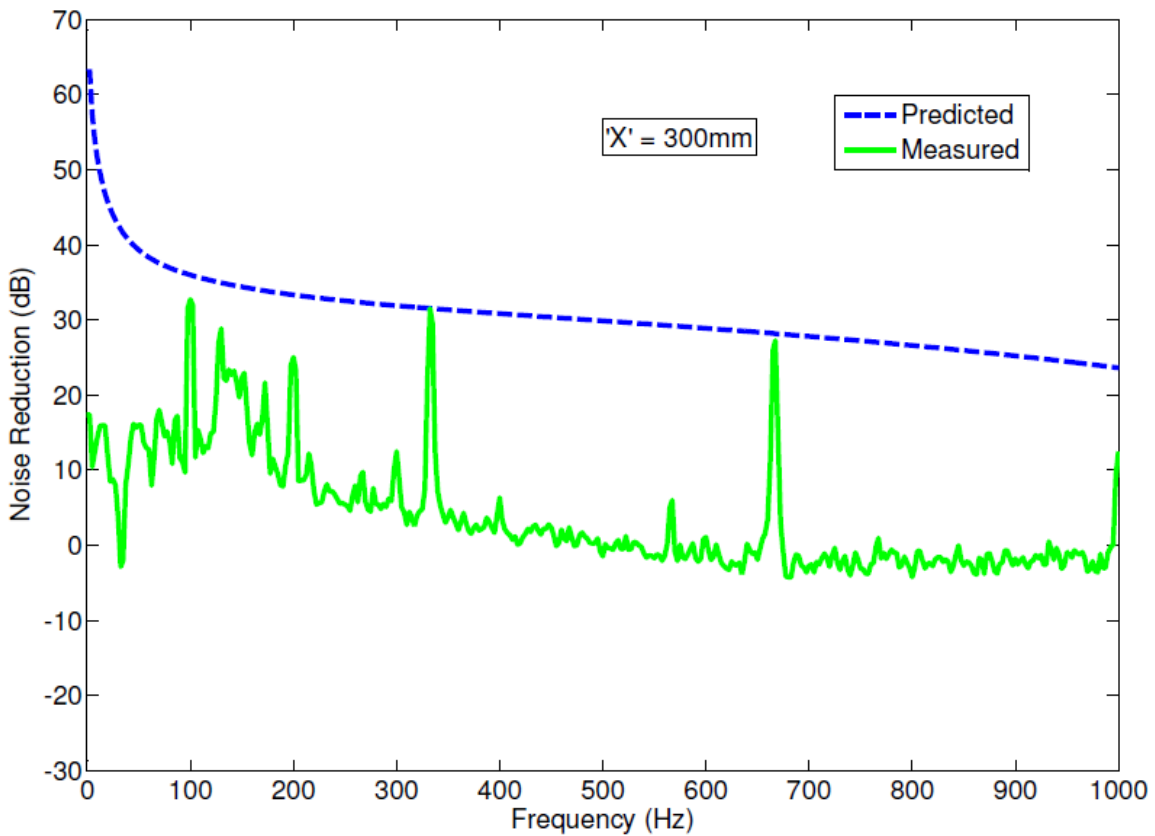


Figure 5-30 Predicted versus Measured Noise Reduction for a 400mm long tuner with a 1mm hole located 300mm from the tuner inlet

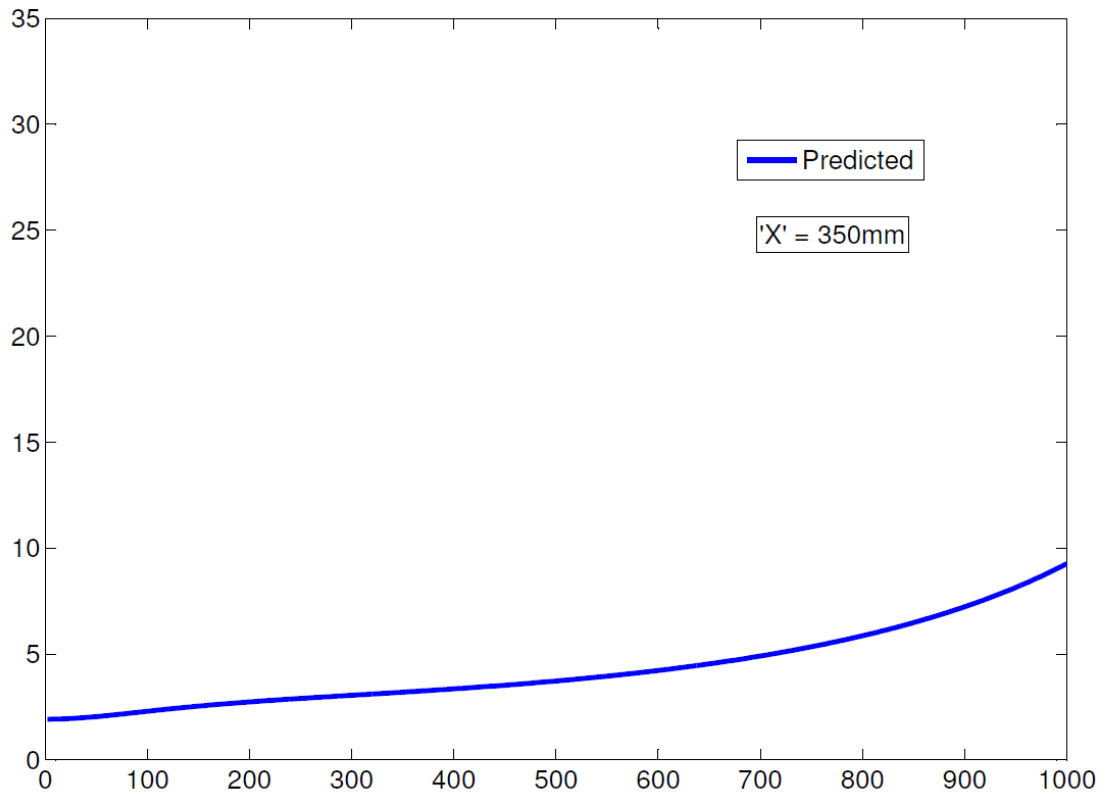


Figure 5-31 Predicted Transmission Loss for a 400mm long tuner with a 1mm hole located 350mm from the tuner inlet

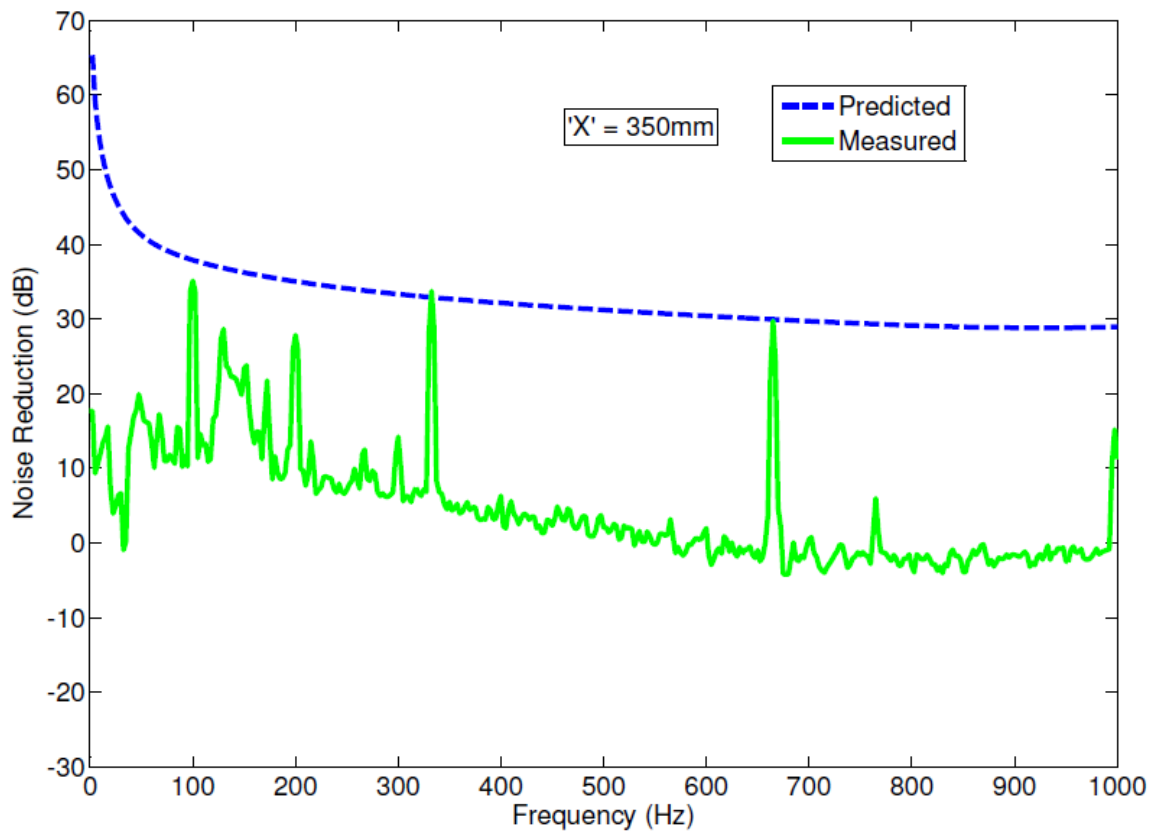


Figure 5-32 Predicted versus Measured Noise Reduction for a 400mm long tuner with a 1mm hole located 350mm from the tuner inlet

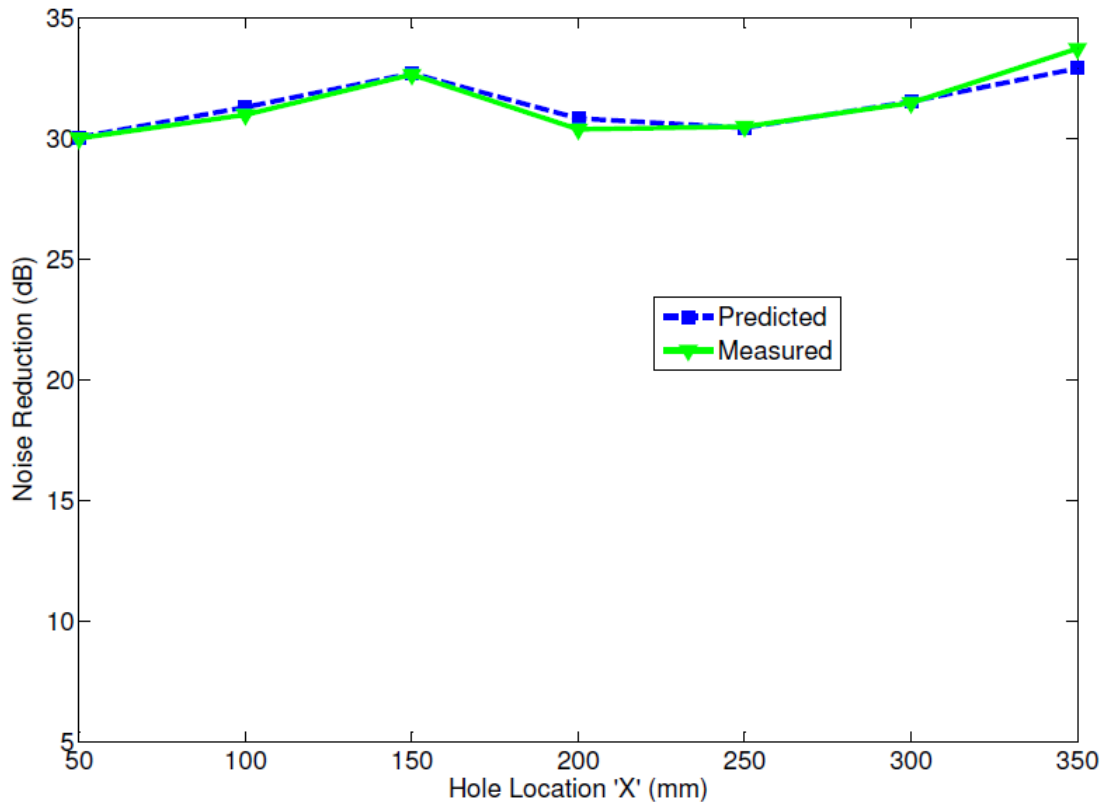


Figure 5-33 Hole Location – Predicted versus Measured Noise Reduction, 1st Pump Order.

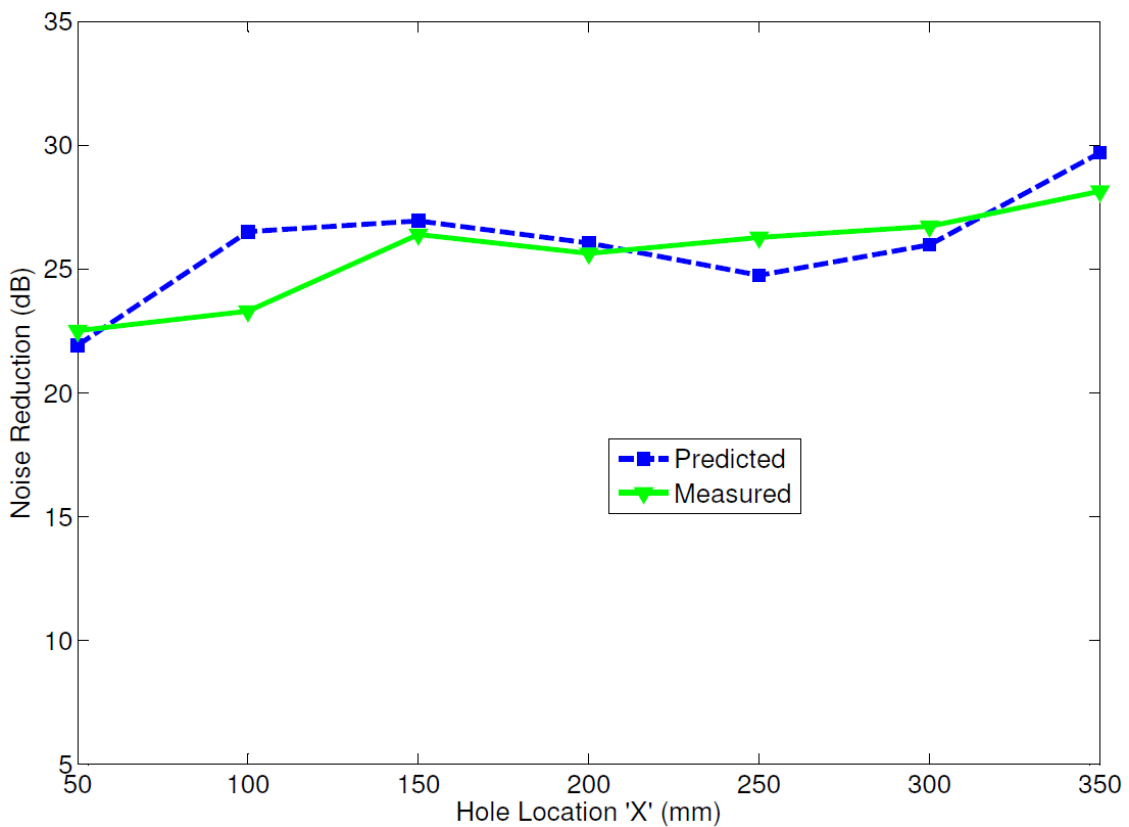


Figure 5-34 Hole Location - Predicted versus Measured Noise Reduction, 2nd Pump Order

Again, good agreement between predicted and experimental results can be observed in Figure 5.33. Analysis of the transmission loss plots suggests that the main influence of the inclusion of a hole in the tuner wall can be observed in the higher frequency range between 500 and 1000 Hz. This result is in agreement with the observations of Kang *et al* (2010), where the transmission loss of a perforated duct muffler tube is small in the low frequency range and increases in the medium to high frequency range (1000-1600 Hz). Noise reduction in this frequency range appears to be decreasing or remaining constant. Figures 5.20, 5.22 and 5.24 contain troughs at 800 Hz, 870 Hz and 950 Hz respectively. It is proposed that these are resonant frequencies for these tuner configurations. Further explanation of the noise reduction mechanisms are provided in section 5.5.6.

5.3 Hole Diameter Validation

This section is concerned with validating the elements of the model concerned with varying the diameter of the pressure relief hole, for a fixed tuner length. As presented in Chapter 3, the model elements used here are the same as those used for the ‘Hole Location’ model, where the diameter properties are varied accordingly.

The model should represent the general form of the results observed during the experiments, in particular where a drop in noise reduction was observed between the 1.0mm and 1.5mm holes at the pump fundamental frequency.

5.3.1 Analysis and discussion

Following the approach to Tuner Length analysis described in Section 5.1.1, Equation 3.3 was used to calculate the theoretical transmission loss of the samples in this experiment. Equation 3.2 was used to predict the theoretical noise reduction of the system in this experiment and Equation 4.1 was used to calculate the experimental noise reduction based on the measured data captured during the experimental phase. Each discrete sample is illustrated in Figures 5.35 – 5.44.

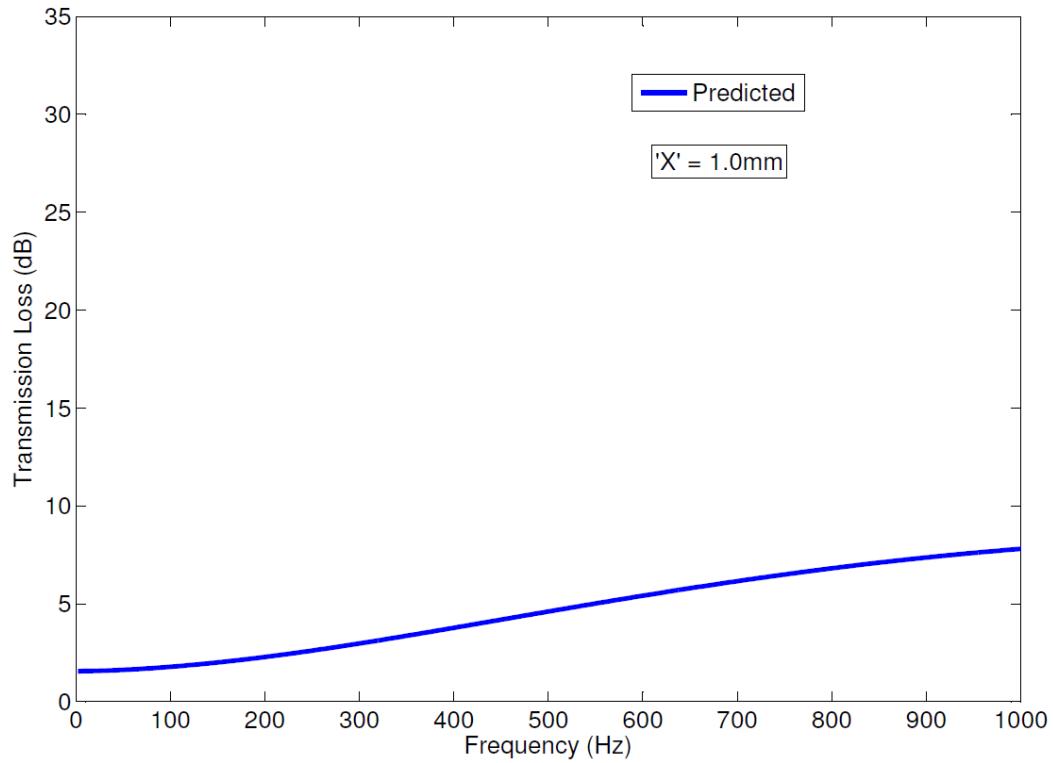


Figure 5-35 Predicted Transmission Loss for a 400mm long tuner with a 1.0mm hole located 100mm from the tuner inlet

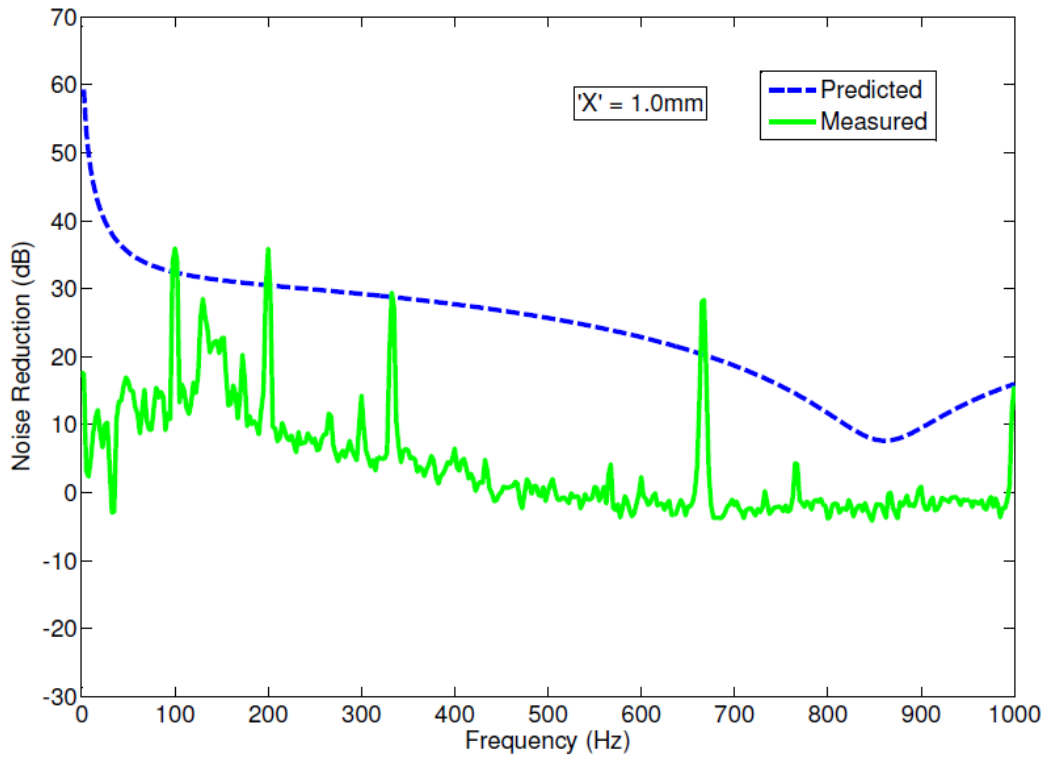


Figure 5-36 Predicted versus Measured Noise Reduction for a 400mm long tuner with a 1.0mm hole located 100mm from the tuner inlet

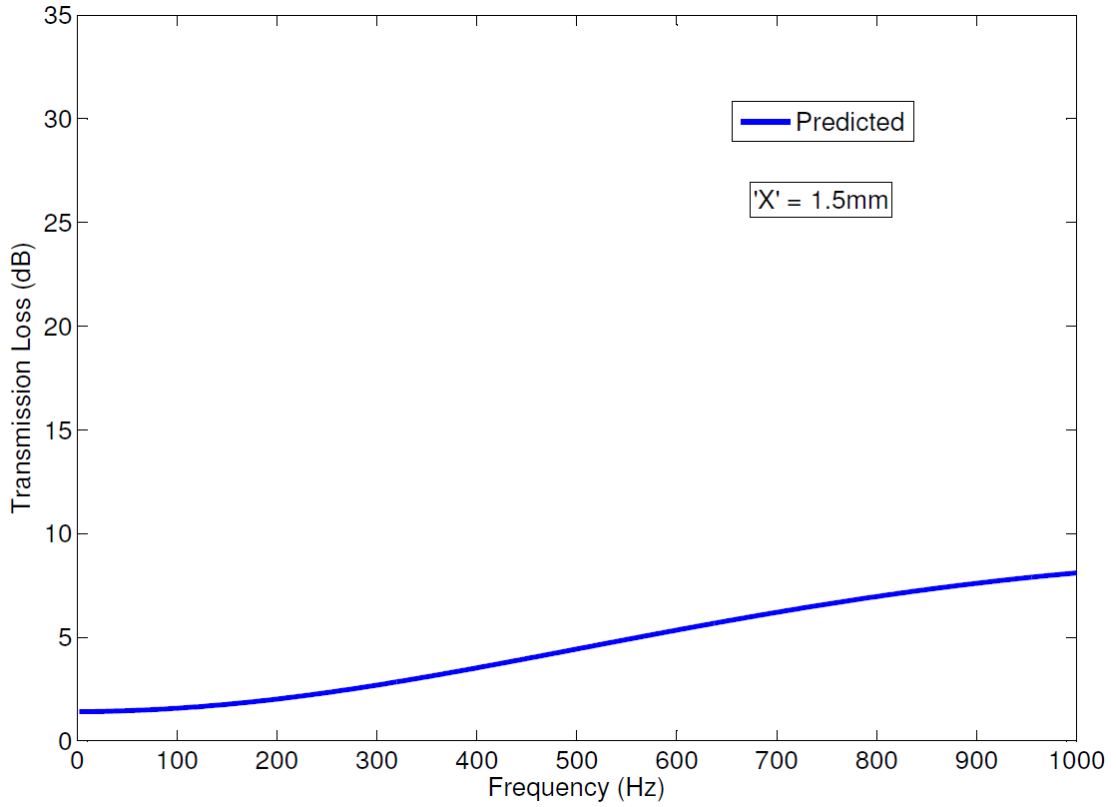


Figure 5-37 Predicted Transmission Loss for a 400mm long tuner with a 1.5mm hole located 100mm from the end of the tuner

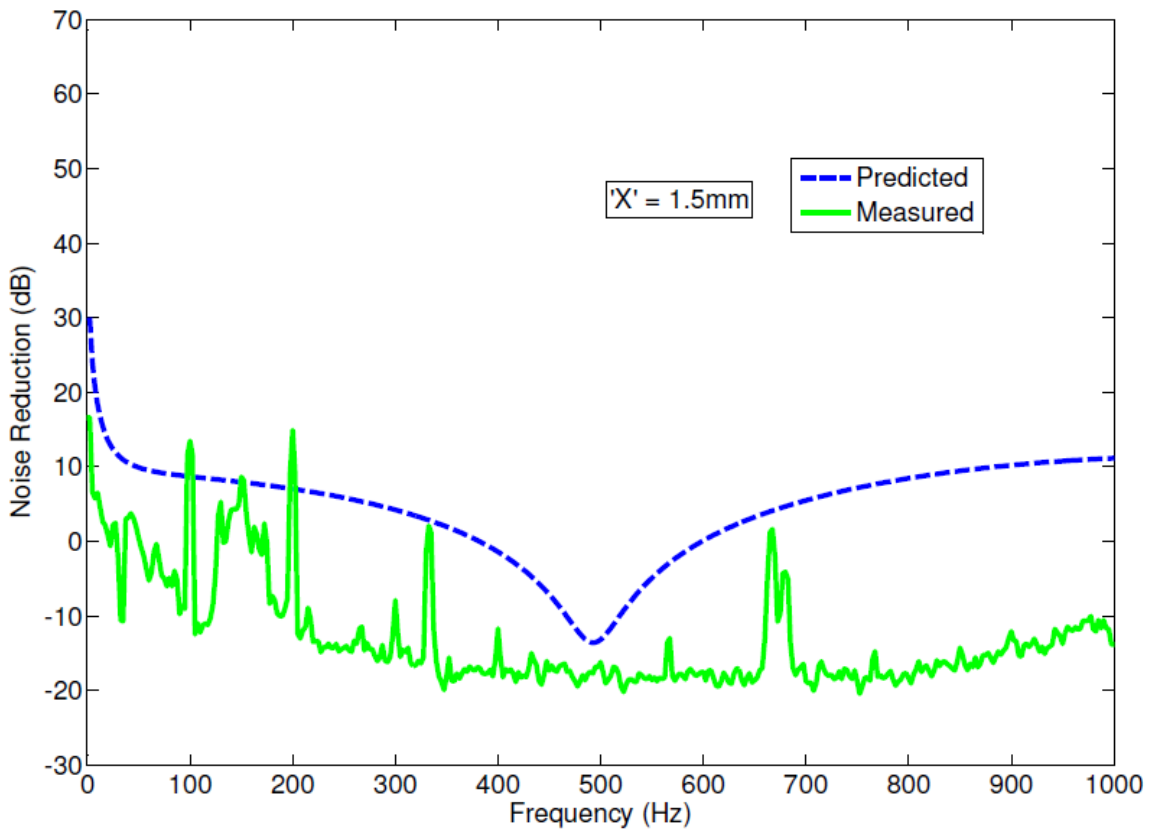


Figure 5-38 Predicted versus Measured Noise Reduction for a 400mm long tuner with a 1.5mm hole located 100mm from the tuner inlet

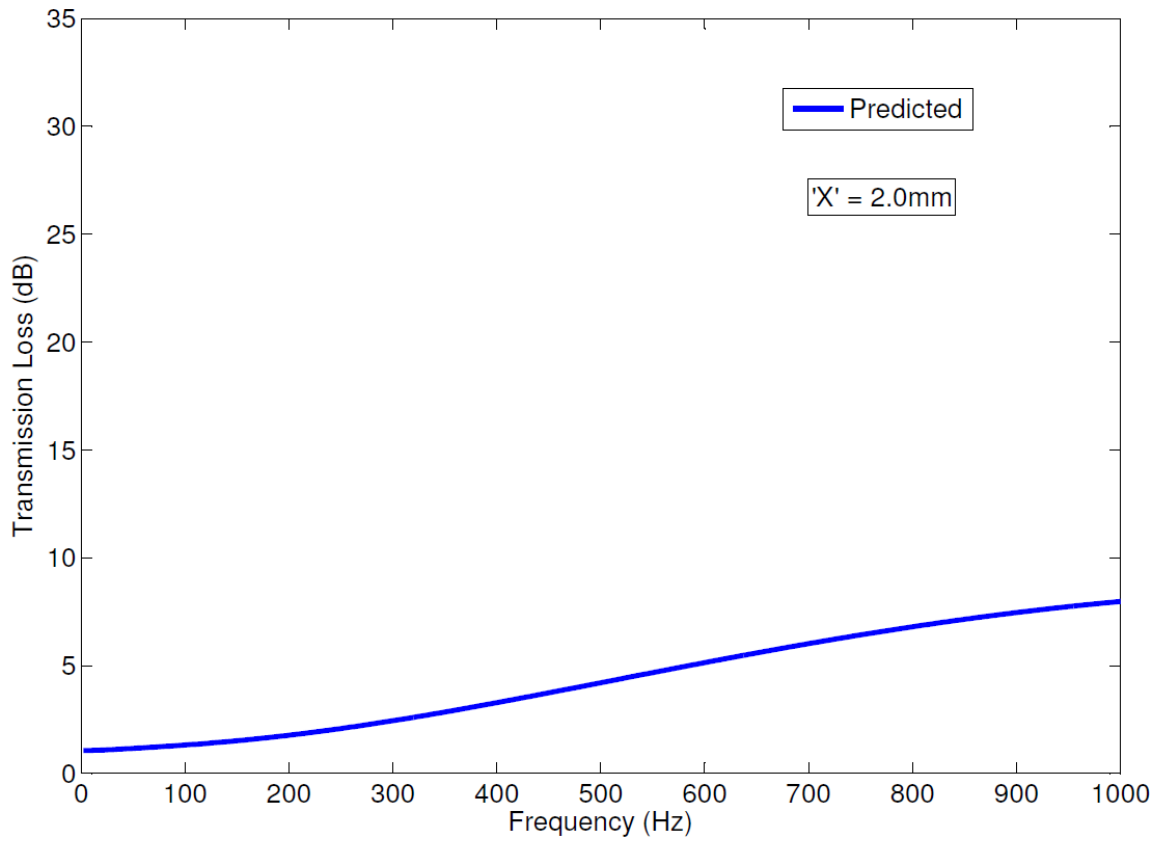


Figure 5-39 Predicted Transmission Loss for a 400mm long tuner with a 2.0mm hole located 100mm from the tuner inlet

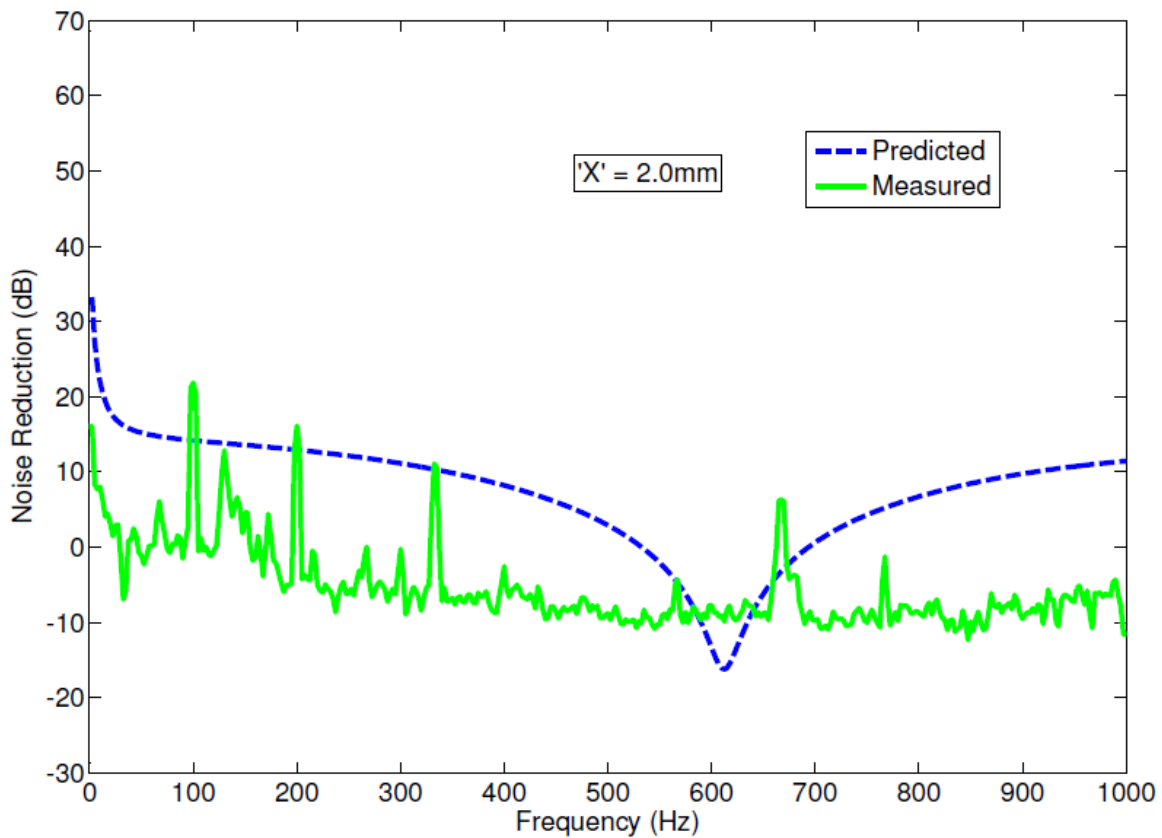


Figure 5-40 Predicted versus Measured Noise Reduction for a 400mm long tuner with a 2.0mm hole located 100mm from the tuner inlet

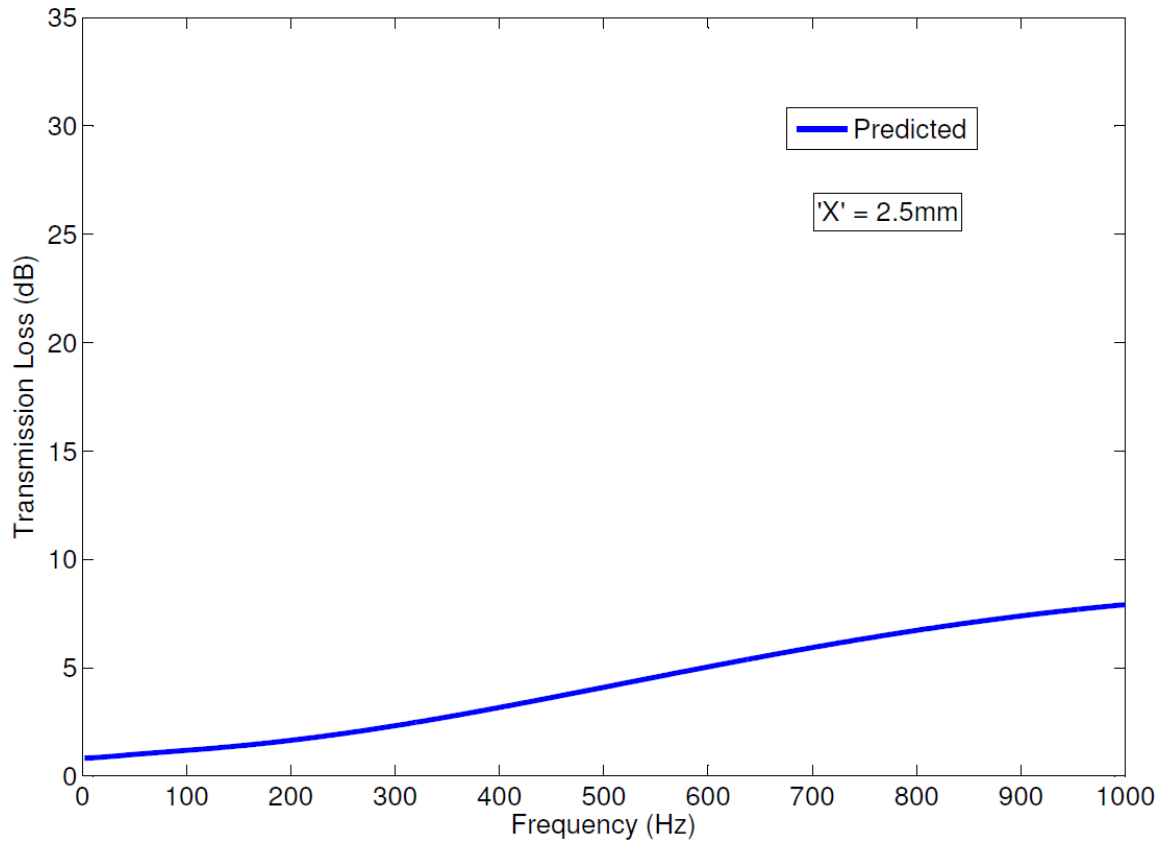


Figure 5-41 Predicted Transmission Loss for a 400mm long tuner with a 2.5mm hole located 100mm from the tuner inlet

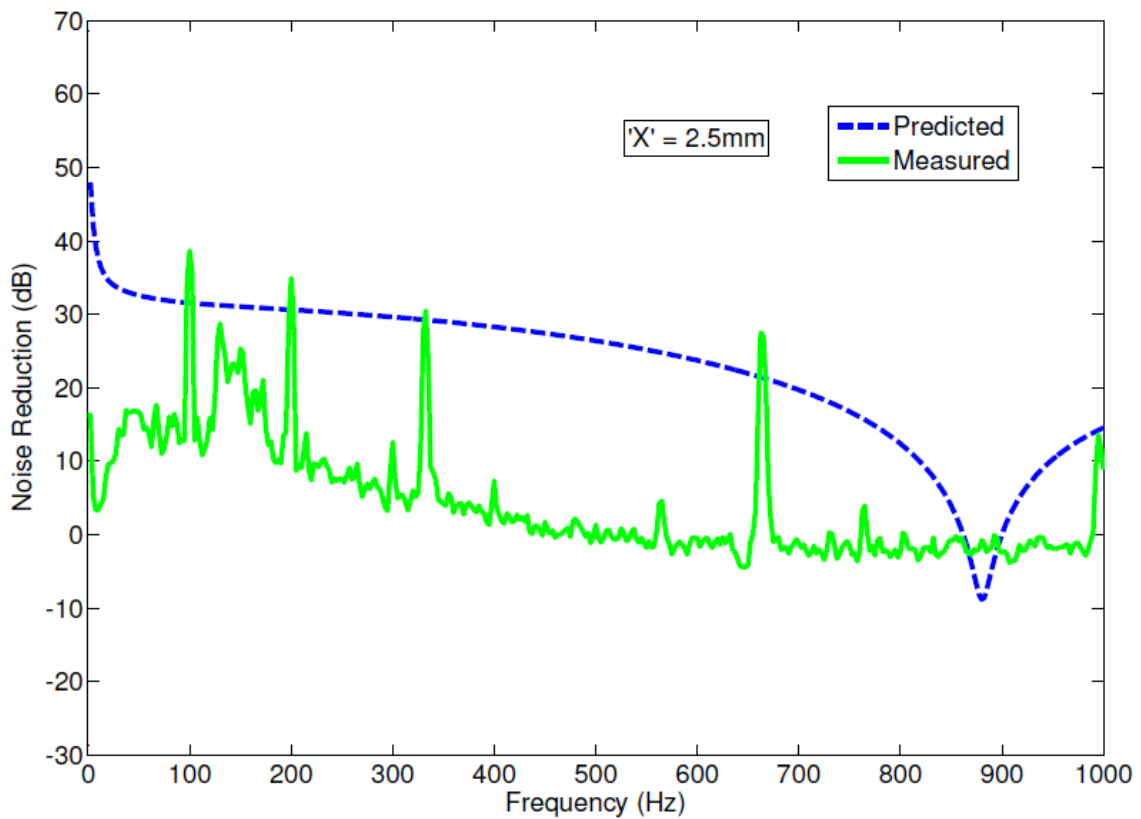


Figure 5-42 Predicted versus Measured Noise Reduction for a 400mm long tuner with a 2.5mm hole located 100mm from the tuner inlet

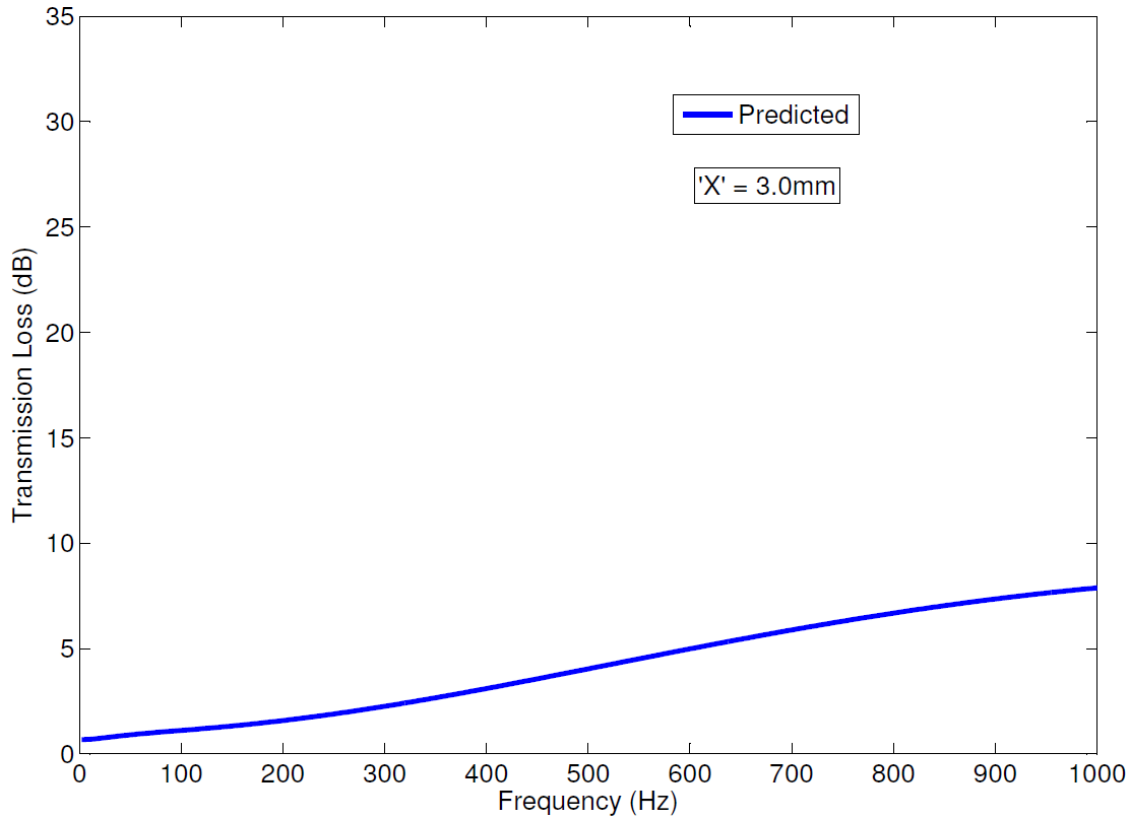


Figure 5-43 Predicted Transmission Loss for a 400mm long tuner with a 3.0mm hole located 100mm from the tuner inlet

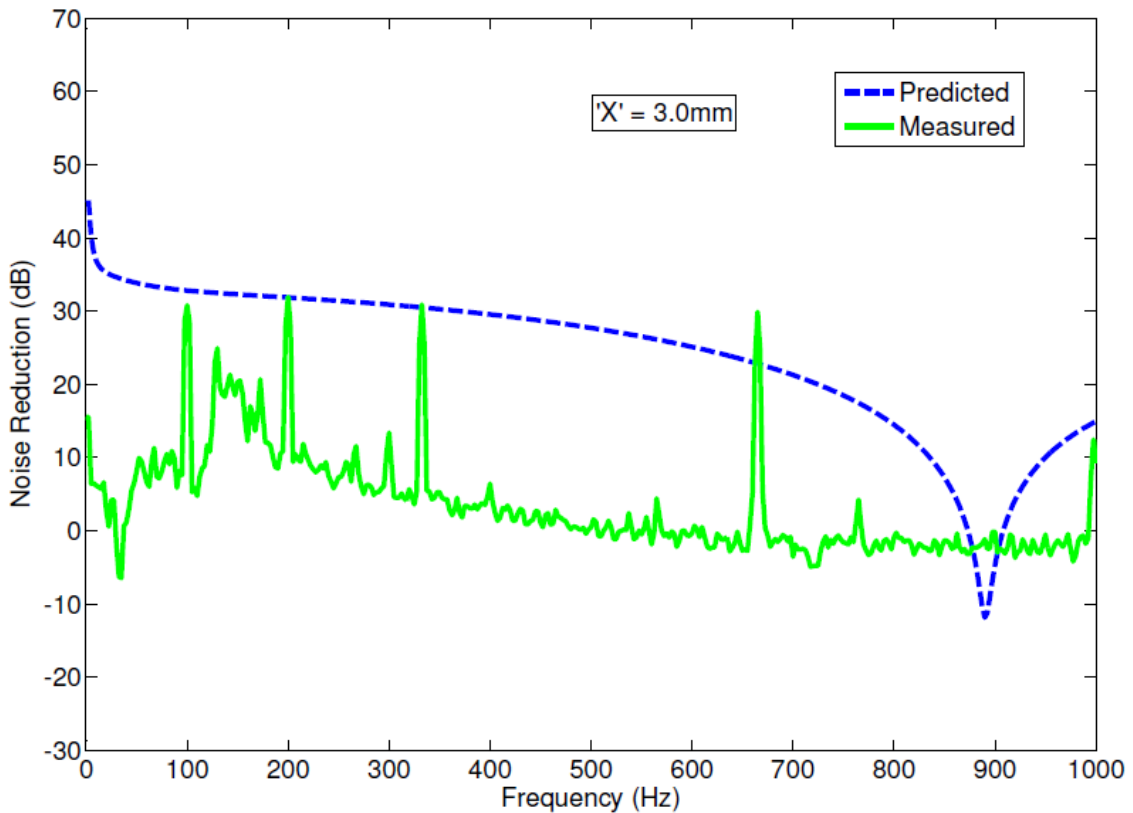


Figure 5-44 Predicted versus Measured Noise Reduction for a 400mm long tuner with a 3.0mm hole located 100mm from the tuner inlet

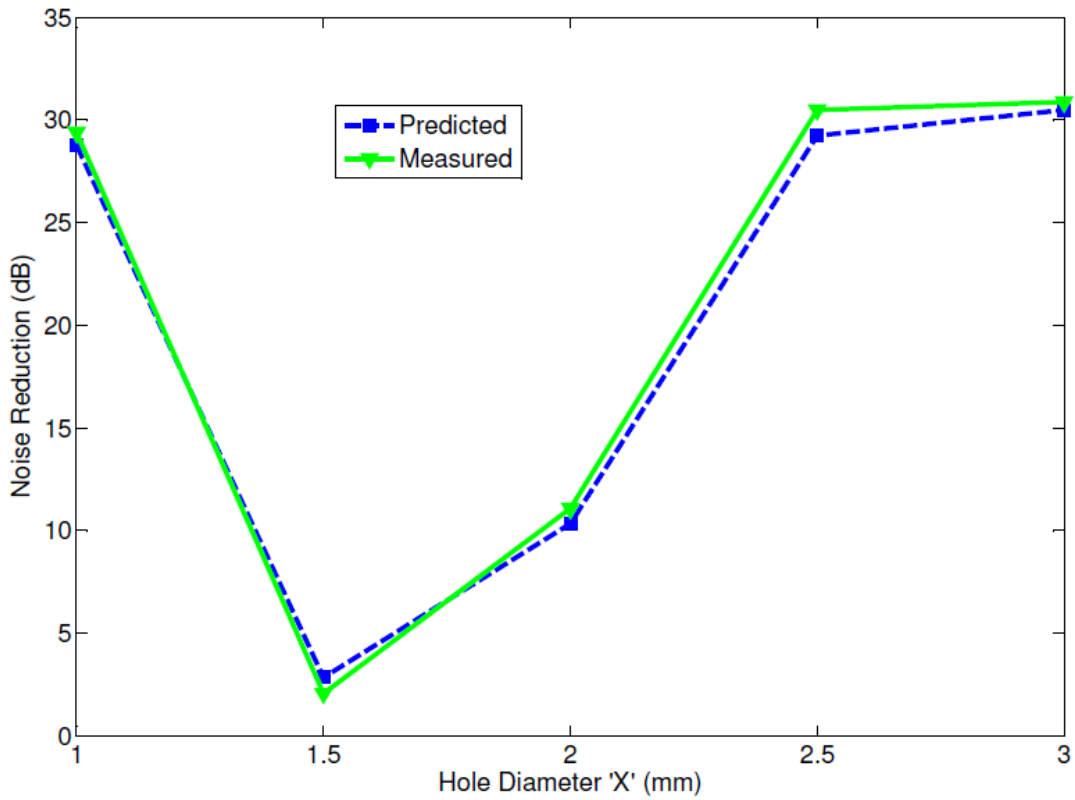


Figure 5-45 Hole Diameter – Predicted versus Measured Noise Reduction, 1st Order

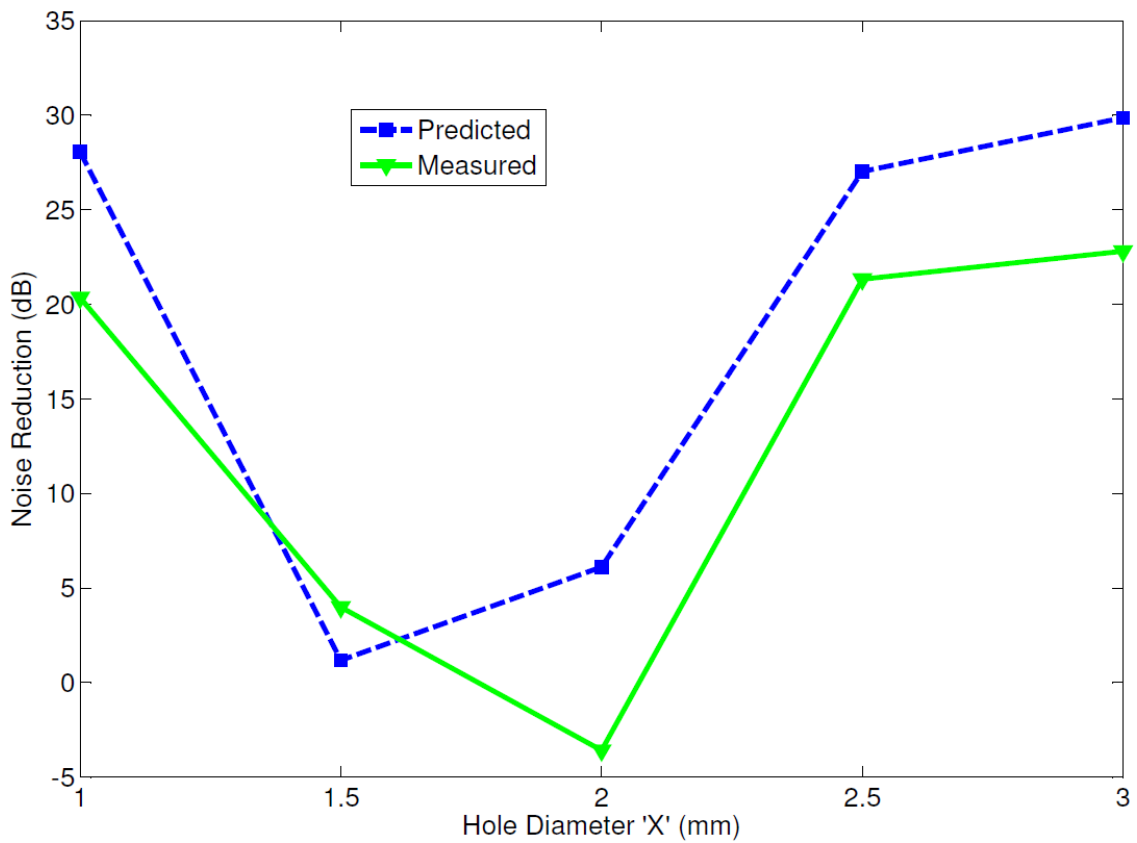


Figure 5-46 Hole Diameter – Predicted versus Measured Noise Reduction, 2nd Order

Good agreement between predicted and experimental results can be observed for 1st pump order noise reduction as can be seen in Figure 5.43. In particular, a significant drop in noise reduction is observed for the 1.5mm and 2.0mm holes. Whilst there is notable change in the form of the predicted noise reduction, there is very little change in the form of the predicted transmission loss. When considering the main difference between these two performance parameters i.e. an assumed anechoic termination for transmission loss and modelled termination impedance for noise reduction, weight is added to the argument that suggests the tuner works by its effect on the overall system, rather than by the modification of one its design parameters viewed in isolation. Taking this argument a step further, these results underline the need for a tuner design to be system specific. For example, a tuner with a 3.0mm hole located 100mm from the tuner inlet isn't necessarily going to provide 30dB or similar levels of noise reduction, in a system which is fundamentally different in terms of the parameters defining acoustic wave progression. Further investigation is required to confirm this theory and details are outlined in Section 6.3.

5.4 Multi-hole Validation

This section is concerned with validating the elements of the model concerned with the inclusion of multiple holes over the tuner length. As presented in Chapter 3, the model elements used here are the same as those used for the 'Hole Location' model, where the diameter and perforation rate properties are varied accordingly.

The model should represent the varied results observed during the experiments, in particular the differences between 2 hole and 3 hole configurations at the pump fundamental frequency.

5.4.1 Analysis and discussion

Following the approach to Tuner Length analysis described in Section 5.1.1, Equation 3.3 was used to calculate the theoretical transmission loss of the samples in this experiment. Equation 3.2 was used to predict the theoretical noise reduction of the system in this experiment and Equation 4.1 was used to calculate the experimental noise reduction based on the measured data captured during the experimental phase. Initially, two-hole configurations are analysed followed by three-hole configurations. Each discrete sample is illustrated in Figures 5.47 – 5.56 for a tuner with two holes, and Figures 5.59 – 5.68 for a tuner with three holes.

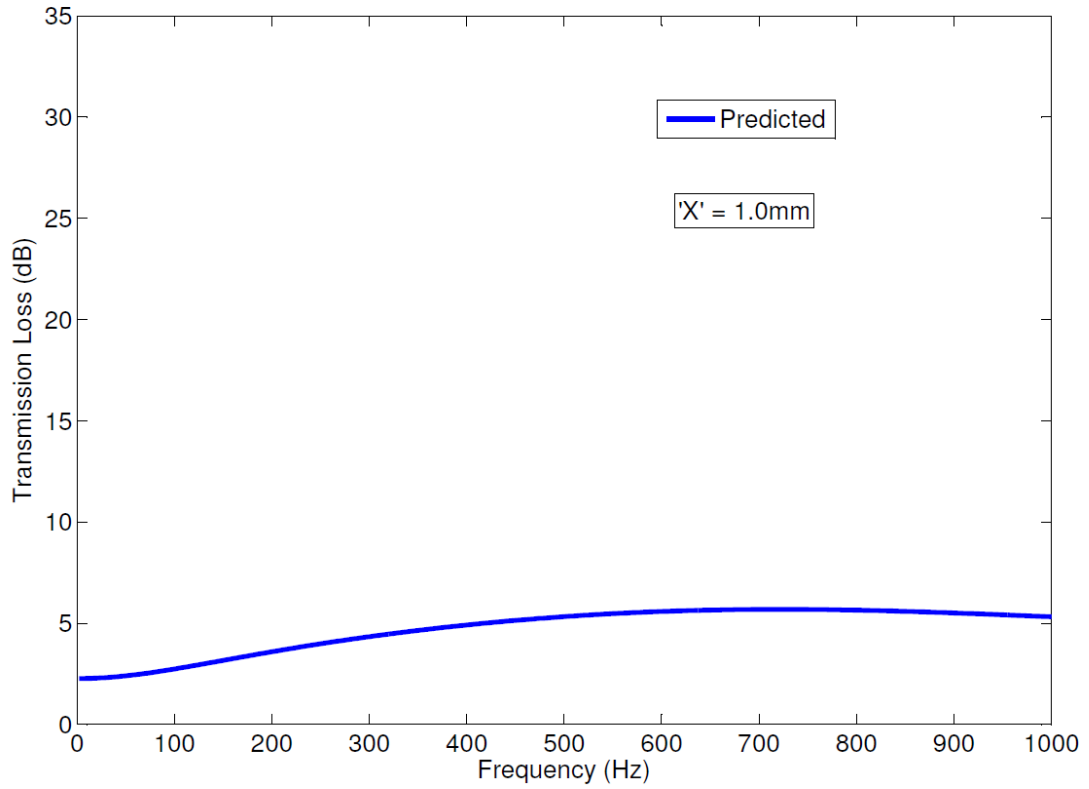


Figure 5-47 Predicted Transmission Loss for a 400mm long tuner with two 1.0mm holes located 100mm and 200mm from the tuner inlet

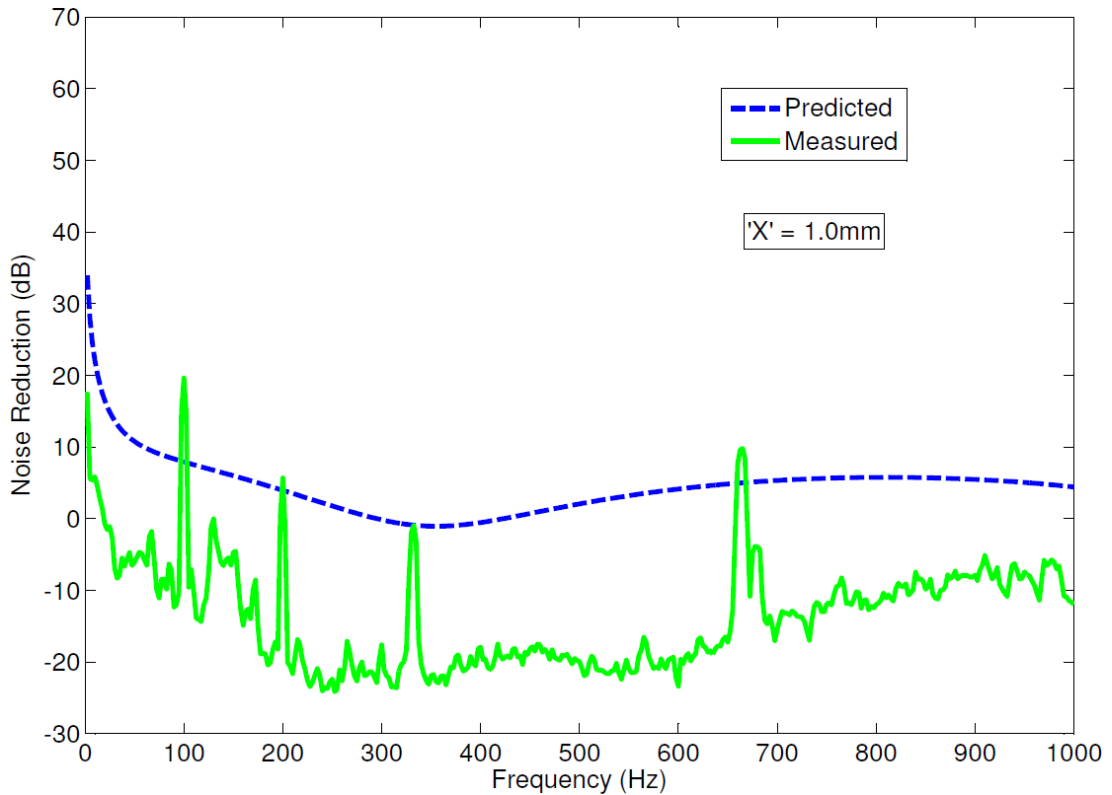


Figure 5-48 Predicted versus Measured Noise Reduction for a 400mm long tuner with two 1.0mm holes located 100mm and 200mm from the tuner inlet

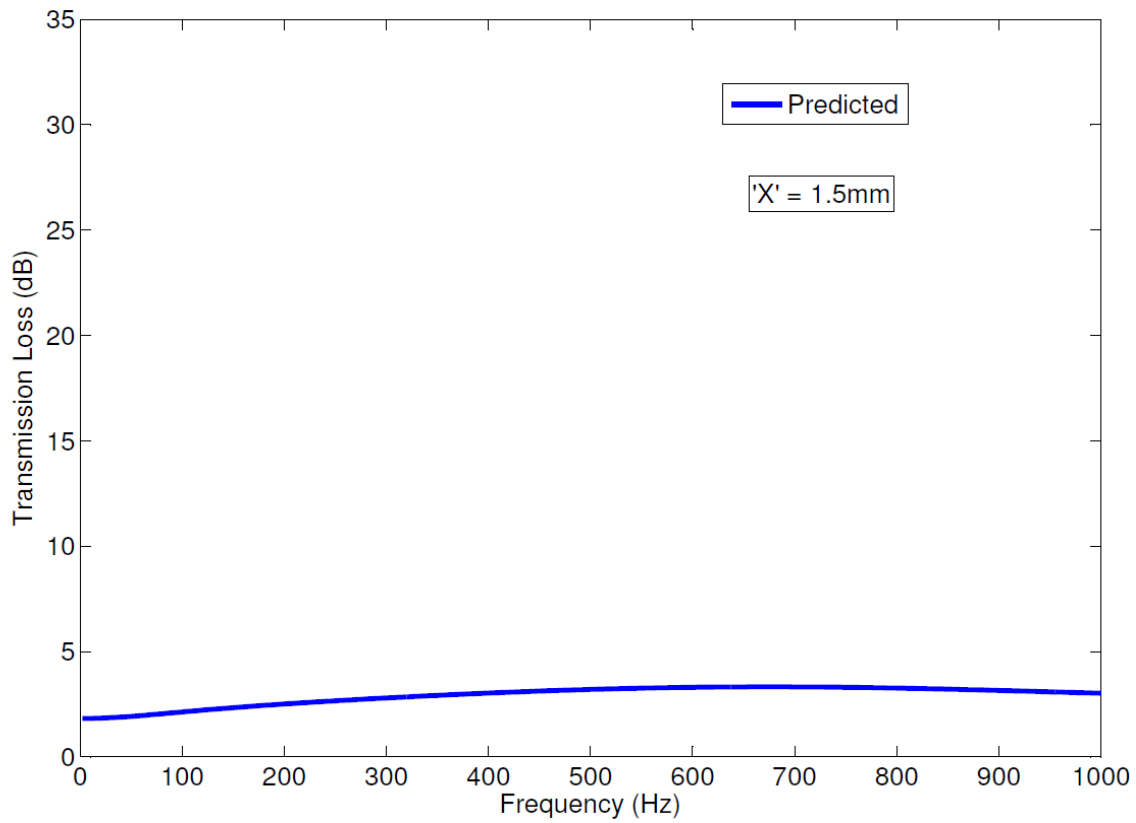


Figure 5-49 Predicted Transmission Loss for a 400mm long tuner with two 1.5mm holes located 100mm and 200mm from the tuner inlet

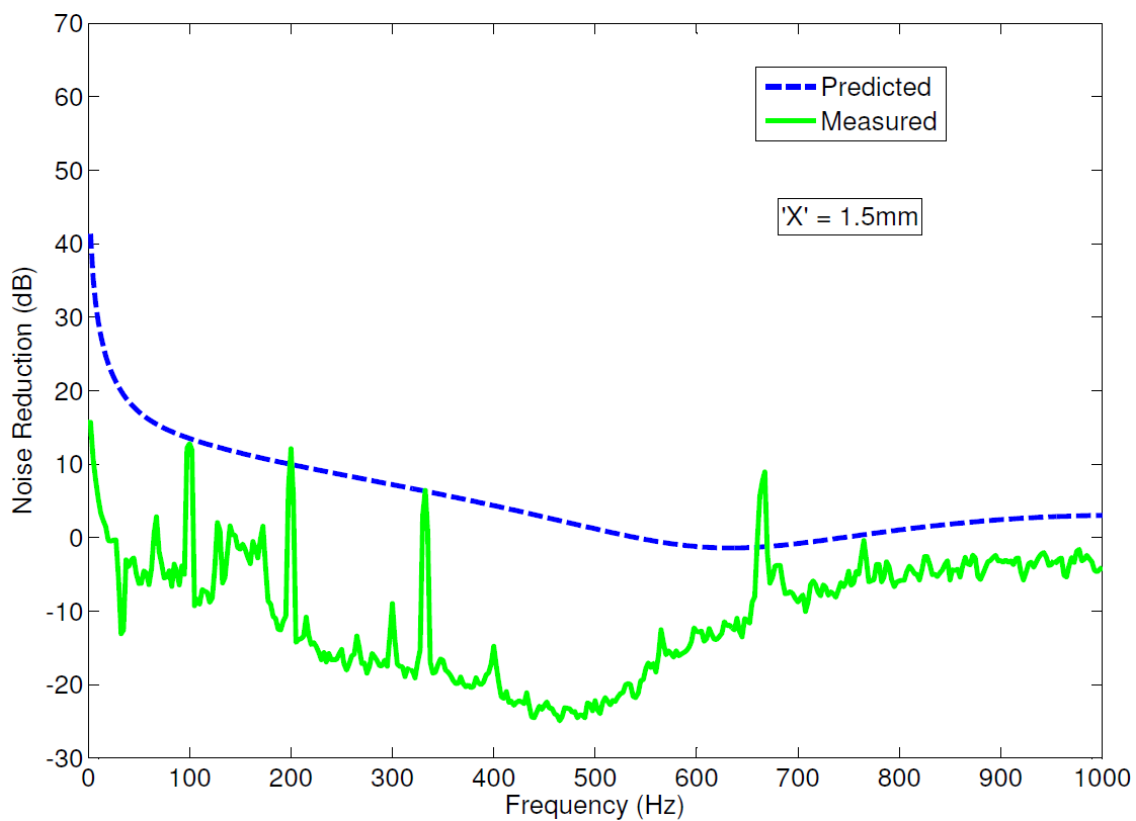


Figure 5-50 Predicted versus Measured Noise Reduction for a 400mm long tuner with two 1.5mm holes located 100mm and 200mm from the tuner inlet

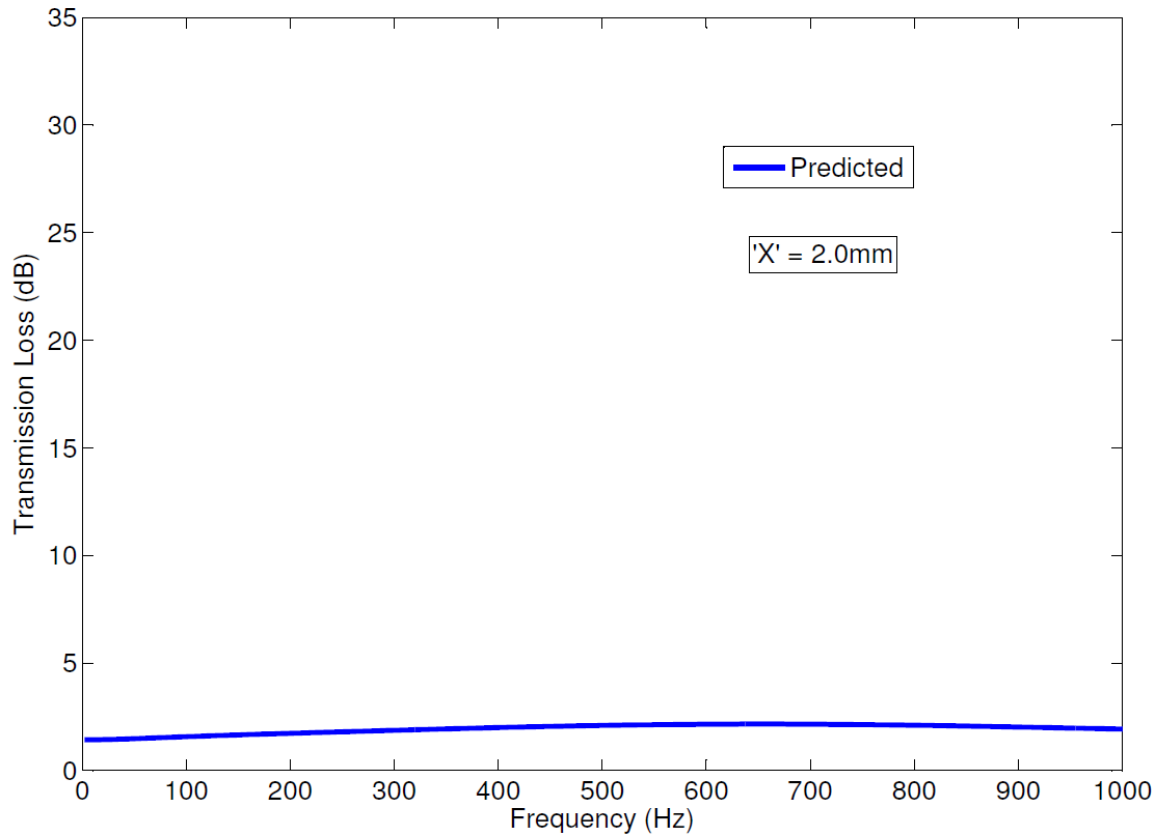


Figure 5-51 Predicted Transmission Loss for a 400mm long tuner with two 2.0mm holes located 100mm and 200mm from the tuner inlet

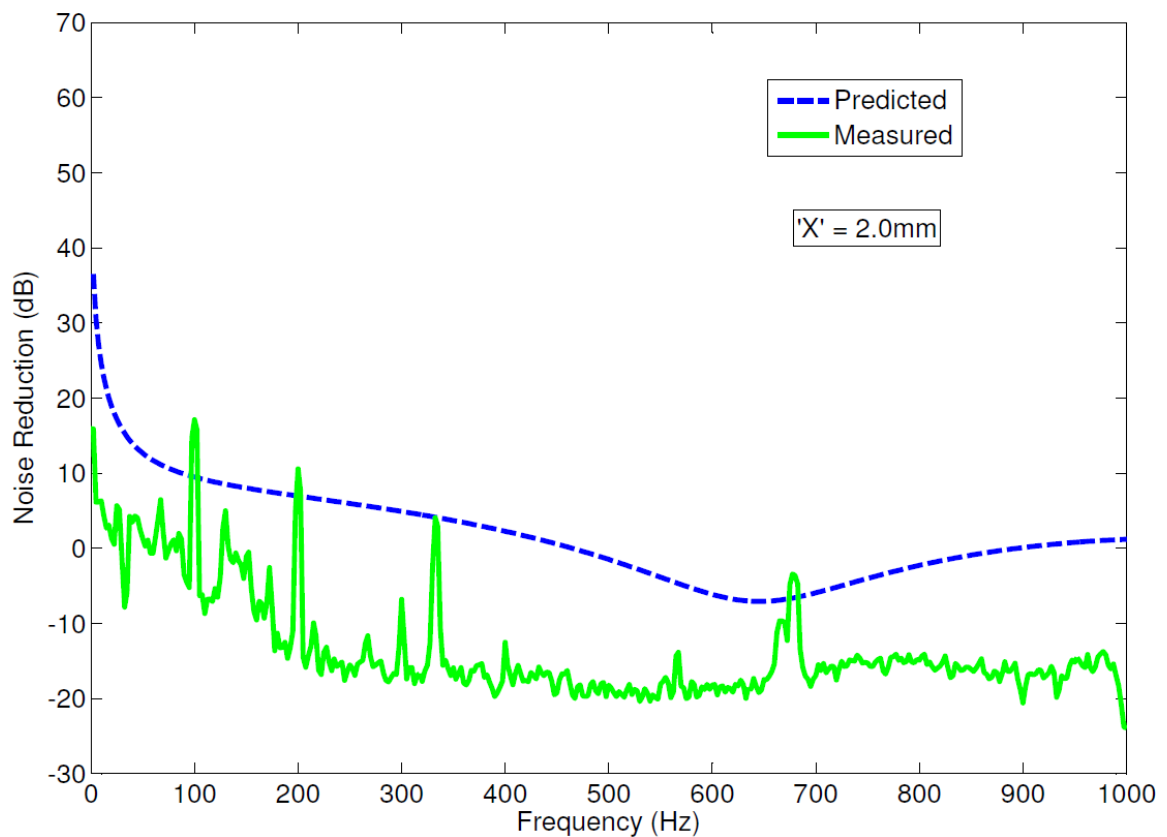


Figure 5-52 Predicted versus Measured Noise Reduction for a 400mm long tuner with two 2.0mm holes located 100mm and 200mm from the tuner inlet

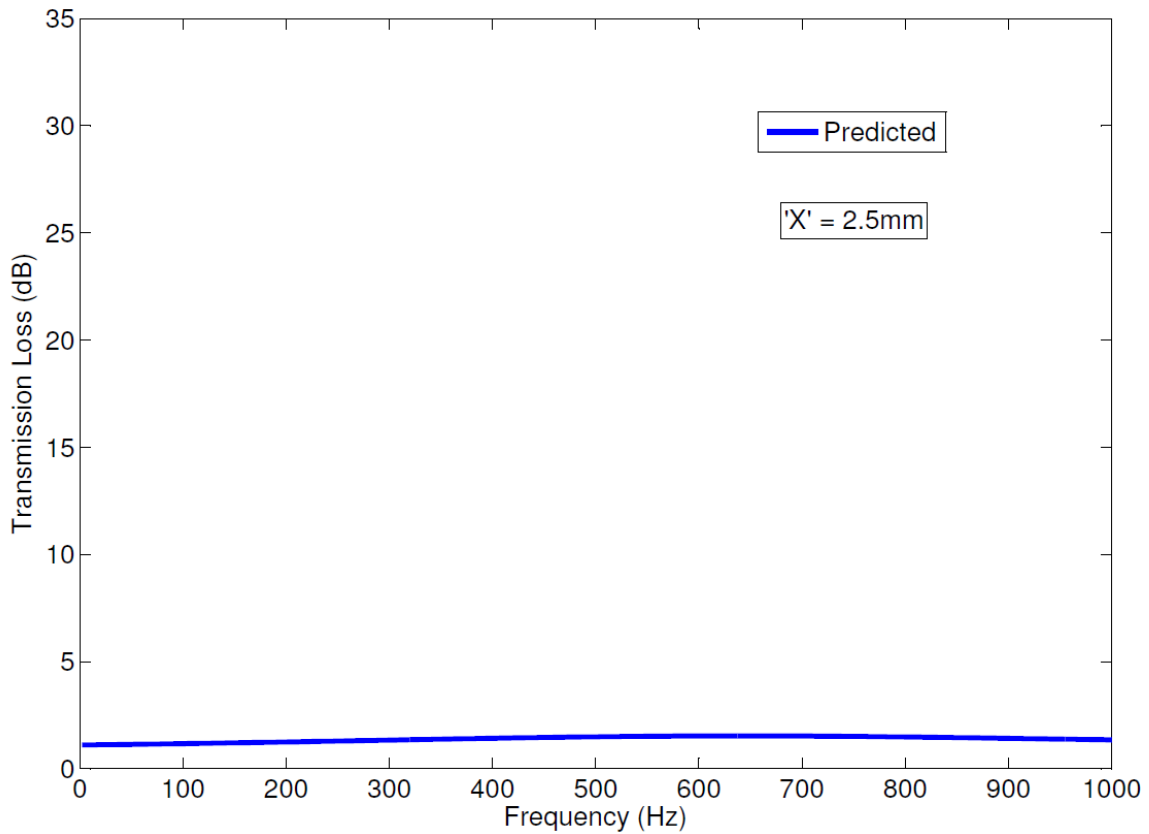


Figure 5-53 Predicted Transmission Loss for a 400mm long tuner with two 2.5mm holes located 100mm and 200mm from the tuner inlet

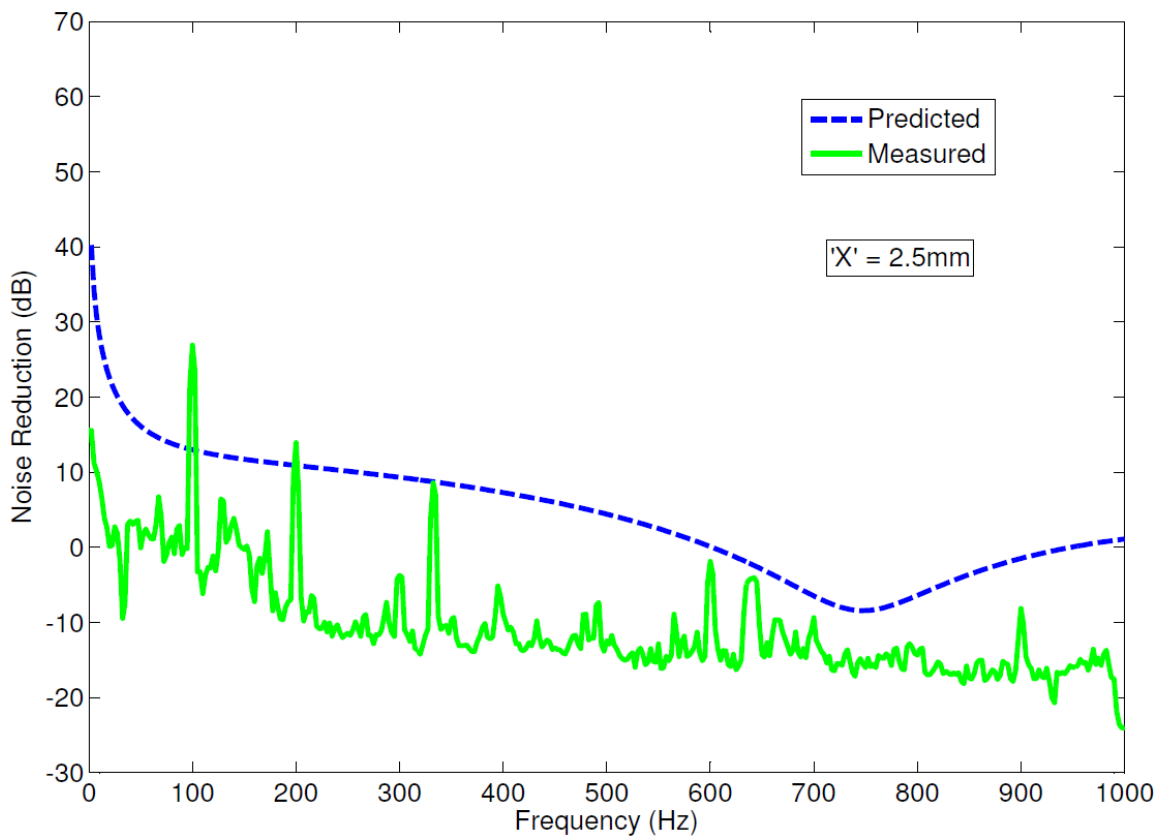


Figure 5-54 Predicted versus Measured Noise Reduction for a 400mm long tuner with two 2.5mm holes located 100mm and 200mm from the tuner inlet

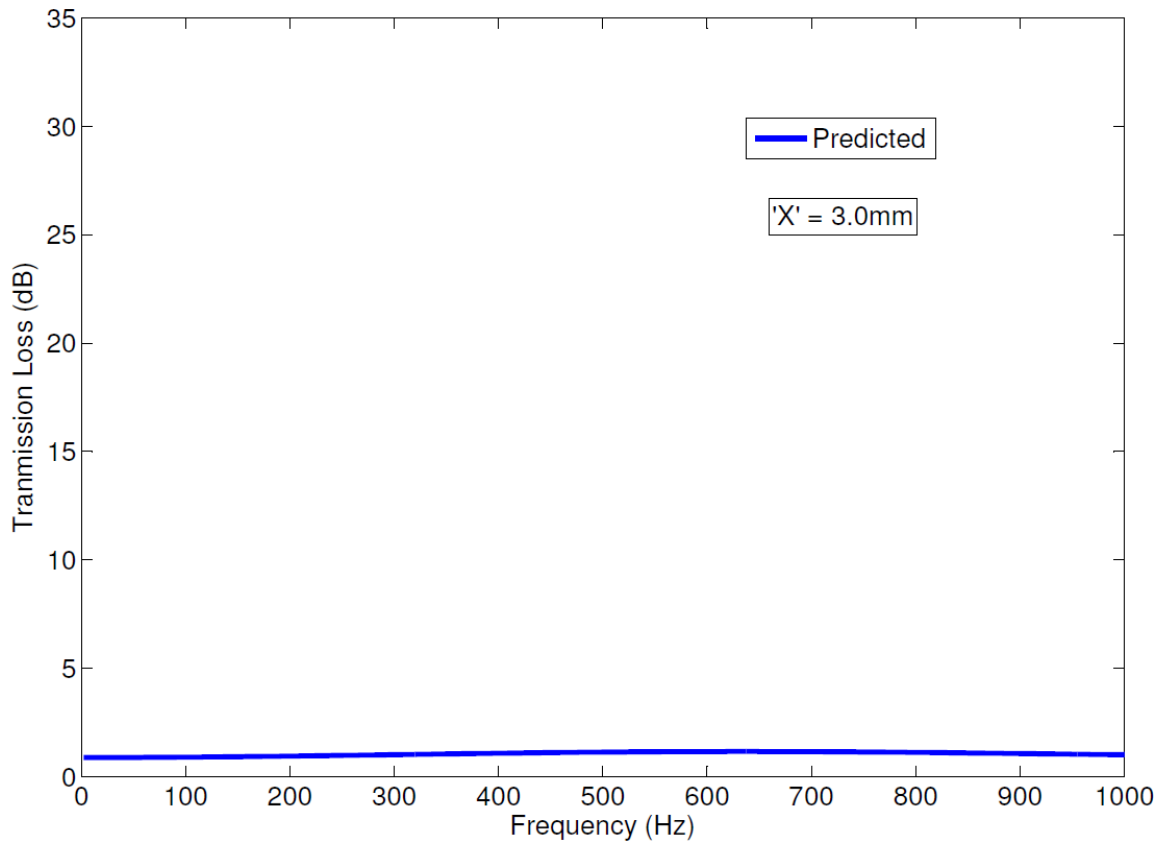


Figure 5-55 Predicted Transmission Loss for a 400mm long tuner with two 3.0mm holes located 100mm and 200mm from the tuner inlet

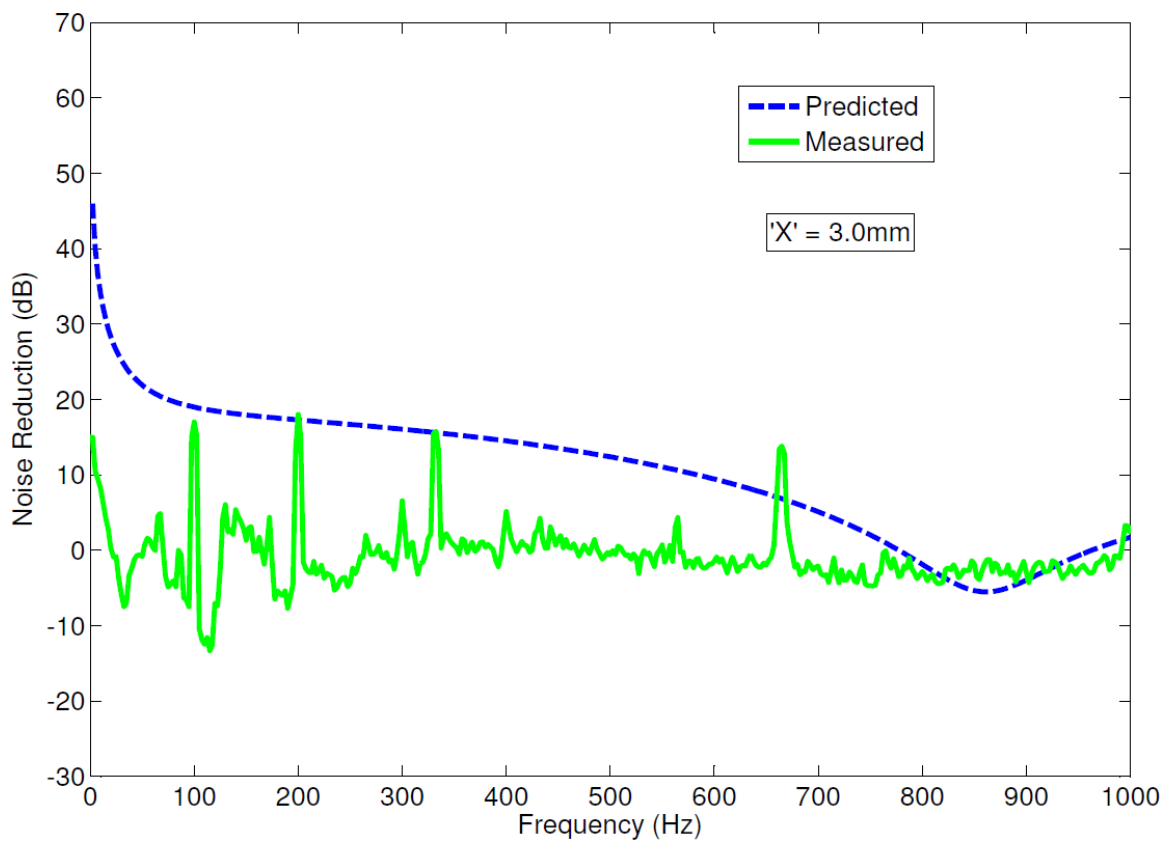


Figure 5-56–Predicted versus Measured Noise Reduction for a 400mm long tuner with two 3.0mm holes located 100mm and 200mm from the tuner inlet

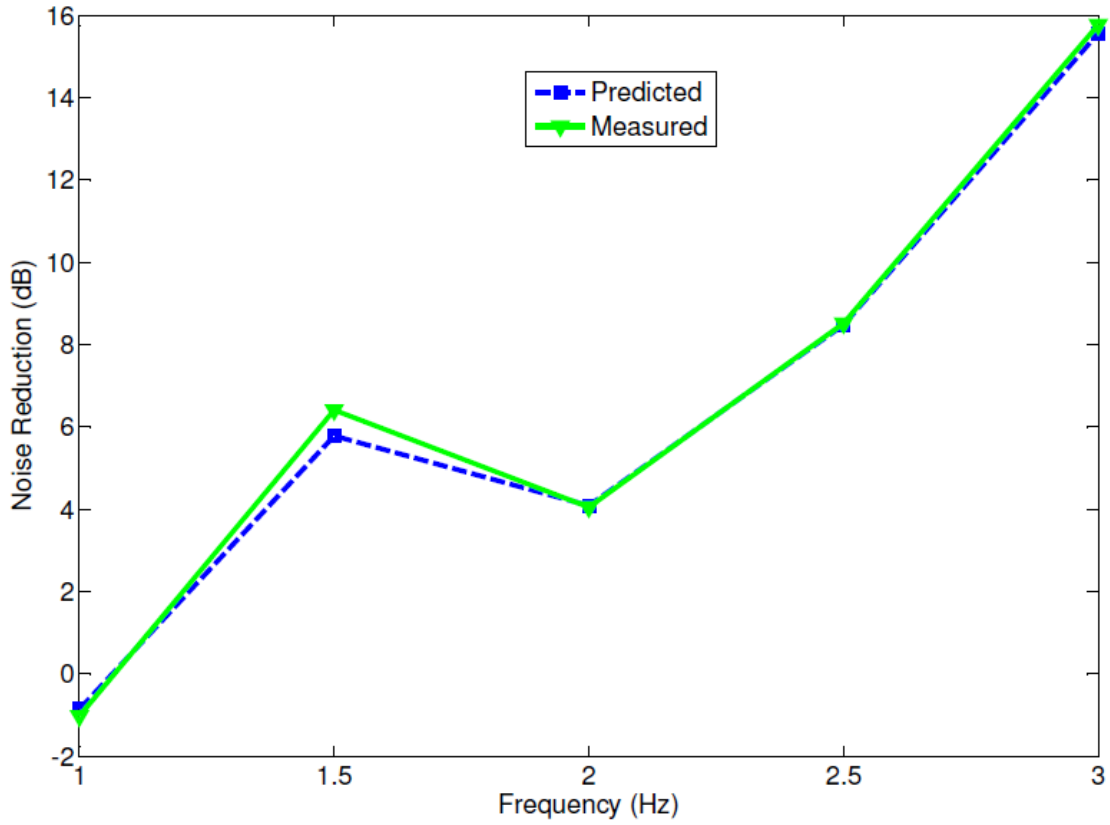


Figure 5-57 Predicted versus Measured Noise Reduction for tuners with two holes, 1st Pump Order.

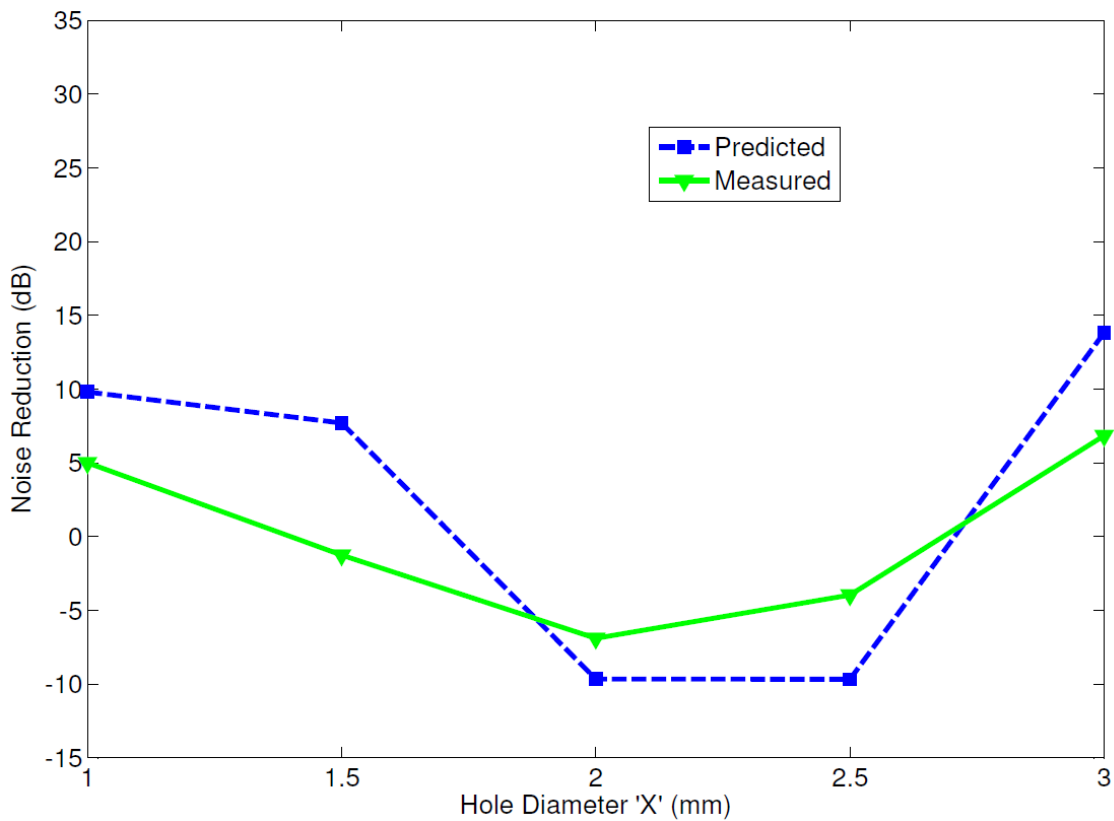


Figure 5-58 Predicted versus Measured Noise Reduction for tuners with two holes, 2nd Pump Order.

As illustrated in Figure 5.57, agreement between predicted and experimental noise reduction results is good for all samples. Comparing Figure 5.45 with Figure 5.57, it can be observed that the addition of a second hole, or increase in perforation rate, can significantly alter the performance of the tuner. Further insight into the multi-hole tuner behaviour is provided in section 5.5.11.

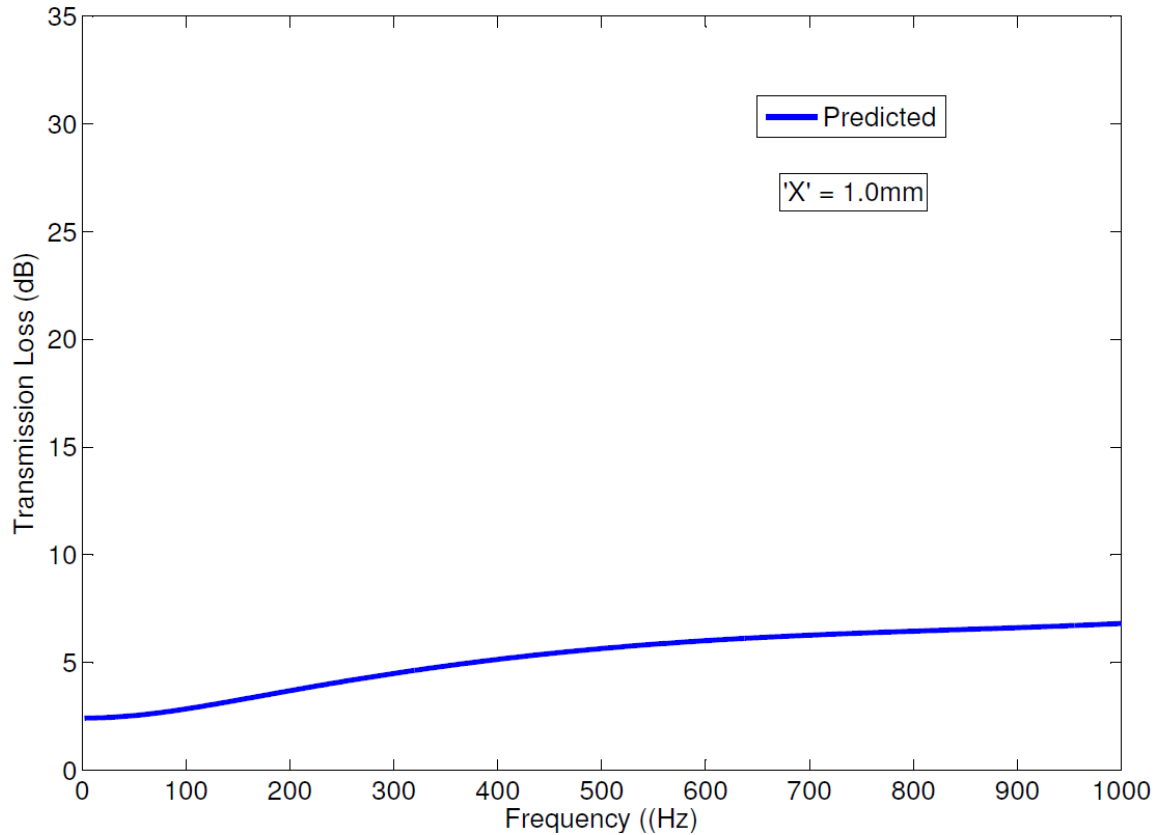


Figure 5-59 Predicted Transmission Loss for a 400mm long tuner with three 1.0mm holes located at 100mm, 200mm and 300mm from the tuner inlet

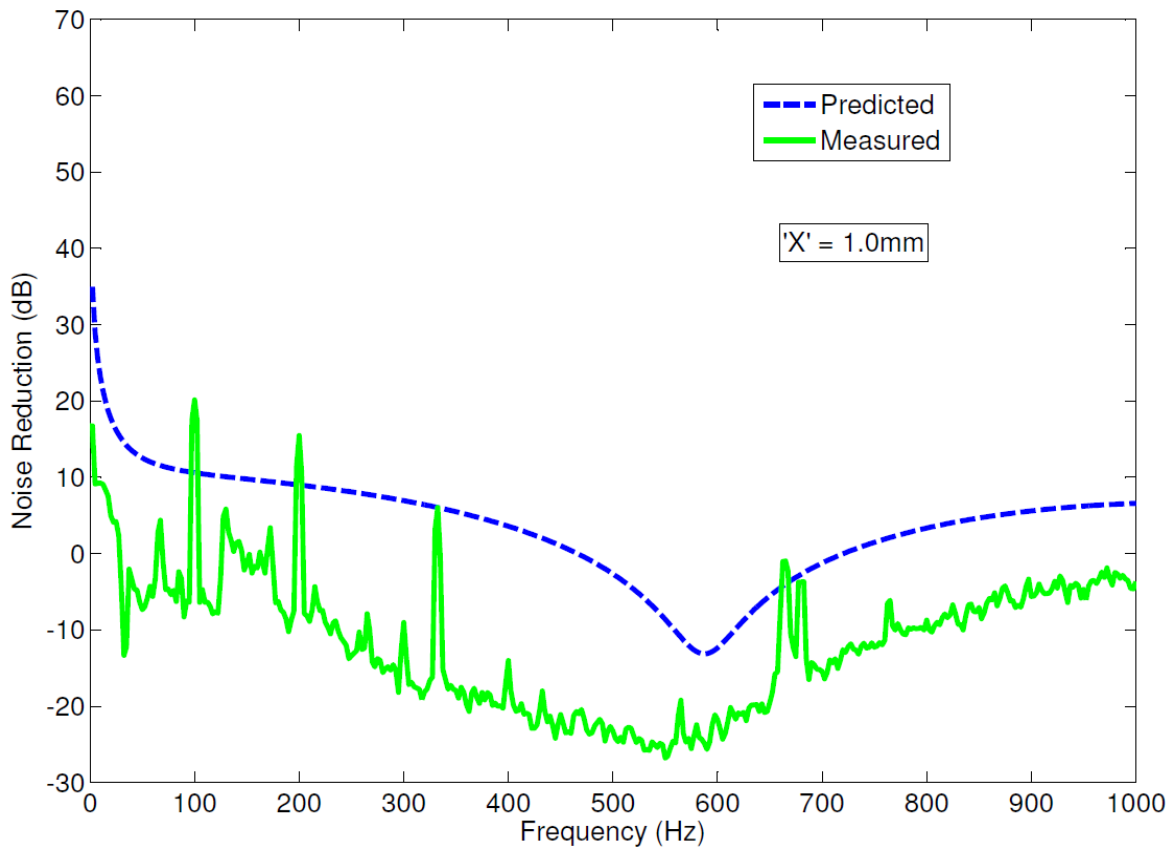


Figure 5-60 Predicted versus Measured Noise reduction for a 400mm long tuner with three 1.0mm holes located 100mm, 200mm and 300mm from the tuner inlet

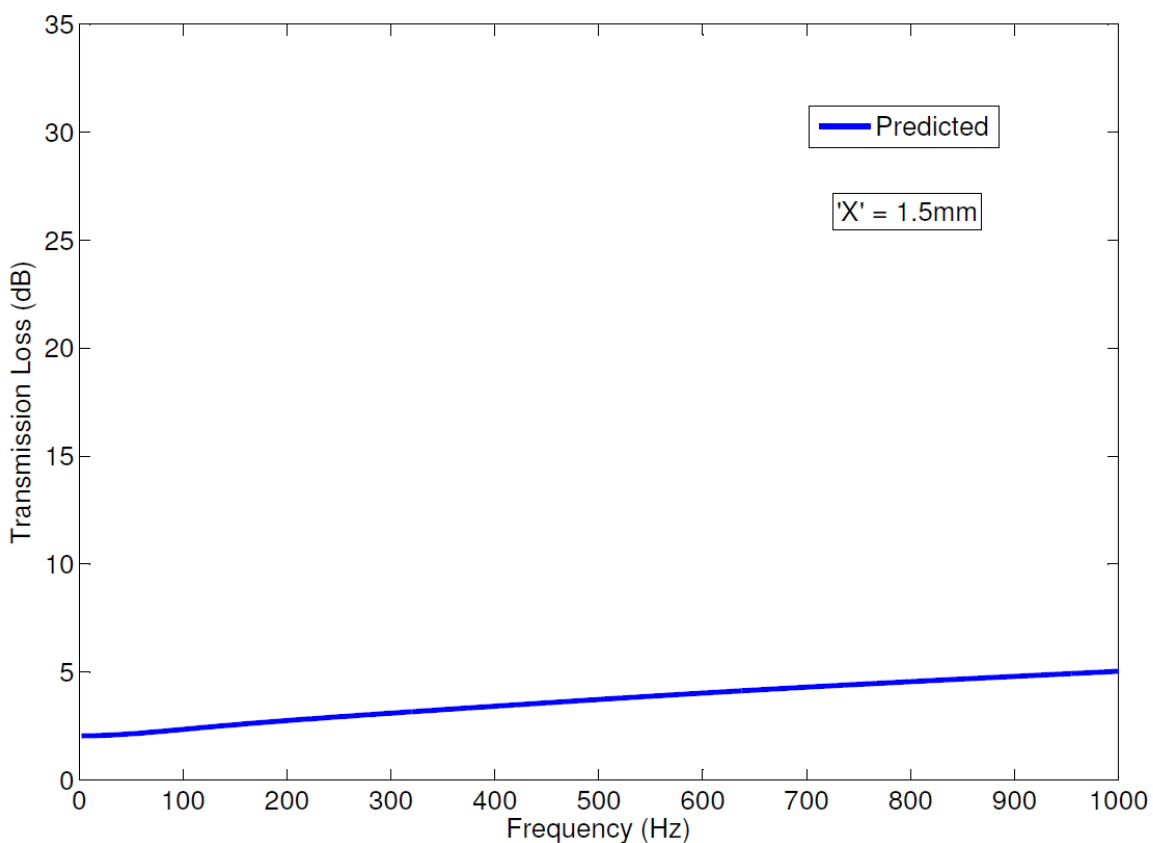


Figure 5-61 Predicted Transmission Loss for a 400mm long tuner with three 1.5mm holes located 100mm, 200mm, and 300mm from the tuner inlet

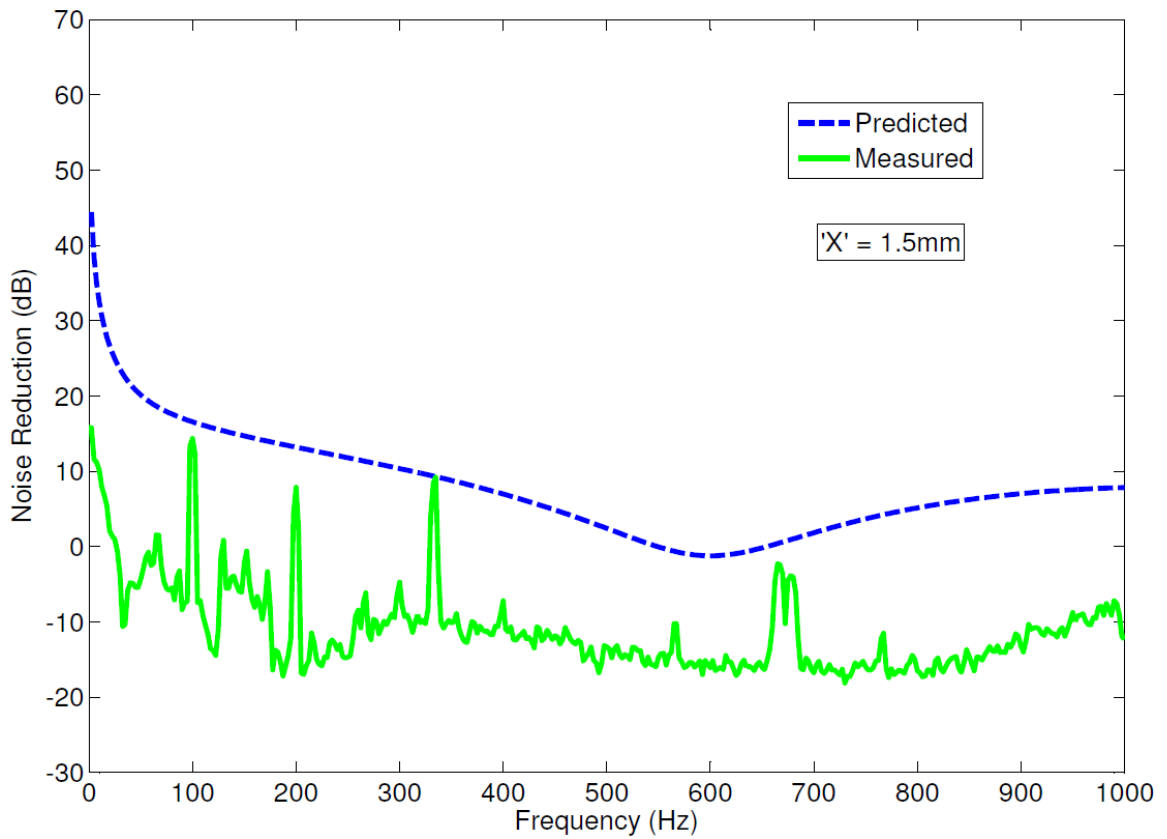


Figure 5-62 Predicted versus Measured Noise Reduction for a 400mm long tuner with three 1.5mm holes located 100mm, 200mm and 300mm from the tuner inlet

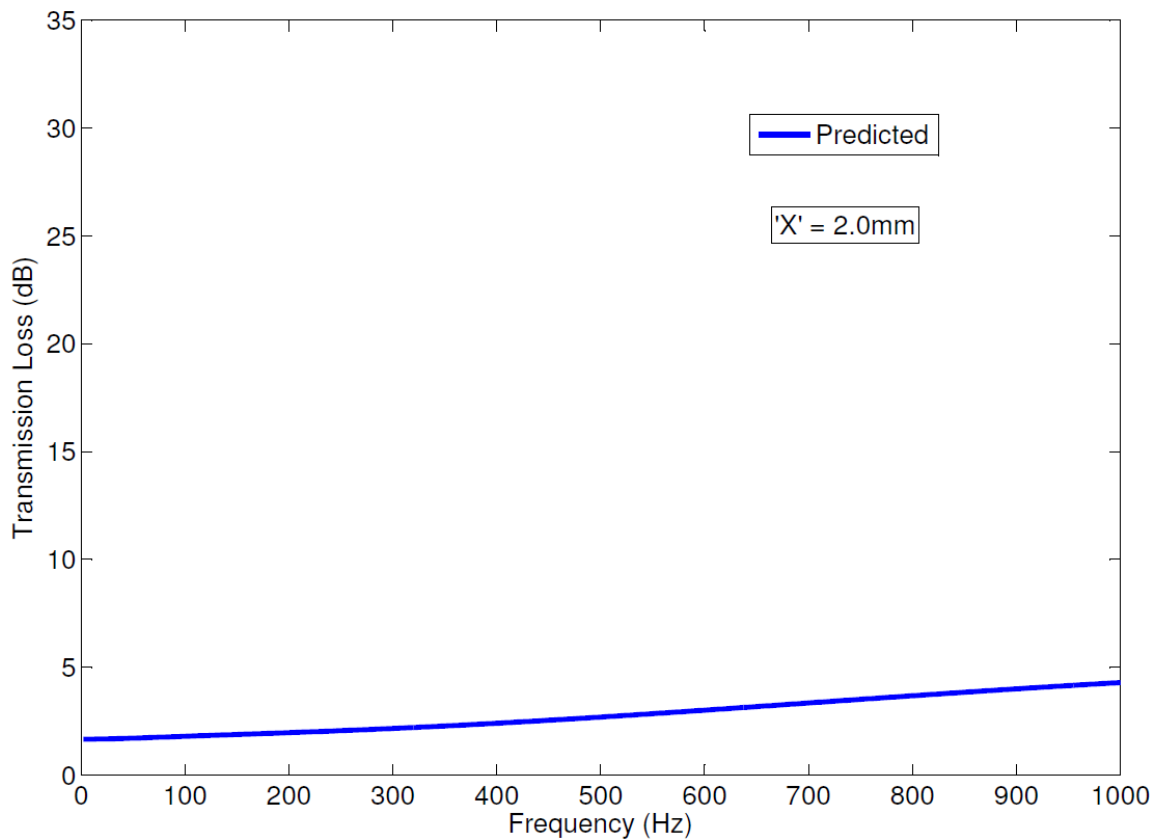


Figure 5-63 Predicted Transmission Loss for a 400mm long tuner with three 1.5mm holes located 100mm, 200mm and 300mm from the tuner inlet

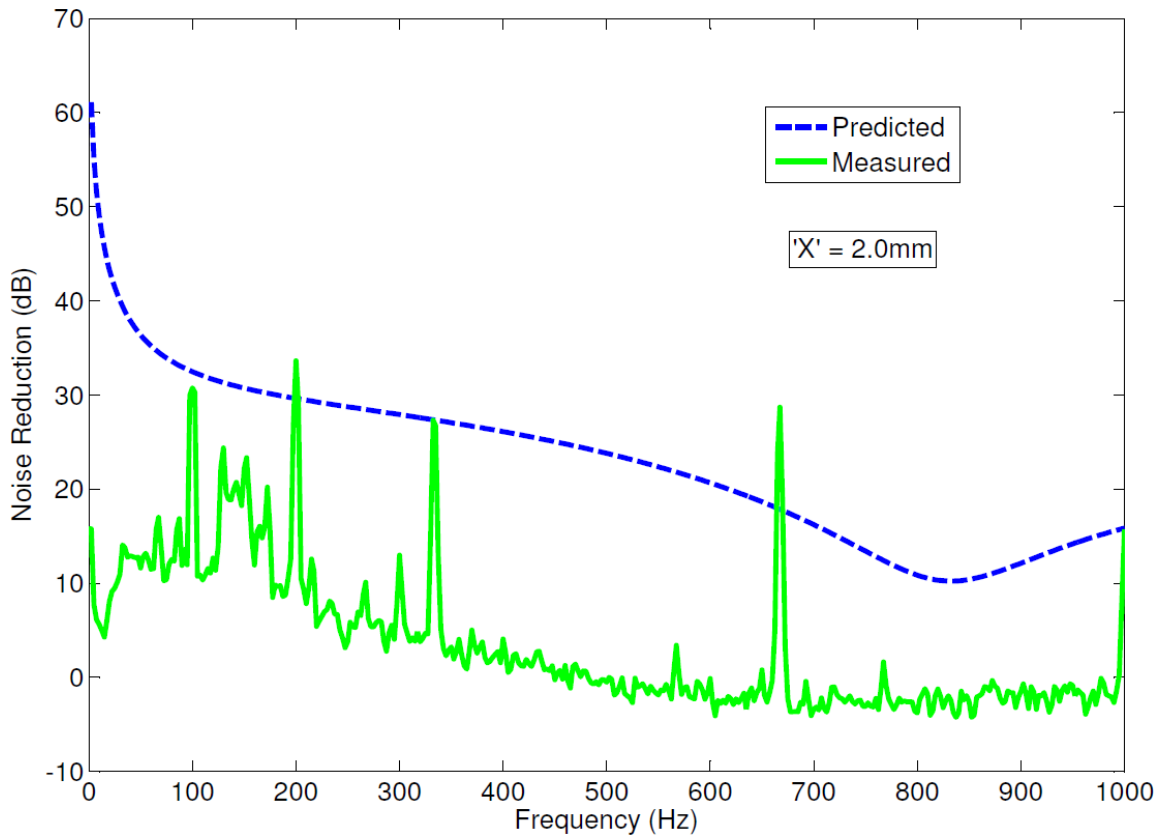


Figure 5-64 Predicted versus Measured Noise Reduction for a 400mm long tuner with three 2.0mm holes located 100mm, 200mm and 300mm from the tuner inlet

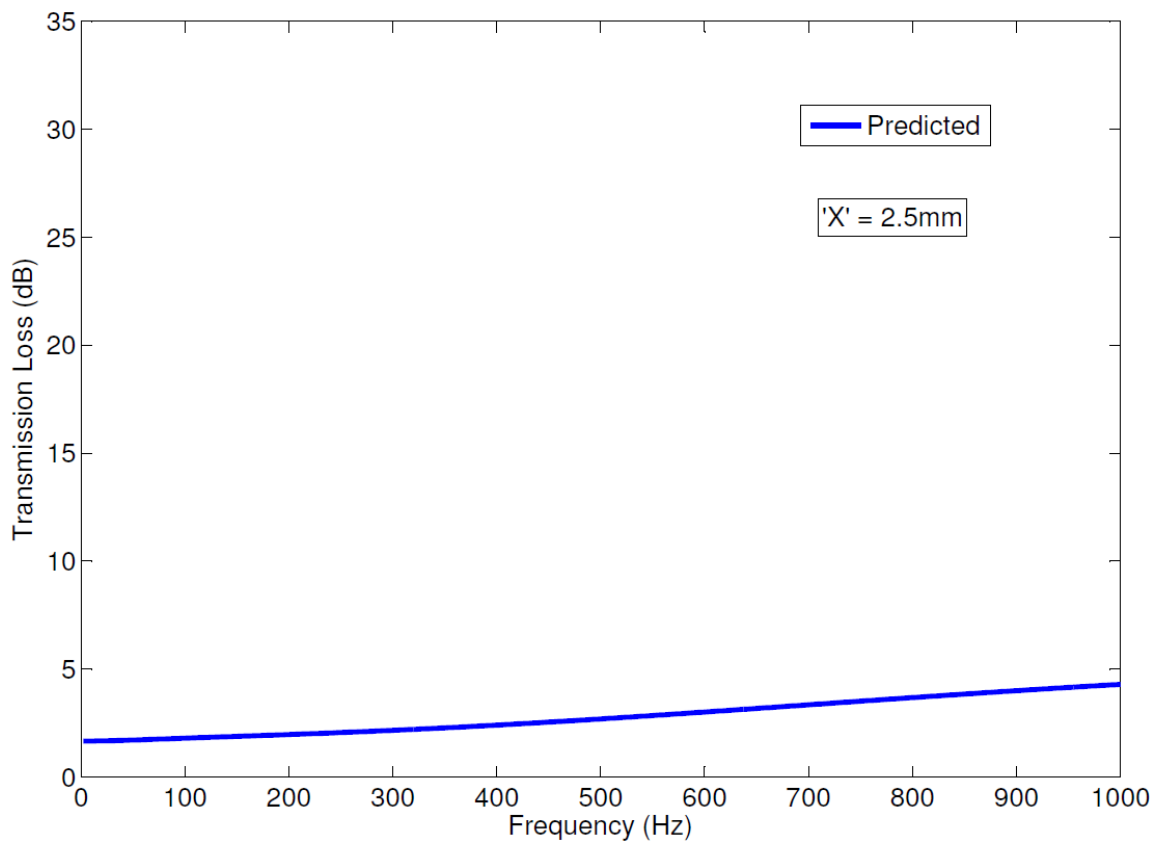


Figure 5-65 Predicted Transmission Loss for a 400mm long tuner with three 3.0mm holes located 100mm, 200mm and 300mm from the tune inlet

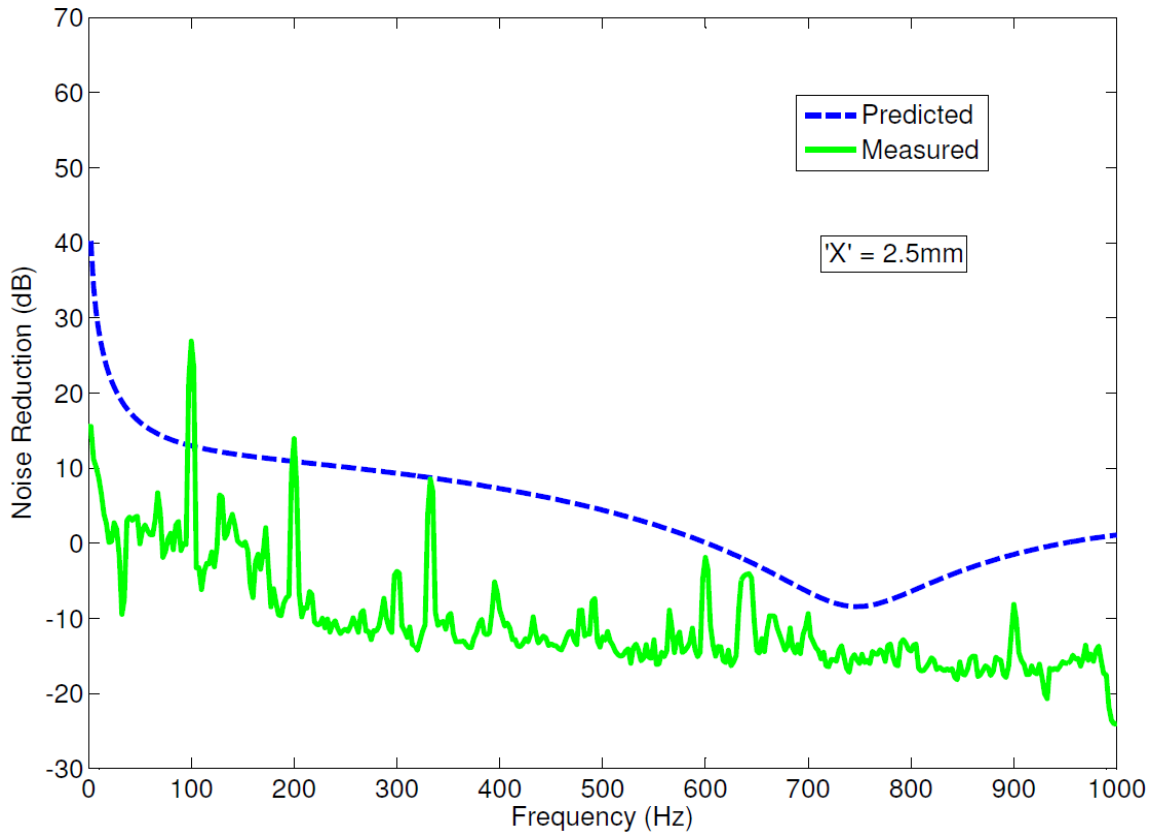


Figure 5-66 Predicted versus Measured Noise Reduction for a 400mm long tuner with three 2.5mm holes located 100mm, 200mm and 300mm from the tuner inlet

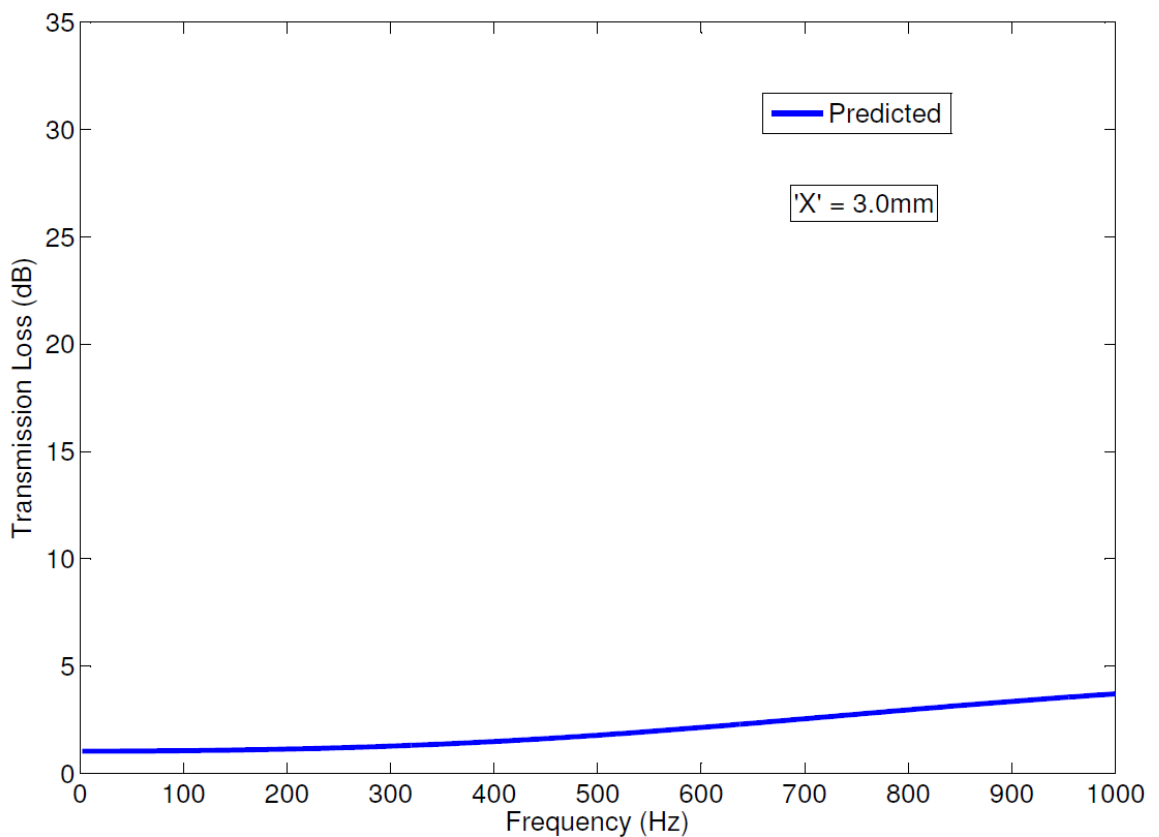


Figure 5-67 Predicted Transmission Loss for a 400mm long tuner with three 3.0mm holes located 100mm, 200mm and 300mm from the tuner inlet

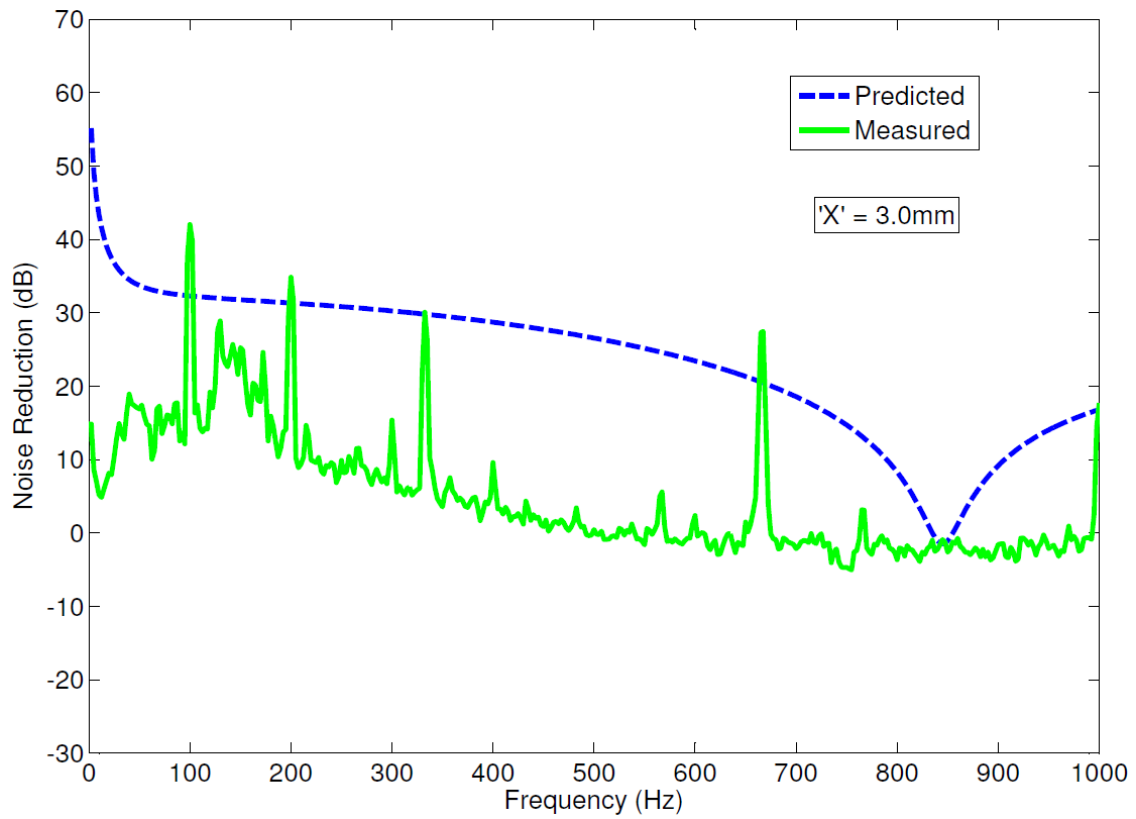


Figure 5-68 Predicted versus Experimental Noise Reduction for a 400mm long tuner with three 3.0mm holes located 100mm, 200mm and 300mm from the tuner inlet

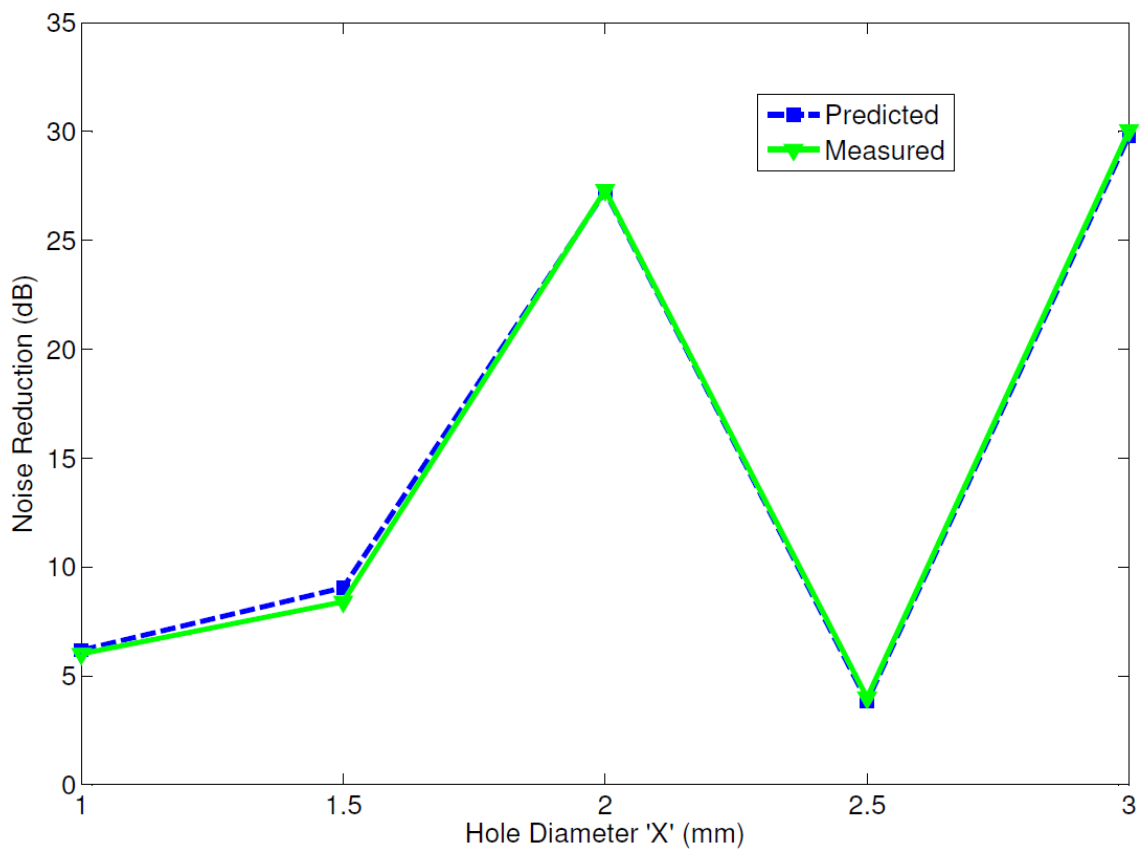


Figure 5-69 Predicted versus Experimental Noise Reduction for three holes tuners, 1st Pump Order.

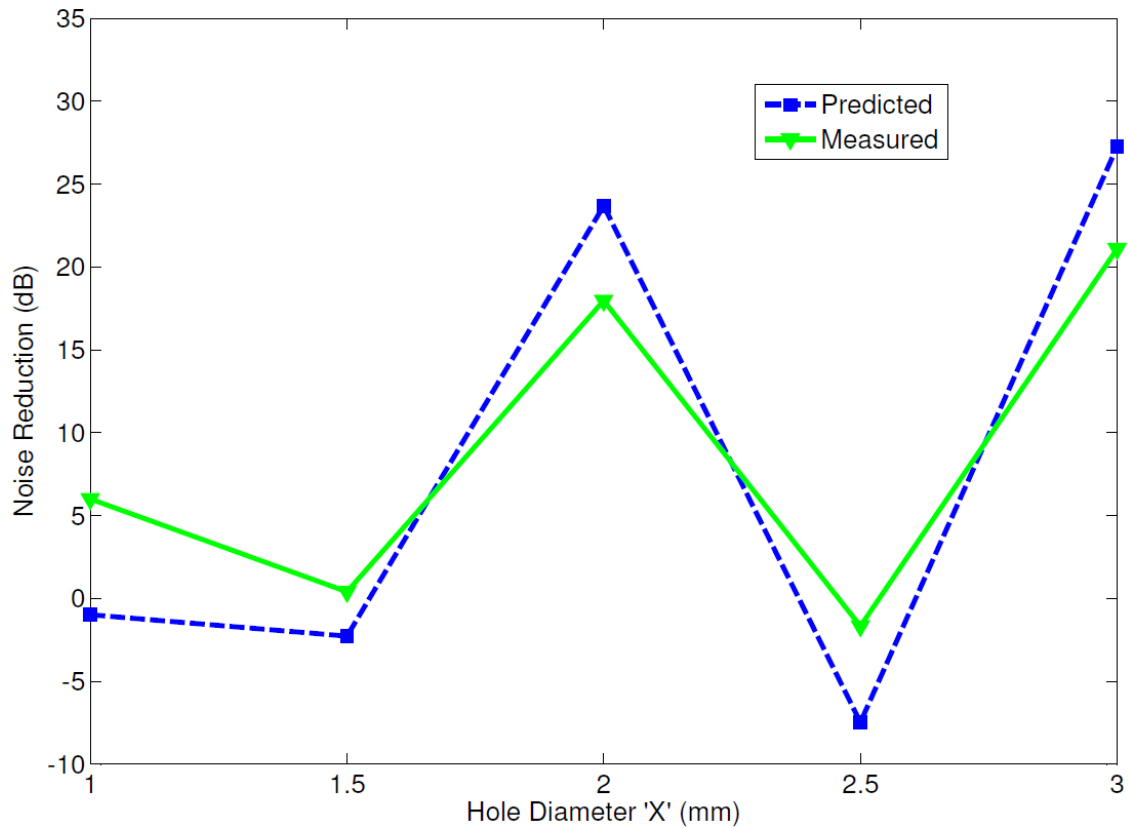


Figure 5-70 Predicted versus Experimental Noise Reduction for three hole tuners, 2nd Pump Order.

As with other experiments, agreement between predicted and experimental noise reduction results is good for all samples. Whilst the 1st pump order is of greatest interest, it is also noted that the coherent magnitudes of the predicted noise reduction is in accordance with the experimental measurements. This is most notable for the 3 x 1.0mm diameter hole tuner shown in Figure 5.60, where the dip at 550 Hz is replicated.

These results have further confirmed the effect of the tuner configuration on the system, which is not immediately apparent from the associated tuner transmission loss. This is most obvious when considering the 1x, 2x and 3x 2.0mm hole tuners; the noise reduction values at the pump fundamental frequency for these tuners are significantly different, however the associated values of transmission loss are reasonably similar. As discussed in Section 5.3.1, it would appear that the change in the tuner design, directly influences the termination impedance in the system, which is simply not considered when evaluating Transmission Loss. For this reason, it is not advisable to design plastic tuners on the basis of Transmission Loss predictions.

The following section will analyse the experimental data presented in Chapter 4, and propose a theoretical solution to determine the termination impedance.

5.5 Termination Impedance

The experimental results presented in Chapter 4 for the termination impedance values suggest that there may be a relationship between the termination impedance and the measured auto power spectrum level of the pressure at the tuner outlet at the first pump order of 333Hz. Before proposing a theoretical solution for this relationship, it is firstly important to confirm that the relationship exists. Once this relationship is confirmed, possible solutions can be analysed and discussed.

5.5.1 Analysis and Discussion

Examining the termination impedance values and the auto power spectrum of the pressure at the first pump order at the tuner outlet, it appears that the relationship is linear in nature. To confirm this, a correlation coefficient was calculated between the two data sets for each experiment. The correlation coefficient determines the tendency for one data set to linearly increase or decrease with respect to the other. Correlation coefficients range from -1 to 1 where

- Values close to 1 suggest there is a positive linear relationship between the two data sets.
- Values close to -1 suggest there is a negative linear relationship between the two data sets
- Values close to 0 suggest there is no linear relationship between the two data sets.

It should be noted that there are potential sources of error with both the experimental measurements and the empirical determination of the termination impedance constant. Whilst these errors may differ from experiment to experiment, it is not expected to significantly affect the results overall. Table 5.1 summarizes the correlation coefficients for each experiment.

Experiment	Correlation Coefficient
Tuner Length	0.9990
Hole Location	0.9369
Hole Diameter	0.9951
Multi-Hole (2 Hole)	0.9004
Multi-Hole (3 Hole)	0.9548

Table 5-1 Experimental Correlation Coefficients between termination impedance values and auto spectrum levels of the pressure at the first pump order at the tuner outlet

As can be seen from Table 5.1, the coefficient values are all very high and close to 1. This confirms the existence of a positive linear relationship between the two data sets. The next step is to define the origin of this relationship by proposing a suitable theoretical expression, and then validating this expression using the empirical data.

5.5.2 Proposed Theory

From Equation 4.2, it was initially proposed that the termination impedance is given by

$$Z_{T_e} = X_u \times Z_T \quad (5.1)$$

where the constant X_u is derived from experimental results and a value matching procedure.

It has been demonstrated in other applications (Ichiyanagi and Nishiumi, 2008) that the termination impedance Z_{T_e} is a quotient of discharge pressure and mean flow

$$Z_{T_e} = \frac{2P_d}{Q} \quad (5.2)$$

where

$$\begin{aligned} P_d &= \text{acoustic pressure at the tuner outlet} \\ Q &= \text{mean flow rate} \end{aligned}$$

Equation 5.2 is unlikely to be suitable in this application as the frequency dependent nature of the response is not captured. However, Equation 5.2 coupled with Z_T from Section 3.6.3 may provide a solution. That is

$$Z_{T_e} = \frac{2P_d}{Q} \times Z_T \quad (5.3)$$

In order to confirm the suitability of Equation 5.3, values of $\frac{2P_d}{Q}$ must be validated against the empirical measurement of X_u .

5.5.3 Validation and Discussion

From the analysis provided in Section 5.5.1, the Tuner Length termination impedance constant provided the greatest correlation. Therefore, this data set is selected for the purpose of validating the new theory. Figure 5.66 illustrates the comparison of X_u and the new theory.

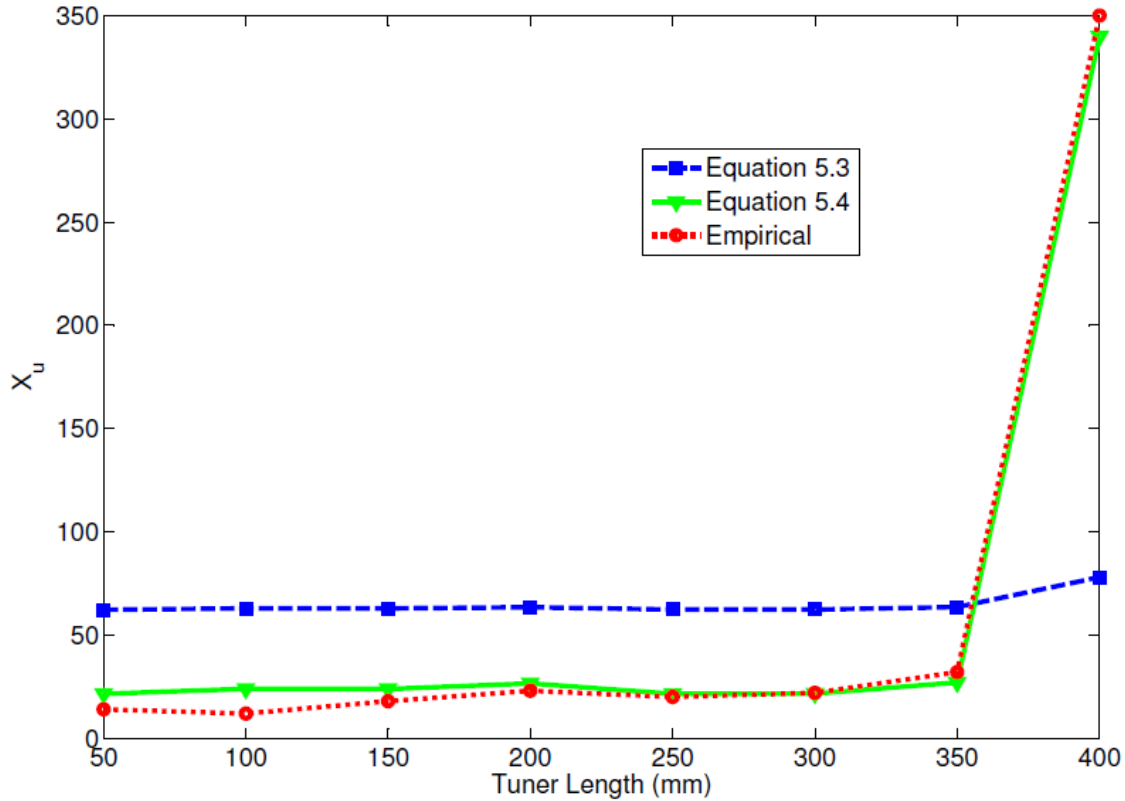


Figure 5-71 Comparison of Termination Impedance Constant and New Theory

As can be seen from Figure 5.71, whilst the trend bears some resemblance, the $\frac{2P_d}{Q}$ term in Equation 5.3 is insufficiently refined to capture the dynamic nature of the empirical values of X_u . Additionally, it is unclear from the work by Ichiyanagi and Nishiumi (2008), exactly where the constant in the $\frac{2P_d}{Q}$ term originates.

In analysing the data, an alternative equation is proposed considering the offset of the results obtained using Equation 5.3 and those obtained empirically, where

$$Z_{T_e} = \frac{C_T P_d}{Q} Z_T \quad (5.4)$$

and the constant C_T is derived from a value matching procedure.

In this case

$$C_T \cong 0.0012 \quad (5.5)$$

The results for the $\frac{C_T P_d}{Q}$ term in Equation 5.4 are in reasonably good agreement with the empirical results of X_u for all values. Mismatch for some values is attributed to the error in calculating the empirical value of X_u .

As shown in Figures 5.72 – 5.79, in order to finally confirm the suitability of Equation 5.4, values for termination impedance calculated using this equation are compared to those generated using Equation 5.1 and empirical values for X_u . ‘Predicted’ denotes results for termination impedance using equation 5.4 and ‘Empirical’ denotes results obtained using equation 5.1. Once again, Tuner Length results are used for this analysis.

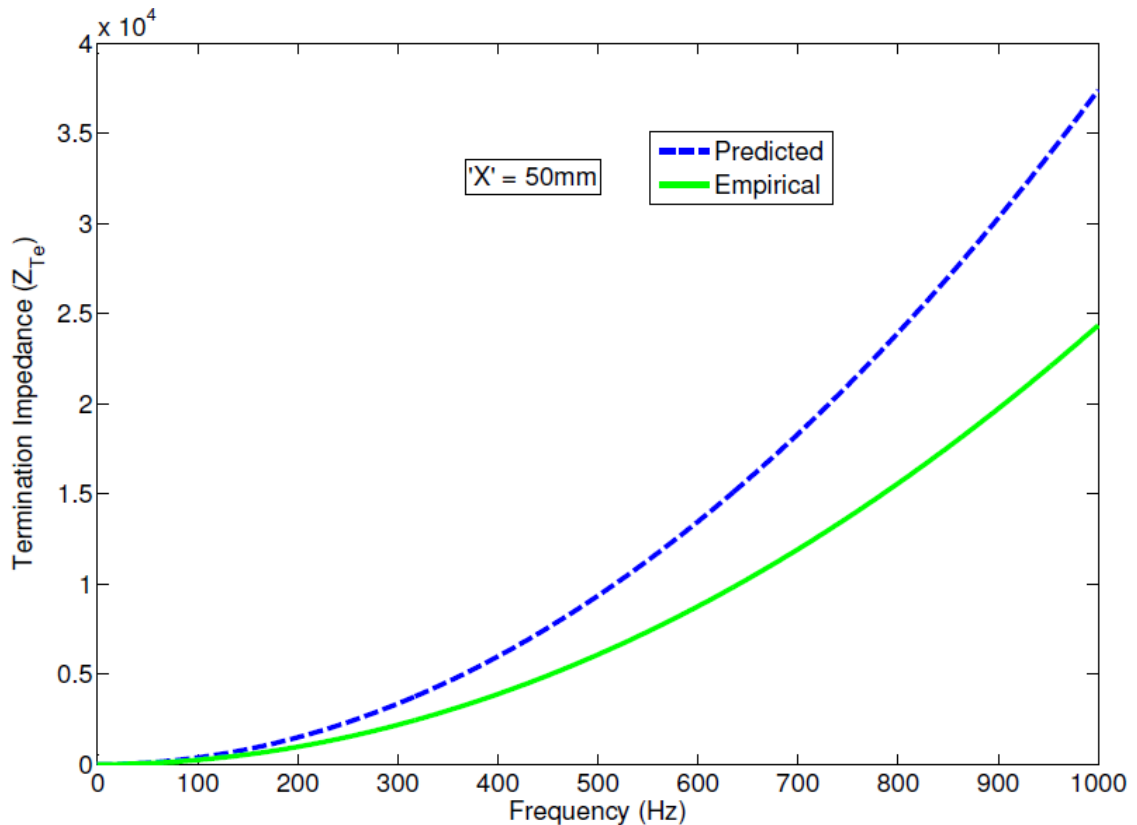


Figure 5-72 Predicted versus Empirical Termination Impedance for a 50mm long tuner

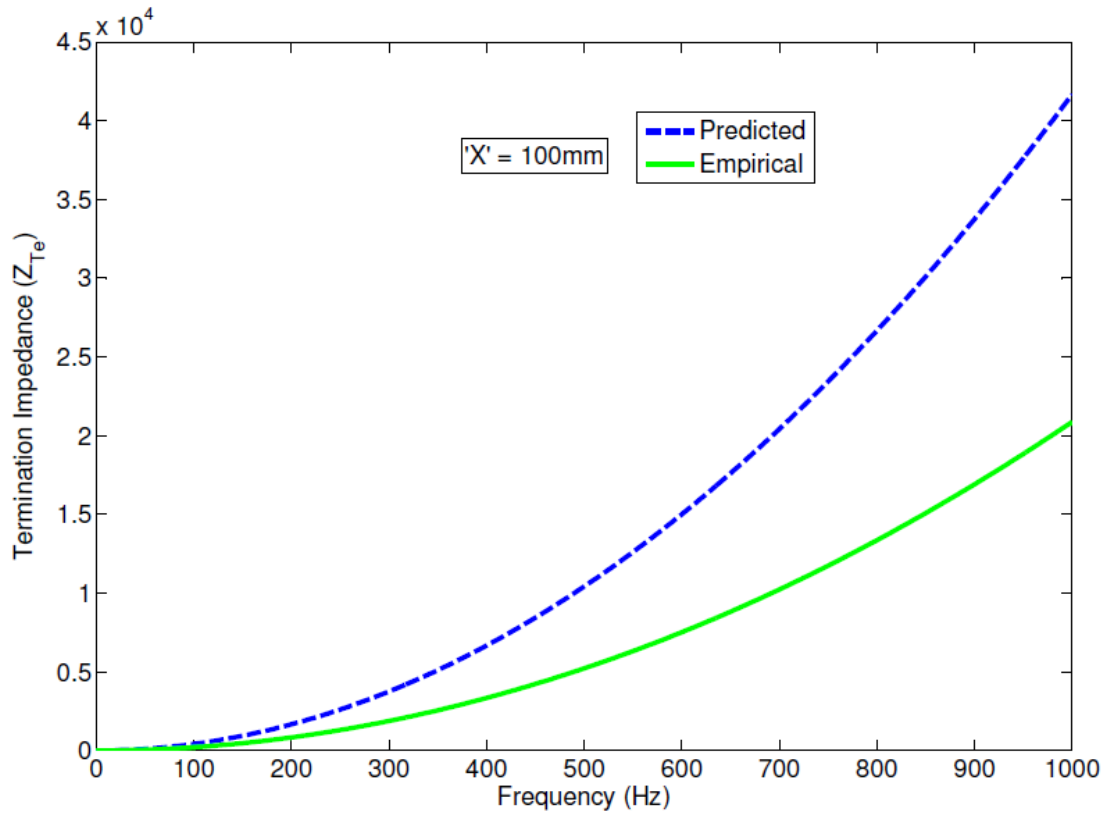


Figure 5-73 Predicted versus Empirical Termination Impedance for a 100mm long tuner

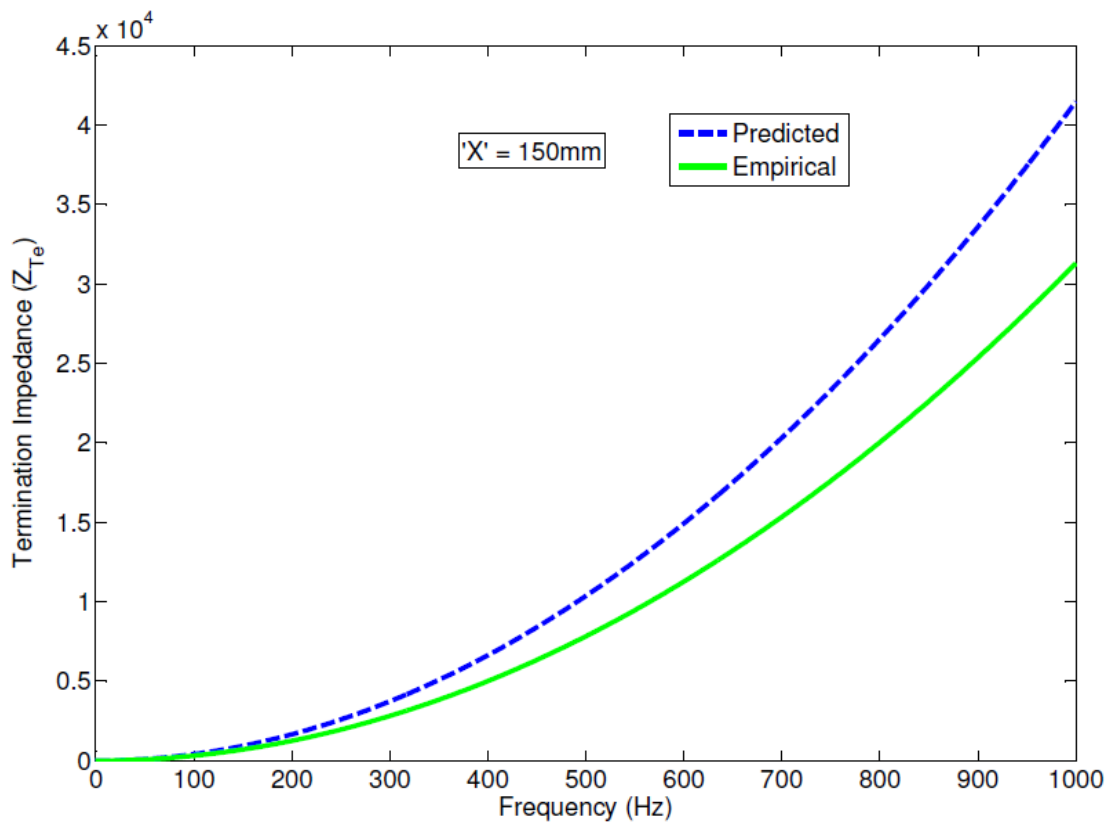


Figure 5-74 Predicted versus Empirical Termination Impedance for a 150mm long tuner

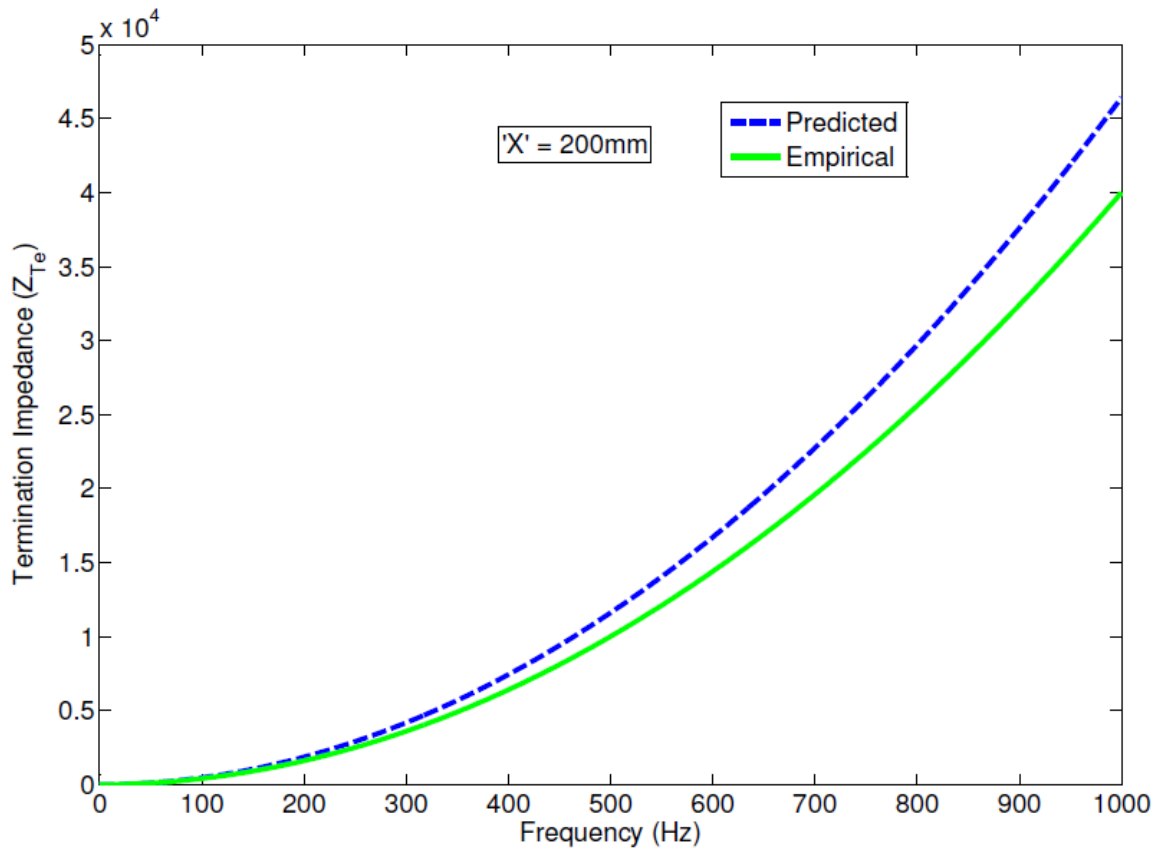


Figure 5-75 Predicted versus Empirical Termination Impedance for a 200mm long tuner

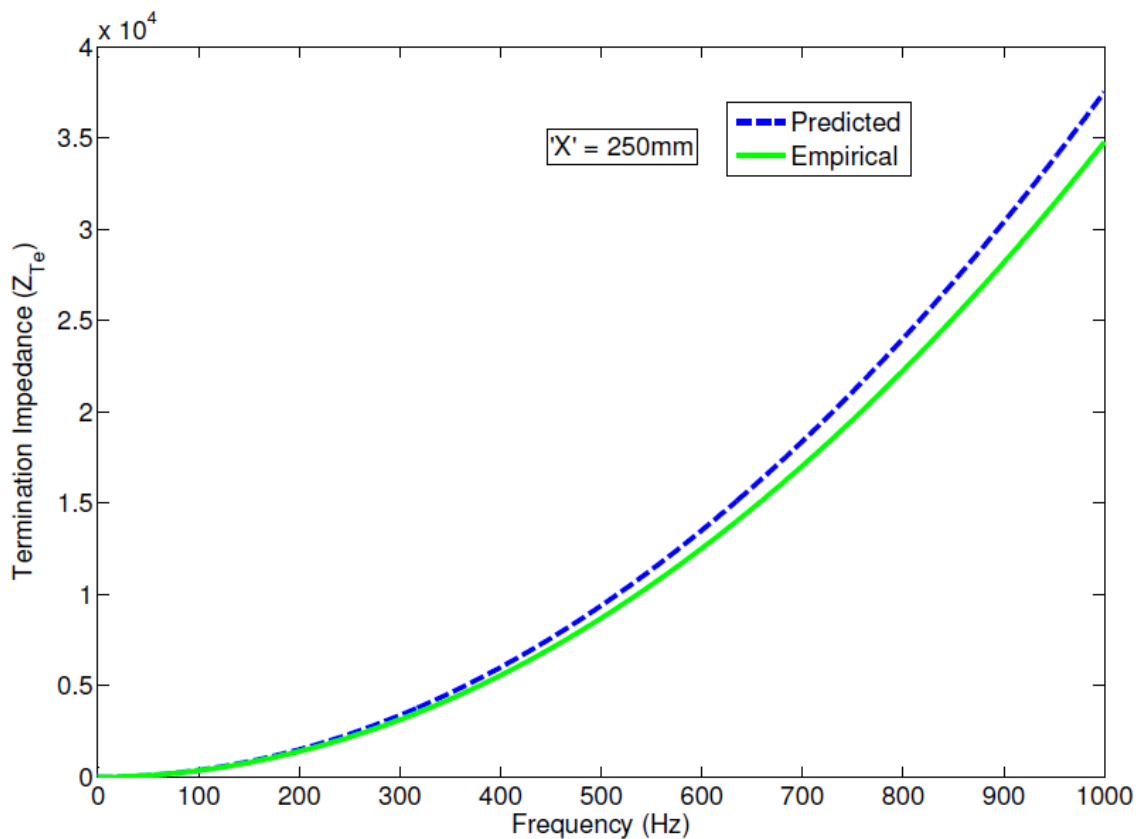


Figure 5-76 Predicted versus Empirical Termination Impedance for a 250mm long tuner

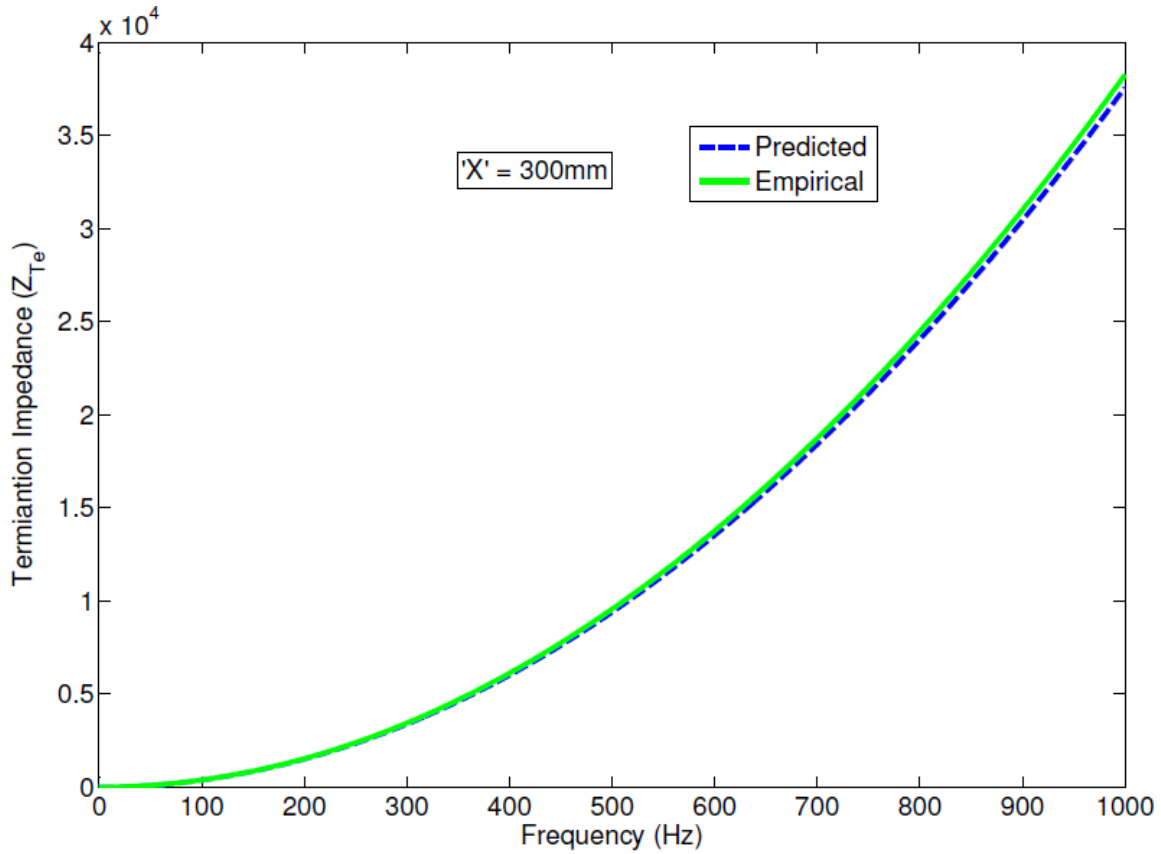


Figure 5-77 Predicted versus Empirical Termination Impedance for a 300mm long tuner

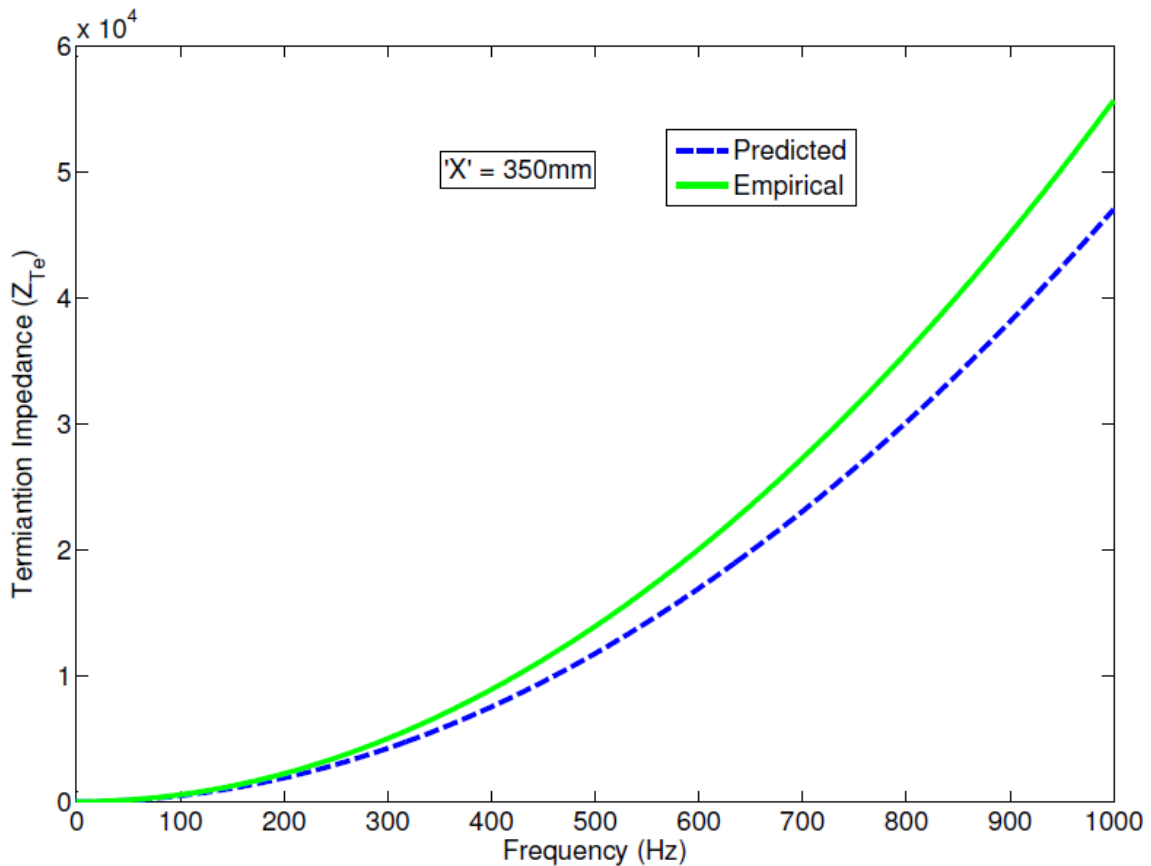


Figure 5-78 Predicted versus Empirical Termination Impedance for a 350mm long tuner

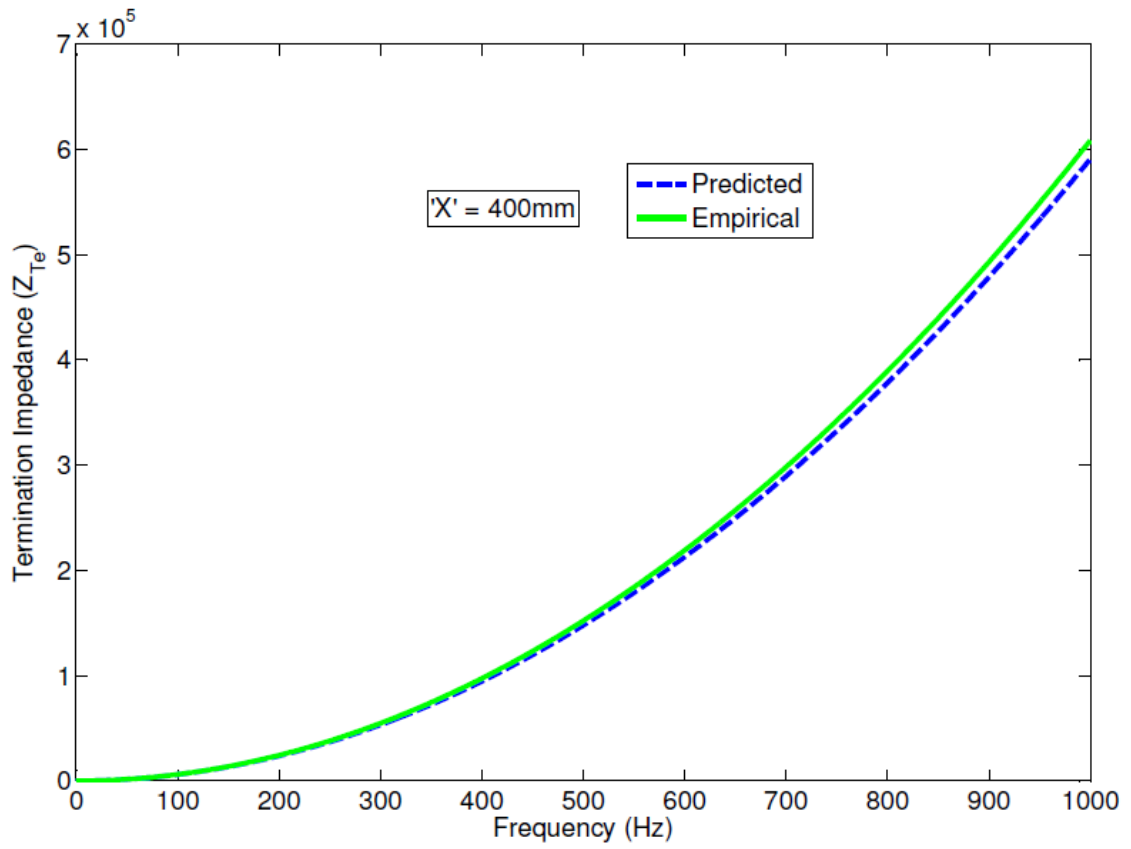


Figure 5-79 Predicted versus Empirical Termination Impedance for a 400mm long tuner

The first impression from Figures 5.72 – 5.79 is that Equation 5.4 is not sufficiently refined to predict the termination impedance in the experiments. However, on closer inspection it is apparent that Equation 5.4 is sufficiently accurate for prediction of the 1st pump order termination impedance, and subsequently, 1st pump order noise reduction. Having said this, it is clearly sensitive to the measured pressure at Transducer 2. As discussed previously, there are potential sources of error with this measurement, which may be skewing results. This is most evident for the 50mm and 100mm tuners.

Considering these common sources of error, results for the 300mm and 400mm tuners still show good agreement between predicted and measured values across the frequency range. This would suggest that Equation 5.4 has some merit, but further evaluation is required to confirm this theory.

5.5.4 Tuner Length Termination Impedance Prediction

Figures 5.80 and 5.81 illustrate a summary of the termination impedance (real and imaginary components respectively) at the first pump order (333 Hz), for each of the tuner lengths illustrated in Figure 4.9 and Table 4.3. Using a high order polynomial curve fitting method, it is possible to derive an equation for the termination impedance, in order to predict the termination impedance at the first pump order, for any given tuner length.

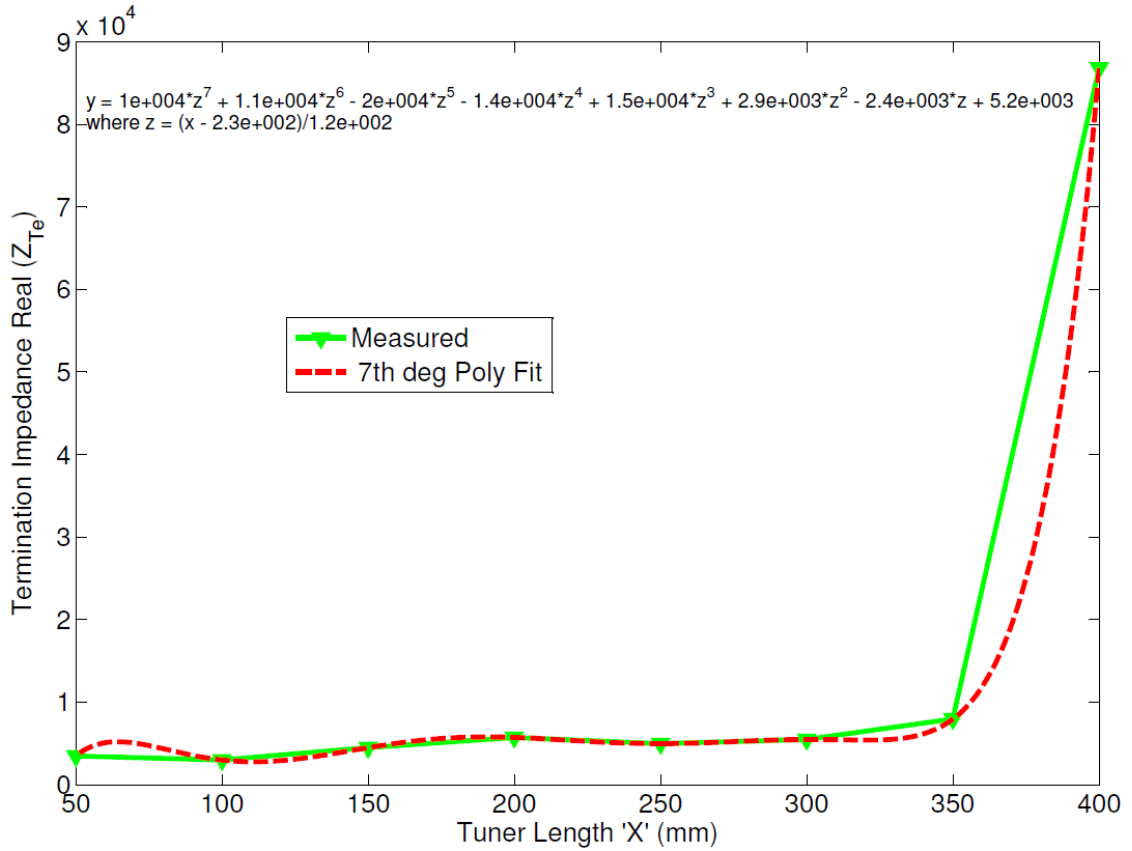


Figure 5-80 1st Pump Order Termination Impedance (Real) for a range of tuner lengths

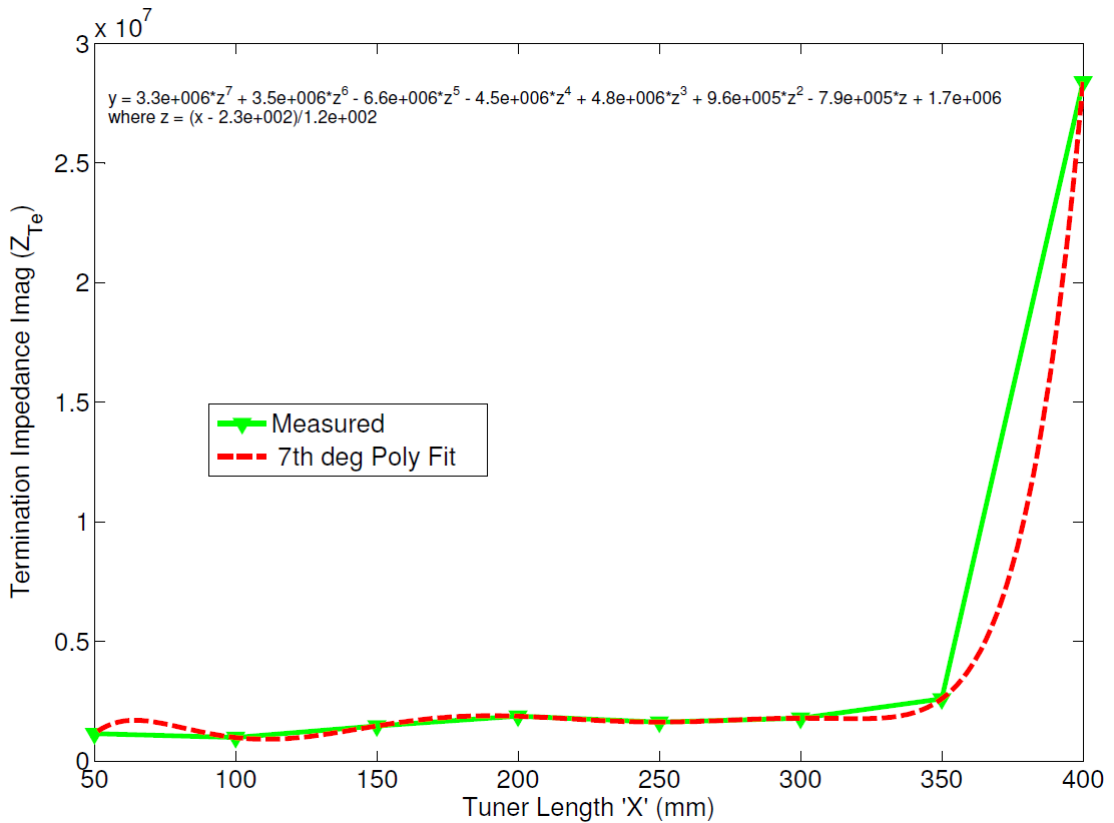


Figure 5-81 1st Pump Order Termination Impedance (Imag) for a range of tuner lengths

5.5.5 Developed Tuner Length Noise Reduction Prediction

Using the polynomial fit equations for the real and imaginary components of the termination impedance shown in Figures 5.80 and 5.81, a complex value for the termination impedance can be generated, which in turn can be used to predict an associated 1st pump order noise reduction for a continuous range of tuner length values. Figure 5.82 illustrates the comparison of predicted and measured 1st pump order noise reduction values for various tuner lengths. ‘Predicted’ refers to the noise reduction calculated using Equation 5.4 and the curve fitting method for termination impedance prediction, and ‘Predicted (Empirical)’ refers to noise reduction calculated using the empirical method of termination impedance as described in Section 4.1.9. Figure 5.82 also includes a 7th order polynomial curve fit of the measured results to provide some context to the ‘Predicted’ results. A 7th order polynomial is selected in this case as this degree provides the best fit of the measured results, i.e. 8 data points, whilst minimising Runge's phenomenon (1901).

In the following sections ‘developed’ is used to describe all predictions using Equation 5.4 and the curve fitting method.

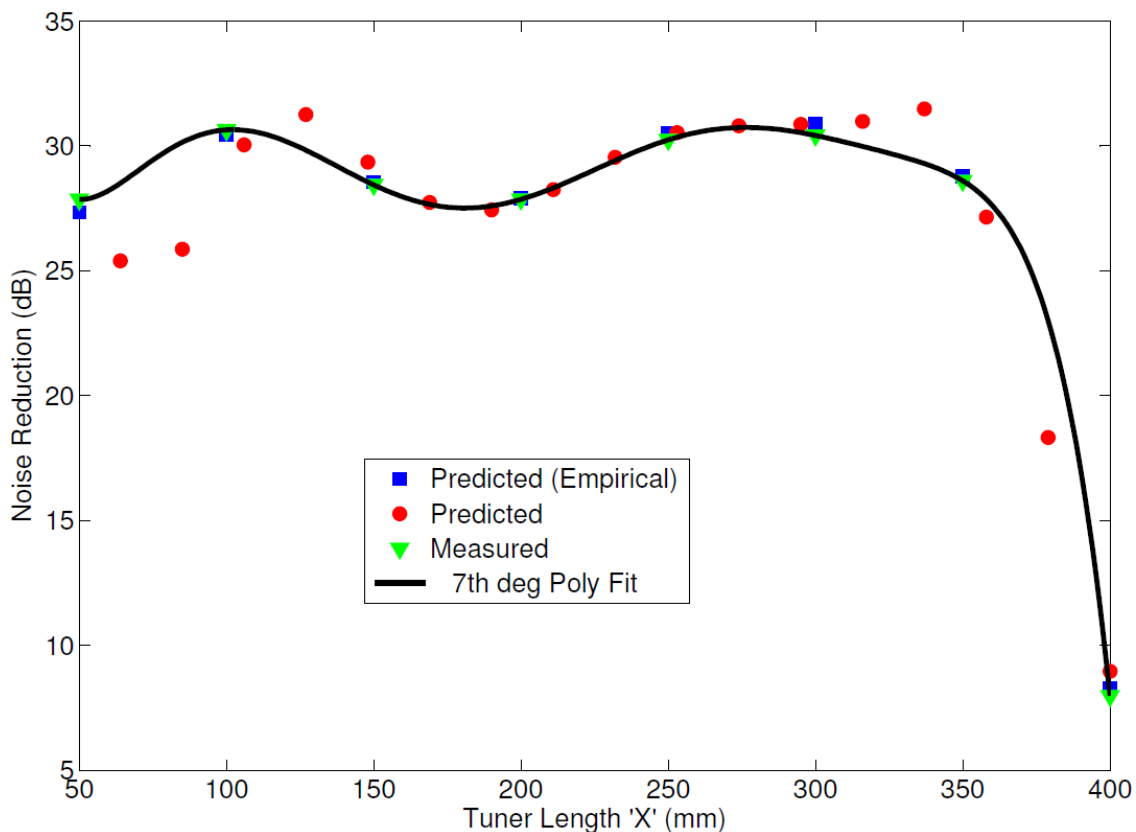


Figure 5-82 Tuner Length - Predicted versus Measured Noise Reduction at 1st Pump Order.

As can be seen from Figure 5.82, the developed predictions are relatively accurate i.e. within 1-2dB, over the range of tuner lengths examined. The predicted data follows the trend of measured results, and hence the empirical predictions are also provided some validation. Certain predicted data points i.e 70.5mm, 91mm, 111.5mm and 338.5mm, are notably different from the polynomial curve fit of the measured results. This is due to the order of the polynomial and the number of measured data points available to generate this curve. This can be observed when considering corresponding points in Figures 5.80 and 5.81.

Despite this calculation error, the developed predictions provide further insight into the behaviour of the tuners containing no holes. Considering the speed of sound in the fluid of $c = 546 \text{ m/s}$ and the first order frequency $f = 333 \text{ Hz}$, and a corresponding wavelength of $\lambda = 1.6 \text{ m}$, it appears that the tuner is operating similarly to an extended inlet resonator muffler, as described previously in Section 3.5.2.

Considering Equation 3.8 in Section 3.5.2, The acoustic impedance or branch impedance Z_B between the extended inlet and the muffler cavity

$$Z_B = -jY \cot(kl_2) \quad (5.6)$$

At certain frequencies Z_B would tend to zero. For the rigid end plate condition, which is assumed in the tuner system, resonance would occur when $\cot(kl_2) \rightarrow 0$ or when

$$kl_2 = (2n + 1)\frac{\pi}{2}, \quad n = 0, 1, 2, \dots \quad (5.7)$$

or

$$l_2/\lambda = (2n + 1)/4, \quad n = 0, 1, 2, \dots \quad (5.8)$$

Considering the average noise reduction performance of an extended inlet resonator (20-25dB), it can be observed that the 400mm tuner is actually amplifying noise in the system. This is most likely due to this tuner length approaching a length associated with resonance of the pump fundamental frequency i.e. $l_2 = \frac{c}{4f_R} = 0.409 \text{ m}$

The procedure followed in this section has provided further insight into the behaviour of a tuner containing no holes. The following sections use the same procedure to predict and analyse the influence of the remaining tuner design parameters of tuner hole location, tuner hole diameter and multi-hole tuners.

5.5.6 Hole Location Termination Impedance Prediction

Figures 5.83 and 5.84 illustrate a summary of the termination impedance (real and imaginary respectively) at the first pump order (333 Hz), for each of the tuner hole locations illustrated in Figure 4.15 and Table 4.4. Using a 5th degree polynomial curve fit, it is possible to derive an equation for the termination impedance, in order to predict the termination impedance at the first pump order, for any given hole location.

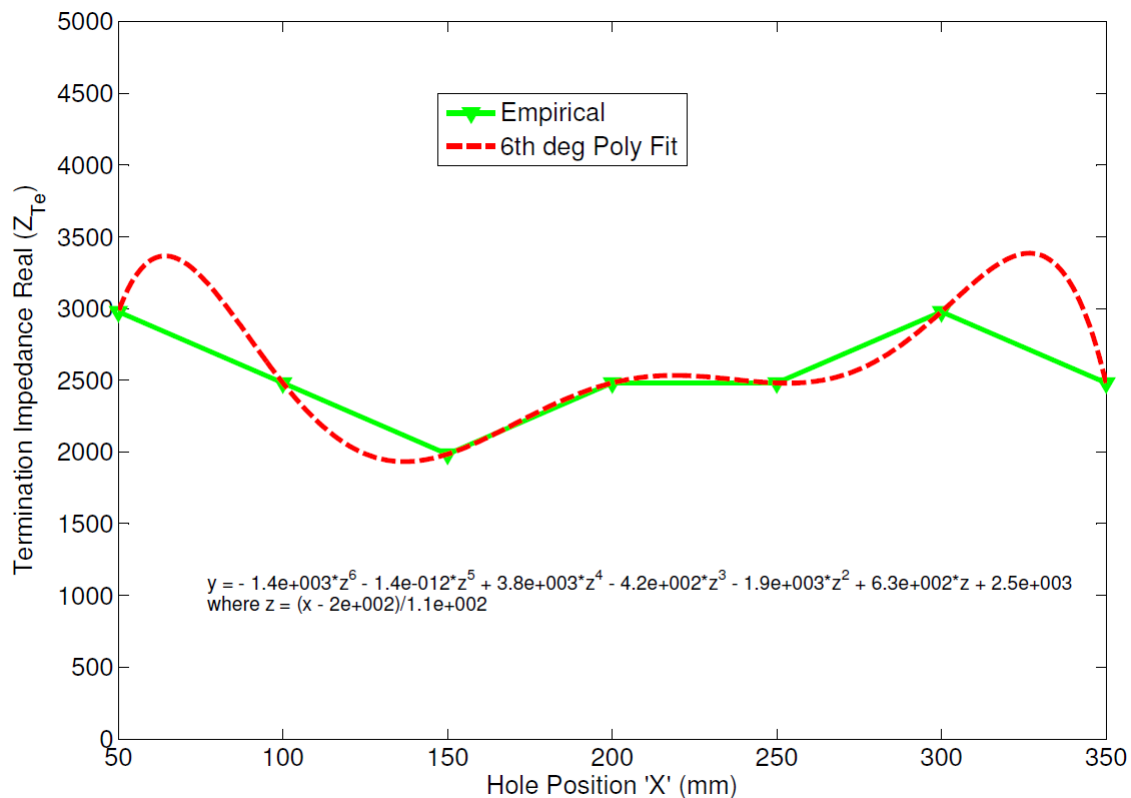


Figure 5-83 1st Pump Order Termination Impedance (Real) for a range of tuner hole locations

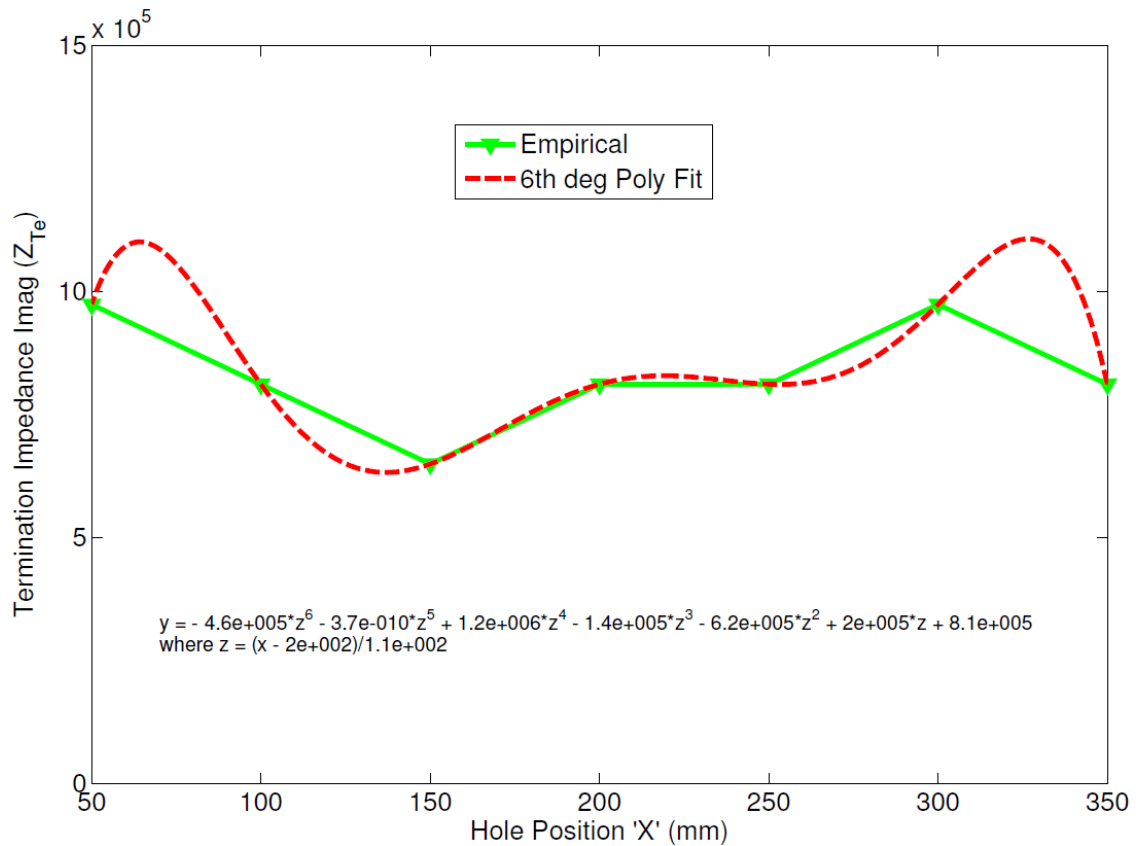


Figure 5-84 1st Pump Order Termination Impedance (Imag) for a range of tuner hole locations

5.5.7 Developed Hole Location Noise Reduction Prediction

Using the polynomial fit equations for the real and imaginary components of the termination impedance shown in Figures 5.83 and 5.84, a complex value for the termination impedance can be generated, which in turn can be used to predict an associated 1st pump order noise reduction for a continuous range of values of tuner hole location. Figure 5.85 illustrates the comparison of predicted and measured 1st pump order noise reduction values, for various tuner hole locations. Figure 5.85 also includes a 6th degree polynomial curve fit of the measured results, to provide some context to the developed predictions.

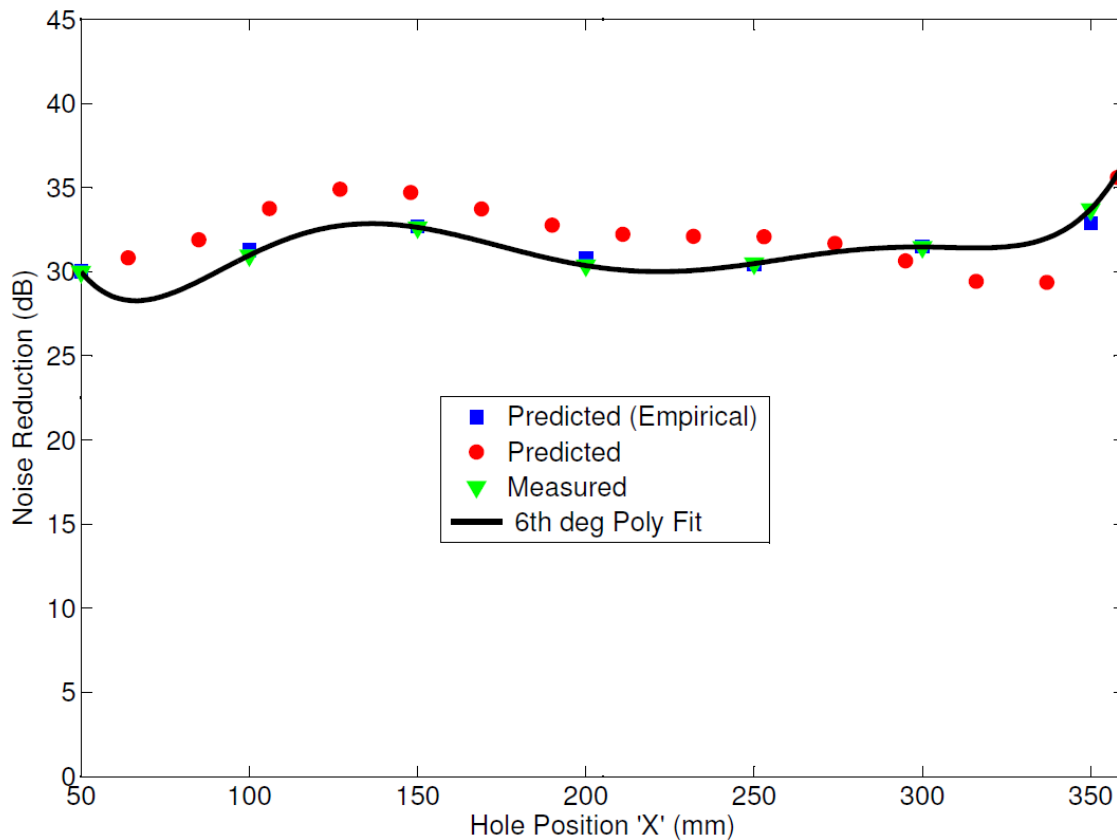


Figure 5-85 Hole Location – Predicted vs Measured Noise Reduction at 1st Pump Order

Comparing the magnitudes of the results presented in Figure 5.85 with Figure 5.82, the developed predictions are consistent with the findings in Section 4.8, i.e. the addition of a hole to the tuner can provide an additional attenuation in the order of 3dB. The location of the hole ($\text{\O}1\text{mm}$ in this case), appears to be the main driver in determining how this potential 3dB either amplifies or further attenuates the existing effects from a tuner containing no holes. Considering the explanation of the extended inlet resonator provided in Section 5.5.5, it is probable that the hole is behaving with a similar noise reduction mechanism, i.e. at certain frequencies the impedance of the hole tends to zero, thus generating a resonant system. With all other parameters remaining equal, changing the location of the hole simply changes the phase difference between the incident and reflected waves, providing for a minor amplification or attenuation of the resultant downstream waveform. This can be observed from the results presented in Figure 5.85, which shows a maximum 3dB change over the range.

Further insight into the attenuation mechanisms associated with the tuner hole diameter are provided in Section 5.59.

5.5.8 Hole Diameter Termination Impedance Prediction

Figures 5.86 and 5.87 illustrate a summary of the termination impedance (real and imaginary components respectively) at the first pump order (333 Hz), for each of the tuner hole diameters illustrated in Figure 4.19 and Table 4.5. Using a 4th degree polynomial curve fit, it is possible to derive an equation for the termination impedance, in order to predict the termination impedance at the first pump order, for any given hole diameter.

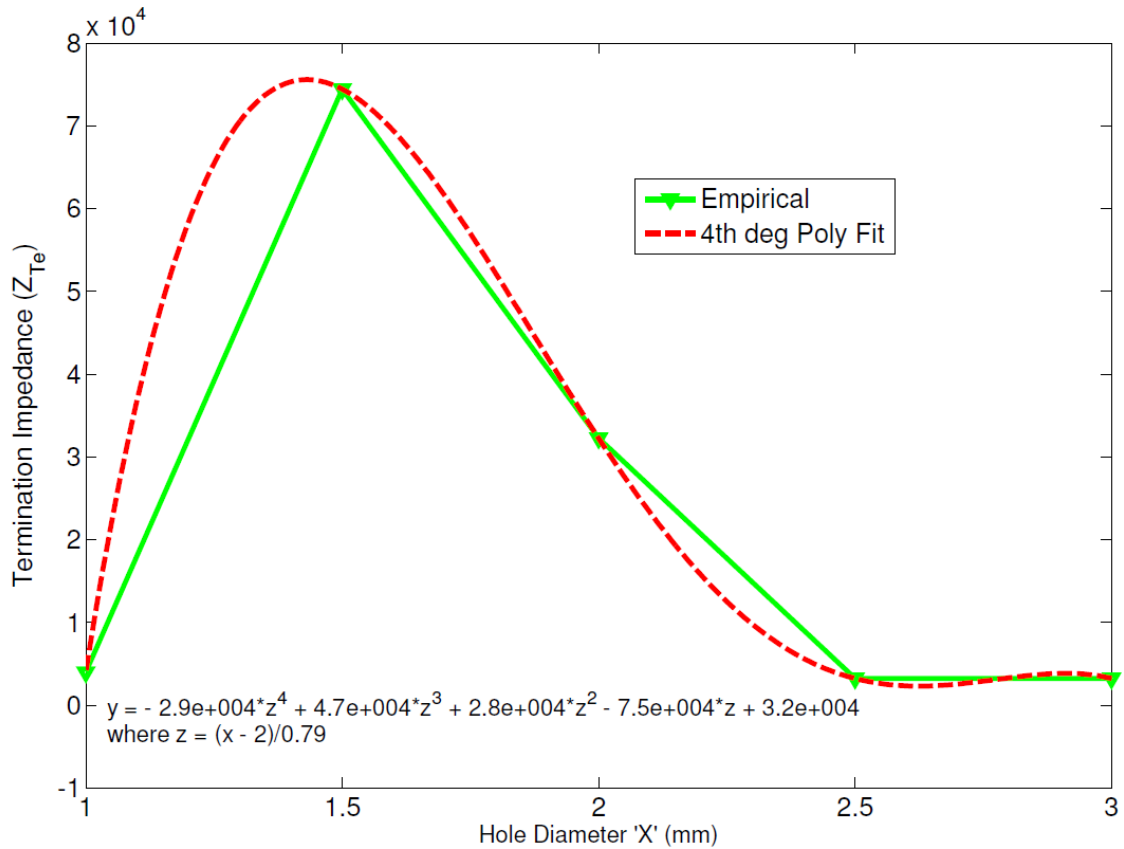


Figure 5-86 1st Pump Order Termination Impedance (Real) for a range of tuner hole diameters

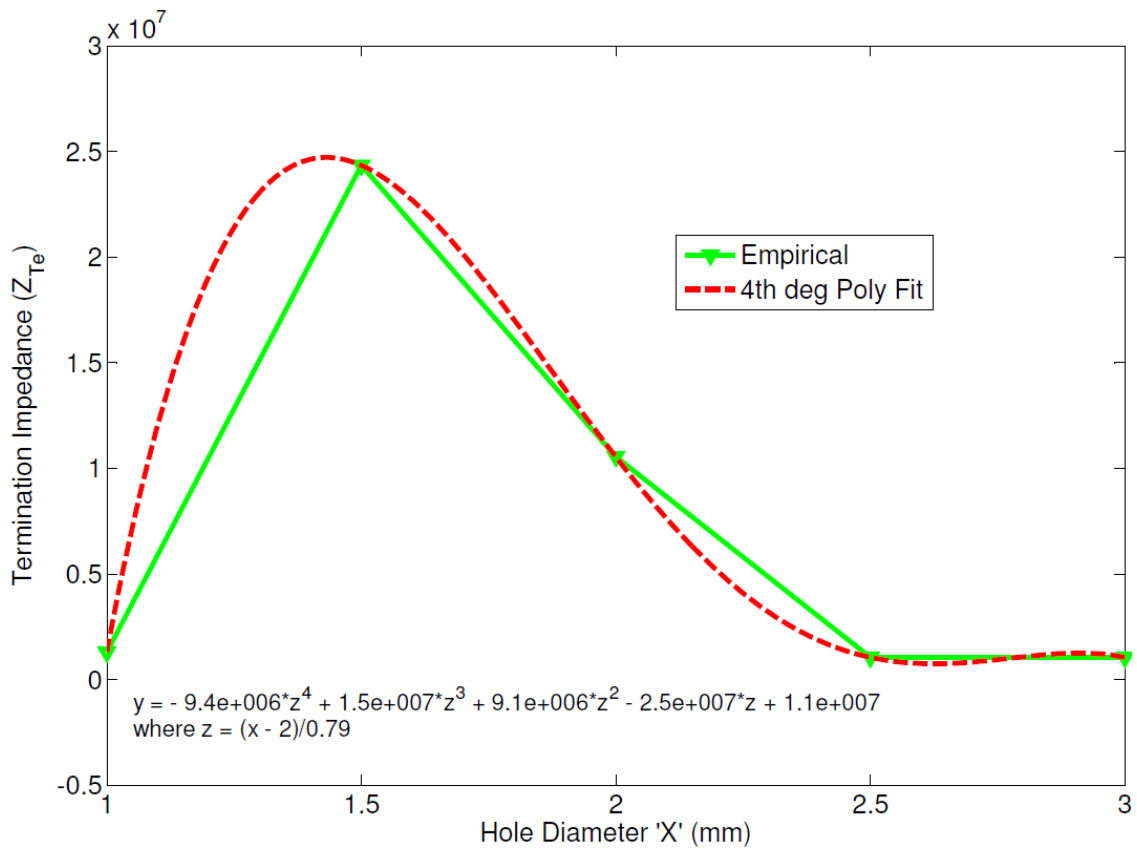


Figure 5-87 1st Pump Order Termination Impedance (Imag) for a range of tuner hole diameters

5.5.9 Developed Hole Diameter Noise Reduction Prediction

Using the polynomial fit equations for the real and imaginary components of the termination impedance shown in Figures 5.86 and 5.87, a complex value for the termination impedance can be generated, which in turn can be used to predict an associated 1st pump order noise reduction for a continuous range of values of tuner hole diameter. Figure 5.88 shows the predicted and measured 1st pump order noise reduction values, for various tuner hole diameters. Figure 5.88 also includes a 4th degree polynomial curve fit of the measured results, to provide some context to the developed predictions.

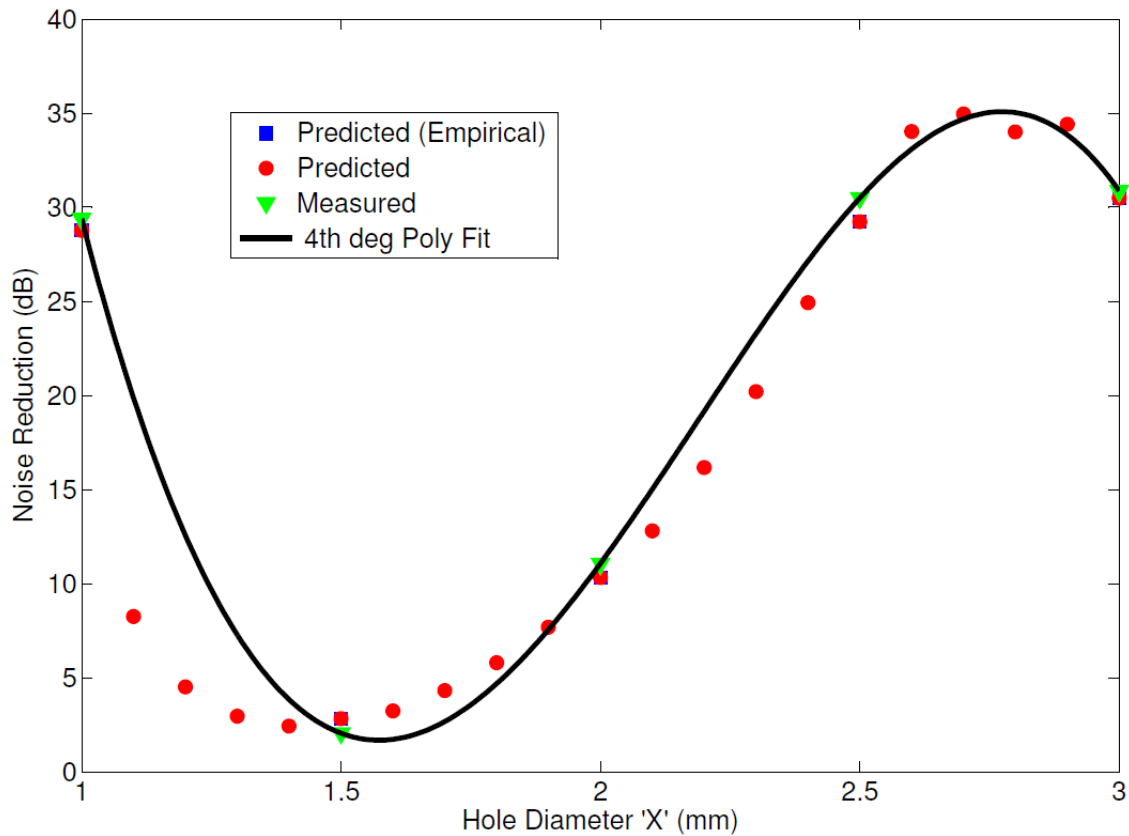


Figure 5-88 Hole Diameter – Predicted vs Measured Noise Reduction at 1st Pump Order

With the exception of the results for 1.1mm, 1.2mm and 1.3mm holes, the developed predictions appear to be consistent with the trend and magnitude of the measured results. Comparing Figure 5.88 with Figures 5.86 and 5.87, it is possible that the termination impedance predictions for holes 1-1.5mm may contain inaccuracies as a result of the curve fitting process. Unfortunately, without further experimental measurements, it is difficult to confirm the extent to which this is affecting noise reduction predictions.

Observing the results presented in Figure 5.88, it would appear that the hole diameter has a much greater influence on tuner noise reduction than tuner hole location. For the 1.5mm hole diameter there is an amplification of pump generated noise to the extent that it almost completely negates the effectiveness of the tuner.

Considering the attenuation mechanisms of the tuner hole, there is a possible correlation with the findings of Ronneberger (1972), where a ‘free shear layer’ builds up in front of the hole in which the propagating acoustic waves are excited due to the pressure difference on both sides of the hole. The acoustic medium (fluid) is blown-in or sucked out of the hole, depending on the ‘free shear layer’ and its positive or

negative displacement, which is a function of the hole diameter. Changing the hole diameter causes a change in the incident wave under consideration resulting in a largely amplified or largely dampened wave downstream of the hole. This holds true for the case where the boundary layer height is small compared to the wavelength under consideration, which is true in this case.

Another possible explanation is provided when considering the theory developed by Maa (1988), in relation to Micro-Perforated Panels. This theory considers not only the influence of the hole on the acoustic properties of the incident wave, but also the influence of the region immediately adjacent to the hole.

NOTE:
This figure/table/image has been removed
to comply with copyright regulations.
It is included in the print copy of the thesis
held by the University of Adelaide Library.

Figure 5-89 Sketch of micro-perforated panel absorber (Maa, 1988), where d = diameter of orifice, b = spacing between orifices, t = thickness of panel and D = air cavity depth between panel and rigid backing wall.

Considering the illustration in Figure 5.89, there is an immediate similarity between a wave incident to the micro-perforated panel absorber and a wave travelling along the internal bore of the tuner, becoming incident to the tuner hole. Having said this, it is important to consider the noise reduction mechanisms of the micro-perforated panel absorber before applying it to analysis of the plastic tuner.

The main noise reduction mechanism associated with the micro-perforated panel is absorption. The micro-perforated panel in front of an air cavity forms an acoustic impedance for the incident wave, thus changing the energy of the wave into another form.

The exact mechanisms for energy dissipation in fluids are complex (Morse and Ingard, 1968) and include internal fluid effects; thermal conductivity, fluid viscosity and molecular effects, and surface energy dissipation; thermal conductivity and viscosity. For the purposes of this research, fluid internal losses are considered negligible compared to energy loss at surfaces. For the micro-perforated panel, viscous effects are the predominant mechanism, which is considered as part of the impedance of the perforation. The hole impedance is given as $Z_{hole} = \theta + j\omega\chi + Z_{cavity}$, where θ is the resistive or real part of the impedance and corresponds to the viscous effects between the fluid and the hole. χ is the reactive or imaginary part of the impedance and is inertial in nature, i.e. it behaves like a mass. Z_{cavity} is the normalised acoustic impedance of the air cavity between the plate and its backing wall.

It has been illustrated (Putra, 2010), that for micro-perforates i.e. holes of diameter 0.05-1.0mm, that the acoustic impedance of the hole is dominated by its resistive component. However, for holes of relatively larger diameter i.e. >1.0mm, the acoustic impedance is dominated by its reactive component and therefore inertial losses are dominant over viscous effects. It is safe to assume therefore that inertial losses will be dominant in the case of the tuner, which has similar hole diameters for the purposes of this research.

It should also be noted that in the case of the micro-perforated panel, the backing wall is considered to be rigid. Any acoustically induced motion (vibration), will drastically affect the impedance of the perforation. In this research and the experiments detailed in Section 4, this assumption is valid i.e. the tuner backing wall is rigid steel. Additionally, non linear effects and higher order modes of the acoustic wave are not considered.

A final consideration when applying the theory of Maa (1988) and Putra (2010) is the fluid medium. In both cases the fluid carrying the acoustic wave is air. However, in the case of the tuner, the fluid under consideration is power steering fluid. It is expected that there would be some scaling effect dependant on the type of fluid involved.

Applying the micro-perforated panel theory, the acoustic impedance for an acoustic wave incident to the tuner hole can be considered as

$$Z_{hole} = Z_{orifice} + Z_{cavity} \quad (5.9)$$

$Z_{orifice}$ is the impedance as a result of acoustic flow within the orifice itself and Z_{cavity} arises in the regions immediately adjacent to the orifice where (Maa, 1988)

$$Z_{orifice} = \frac{32Nt}{pd^2} \left(1 + \sqrt{\frac{K^2}{32}} + \frac{\sqrt{2}Kd}{32t} \right) + \frac{jw\rho t}{p} \quad (5.10)$$

and

$$Z_{cavity} = -j \cot\left(\frac{\omega D}{c}\right) \quad (5.11)$$

where

- N = viscosity of fluid
- p = perforation ratio
- d = hole diameter
- t = tuner wall thickness
- ρ = fluid density
- D = depth of fluid cavity
- ω = wavenumber

- K = perforation constant
- = $d\sqrt{\omega\rho/4N}$

The depth of the fluid cavity D in the case of the tuner is considered to be the distance between the outer diameter of the tuner and the internal surface of the power steering hose wall. For the experiments performed in Section 4, this distance is 2.87mm.

From Equations 5.9 and 5.10, it is clear that the impedance Z_{hole} will be dominated by the cavity impedance Z_{cavity} for changing frequency. Conversely, for a fixed frequency e.g. the pump fundamental frequency of interest, Z_{hole} will only be affected by changing the geometry of the perforation, with all other parameters remaining equal.

Having determined an expression for the impedance of the tuner hole Z_{hole} , the absorption coefficient α for a plane wave incident to the tuner hole can be calculated from

$$\alpha = 1 - \left| \frac{(Z_{hole} - \rho c)^2}{(Z_{hole} + \rho c)^2} \right| \quad (5.12)$$

The absorption coefficient for a single hole in the tuner wall where $d = 1.0\text{mm}$, 1.5mm , 2.0mm , 2.5mm and 3.0mm is presented in Figure 5.90.

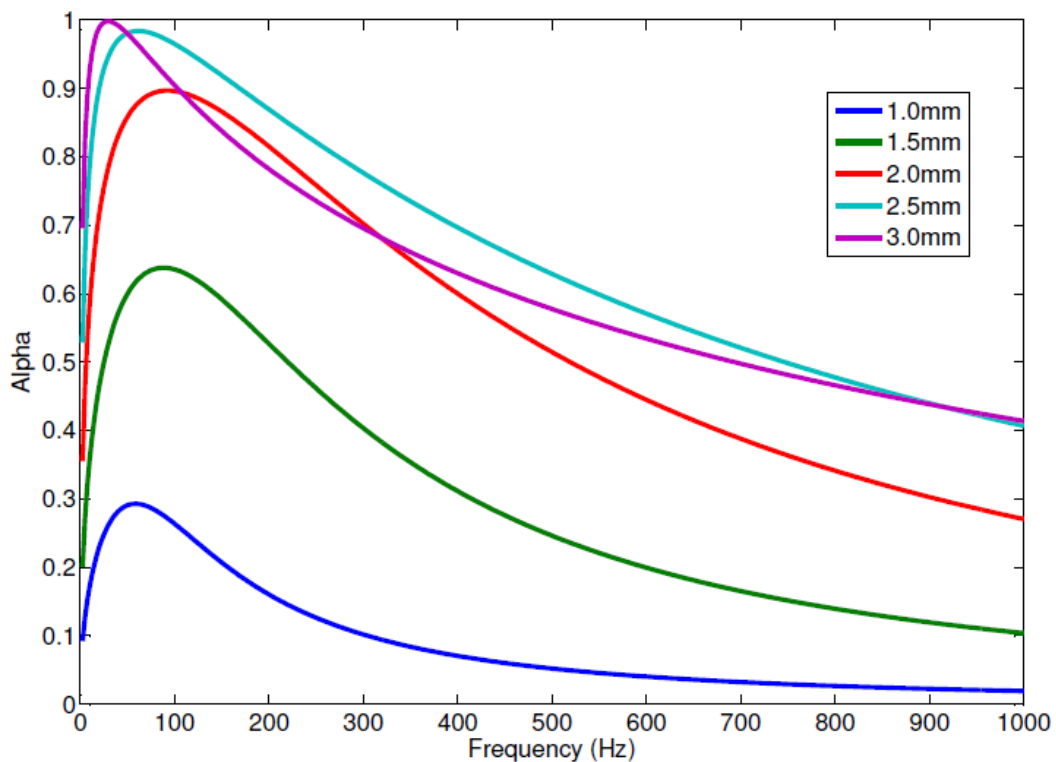


Figure 5-90 Absorption coefficient for a single hole in the tuner wall with varying diameter

As can be observed from Figure 5.90, in accordance with theory relating to perforated plates (Ingard, 1954), peak absorption for the geometries presented occur in a very narrow frequency band between 0 and 100Hz. The absorption coefficient at the pump fundamental frequency 333 Hz, varies significantly according to hole diameter, which is consistent with the findings of Maa (1988) and Putra (2010), discussed earlier in this section.

Comparing the results presented in Figure 5.90 and Figure 5.88, there appears to be a correlation between the theoretical absorption coefficient of the hole, and the corresponding noise reduction of the tuner i.e. 1.0 – 1.5mm hole tuners have the lowest noise reduction, there is then a significant jump for the 2.0mm hole tuner, and the maximum noise reduction can be found between the 2.0mm and 3.0mm tuners over this range. This would suggest that the tuner hole, in particular its diameter, has the largest influence on noise reduction for this type of tuner.

5.5.10 Multi Hole Termination Impedance Prediction

Figures 5.91 and 5.92 (two hole) and Figures 5.93 and 5.94 (three hole) illustrate a summary of the termination impedance (real and imaginary respectively) at the first pump order (333 Hz), for each multi hole tuner configuration illustrated in Figure 4.24 and Table 4.6. Using a 4th degree polynomial curve fit, it is possible to derive an equation for the termination impedance, in order to predict the termination impedance at the first pump order, for any given multi hole tuner.

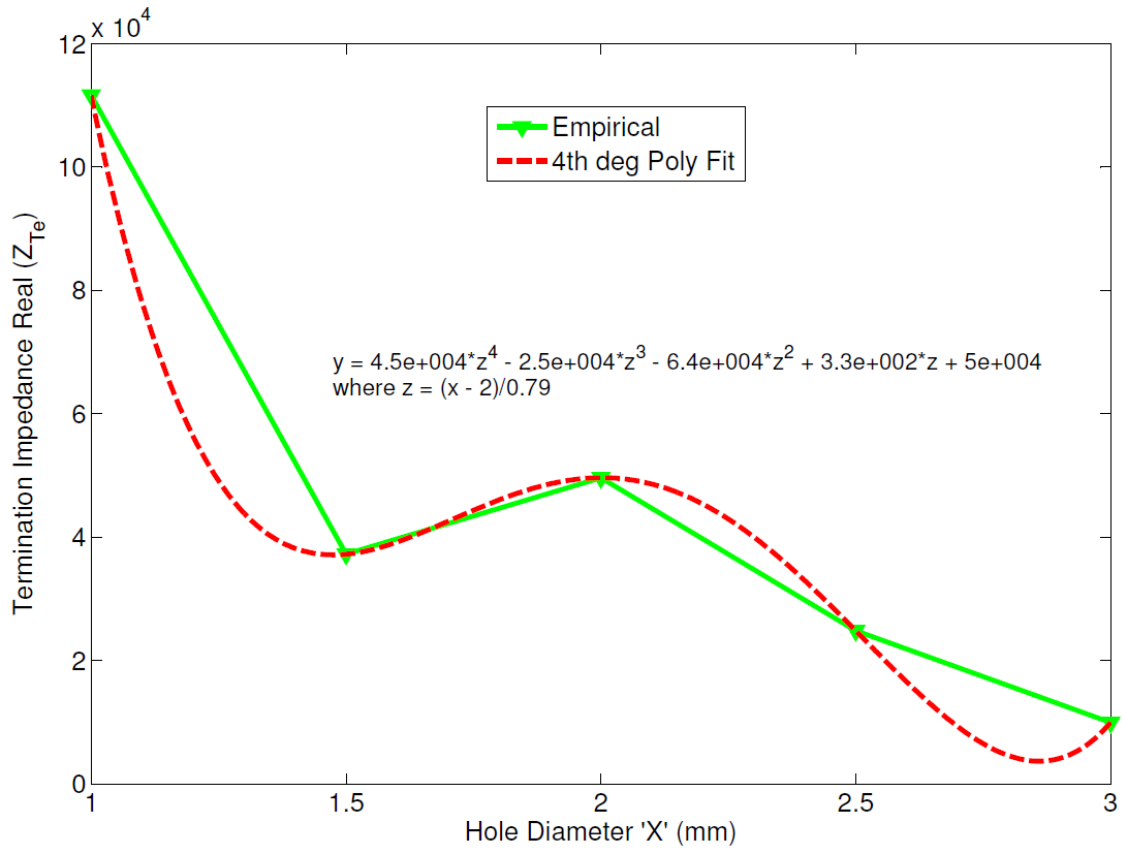


Figure 5-91 1st Pump Order Termination Impedance (Real) for two hole tuners with a range of hole diameters

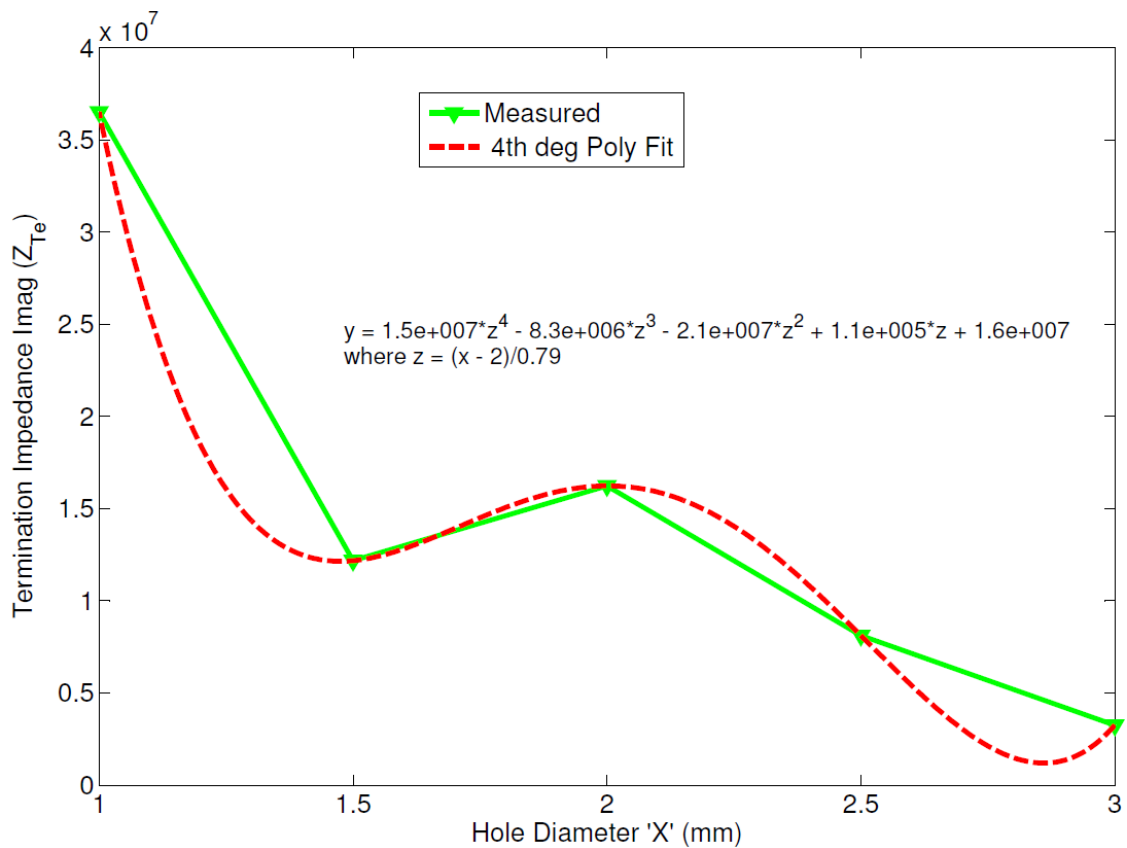


Figure 5-92 1st Pump Order Termination Impedance (Imag) for two hole tuners with a range of holes diameters

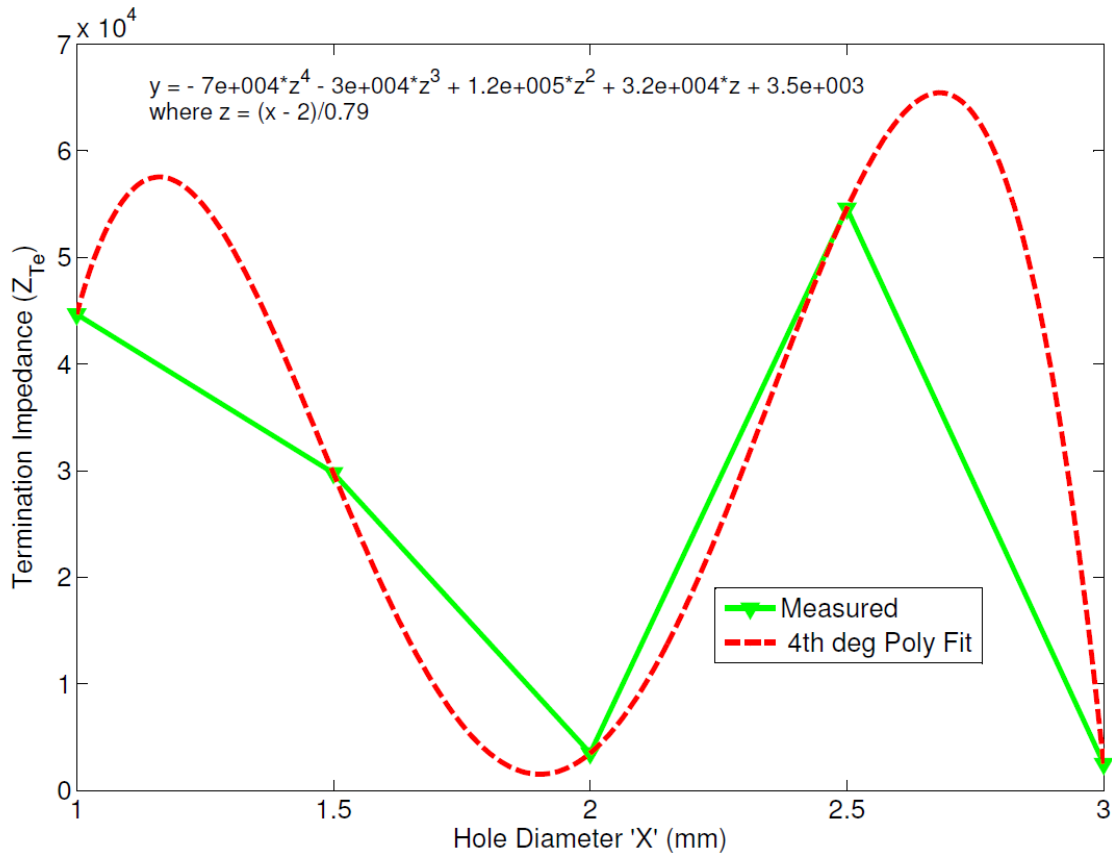


Figure 5-93 1st Pump Order Termination Impedance (Real) for three hole tuners with a range of hole diameters

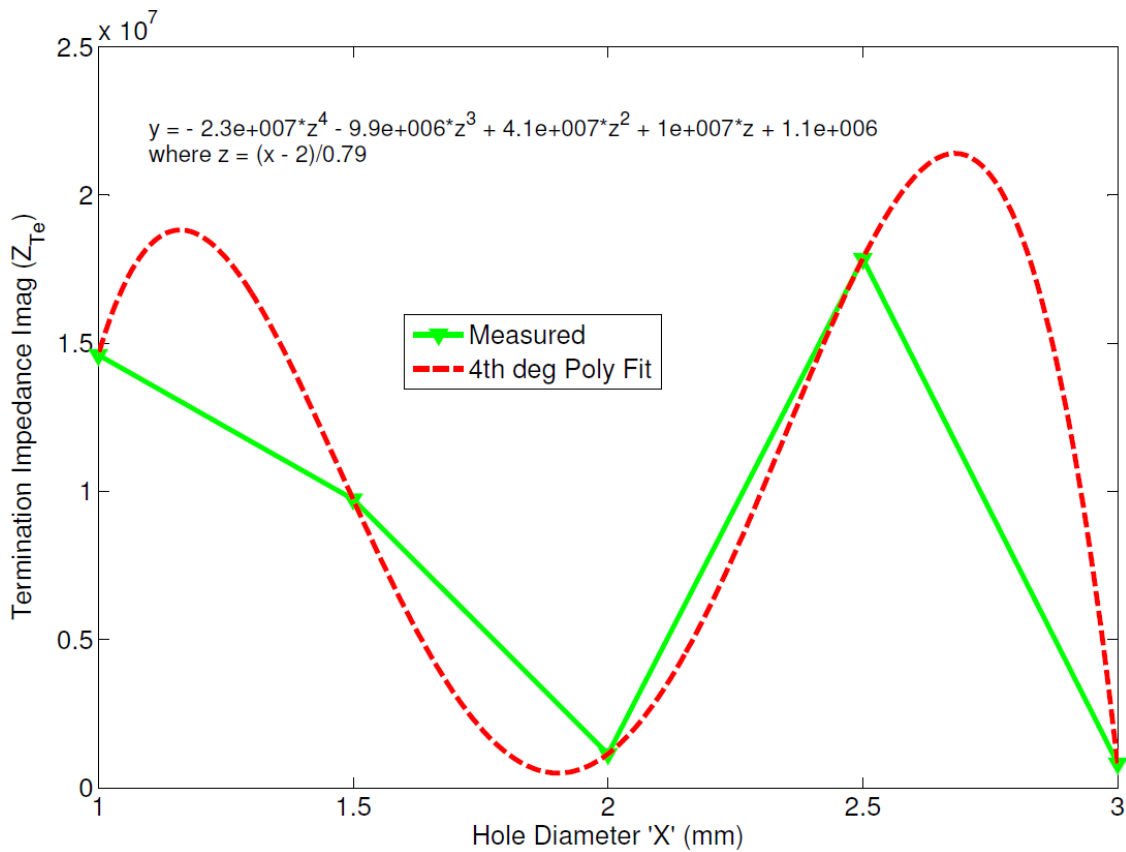


Figure 5-94 3-Hole 1st Pump Order Termination Impedance (Imag) for three hole tuners with a range of hole diameters

5.5.11 Developed Multi Hole Noise Reduction Prediction

Using the polynomial fit equations for the real and imaginary components of the termination impedance shown in Figures 5.91 – 5.94, complex values for the termination impedance for two and three hole tuners can be generated, which in turn can be used to predict associated 1st pump order noise reductions for a continuous range of values of hole diameter. Figure 5.95 (two hole) and Figure 5.96 (three hole) illustrate the predicted and measured 1st pump order noise reduction values, for various tuner hole diameters. Figures 5.95 and 5.96 also include a 4th degree polynomial curve fit of the measured results, to provide some context to the developed predictions.

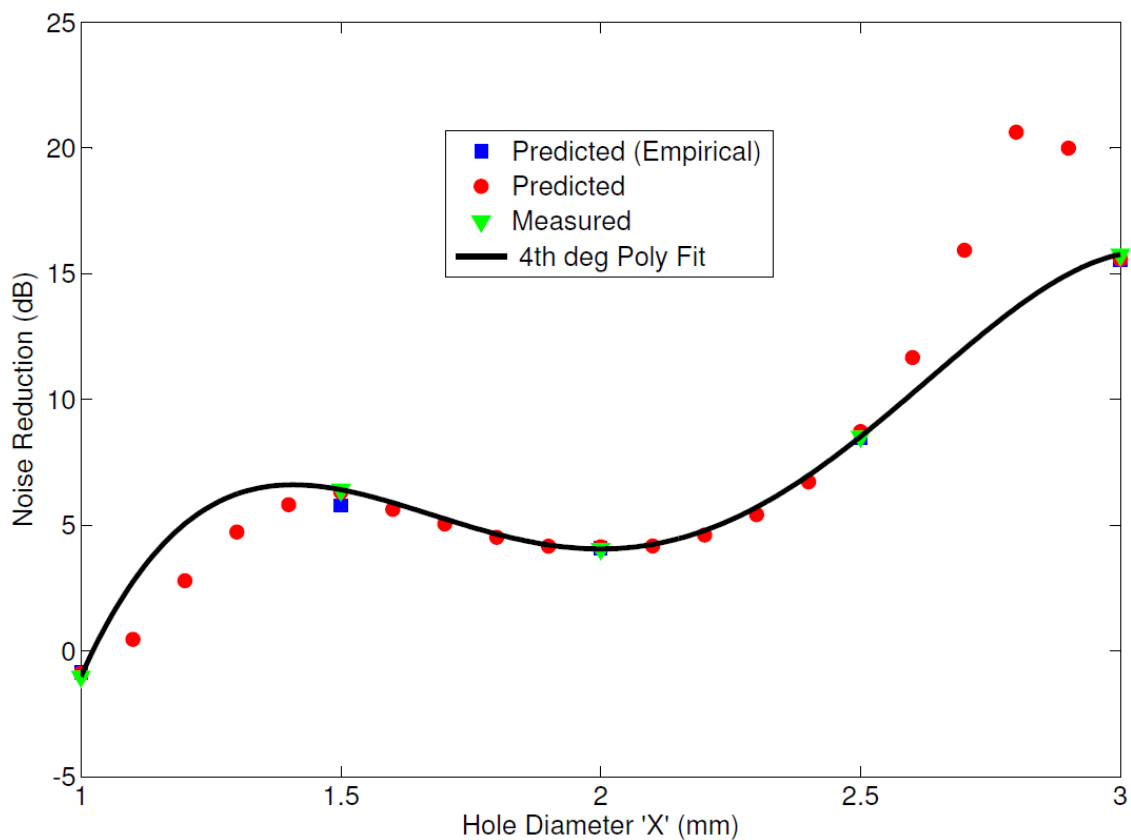


Figure 5-95 Two Hole Tuner – Predicted vs Measured Noise Reduction 1st Pump Order

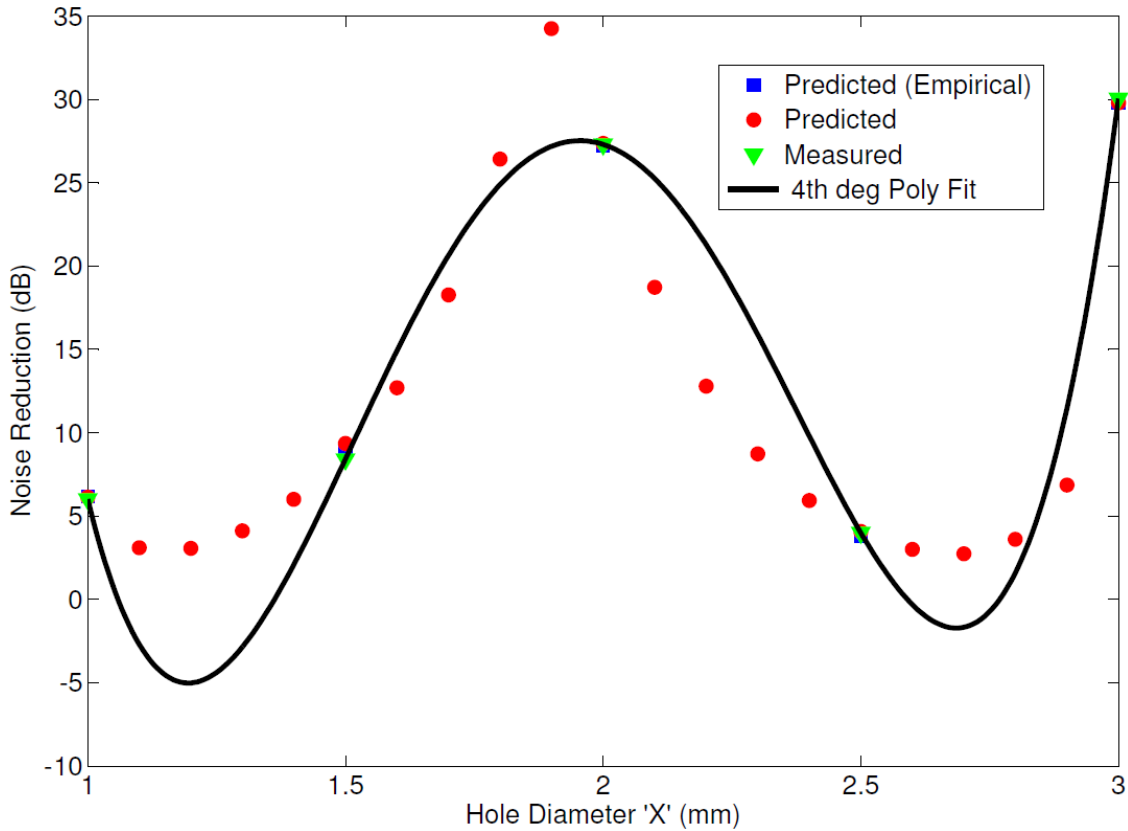


Figure 5-96 Three Hole Tuner – Predicted vs Measured Noise Reduction 1st Pump Order

Comparing the results illustrated in Figures 5.95 and 5.96 with those illustrated in Figure 5.88, and considering in addition the explanation given on tuner hole behaviour in Section 5.5.9, it is possible to gain further insight into the performance of multi-hole tuners. In general the developed predictions for the two hole tuners are well predicted. The developed predictions for the three hole tuner follow the trend of the curve fit of the measured results, however they appear to have a discrepancy introduced by a damping. Examining the results for a 1.5mm hole; one hole provides a noise reduction magnitude of 3dB, two holes provide a noise reduction magnitude of 6dB, and three holes provide a noise reduction magnitude of 9dB. Analysing other hole diameters, this apparent linear relationship does not always follow. However, there does seem to be some consistency with single hole magnitude values. The difference appears to be the way in which the holes or their associated impedances interact with each other to provide a resultant noise reduction for the tuner.

The impedance of a single hole in the tuner has been discussed in Section 5.5.9 and modelled based on perforated plates. As the multi-hole tuner design is simply a collection of single holes, it would be reasonable to assume that the attenuation

mechanisms are consistent. Having said this, consideration should be given to the interaction between the holes and its potential to affect single hole behaviour.

Melling (1973) has shown that the interaction between holes cannot be considered separately from the effect of porosity. The distance between the holes decreases as porosity is increased. Considering the resistive impedance of the tuner hole, a convenient way to explain this is that as the distance between the holes is decreased, the shear region around each hole becomes shared with the shear region of adjacent holes. As a result, the resistive impedance of each hole reduces and the overall acoustic impedance of the plate, or in this case the tuner, is reduced.

Considering the results presented in Figures 5.88, 5.95 and 5.96, it does not appear that for a given hole diameter, the overall acoustic impedance of the holes is reduced as porosity is increased. For example, the predicted and measured results for the three hole 2.0mm tuner provide significantly greater noise reduction than its two hole counterpart, where the two hole tuner provides less noise reduction than the single hole 2.0mm tuner. This would suggest that interaction between multi-tuner holes is not significantly affecting the overall attenuation mechanisms of the tuner in the same way the interaction operates for perforated plates as detailed by Melling (1973). This is most likely due to the relatively small hole size and the relatively large spacing of the tuner holes.

It is more likely that, consistent with the findings of Ronneberger (1972), each hole provides either an amplification or attenuation of an incident wave. The magnitude of the resultant waveform is constant and defined by the hole geometry, however the direction is influenced by any upstream holes, and the length of the interconnecting duct between the holes. This duct provides for a phase change of the acoustic wave and in theory, could be used to develop a resonant system. However, practically this would not be possible given the geometry of the power steering system.

Finally, consistent with the findings of Maa (1988), it is clear that multi-hole tuners provide for a significant increase compared to single hole tuners. Absorption coefficients for two hole and three hole tuners where $d = 1.0\text{mm}$, 1.5mm , 2.0mm , 2.5mm and 3.0mm and $D = 2.87\text{mm}$ are presented in Figures 5.97 and 5.98.

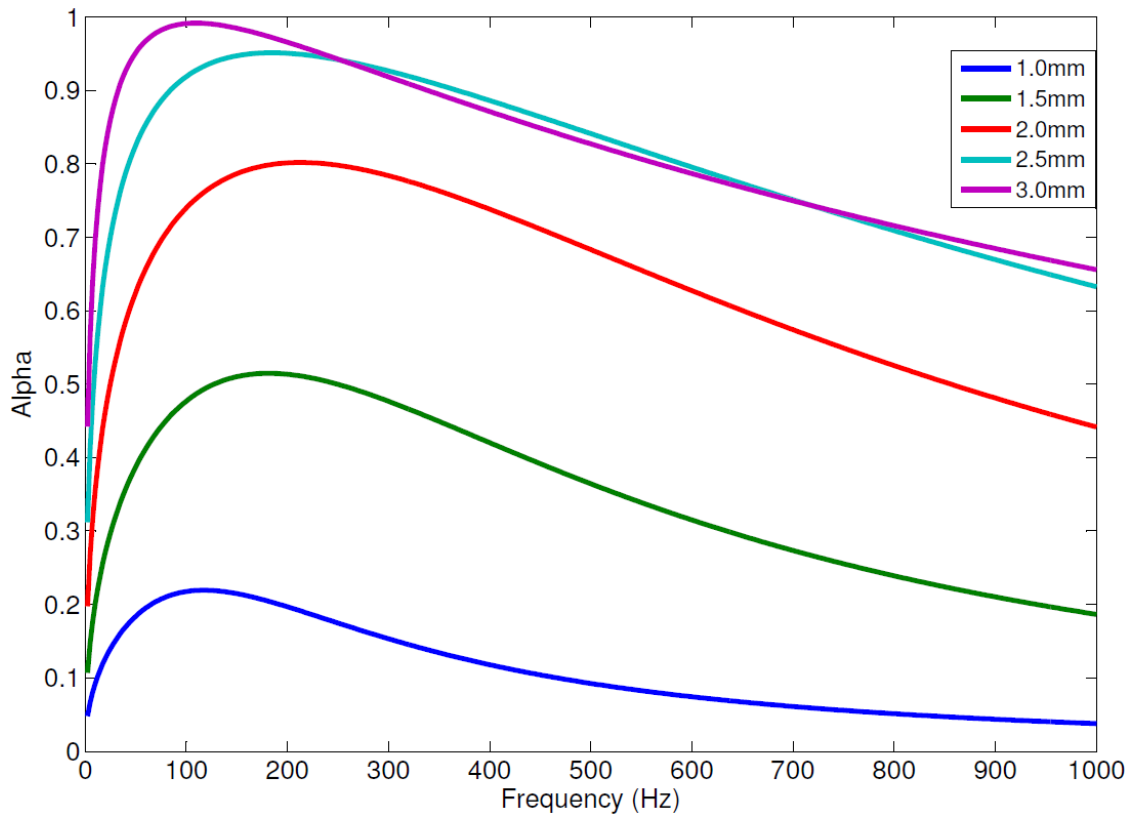


Figure 5-97 Absorption coefficient for a 2 hole tuners with varying diameter

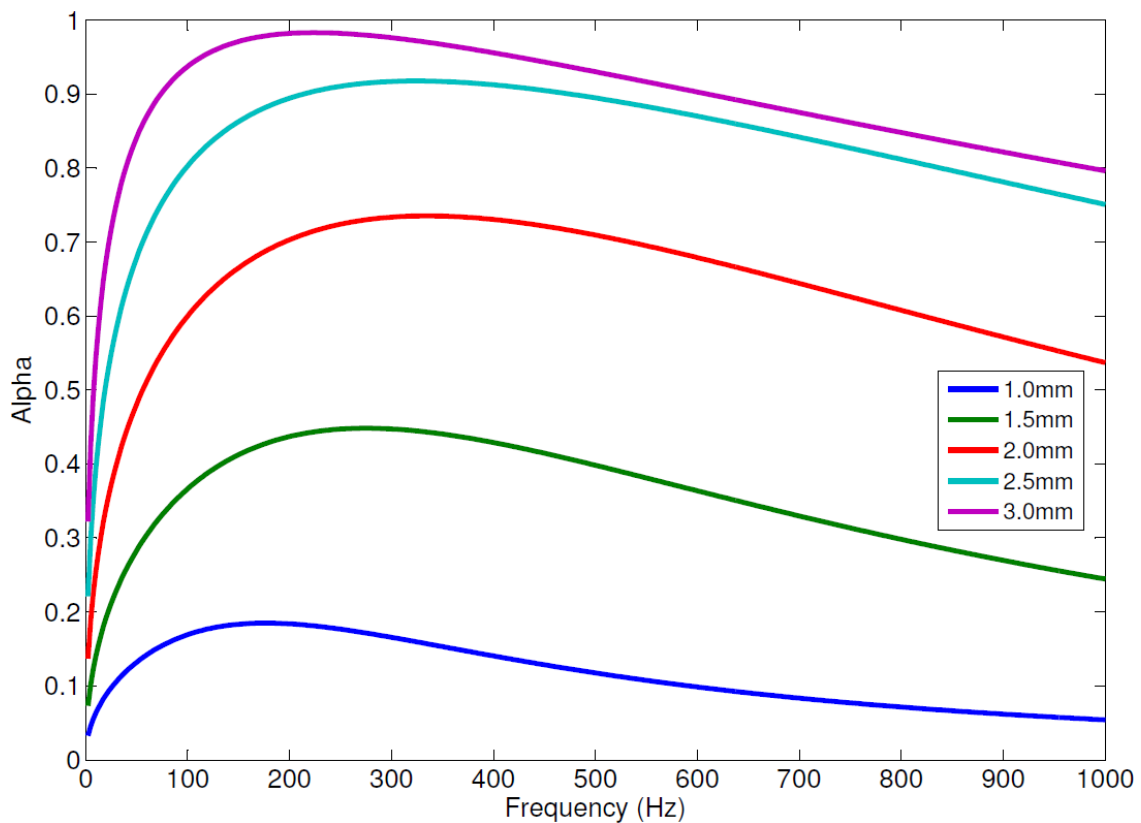


Figure 5-98 Absorption coefficient for a 3 hole tuners with varying diameter

It should be noted that the results presented in Figures 5.97 and 5.98 represent absorption coefficients calculated based on the assumption of the tuner holes seeing the same incident waveform simultaneously. As discussed earlier, in practise the holes will in fact progressively interact with the waveform, which will experience a phase change from hole to hole. In the case of the two and three hole tuners, the hole spacing is significantly less than the wavelength at the frequency of interest, such that this approach and associated results may be considered representative of multi-hole tuner behaviour.

5.6 Summary

The results presented in this section cover a wide range of tuner design configurations predicted using the theoretical model proposed in Chapter 3. These results have been validated using corresponding experimental measurements. Overall, good correlation exists between the experimental and theoretical results, in particular for the 1st pump order magnitudes, which are of greatest interest to this research.

For each of the tuner design parameters of interest i.e. tuner length, tuner hole location, tuner hole diameter, and multi-hole tuners, an examination of the various attenuation mechanisms has been provided. This analysis has illustrated that the acoustic impedances for the various tuner elements is consistent with well published theories covering quarter wavelength resonators and perforated plates.

In addition to achieving the key objectives of this research, this chapter has also presented and validated a new approach to modelling the complex termination impedance present in the power steering system. Furthermore, it has been demonstrated how this in turn can be used to predict associated noise reductions for a range of tuner design parameters.

6 Conclusions and Future Work

6.1 Summary

The aim of the work presented in this thesis is to investigate the noise reduction characteristics of plastic tuners and use this knowledge to develop a new theoretical model. The main reason for this was to improve the design and development process of these devices. Currently within the automotive industry, this process is rather lengthy, extremely laborious and somewhat inaccurate. To this end, the thesis has presented a theoretical model, which with the provision of some simple measurements, can be used to accurately predict tuner performance in a much reduced timeframe.

As explained in the introductory chapter, the frequency of greatest interest in power steering noise reduction is the fundamental or 1st order frequency of the power steering pump. Theoretical noise reduction for a number of different tuner design configurations was predicted using the transmission matrix method. The results showed that the tuner performance was not only a function of the tuner design, but primarily a result of the influence of the tuner on the power steering system, specifically the system termination impedance. Initially, an empirical approach was used to predict this impedance, which supported accurate 1st pump order results for tuner noise reduction. In addition, and following analysis of the empirical results, a new theory used to predict the complex termination impedance of the system under analysis was proposed and validated using the measured data. This theory removes the need for the empirical approach to termination impedance modelling, and therefore further reduces the tuner design and development timeframe by removing the time associated with taking these experimental measurements. Indeed, in the future, it may be possible to accurately model the noise reduction for a prototype tuner design, without the need for any experimental measurements.

A large number of tuner designs were investigated experimentally to quantify the noise reduction performance of commonly varied design parameters. These parameters included; tuner length, tuner hole position, tuner hole diameter and multi-hole tuners. The experiments also served to validate the theoretical model. In both cases, the tuner hole diameter was confirmed as the single most influential design parameter, which is in accordance with well researched acoustic duct, perforated plate and resonator theory,

but represents a new insight in terms of the acoustic wave propagation in a plastic tuner.

6.2 Key Objectives Achieved

Considering the main aim of the thesis outlined in Section 1.1, this work has been deemed to be successful since the knowledge of plastic tuners has been progressed and the plastic tuner development process has the potential to be improved using this new information. Specifically, a number of key areas of knowledge have been progressed as planned in Sections 1.2.1 – 1.2.6. These findings are summarised in the following sections.

6.2.1 Baseline Evaluation Summary

The purpose of this exercise was to experimentally compare and quantify the performance of the plastic tuner with a known baseline, in this case the spiral wound steel tuner. In addition, it was important to understand other system effects associated with the plastic tuner design introduction, which can also drive design development decisions.

Several experiments were conducted with plastic tuner design configurations selected at random. As a result, it was clearly noted that based on appropriately selected design parameters such as tuner length, hole position and number of holes, an attenuation performance equal to or better than a spiral wound steel tuner can be realised with a plastic tuner design. This is a finding that is certainly not widely understood in the automotive community. Furthermore, it was found that not only can a plastic tuner outperform a spiral wound steel tuner in terms of noise reduction, it can also improve the life of power steering system components such as the power steering pump, by reducing system back-pressure.

In summary, it is believed that this objective has been achieved and this component of the thesis has contributed to the existing knowledge base.

6.2.2 Tuner Length Summary

The objective in this section was to develop the understanding of the tuner length as a variable design parameter, and subsequently quantify its impact on system noise reduction.

Plastic tuners in the commonly used length range of 50-400mm were investigated by experimental analysis. It was found that overall the tuner length can contribute to noise reduction in the range of 5-10dB. Whilst this is not necessarily new information, it also illustrated that an optimal length of tuner can be determined. This knowledge is of value to development engineers as there is therefore potential to reduce cost (material cost) whilst maintaining performance.

It was also illustrated that the tuners containing no holes appear to have similar noise reduction mechanisms to an extended inlet resonator muffler (quarter wavelength resonator), with a clear resonant peak observed and predicted at $X = \lambda/4 \cong 400mm$.

Based on these findings this objective is believed to have been satisfied.

6.2.3 Tuner Hole Location Summary

The objective in this section was to develop an understanding of the tuner hole location as a design parameter, and subsequently quantify its impact on system noise reduction.

Plastic tuners 400mm in length, with a 1mm diameter hole progressively located along the tuner, were investigated. It was found that the location of the hole was not a significant design parameter for tuner performance. Over the range of the test samples, the maximum noise reduction attributed to this feature alone was around 3dB. The noise reduction mechanism associated with the hole was deemed to operate by providing acoustic impedance to the forward travelling wave. The hole location along the tuner length simply changed the phase of the incident wave, such that the downstream magnitude for a given frequency was either amplified or attenuated.

Quantifying this performance is considered to be of value as this specific knowledge was not widely available in the automotive community.

6.2.4 Tuner Hole Diameter Summary

The objective in this section was to develop an understanding of the tuner hole diameter as a design parameter, and subsequently quantify its impact on system noise reduction.

Plastic tuners 400mm in length, with a fixed location hole, of incremental diameter were investigated. The results for this design parameter were quite significant, in that they demonstrated a potential for up to 25dB noise reduction to be gained from an

appropriately selected hole diameter. In addition, it illustrated from a manufacturing process viewpoint, that it is very important to control the hole creation process so as to maintain the designed attenuation properties.

The noise reduction mechanisms associated with the tuner hole diameter were analysed with reference to micro-perforated panels and the theory developed by Maa (1988). Whilst the energy loss attributed to the ‘cavity’ between the tuner and the test tube wall behaved in accordance with Maa’s theory, due to the hole diameter size, the losses in the hole region are predominantly inertial rather than viscous in accordance with the findings of Putra (2010).

From the analysis of the noise reduction mechanisms, absorption coefficients for a range of tuner hole diameters were calculated. There appeared to be good correlation between the measured noise reduction for a given hole diameter and the corresponding absorption coefficient over the range.

Based on the results and analysis presented on the tuner hole diameter, the objective of this section is considered to have been met.

6.2.5 Multi-hole Summary

The objective in this section was to develop an understanding of multi-hole tuners and their performance characteristics, based on the range of commercially available tuners and their various hole configurations.

To achieve this objective a number of different tuner configurations were investigated. These included two and three hole configurations for a range of hole diameters. The experimental results alone provided a contribution to the existing knowledge base, as this type of data is not widely available. Significantly it was concluded that multi-hole tuners did not always provide enhanced performance when the hole diameter was maintained. The main reason for this, considering the explanations provided for tuner hole location and tuner hole diameter in Sections 5.5.7 and 5.5.9 respectively, was that the holes do not operate independently of each other with respect to overall noise reduction of the tuner.

Initially it was considered that the holes may be behaving in a manner similar to that proposed by Melling (1973), where the acoustic impedance of the hole, in particular the real or resistive component of the impedance is reduced by increased porosity, thus reducing overall acoustic impedance of the tuner. However it was demonstrated that this is not the case for the tuner samples analysed. Instead, the tuner hole interaction is characterised by the spacing or the length of the interconnecting duct, which promotes a phase shift of the incident waveform, and further attenuation or amplification of the upstream hole effects, in the resultant waveform.

Considering this finding, multi-hole tuners would potentially be better performers than single hole tuners, provided the design considered optimal hole diameter and spacing. However, it is likely based on the results presented in this thesis that similar performance could be achieved with a single hole tuner of appropriate length, hole size and hole position. From a manufacturing (cost) point of view, this would be the preferred solution.

The objective of this section is considered to have been met.

6.2.6 Plastic Tuner Model Summary

As detailed in the main aims and objectives, ideally a plastic tuner model could be developed, which would assist with the current design / development process for plastic tuners.

To achieve this, the plastic tuner was broken into various mathematical elements, which were then coupled using the transmission matrix methodology, to generate an overall model for the plastic tuner.

The assessment criterion for a plastic tuner is its noise reduction performance at the fundamental frequency of the power steering pump. The models presented here accurately predicted the noise reduction at this frequency for a wide range of plastic tuner design configurations.

In addition, during the course of the theoretical model development, a new equation capturing the acoustic pressure and velocity interaction within the power steering system termination has been outlined. Using this equation it was possible to generate a

complex model of the termination impedance, and subsequently use this to predict noise reductions for a continuous range of tuner design considerations.

The model generated has the potential to significantly reduce the design / development process for plastic tuners. The objective is considered to have been met.

6.3 Future Work

Leading from the analysis performed in this work, a definite area of future focus would be in the validation of the termination impedance theory. Results presented here suggest that the theory has merit in this application, however it certainly requires validation over a wider range of system parameters, in particular high and low pressure systems and systems of differing fluid density.

The theoretical model of the plastic tuner could be developed to incorporate pressure loss elements in the transmission matrix. One of the limiting aspects of the current model is that it is largely based on theory where the systems under consideration contain acoustic waves propagating in air. At certain points in the tuner, in particular the tuner hole region, the fluid under consideration i.e. power steering fluid, will behave such that loss effects may need to be considered. In this case, it would be useful to capture the loss with an appropriate element that accurately represents transmission through this region.

Further development of the tuner hole element, in particular its application in multi-hole tuners would be useful. It has been shown in Section 5 that the interaction between holes is not necessarily consistent with existing theory due to the spacing between the holes and the length of the interconnecting duct. However, it would be useful to understand the limitations in this regard. Application of Maa's (1988) theory to the transmission matrix model would assist in furthering the knowledge into multi-hole tuners.

Development of the tuner model also promotes the ability to apply optimisation techniques based on noise reduction performance. Manufacturing (cost) weighting could be applied to each of the tuner design parameters, which would further promote the concept of an optimal tuner design for a given application.

Other potential future work includes the application of the theory outlined here to pump generated noise reduction in a vast range of non power steering applications, including household washing machines, naval combatant vessels, and large-scale fluid transmission such as that associated with desalination plants.

7 References

- Bell, L** (1994). "Industrial Noise Control." Marcel Dekker, New York.
- Beranek, L and Ver, I** (1992). "Noise and Vibration Control Engineering: Principles and Applications." John Wiley and Sons Inc., New York.
- BS6335** (1990). "Methods for determining pressure ripple levels generated in hydraulic fluid power steering systems and components." British Standards Institution, London.
- Burdisso, R and Smith, J** (2000). "Control of Noise from Turbofan Engines Using Herschel-Quincke Waveguides." 6th AIAA Aeroacoustics Conference, Hawaii, USA, 12th - 14th June, 2000.
- Burgemeister, K and Hansen, C** (1996). "Calculating resonance frequencies of perforated panels." Journal of Sound and Vibration, 196(4): 387-399.
- Casalino, D, Diozzi, F, Sannino, R and Paonessa, A** (2008). "Aircraft noise reduction technologies: A bibliographic review." Aerospace Science and Technology, 12: 1-17.
- Chen, Y, Tse, C and Lao, H** (1992). "A study on the transmission loss of straight through type reactive mufflers." National Science Council, Report No. NSC 81-0403-E-002-05.
- Chu, W** (1986). "Transfer function technique for impedance and absorption measurements in and impedance tube using a single microphone." Journal of the Acoustical Society of America, 80(2): 555-560.
- Chung, J and Blaser, D** (1980). "Transfer function method of measuring in-duct acoustic properties." Journal of the Acoustical Society of America, 68(3): 907-913.

Cooper Standard Automotive (2007). "B265 Spiral Wound Steel Tuner." 7205-508-0004, Adelaide, Australia.

Davies, P, Bhattacharya, M and Beuto, J (1980). "Measurement of plane wave acoustic field in flow ducts." *Journal of Sound and Vibration*, 72: 539-542.

Dickinson, A, Edge, K and Johnston, D (1994). "Measurement and prediction of power steering vane pump fluid borne noise." SAE Noise and Vibration Conference, Traverse City, Michigan, May 1993, Proc SAE International 1993(931294): 267-275.

Drew, J (1997). "The use of flexible hose to reduce pressure ripple in power steering." Phd Thesis, University of Bath, UK.

Drew, J, Longmore, D and Johnston, D (1998). "Theoretical analysis of pressure and flow ripple in flexible hoses containing tuners." *Proceedings of the Institute of Mechanical Engineers, Part I: Journal of Systems and Control Engineering* 212(6): 405-422.

Dupont, T, Pavic, G and Laulagnet, B (2003). "Acoustic properties of lightweight micro-perforated plate systems." *Applied Acoustics*, 89(2): 201-12.

Edge, K and Johnston, D (1990). "The secondary source method for pump pressure ripple characteristics." *Proceedings of the Institute of Mechanical Engineers*, 204(A00989/1).

Fahy, F (1984). "Rapid method for the measurement of sample acoustic impedance in a standard wave tube." *Journal of Sound and Vibration*, 97: 168-170.

Ford Motor Company of Australia (1979). "DVT 11.07, Attenuator Performance Evaluation."

-
- Foster, K and Hannan, D** (1977). "Fundamental fluidborne and airborne noise generation of axial piston pumps." Institute of Mechanical Engineers, London, Seminar on Quiet Oil Hydraulic Systems pp. 29-40. Page 336
- Furnell, G and Bies, D** (1989). "Matrix analysis of acoustic wave propagation within curved ducting systems." *Journal of Sound and Vibration*, 132(2): 245-263.
- GE Sensing** (2005). "PTX / PMP 1400 Series Industrial Pressure Sensors." (920-097A).
- Griffen, S, Huybrechts, S and Lane, S** (1999). "An adaptive Herschel-Quincke Tube." *Journal of Intelligent Material Systems and Structures*, 10(12): 956-961.
- Hallez, R and Burdisso, R** (2001). "Investigation of the Herschel-Quincke tube concept as a noise control device for turbofan engines." 39th AIAA Aerospace Sciences Meeting & Exhibition, Reno, Nevada, USA, 8th-11th Jan 2001, AIAA-200LO816.
- Hastings, M and Chen, C** (1993). "Analysis of tuning cables for reduction of fluidborne noise in automotive power steering hydraulic lines." SAE Technical Paper Series, 1st May, 1993, SAE(931295).
- Herschel, J** (1883). "On the absorption of light coloured media, viewed in connexion with undulated theory." *Philosophical magazine and Journal of Science*, 3: 401-412.
- Howstuffworks.** (2001). "Steering Pump Diagram and Flow Chart." Retrieved 27 May, 2009, from <http://static.howstuffworks.com/gi/steering-pump-diagram.jpg>.
- Hydraulic Equipment Manufacturers.** (2011). "Power Steering Diagram." Retrieved 2 March, 2008, from <http://www.hydraulic-equipment-manufacturers.com/gifs/powersteer.jpg>.
-

Ichiyanagi, T and Nishiumi, T (2008). "Insertion Loss of a Side Branch Resonator in a Hydraulic Line." Department of Mechanical Systems Engineering, School of Systems Engineering, National Defence Academy, Hashirimizu, Yokosuka, Kanagana, Japan, 1-10-20: 239-868.

Igarashi, J (1958). "Fundamentals of acoustic silencers." Aeronautical Research Institute, University of Tokyo, Report No. 344: 67-85.

Ingard, U (1948). "On the radiation of sound into a circular tube with an application to resonators." Journal of the Acoustic Society of America, 20: 665-682.

Ingard, U (1954). "Perforated facing and sound absorption." Journal of the Acoustical Society of America, 26: 151-154.

Ingard, U and Ising, H (1967). "Acoustic nonlinearity of an orifice." Journal of the Acoustical Society of America, 21: 94-97.

ISO 10767-1 (1996). "Determination of pressure ripple levels generated in systems and components - Part 1: Precision methods for pumps." International Organisation for Standardisation.

Jayaraman, K and Yam, K (1981). "Decoupling approach to modelling perforated tube muffler components." Journal of the Acoustical Society of America, 69(2): 390-396.

Johnston, D, Way, T and Cone, K (2010). "Measured dynamic properties of flexible hoses." Journal of Vibration and Acoustics, 132(021011-1).

Jones, P and Kessissoglou, N (2010). "A Numerical and Experimental Study of the Transmission Loss of Mufflers used in Respiratory Medical Devices." Acoustics Australia, 38(1): 13-19.

-
- Kang, J and Fuchs, H** (1999). "Predicting the absorption of open weave textiles and micro-perforated membranes backed by an air space." *Journal of Sound and Vibration*, 220(5): 905-920.
- Kang, Z, Zheng, S and Lian, X** (2010). Study of the acoustic performance of a perforated duct muffler. State Key Laboratory of Automobile Safety and Energy Beijing, China, Tsinghua University. 978-1-4244-7739.
- Kinsler, L and Frey, A** (1962). "Fundamentals of Acoustics." John Wiley and Sons Inc., New York, 2nd edition.
- Klees, G** (1967). "Attenuating Device." US Patent 3323305.
- Kobayashi, M and Oshima, A** (2001). "Analysis of Hammering in Power Steering Systems by Simulation." *KOYO Engineering Journal English Edition*,(159E).
- Lapka, W and Cempel, C** (2007). "Noise Reduction of Spiral Ducts." *International Journal of Safety and Ergonomics*, 13(4): 419-426.
- Lee, D and Kwon, Y** (2004). "Estimation of the absorption performance of multiple layer perforated panel systems by transfer matrix method." *Journal of Sound and Vibration*, 278: 847-860.
- Lee, J and Swenson, G** (1992). "Compact sound adsorbers for low frequencies." *Noise Control Eng Journal*, 38(3): 109-117.
- Long, M** (1999). "Isolating hydraulic noise from mechanical noise in power rack and pinion steering systems." *SAE*,(1999010397).
- Longmore, D** (1977). "The transmission and attenuation of fluid borne noise in hydraulic hose." *Proceedings of the Institute of Mechanical Engineers: Seminar on Quiet Oil Hydraulic Systems*, 127(138) : C267/77

-
- Longmore, D and Schlesinger, A** (1991). "Transmission of vibration and pressure fluctuations through hydraulic hoses." Proceedings of the Institute of Mechanical Engineers, 205(12): 97-104.
- Maa, D** (1998). "Potential of microperforated panel absorber." Journal of the Acoustical Society of America, 104(5): 2861-2866.
- Mangiarotty, R** (1971). "The reduction of aircraft engine fan-compressor noise using acoustic linings." Journal of Sound and Vibration, 18(4): 565-576.
- Melling, T** (1973). "The acoustic impedance of perforates at medium and high sound pressure levels." Journal of Sound and Vibration, 29(1): 1-65.
- Merkel, R** (2004). "Specification for Acoustic Tuners." Eaton Fluid Power, Germany.
- Morse, P and Ingard, U** (1968). "Theoretical Acoustics." McGraw-Hill, New York.
- Munjal, M** (1987). "Acoustics of ducts and mufflers." John Wiley and Sons Inc., New York.
- Pan, J, Guo, J and Ayres, C** (2005). "Improvement of sound absorption of honeycomb panels." School of Mechanical Engineering, University of Western Australia , Proceedings of Acoustics, Busselton, Western Australia (2005): 195-200.
- Patrick, W** (1968). "Sound transmission through lined ducts in parallel." Phd Thesis, Massachusetts Institute of Technology, MA, USA.
- Putra, A and Thompson, D** (2010). "Sound radiation from perforated plates." Journal of Sound and Vibration, 329: 4227-4250.
- Quincke, G** (1866). "Ueber interferenzapparate fur schallwellen." Annalen der Physik und Chemie, 128: 177-192.

-
- Rao, K** (1984). "Prediction and verification of aeroacoustic performance of perforated element mufflers." PHD Thesis, Indian Institute of Science, Bangalore.
- Ronneberger, D** (1972). "The acoustic impedance of holes in the wall of flow ducts." *Journal of Sound and Vibration*, 24: 133-150.
- Runge, C** (1901). "Über empirische Funktionen und die Interpolation zwischen äquidistanten Ordinaten", *Zeitschrift für Mathematik und Physik* 46: 224–243.
- Sciortino, G and Bamdad-Soufi, D** (1998). "Vibration diagnostics and optimization of a test bench to characterise power steering pump noise using vibration measurements." IMechE, Delphi Automotive Systems, Paris, C521/007.
- Selamet, A** (1994). "The Herschel-Quincke tube: A theoretical, computational, and experimental investigation." *Journal of the Acoustical Society of America*, 96(5): 3177-3185.
- Selamet, A and Ji, Z L** (1998). "Acoustic Attenuation Performance of Circular Expansion Chambers with Extended Inlet / Outlet." *Journal of Sound and Vibration*, 223(2): 197-212.
- Seybert, A and Ross, D** (1977). "Experimental determination of acoustic properties using a two-microphone random excitation technique." *Journal of the Acoustical Society of America*, 61(5): 1362-1370.
- Seybert, A and Soenarko, B** (1981). "Error analysis of spectral estimates with application to the measurement of acoustic parameters using random sound fields in ducts." *Journal of the Acoustic Society of America*, 69(1190-1199).
- Sreenath, A and Munjal, M** (1970). "Evaluation of noise attenuation due to exhaust mufflers." *Journal of sound and vibration*, 12(1): 1-19.
- Stewart, G** (1928). "The theory of the Herschel-Quincke tube." *Physics Revised*, 31: 696-698.
-

-
- Stinson, M and Shaw, E** (1985). "Acoustic impedance of small, circular orifices in thin plates." *Journal of the Acoustical Society of America*, 77(6): 2039-2042.
- Sullivan, J** (1979). "A method for modelling perforated tube muffler components: 1 Theory,." *Journal of the Acoustic Society of America*, 1979, 66(3): 772-778.
- Thawani, P and Jayaraman, K** (1983). "Modelling and applications of straight through resonators." *Journal of the Acoustical Society of America*, 73(4): 1387-1389.
- Thomas, R, Burdisso, R, Fuller, C and O'Brien, W** (1993). "Preliminary experiments on active control of fan noise from a turbofan engine." *Journal of Sound and Vibration*, 161(3): 532-537.
- Tuc, B** (1981). "The use of flexible hoses for reducing pressure ripple in hydraulic systems." Phd Thesis,, University of Bath.
- Washio, S and Konishi, T** (1985). "Research on wave phenomena in hydraulic lines." *Japanese Society of Mechanical Engineers, Bulletin of the JSME*, 28(241): 1409-1415.
- ZF.** (2011). "Servotronic 2." Retrieved 2 March, 2008, from http://www.zf.com/media/media/img_1/brands_1/zf_parts/products_zf_parts/steering_gear_zf_parts/zf_servotronic/ZF_Servotronic_2.jpg.
- Zhang, Z and Gu, X** (1998). "The theoretical and application study on a double layer microperforated sound absorption structure." *Journal of Sound and Vibration*, 215(3): 339-405.

Appendix A

A.1 Matlab Code – Tuner Duct Element

The following code illustrates an example of the Matlab function used to compute a forward transmission matrix of a tuner duct element in the $(p; \rho*s*u)$ form.

```
%
%Input Parameters
%
%   f = frequency (Hz)
%   r_a = duct radius @ a (m)
%   S_a = duct area @ a (m^2)
%   l = length of duct (m)
%   rho = density (kg/m^3)
%
r_3 = 0.002;
S_3 = (pi*(r_3^2));
l_3 = 0.1;
rho = 870;
c = 546;
%
%
%Output Parameters
%
%   t11 = t11 of forward transmission matrix
%   t12 = t12 of forward transmission matrix
%   t21 = t21 of forward transmission matrix
%   t22 = t22 of forward transmission matrix
%
%Loop - Generate transmission matrix values for each value of f
%
t11_3 = zeros(401,1);
t12_3 = zeros(401,1);
t21_3 = zeros(401,1);
t22_3 = zeros(401,1);
%
for i = 1 : 401
    f(i,1) = G2_2(i,1);
    M = 0.02;
    k = (2*pi*f(i,1))/c;
    k_c = k/(1-M^2);
    y_3 = c/S_3;
    coeff_3 = exp(-j*k*M*l_3);
    t11 = coeff_3*cos(k*l_3);
    t12 = j*coeff_3*y_3*sin(k*l_3);
    t21 = j*coeff_3*sin(k*l_3)/y_3;
    t22 = coeff_3*cos(k*l_3);

%
%
```

```
t11_3(i,1) = t11;  
t12_3(i,1) = t12;  
t21_3(i,1) = t21;  
t22_3(i,1) = t22;
```

```
end
```

A.2 Matlab Code – Tuner Expansion Element

The following code illustrates an example of the Matlab function used to compute a forward transmission matrix of a tuner expansion element in the (p; rho*s*u) form.

```
%  
%Input Parameters  
% f = frequency (Hz)  
% S_a = duct radius @ location (a) (m^2)  
% l_a = length of duct a (m)  
% rho = density (kg/m^3)  
%  
r_2 = 0.002;  
S_2 = (pi*(r_2^2));  
l_2 = 0.1;  
%  
r_3 = 0.005;  
S_3 = (pi*(r_3^2));  
l_3 = 0.1;  
%  
rho = 870;  
c = 546;  
%  
%Output Parameters  
%  
% t11 = t11 of forward transmission matrix  
% t12 = t12 of forward transmission matrix  
% t21 = t21 of forward transmission matrix  
% t22 = t22 of forward transmission matrix  
%  
%Loop - Generate transmission matrix values for each value of f  
%  
t11_5 = zeros(401,1);  
t12_5 = zeros(401,1);  
t21_5 = zeros(401,1);  
t22_5 = zeros(401,1);  
Z_5 = zeros(401,1);  
%  
  
%  
for i = 1 : 401
```

```

f(i,1) = G2_2(i,1);
K_5 = ((S_2/S_3)-1)^2;
M = 0.02;
t11 = 1;
t12 = K_5*M*y_2;
t21 = 0;
t22 = 1;
%
t11_5(i,1) = t11;
t12_5(i,1) = t12;
t21_5(i,1) = t21;
t22_5(i,1) = t22;

end

```

A.3 Matlab Code – Tuner Contraction Element

The following code illustrates an example of the Matlab function used to compute a forward transmission matrix of a tuner contraction element in the (p; rho*s*u) form.

```

%
%Input Parameters
% f = frequency (Hz)
% S_a = duct radius @ location (a) (m^2)
% l_a = length of duct a (m)
% rho = density (kg/m^3)
%
r_9 = 0.005;
S_9 = (pi*(r_9^2));
l_9 = 0.1;
%
r_12 = 0.002;
S_12 = (pi*(r_12^2));
l_12 = 0.1;
%
rho = 870;
c = 546;
%
%Output Parameters
%
% t11 = t11 of forward transmission matrix
% t12 = t12 of forward transmission matrix
% t21 = t21 of forward transmission matrix
% t22 = t22 of forward transmission matrix
%
%Loop - Generate transmission matrix values for each value of f
%
t11_11 = zeros(401,1);

```

```

t12_11 = zeros(401,1);
t21_11 = zeros(401,1);
t22_11 = zeros(401,1);
Z_11 = zeros(401,1);
%

for i = 1 : 401
    f= G2_2(i,1);
    K = (1-(S_9/S_12))/2;
    Y_11 = c/S_11;
    %
    t11_11(i,1) = 1;
    t12_11(i,1) = K*M*Y_11;
    t21_11(i,1) = 0;
    t22_11(i,1) = 1;

end

```

A.4 Matlab Code – Parallel Branch Element

The following code illustrates an example of the Matlab function used to compute a forward transmission matrix of a parallel branch element in the $(p; \rho*s*u)$ form.

```

%
%Input Parameters
%    T_** Transmission matrix of various flow paths comprising the parallel branch.
%
%Output Parameters
%
%    t11_11(i,1) = t11 of forward transmission matrix
%    t12_11(i,1) = t12 of forward transmission matrix
%    t21_11(i,1) = t21 of forward transmission matrix
%    t22_11(i,1) = t22 of forward transmission matrix
%

T_B1 = T_12*T_9*T_3*T_3_5;
t11_L1 = T_B1(1,1);
t12_L1 = T_B1(1,2);
t21_L1 = T_B1(2,1);
t22_L1 = T_B1(2,2);
%

T_B2 = T_5*T_4*T_7;
t11_L2 = T_B2(1,1);
t12_L2 = T_B2(1,2);
t21_L2 = T_B2(2,1);
t22_L2 = T_B2(2,2);

%

B_1 = 1./(1./t12_L1+1./t12_L2);

```

```

A_1 = (t11_L1./t12_L1+t11_L2./t12_L2)*B_1;

C_1 = (t21_L1+t21_L2+A_1*(t22_L1./t12_L1+t22_L2./t12_L2)-
(t22_L1.*t11_L1./t12_L1+t22_L2.*t11_L2./t12_L2));

D_1 = B_1 * (t22_L1./t12_L1+t22_L2./t12_L2);

t11_brn_1(i,1) = A_1;
t12_brn_1(i,1) = B_1;
t21_brn_1(i,1) = C_1;
t22_brn_1(i,1) = D_1;

end

```

A.5 Matlab Code – Transmission Loss

The following code illustrates an example of the Matlab function used to compute the transmission loss of a system of matrices in the (p; rho*s*u) form.

```

%Input Parameters
% t11_f = t11 of transmission matrix @ frequency f
% t12_f = t12 of transmission matrix @ frequency f
% t21_f = t21 of transmission matrix @ frequency f
% t22_f = t22 of transmission matrix @ frequency f
%
%
Tsys = zeros(401,1);
Tsys11 = zeros(401,1);
Tsys12 = zeros(401,1);
Tsys21 = zeros(401,1);
Tsys22 = zeros(401,1);
%
r_5 = 0.002;
S_5 = (pi*(r_5^2));
r_1 = 0.005;
S_1 = (pi*(r_1^2));
%
%Loop - Generate transmission loss and P1 for each value of f
%
for i = 1 : 401
    %
    T_brn_1 = [t11_brn_1(i,1) t12_brn_1(i,1); t21_brn_1(i,1) t22_brn_1(i,1)];
    T_5 = [t11_5(i,1) t12_5(i,1); t21_5(i,1) t22_5(i,1)];
    T_4 = [t11_4(i,1) t12_4(i,1); t21_4(i,1) t22_4(i,1)];
    T_3 = [t11_3(i,1) t12_3(i,1); t21_3(i,1) t22_3(i,1)];
    T_2 = [t11_2(i,1) t12_2(i,1); t21_2(i,1) t22_2(i,1)];
    T_1 = [t11_1(i,1) t12_1(i,1); t21_1(i,1) t22_1(i,1)];
    %
    Tsys = T_brn_1*T_3*T_5*T_4*T_2*T_1
    Tsys11 = Tsys(1,1);

```

```

Tsys12 = Tsys(1,2);
Tsys21 = Tsys(2,1);
Tsys22 = Tsys(2,2);

sum(i,1) = ((abs(Tsys11+Tsys12*(S_5/c)+Tsys21*(c/S_1)+Tsys22))/2);
tl_p(i,1) = 20*log10(sum(i,1));

```

```
end
```

A.4 Matlab Code – Noise Reduction

The following code illustrates an example of the Matlab function used to compute the noise reduction of a system of matrices in the $(p; \rho * s * u)$ form.

```

%Input Parameters
% t11_f = t11 of transmission matrix @ frequency f
% t12_f = t12 of transmission matrix @ frequency f
% t21_f = t21 of transmission matrix @ frequency f
% t22_f = t22 of transmission matrix @ frequency f
% Tsys = resultant transmission matrix
%
% Set Parameters
%
tl_p = zeros(401,1);
sum_2 = zeros(401,1);
NR_P = zeros(401,1);
Tsys = zeros(401,1);
Tsys11 = zeros(401,1);
Tsys12 = zeros(401,1);
Tsys21 = zeros(401,1);
Tsys22 = zeros(401,1);
%
%Loop - Generate transmission loss and P1 for each value of f
%
for i = 1 : 401
    %
    f = G2_2(i,1);
    l_e = 0.6133*r_0;
    k = (2*pi*f)/c;
    y_0 = c/S_0;
    Q = 0.00024;
    V = 0.012*( (X2_50(134,2)) / (Q/S_0) );
    Z_t(i,1) = V*(y_0*((0.5*k*r_0)^2+j*k*l_e));
    %
    %
    T_5 = [t11_5(i,1) t12_5(i,1); t21_5(i,1) t22_5(i,1)];
    T_4 = [t11_4(i,1) t12_4(i,1); t21_4(i,1) t22_4(i,1)];
    T_3 = [t11_3(i,1) t12_3(i,1); t21_3(i,1) t22_3(i,1)];
    T_2 = [t11_2(i,1) t12_2(i,1); t21_2(i,1) t22_2(i,1)];
    T_1 = [t11_1(i,1) t12_1(i,1); t21_1(i,1) t22_1(i,1)];

```

```
%  
Tsys = T_3*T_5*T_4*T_2*T_1  
Tsys11 = Tsys(1,1);  
Tsys12 = Tsys(1,2);  
Tsys21 = Tsys(2,1);  
Tsys22 = Tsys(2,2);  
%  
sum_2(i,1) = abs(Tsys11+Tsys12/Z_t(i,1)/cos(k*l_e)+j*y_0*(sin(k*l_e)/Z_t(i,1)));  
NR_P(i,1) = 20*log10(sum_2(i,1));
```

```
end
```